

## Durham E-Theses

---

### *Understanding the cellular behaviour of the luminescent lanthanide complexes*

New, Elizabeth Joy

#### How to cite:

---

New, Elizabeth Joy (2009) *Understanding the cellular behaviour of the luminescent lanthanide complexes*, Durham theses, Durham University. Available at Durham E-Theses Online:  
<http://etheses.dur.ac.uk/2109/>

#### Use policy

---

The full-text may be used and/or reproduced, and given to third parties in any format or medium, without prior permission or charge, for personal research or study, educational, or not-for-profit purposes provided that:

- a full bibliographic reference is made to the original source
- a [link](#) is made to the metadata record in Durham E-Theses
- the full-text is not changed in any way

The full-text must not be sold in any format or medium without the formal permission of the copyright holders.

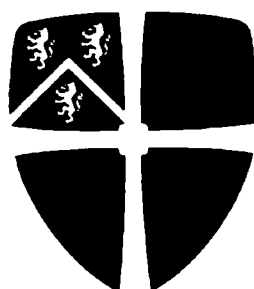
Please consult the [full Durham E-Theses policy](#) for further details.

# UNDERSTANDING THE CELLULAR BEHAVIOUR OF LUMINESCENT LANTHANIDE COMPLEXES

**Elizabeth Joy New**

A thesis submitted for the degree of Doctor of Philosophy

The copyright of this thesis rests with the author or the university to which it was submitted. No quotation from it, or information derived from it may be published without the prior written consent of the author or university, and any information derived from it should be acknowledged.



12 OCT 2009

Department of Chemistry  
Durham University

2009



## **DECLARATION**

The research described herein was undertaken at the Department of Chemistry at Durham University between October 2006 and July 2009. All of the work is my own, except where specifically stated otherwise. No part of it has previously been submitted for a degree at this or any other university.

## **STATEMENT OF COPYRIGHT**

The copyright of this thesis rests with the author. No quotations should be published without prior consent and information derived from it should be acknowledged.

## ABSTRACT

The design of responsive optical cellular probes remains a key challenge for biology and medicine. Luminescent lanthanide complexes are well suited for this purpose, with their information-rich emission profiles, and long luminescence lifetimes which allow gating out of interfering background signals. In order to design complexes for *in cellulo* applications, it is important to gain a greater understanding of the cellular behaviour of such complexes. This thesis describes work performed to this end.

The studies described herein utilise a broad range of complexes synthesised in Durham. These complexes comprise a  $\text{Eu}^{3+}$  or  $\text{Tb}^{3+}$  ion encapsulated in a cyclen macrocycle to which is attached a sensitising chromophore and two or three amide- or carboxylate-based pendant arms. The synthesis and characterisation of one set of such complexes is described. Modification of the pendant arm was shown to result in considerable variation of the complex helicity and structure, but with no alteration in the cellular behaviour.

This thesis also describes work which was performed to explore various aspects of cellular behaviour. The range of observed sub-cellular localisations are described, structure-localisation relationships presented and the observation of nucleolar localisation in some cases investigated. Studies of uptake mechanisms indicated that all complexes are transported across the cell membrane by a common pathway of macropinocytosis. Examples of various sub-cellular speciation states are presented, with detailed investigation of one case of reversible protein binding which induces a helicity change in the complex in an enantioselective fashion. Finally, the effect of the complexes on the cellular homeostasis is discussed, with the finding that complexes do not generally perturb the normal function of the cell.

This work therefore demonstrates that most luminescent lanthanide complexes do exhibit behaviour which makes them suitable for use as cellular probes. They are generally non-toxic, readily internalised and localise to specific organelles, and have demonstrated utility in reporting on the sub-cellular environment.

## ACKNOWLEDGEMENTS

So many people have played a role in ensuring that the three years I have spent in Durham were not only productive, but also enjoyable. I would firstly like to thank my supervisor, Professor David Parker, for continued guidance, optimism and support throughout the years.

It has been a delight to work in the Parker group. Thank you to my fellow PhD students Kirsten, Elena, James, David, Brad, Craig, Ben, Robek, Filip, Elisa and Siobhan, and to other members of the group, including Kanthi, Ga-Lai, Phil, Roy, Raman and Shashi, for their friendship, and their readiness to lend a helping hand.

Special thanks must go to Dr Aileen Congreve for her help with flow cytometry, to Dr Christine Richardson of the School of Biological Sciences for assistance with the confocal microscope, and to Dr Bob Peacock of Glasgow University for use of his CPL spectrometer.

Much of my work relied on the help of many others in the chemistry department. Thanks to the stores staff, to Dr Alan Kenwright, Catherine Heffermann and Ian McKeag for NMR spectroscopy, and Dr Mike Jones, Dr Jackie Mosely and Lara Turner for mass spectrometry. Many others in the chemistry department were always willing to give me advice: thanks to my associate supervisor Dr Andrew Beeby, Dr John Sanderson, Dr Ehmke Pohl, Dr Lars Olof-Pålsson and Dr Ilya Kuprov.

Thanks also to Dr Chris Ottley in the Department of Earth Sciences for ICP-MS analysis, and Professor Carlos Geraldés, João Teixeira and David Dias at the University of Coimbra (Portugal) for STD-NMR data.

My studies in Durham have been made possible by financial support from the Association of Commonwealth Universities, and the Durham Doctoral Fellowship Scheme.

Finally, I would like to thank all my family and friends who supported, encouraged and prayed for me over the years. My parents in particular have been such a great support.

# TABLE OF CONTENTS

ABSTRACT .....	i
ACKNOWLEDGEMENTS .....	ii
ABBREVIATIONS .....	vii
CHAPTER ONE: INTRODUCTION	
1.1 Overview .....	1
1.2 Molecular imaging .....	1
1.2.1 Luminescence imaging .....	3
1.2.2 Classes of luminescence signalling .....	3
1.2.3 The challenge of designing luminescent cellular probes .....	6
1.2.3.1 Probe suitability .....	6
1.2.3.2 Cellular behaviour .....	8
1.3 Luminescent cellular probes .....	10
1.3.1 Fluorescent organic dyes .....	10
1.3.2 Fluorescent proteins .....	11
1.3.3 Quantum dots .....	12
1.3.4 Transition metal complexes .....	13
1.3.5 Luminescent lanthanides .....	14
1.4 Luminescent lanthanide complexes .....	14
1.4.1 Photophysical properties .....	14
1.4.1.1 The need for sensitised emission .....	15
1.4.1.2 Energy processes of sensitised emission .....	16
1.4.1.3 Mechanisms of energy transfer .....	17
1.4.1.4 Basic features of europium(III) and terbium(III) spectra .....	17
1.4.2 Ligand design .....	19
1.4.2.1 The choice of ligand .....	19
1.4.2.2 The choice of chromophore .....	20
1.5 Luminescent lanthanide complexes as cellular probes .....	21
1.5.1 Examples of responsive systems .....	21
1.5.1.1 Probes for pH .....	22
1.5.1.2 Probes for endogenous anions .....	23
1.5.1.3 Probes for metal ions .....	25
1.5.1.4 Probes for sub-cellular events .....	26
1.5.2 Examples of cell-permeating systems .....	28
1.5.3 The challenge of an informative, cell-permeating probe .....	31
1.6 Objectives .....	32
1.6.1 Outline .....	33
CHAPTER TWO: SYNTHESIS AND CHARACTERISATION OF A SET OF COMPLEXES	
2.1 Introduction .....	35
2.2 Synthesis .....	36
2.3 Structural analysis .....	38
2.3.1 The method of structural analysis .....	39
2.3.2 Emission spectroscopy .....	41
2.3.3 Circularly polarised luminescence spectroscopy .....	44
2.3.4 <sup>1</sup> H NMR spectroscopy .....	48

2.3.5	Infrared spectroscopy.....	50
2.3.6	Conclusions of the structural analyses.....	52
2.4	Excited state quenching processes .....	55
2.4.1	Quenching by urate, ascorbate and iodide .....	55
2.4.2	Quenching by serum albumin .....	60
2.5	Preliminary studies of cellular behaviour.....	63
2.6	Conclusions.....	66
<b>CHAPTER THREE: SUB-CELLULAR LOCALISATION OF COMPLEXES</b>		
3.1	Introduction.....	67
3.1.1	Mechanisms of sub-cellular trafficking .....	67
3.1.2	Strategies for controlling localisation.....	69
3.1.3	Localisation of lanthanide complexes .....	70
3.2	Overview .....	71
3.2.1	Complexes selected for further study .....	72
3.3	Classification of complexes.....	744
3.3.1	Lysosomally-localising complexes .....	75
3.3.2	Mitochondrially-localising complexes .....	76
3.3.3	Complexes which localise to the mitochondria and lysosomes .....	777
3.3.4	Complexes which localise to the nucleoli.....	79
3.4	Understanding nucleolar localisation .....	80
3.4.1	Evidence for altered behaviour .....	80
3.4.2	Studies of a permeabilised membrane.....	82
3.4.3	Understanding transport across the nuclear membrane.....	84
3.4.4	Conclusions regarding nucleolar localisation .....	86
3.5	Structural factors affecting localisation.....	87
3.5.1	Effect of chromophore.....	87
3.5.2	Effect of pendant arms.....	89
3.5.3	Effect of charge and counterion .....	90
3.5.4	Effect of geometry .....	91
3.5.5	Effect of lanthanide ion.....	92
3.5.6	Deriving structure-localisation relationships .....	92
3.6	Assessing for nuclear localisation.....	93
3.6.1	DNA quenching studies.....	93
3.6.2	Nuclear extraction experiments.....	95
3.6.3	Further experiments.....	96
3.7	Understanding trafficking.....	96
3.8	Conclusions .....	99
<b>CHAPTER FOUR: CELLULAR UPTAKE OF COMPLEXES</b>		
4.1	Introduction.....	101
4.1.1	Cellular uptake pathways.....	101
4.1.2	Strategies for cellular delivery .....	105
4.1.3	Uptake of lanthanide complexes .....	105
4.2	Exploring effects of structure on cellular uptake .....	107
4.2.1	Comparing the absolute cellular uptake.....	108
4.2.2	Comparing <i>in cellulo</i> quenching .....	112
4.2.3	Conclusions regarding poorly visible complexes.....	113
4.2.4	General observations of cellular uptake.....	113
4.3	Determining the energy dependence of uptake.....	114
4.3.1	Correlating lipophilicity with uptake.....	114

4.3.2	Preliminary low-temperature experiments .....	116
4.3.3	Further evidence for active transport.....	117
4.4	Refining uptake measurements .....	118
4.4.1	A new method for quantifying uptake.....	118
4.4.2	Testing the uptake method .....	119
4.4.3	Determining the optimum incubation time.....	119
4.5	Determining the mode of endocytosis.....	120
4.5.1	Selection of inhibitors and activators .....	120
4.5.2	Microscopy studies of uptake.....	122
4.5.3	Results of ICP-MS analysis .....	125
4.6	Exploring the macropinocytotic pathway .....	127
4.6.1	Confirmation of macropinocytosis.....	127
4.6.2	Implications of uptake by macropinocytosis .....	128
4.7	Conclusions .....	129
<b>CHAPTER FIVE: SUB-CELLULAR SPECIATION OF COMPLEXES</b>		
5.1	Introduction.....	130
5.2	Sub-cellular speciation .....	131
5.2.1	Enzyme hydrolysis .....	131
5.2.2	Complex dissociation.....	134
5.2.3	Anion binding.....	135
5.2.4	Protein binding .....	137
5.3	Stereoselectivity of protein interactions .....	140
5.3.1	CPL studies in the presence of protein .....	142
5.3.2	Probing the protein binding site .....	147
5.3.3	NMR studies of protein binding.....	152
5.3.4	A unique example of dynamic helicity inversion.....	157
5.4	Conclusions.....	158
<b>CHAPTER SIX: EFFECTS OF COMPLEXES ON CELLULAR HOMEOSTASIS</b>		
6.1	Introduction.....	159
6.2	Cytotoxicity .....	159
6.2.1	Measuring cytotoxicity .....	159
6.2.2	General comments about cytotoxicity .....	162
6.2.3	An alternative method for assessing cytotoxicity .....	163
6.2.4	Understanding cytotoxicity of selected lanthanide complexes.....	164
6.3	Mitochondrial membrane potential.....	168
6.4	Conclusions.....	172
<b>CHAPTER SEVEN: CONCLUSIONS</b>		
7.1	General conclusions .....	174
7.2	Implications for probe design .....	176
7.3	Future work.....	177
7.4	Final remarks .....	178
<b>CHAPTER EIGHT: EXPERIMENTAL METHODS</b>		
8.1.	General experimental .....	180
8.1.1.	Spectroscopy .....	180
8.1.2.	Cellular studies.....	182
8.1.2.1.	Microscopy.....	183
8.1.2.2.	Uptake studies .....	183

---

8.1.2.3.	Cytotoxicity .....	186
8.1.2.4.	Flow cytometric assays .....	188
8.1.2.5	Expression of RFP-tagged proteins .....	190
8.1.2.6	Sub-cellular fractionation .....	190
8.1.3.	Lipophilicity .....	191
8.2.	Syntheses .....	192
REFERENCES	.....	211
APPENDIX ONE – SELECTED COMPLEXES	.....	221
APPENDIX TWO – RELEVANT PUBLICATIONS	.....	223

## ABBREVIATIONS

AAG	$\alpha_1$ -acid glycoprotein
ATP	adenosine triphosphate
BCA	bicinchoninic acid
BSA	bovine serum albumin
CFP	cyan fluorescent protein
CHEF	chelation enhanced fluorescence
CHEQ	chelation enhanced quenching
CHO	a cultured cell line derived from transformed Chinese Hamster Ovary cells
CMXRos	chloromethyl-X-rosamine
COSY	correlation spectroscopy
CPL	circularly polarised luminescence
CPP	cell-penetrating peptide
Ctrl	copper transporter 1
cyclen	1,4,7,10-tetraazacyclododecane
DMEM	Dulbecco's modified Eagle medium
DMSO	dimethylsulfoxide
DNA	deoxyribonucleic acid
DOTA	1,4,7,10-tetraazacyclododecane-N,N',N'',N'''-tetraacetic acid
DTPA	diethylene triamine pentaacetic acid
dpqC	10,11,12,13-tetrahydrodipyrido[3,2-a:2',3'-c]phenazine
FAD	flavin adenine dinucleotide
FBS	foetal bovine serum
FCCP	carbonyl cyanide <i>p</i> -trifluoromethoxyphenyl-hydrazone
FITC	fluorescein isothiocyanate
FRET	Förster resonance energy transfer
GFP	green fluorescent protein
HeLa	a cultured cell line derived from human cervical carcinoma cells
HEPES	4-(2-hydroxyethyl)-1- piperazineethanesulfonic acid
HPLC	high pressure liquid chromatography
HSA	human serum albumin
IC <sub>50</sub>	half-maximal inhibitory concentration
ICP-MS	inductively coupled plasma – mass spectrometry

---

IR	infra-red
ISC	inter-system crossing
LP	long pass
LTG	LysoTracker Green™
MMP	mitochondrial membrane potential
MRI	magnetic resonance imaging
MTG	MitoTracker Green™
MTT	3-(4,5-dimethylthiazol-2-yl)-2,5-diphenyltetrazolium bromide
NADH	reduced nicotinamide adenine dinucleotide
NIH 3T3	a cultured cell line derived from transformed mouse embryonic fibroblast cells
NLS	nuclear localisation sequence
NMR	nuclear magnetic resonance
PBR	peripheral benzodiazepine receptor
PBS	phosphate-buffered saline
PEG	polyethylene glycol
PeT	photoinduced electron transfer
PI	propidium iodide
PLE	pig liver esterase
ppb	parts per billion
ppm	parts per million
PS	phosphatidyl serine
RFP	red fluorescent protein
RNA	ribonucleic acid
rpm	revolutions per minute
QD	quantum dot
SAP	square antiprism
SD	standard deviation
STD	saturation transfer difference
TSAP	twisted square antiprism
v/v	volume / volume
WST-1	4-[3-(4-Iodophenyl)-2-(4-nitrophenyl)-2H-5-tetrazolio]-1,3-benzene disulfonate
YFP	yellow fluorescent protein

# CHAPTER ONE

---

## **INTRODUCTION**

## 1.1 Overview

Much current research focuses on the development of more sophisticated systems to report on sub-cellular conditions. This chapter reviews the various molecular imaging techniques, with particular focus on luminescence imaging. The challenges of optical probe design are discussed, in addition to an overview of the diverse range of luminescent probes which are currently available. Luminescent lanthanide complexes are presented as a class which possess attractive properties for use as cellular probes. Particular attention is given to the current understanding of the interaction of these complexes with biological systems.

## 1.2 Molecular imaging

The study of biological processes in living cells requires techniques which allow for the observation of changes *in cellulo* and in real time. This can be achieved by the use of molecular imaging, which is the *in vivo* characterisation and measurement of processes at the cellular and molecular level.<sup>1, 2</sup> Advances in the field of molecular imaging require simultaneous improvements of imaging technologies and probe design. There are a number of widely-used molecular imaging techniques, which span the electromagnetic spectrum from long wave to X-ray frequencies (Figure 1.1).

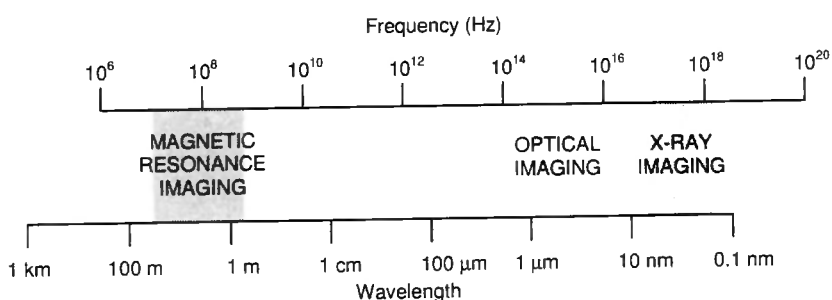


**Figure 1.1:** Imaging techniques according to their position in the electromagnetic spectrum.

The efficacy of a molecular imaging system is measured in terms of its sensitivity and resolution. The sensitivity is the minimum signal that can be distinguished from background noise, and is usually manifested in the minimum concentration required for detection. The terms spatial and temporal resolution refer to the precision of the measurement with respect to location and time, respectively. In addition to high

resolution and sensitivity, effective whole body imaging requires good tissue penetration to allow study of all tissue and organs.

Magnetic resonance imaging (MRI) detects molecules according to their nuclear spin.<sup>3</sup> While the technique allows for good temporal (ms) and spatial ( $\mu\text{m}$ ) resolution, as well as good depth penetration ( $>10\text{ cm}$ ), it is limited by its low sensitivity (mM concentrations).<sup>4, 5</sup> This can be alleviated, in part, by the use of contrast agents. X-ray imaging measures the decay of an administered radioactive isotope. This technique allows for extremely high sensitivity ( $10^{-12}\text{ M}$ ) but at the expense of spatial resolution (5-10 mm).<sup>6</sup> Optical imaging is based on the detection of transmitted light, and allows for very high spatial resolution (sub- $\mu\text{m}$ ) and good sensitivity.<sup>7</sup> It is this imaging system which will be explored in this thesis.

The advantage of optical imaging over other systems lies in its intermediate location on the electromagnetic spectrum, which allows for a maximisation of both sensitivity and resolution. The intermediate wavelengths and energies also require the simplest equipment, which is generally the most cost-efficient. The most basic optical imaging device is the light microscope, enhanced by the development of many new technologies such as flow cytometry and confocal microscopy. Recent technological advances in fibre optics, lasers and computer systems have led to great improvements in optical imaging techniques.<sup>8</sup>

The principal disadvantage of optical imaging results from its poor depth penetration. This is limited to a few mm, but can be as high as 10 cm in the near-infrared spectral region.<sup>9</sup> As a result of this limitation, optical imaging has found greatest utility in tissue culture studies, but has also found valuable clinical applications in retinal angiography, cardiovascular surgery and gastrointestinal endoscopy.<sup>10</sup>

There are a number of different forms of optical imaging. These include diffuse optical tomography in the near infra-red, optical projection tomography – in which a fixed sample is rotated  $360^\circ$  and stepwise images are collected, bioluminescence imaging – utilising a chemiluminescent enzyme-substrate reaction – and luminescence imaging.<sup>4</sup> The latter technique will be discussed here.

### **1.2.1 Luminescence imaging**

Luminescence is the emission of light from an electronically excited state of a substance.<sup>11</sup> It can be divided into two classes, fluorescence and phosphorescence, according to the nature of the excited state. Fluorescence arises from the relaxation of an electron from an excited singlet state to the ground state. This is a rapid, spin-allowed process, and fluorescence lifetimes are therefore very short, typically nanoseconds. Phosphorescence is the emission of light from a triplet excited state. As such transitions are forbidden, phosphorescence lifetimes are of the order of milliseconds to seconds.

Luminescence imaging is an optical imaging technique in which information is derived from the emission output of luminescent molecules within the cell. Some luminescent molecules, such as chlorophyll, reduced nicotinamide adenine dinucleotide (NADH) and oxidised flavin adenine dinucleotide (FAD) are intrinsic, occurring naturally within the cell. The relative lack of naturally occurring fluorescent molecules, however, requires the use of extrinsic luminophores, which are added to the cell in order to derive information about the system. Such species are generally referred to as luminescent probes.

By selecting luminescent probes that are sensitive to their microenvironment, information can be gained about the local chemical environment, such as the pH or ion concentration,<sup>12</sup> and about aspects of the local physical environment including polarity, fluidity and distance.<sup>13</sup> The challenge is therefore to design luminescent probes that can provide useful information about their environment. The next sections outline types of luminescence signalling which may be utilised, and the criteria for luminescence probes. The subsequent section briefly presents existing classes of luminescent cellular probes.

### **1.2.2 Classes of luminescence signalling**

The most rudimentary class of signalling molecules comprises cellular stains. These are luminescent molecules which localise to particular organelles or sub-cellular locations. The luminescent output of these stains can therefore give information about the physical lay-out of the cell.<sup>14</sup> While such stains have found wide commercial use as organelle

markers,<sup>15</sup> their emission is not sensitive to cellular conditions. To better understand biological systems, it is important to use probes which can report on their environment.

In order for a molecule to act as an informative probe, the presence of a species or a biochemical event must be signalled by some form of luminescence change. Such a signal can take one of a number of forms (Figure 1.2). Each signalling behaviour will be discussed below.

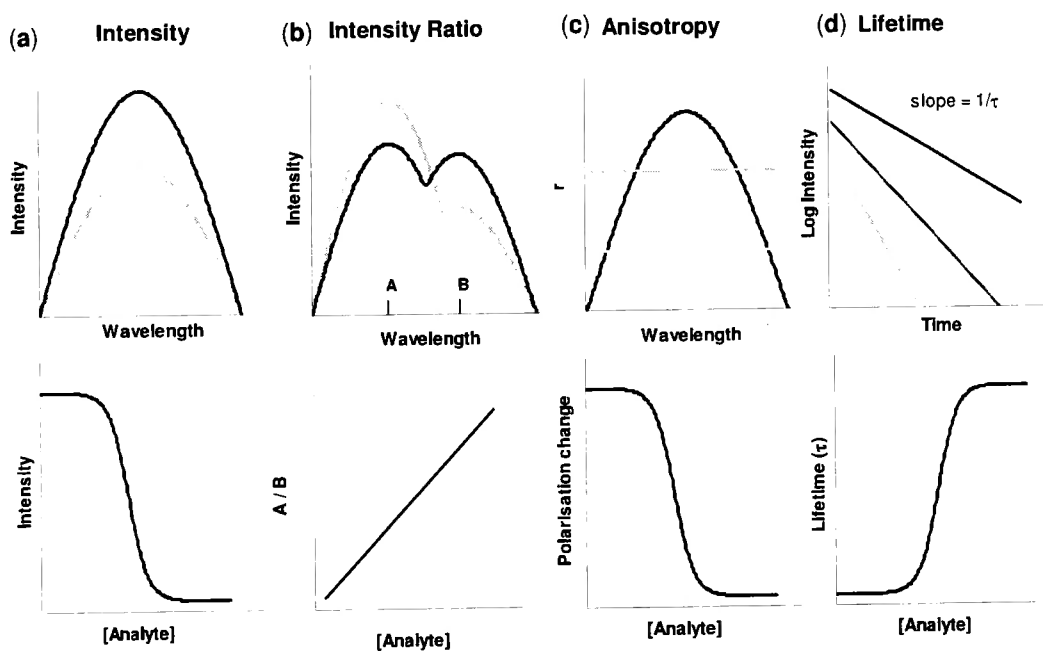


**Figure 1.2:** Types of luminescence signals which can be employed for probing applications: (a) intensity, (b) intensity ratio, (c) anisotropy and (d) lifetime. The lower curve of each pair describes the relationship between the measured signal and the analyte concentration. Adapted from Lakowicz.<sup>16</sup>

The most common mode of luminescence modulation is the increase or decrease in emission intensity on analyte binding (Figure 1.2a). By fitting the emission intensity at known analyte concentrations to a curve, the concentration of unknown solutions can be determined. Changes in emission intensity can be the result of a variety of mechanisms, such as dynamic quenching, the enhancement or inhibition of photoinduced electron transfer (PeT) and changes in the microenvironment, such as the polarity.<sup>17</sup>

The principal drawback of a sensor which relies on the luminescence intensity change at a single wavelength is the heavy dependence of emission intensity on factors such as pH, concentration, light scattering and photobleaching. As a result, much luminescent

probe technology utilises complementary responses at different wavelengths (Figure 1.2b). The ratio of intensities at these two wavelengths ( $A/B$ ) can be calibrated to provide information about the analyte, independent of external factors.<sup>18</sup> Ratiometric information can also be obtained from systems in which ligand binding or dissociation results in excimer formation.<sup>19</sup>

The third luminescence signal which can be utilised is that of luminescence polarisation, or anisotropy (Figure 1.2c). The technique is based on the principle that the anisotropy of a molecule is a function of its tumbling speed, which in turn relies on the molecular size and shape. For a bound probe in equilibrium with its free form, therefore, the anisotropy will be a weighted average of anisotropies of the free and bound forms.<sup>11</sup> A calibration curve can be constructed in which the polarisation change is plotted against analyte concentration. As with the ratiometric method, anisotropy is independent of the concentration of the probe.

The final approach, which is also independent of probe concentration, involves monitoring of the luminescence lifetime (Figure 1.2d). In many cases, interaction with an analyte will result in a change to the lifetime of a luminophore.<sup>20</sup> While this method requires more sophisticated technology, it affords the added advantage of reduced interference from other molecules.

This survey has shown that there is a wide variety of methods by which a probe can signal a biochemical event or the presence of a sub-cellular species. For a cellular probe, it is impractical to determine the concentration of the probe at every sub-cellular location or to derive calibration curves for all possible cellular conditions. Therefore, a luminescence signal which is independent of these factors is desirable. This precludes the use of a simple change in emission intensity, and requires the development of probes which signal analyte binding by changes in luminescence lifetime, anisotropy, or the ratio of emission peaks. It is the latter class of probes which will be primarily explored in this work.



As discussed above, luminescence is an attractive method for probing living cells as it is non-invasive and allows high resolution. The spectroscopic properties of the probe, however, must be optimised to give greatest possible detectability. This requires consideration of a number of factors, and is also influenced by the sensitivity of the detection instrument – usually a microscope. The molar absorption coefficient and luminescence quantum yield must be high enough that the fluorescence output of the probe will be sufficient to allow detection of the target under normal cellular conditions and concentrations, when excited by wavelengths of minimal energy. While absorption coefficients are not usually significantly affected by environment, quantum yields are sensitive to the solvent, and are limited by quenching processes involving cellular species, so it is important to maximise the quantum yield under cellular conditions. To this end, it is desirable to design probes that minimise the quenching by endogenous species, such as protein and DNA.

The properties of the detection instrument must be considered when selecting the excitation wavelength. The absorption maximum of the probe should be closely matched to the available excitation sources, such as lasers. Higher excitation wavelengths are also desirable as they result in less interference from background autofluorescence,<sup>23</sup> decreased photochemical damage to the cell<sup>24</sup> and greater penetration into samples due to less light scattering. In addition, probes with a large Stokes shift allow greater resolution of incident from emitted light (Figure 1.4). Finally, the excited state lifetime of the probe must be matched to its use: for flow cytometry, a short lifetime is desired due to the short timescale of the experiment<sup>25</sup> whereas in microscopy, longer lifetimes allow removal of background autofluorescence by time-gating.<sup>26</sup>

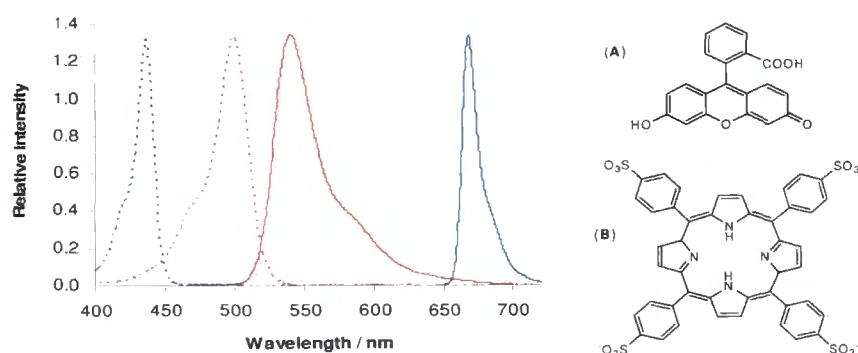


**Figure 1.4:** Excitation (---) and emission (—) spectra demonstrating the small Stokes shift of fluorescein (A; red)<sup>15</sup> compared to that of a porphyrin derivative (B; blue).<sup>27</sup>

The final criterion of a luminescent probe is that interaction with the target must be signalled by a luminescence response, as discussed in Section 1.2.2 above. For organelle stains, this response may take the form of the distribution of luminescence in the cell, but for probes of sub-cellular species and events, a luminescence change following binding is required. Ideally, this change would be independent of probe concentration. An additional luminescence response that can be utilised is Förster resonance energy transfer (FRET), in which emission of one fluorophore is coupled to the excitation of another in a distance-dependent manner.<sup>11</sup>

### 1.2.3.2 Cellular behaviour

The development of cellular probes requires certain key cellular behaviour. It is important, therefore to ensure efficient delivery, targeting to the region of interest, and minimal perturbation of cellular homeostasis.<sup>25, 28</sup> Each will be discussed in turn below.

The principal requirement for a cellular probe is that it is able to enter the cells on which it is to report. Ideally, the probe would be cell-permeating, so that introducing a stock solution to the extracellular medium would result in cellular uptake, by an active or passive mechanism. In some cases, however, it is necessary to induce uptake by bulk loading methods such as electroporation<sup>29</sup> or ATP-induced permeabilisation.<sup>30</sup> Another commonly-used technique is the conversion of the probe to its acetate or acetoxymethyl ester form, which is membrane-permeating. The added group is subsequently hydrolysed *in cellulo* to give the desired probe.<sup>31</sup> In order for probes to have widespread applicability, it is also important that they be readily introduced into a wide variety of tissues and organisms.

In order to use a probe to study the structure and function of a cell, it is necessary to ensure that the probe encounters the molecular species about which it will report. Thus, the probe must have affinity for the relevant target. In addition, a probe that is designed to report on the conditions within a particular region of the cell, such as an organelle, must be trafficked to that region. In some cases, this may be achieved by incorporating a targeting group into the probe or by attaching a transducer protein that carries the probe to a specific location. A wide range of sub-cellular localisations are possible (Figure 1.5).

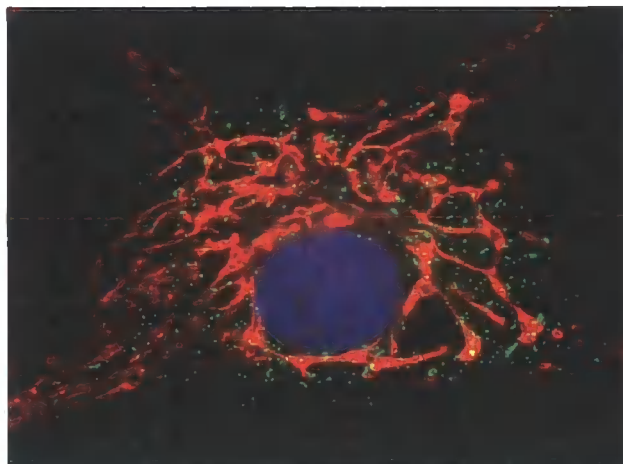


**Figure 1.5:** Multichannel fluorescence image showing localisation of commercially-available dyes. Peroxisomes (green) are labelled with a primary antibody –Alexa Fluor 488 conjugate, mitochondria (red) are labelled with MitoTracker Red CMXRos, and the nucleus (blue) is stained with DAPI.<sup>15</sup>

The impetus for the development of cellular probes is the need for methods to study the structure and function of cells. Probes must therefore report on the cell's physiology without interfering with cellular processes. It is an important design consideration that the probe should not alter the homeostasis of the cell. The primary manifestation of this is that the probe, whether in its natural state, or in its photoactive state, does not have toxic effects on the cell (Figure 1.6). In addition, the probe should not interfere with cellular function and structure. For example, if part of the probe lodged in the cell membrane, it could alter the membrane properties, while a protein-binding probe could inhibit enzyme activity.

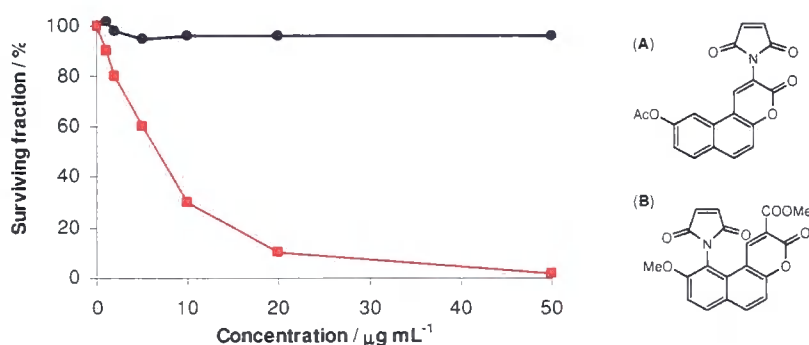


**Figure 1.6:** Cytotoxicity of naphthopyranone-based dyes as a function of dye concentration showing the relative non-toxicity of A (●) compared to the toxicity of B (■).<sup>32</sup>

Many different classes of compound have been developed for use as cellular probes. Each class will be discussed briefly, with particular attention to the criteria outlined above. The subsequent discussion will then focus on the class of luminescent lanthanide complexes, which is the topic of this thesis.

### 1.3 Luminescent cellular probes

#### 1.3.1 Fluorescent organic dyes

The first widely studied fluorescent organic molecule was the natural product quinine. Its visible emission in aqueous solution was reported by Herschel in 1845.<sup>33</sup> Quinine was also one of the first molecules used as a fluorescent probe: during the Second World War, the composition of anti-malarial cocktails was determined by measuring quinine fluorescence.<sup>34</sup> Since that time, the library of fluorescent organic dyes has expanded and developed. There are now a wide range of dyes available, which span the UV-visible spectrum, and offer various chemical and photophysical properties.<sup>35</sup>

While the synthesis of new classes of efficient dyes remains a challenge, the structures of common dyes such as fluorescein can be modified slightly to generate vastly different fluorescence properties.<sup>36, 37</sup> The most common classes of fluorescent dyes are derivatives of fluorescein and rhodamine (Figure 1.7),<sup>15</sup> each of which has a relatively high molar absorption coefficient, excellent fluorescent quantum yield and good water solubility. Each fluorophore can be easily conjugated to other compounds through reactive ester or amine derivatives.

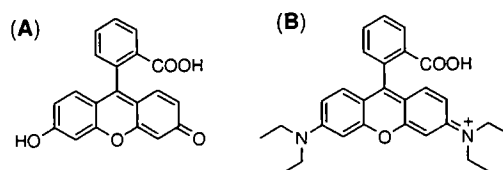


**Figure 1.7:** Common classes of fluorescent dyes are based on (A) fluorescein and (B) rhodamine

Fluorescein- and rhodamine-based dyes are limited by their relatively high rates of photobleaching, pH-dependent fluorescence and broad emission and absorption bands. In response, new generations of fluorescent dyes based on the core structures of BODIPY<sup>®</sup> and Alexa Fluor<sup>®</sup> were developed (Figure 1.8).<sup>15, 38</sup> These dyes are less

susceptible to photobleaching and show negligible fluorescence changes over the range of pH 4-9. They also have advantages of fluorescein and rhodamine in their high molar absorption coefficients and quantum yields. Again, slight modification of the structure gives rise to a change in the fluorescence properties, and dyes are therefore available with excitation and emission at various wavelengths across the visible spectrum.

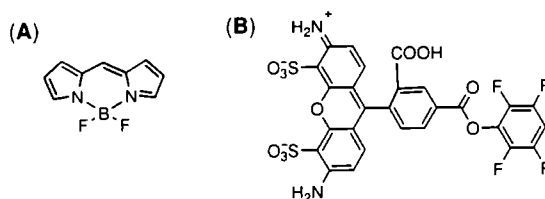


**Figure 1.8:** Examples of improved organic fluorophores: (A) BODIPY and (B) Alexa Fluor 488

Despite their great versatility, the use of organic dyes as luminescent probes is limited by the low signal to noise ratios observed in fluorescence microscopy due to their short emissive lifetimes and the interference from cellular autofluorescence. In addition, the design of organic dyes with large enough Stokes shifts for microscopy applications remains a challenge.<sup>39</sup> The utility of organic dyes is further compromised by the fact that they have broad and featureless emission profiles, so it is difficult to develop ratiometric probes which allow study of the analyte without interference from the environment. As a result of these drawbacks, various alternative classes of luminescent probes have been explored and developed.

### 1.3.2 Fluorescent proteins

The sophisticated recognition capabilities possessed by biological organisms has driven much study towards sensors built from biological components.<sup>40</sup> Chief amongst these are fluorescent proteins, which are biological in nature, but can easily be tailored for specific purposes.

The first fluorescent proteins to be used in cell biology were the phycobiliproteins, which are the pigment proteins involved in photosynthesis in cyanobacteria.<sup>41</sup> The tetrapyrrole bilin fluorophores are held within a rigid framework, minimising deactivation of the excited state, and rendering phycobiliproteins detectable at concentrations as low as  $10^{-15}$  M. A further advantage of this class of proteins is the

emission in the orange-red, thus minimising the interference from auto-fluorescence.<sup>42</sup> Phycobiliproteins have found use in antibody conjugates for surface labelling of cells for flow cytometry. The use of phycobiliproteins is limited, however, by aspects of their uptake. The proteins are very large (200 kDa), and therefore do not readily diffuse into and within the cell. In addition, the proteins cannot be genetically expressed *in situ* as the bilin moieties must be physically inserted into the apoproteins.

The use of fluorescent proteins as cellular probes gained momentum with the discovery<sup>43</sup> and molecular cloning<sup>44</sup> of the green fluorescent protein (GFP). The fluorescent chromophore of GFP is generated by autocatalytic cyclisation and oxidation of three amino acid residues at the centre of the protein. GFP fulfils many of the criteria for fluorescent probes outlined above. It can be readily delivered to its targets, as introduction of the GFP gene into cellular DNA results in synthesis of the protein. Furthermore, as an endogenous species, the protein does not affect the homeostasis of the cell. However, the great attractiveness of GFP lies in its adaptability. The protein can be engineered to vary the emission wavelengths, generating variants such as cyan fluorescent protein (CFP) and yellow fluorescent protein (YFP).<sup>45</sup> Furthermore, GFP can be used to study the cellular localisation of other proteins; the GFP gene can be fused to the gene of interest, giving rise to a fluorescent fusion protein. The principal limitations of GFP and other related fluorescent proteins lie in their fluorescence properties. The Stokes shifts in these proteins are relatively small,<sup>46</sup> and the fluorescence spectra are broad and formless. As a result, it is not possible to elicit information from the emission profiles. While GFP and its variants have proved to be an invaluable contribution to the library of fluorescent probes, their utility lies primarily in the spatial and temporal study of proteins. They are unable to provide information about other endogenous molecules, or about biochemical events within the cell.

### 1.3.3 Quantum dots

The development of the third class of luminescent probes, quantum dots, arose from Louis Brus' observations that the conductivity of liquids changed with the particle size of materials.<sup>47</sup> Brus and his co-workers developed this concept into nanocrystals, which he named "quantum dots", whose emission wavelength depends on size.<sup>48</sup>

Quantum dots are fluorescent semiconducting nanocrystals of diameters 2-8 nm, generally containing elements from groups II and VI or from groups III and V. For *in cellulo* applications, they are surrounded by an amphiphilic polymer coating to ensure cell uptake, and ligands can be attached to this coating for interaction with cellular species. Principal among their advantages are the size- and composition-tunable emission throughout visible and infrared wavelengths, large absorption coefficients and high brightness and photostability.<sup>49</sup> Quantum dots can also be employed in combinatorial optical coding, in which particles of different colours and intensities are combined to encode an array of genes, proteins or small-molecule compounds.<sup>50, 51</sup> Quantum dots have been widely used as replacements for fluorescent proteins, for the labeling of cellular proteins.<sup>52</sup> A challenge in the use of quantum dots is in the intracellular delivery of these relatively large particles. An additional limitation is that they are unresponsive to their local environment, and can therefore only act as fluorescent tags.

#### 1.3.4 Transition metal complexes

In parallel to the development of quantum dots, luminescent transition metal complexes have arisen in the past twenty years as another alternative to small organic dyes and fluorescent proteins.<sup>53</sup> These complexes are primarily based on the  $d^6$  and  $d^8$  metal ions of the platinum group elements including Ru(II), Os(II), Re(I), Rh(III), Ir(III), Pt(II) and Co(III). The use of organic ligands which are generally highly conjugated gives rise to intense metal-to-ligand and ligand-to-metal charge transfer transitions which are symmetry allowed.<sup>54</sup>

The advantages of such complexes are their long luminescence lifetimes ( $10^{-7}$  to  $10^{-4}$  s) that can allow for time-gating to reduce background noise, their relatively high luminescence quantum yields, intense visible absorptions and high thermal, chemical and photochemical stability.<sup>55</sup> The photophysical and selectivity properties of transition metal complexes can also be modified by simple changes to the ligand structure. One recent example of a transition metal complex with potential use as a luminescent probe is the phenanthridine-containing RuEth (Figure 1.9A), which binds to RNA.<sup>56</sup> Preliminary fluorescence microscopy images were interpreted as demonstrating greatest luminescence in RNA-rich regions of the cell, but co-localisation studies would be

required to confirm this. Recent studies of Pt(II) complexes containing dipyriddy benzene derivatives have also demonstrated promising photophysical and cellular behaviour, with great potential for tuning properties for use in two-photon excitation microscopy (Figure 1.9B).<sup>57</sup>

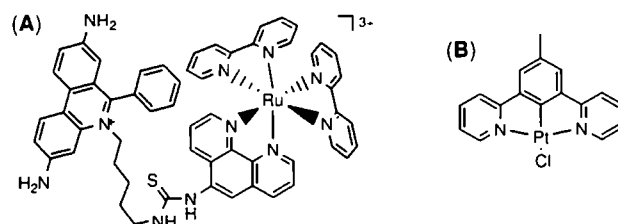


**Figure 1.9:** Examples of transition metal complexes with potential use as luminescent probes (A)  $[\text{RuEth}]^{3+}$  and (B)  $\text{PtLCI}$

### 1.3.5 Luminescent lanthanides

In addition to complexes of the platinum group transition metals, other luminescent metal complexes have been investigated for use as luminescent cellular probes. Amongst these are the luminescent lanthanide complexes. The appropriate lanthanide can be selected to span a wide range of emission wavelengths, and the ligands are chosen to allow water solubility and high luminescence quantum yields. Luminescent lanthanide complexes have long emissive lifetimes, allowing the use of time-gated detection methods. A discussion of the properties of these complexes follows.

## 1.4 Luminescent lanthanide complexes

The term lanthanide is used to refer to the fourteen elements from cerium to lutetium which contain a partially-filled 4f orbital.<sup>58</sup> For all lanthanides, the +3 state is the most stable in solution, with the only other observed forms being  $\text{Ce}^{4+}$ ,  $\text{Eu}^{2+}$ ,  $\text{Yb}^{2+}$  and  $\text{Sm}^{2+}$ , of which the divalent ions are rapidly oxidised in aqueous media.<sup>59</sup>

### 1.4.1 Photophysical properties

In order to account for the emission and absorption spectra of the lanthanide(III) ions, the ions can be considered to consist of energy levels described by the Russell Saunders coupling scheme, a model which can be applied in this case of strong coupling, although

is normally considered most appropriate for weak spin-orbit coupling.<sup>60</sup> Neighbouring terms are typically separated by an energy gap of 5,000 to 10,000  $\text{cm}^{-1}$ , with the  $J$  levels of each term being separated by a further 1,000  $\text{cm}^{-1}$ .

The  $f-f$  transitions of the lanthanide(III) ions have a number of important characteristics. The small ligand-field splitting (of approximately 100  $\text{cm}^{-1}$ ) gives rise to spectra which are largely independent of coordination environment. Just as  $d-d$  transitions are Laporte forbidden, so are  $f-f$  transitions, but they experience less perturbation by ligands, so experience a reduced ligand field. The  $f-f$  transitions become only partially allowed by weak coupling with asymmetric ligand vibrations, resulting in very low extinction coefficients (less than 1  $\text{M}^{-1} \text{cm}^{-1}$ ).<sup>61</sup>

In order for a lanthanide ion to be utilised in a luminescent probe, it must have certain photophysical characteristics. Most importantly, there must be a sufficient energy gap between the ground and first excited states, to ensure that energy will be emitted as luminescence rather than being lost by non-radiative processes.<sup>62</sup> To this end, the lanthanide ions which lie in the centre of the series –  $\text{Eu}^{3+}$ ,  $\text{Gd}^{3+}$  and  $\text{Tb}^{3+}$ , with energy gaps of 12300 ( $^5\text{D}_0 \rightarrow ^7\text{F}_6$ ), 32200 ( $^6\text{P}_{7/2} \rightarrow ^8\text{S}_{7/2}$ ) and 14800 ( $^5\text{D}_4 \rightarrow ^7\text{F}_0$ )  $\text{cm}^{-1}$  respectively, are the most useful. While  $\text{Eu}^{3+}$  and  $\text{Tb}^{3+}$  emit in the visible region of the spectrum,  $\text{Gd}^{3+}$  emission is in the ultraviolet, rendering it unsuitable for use in luminescent probes for biological applications. Subsequent discussion will therefore focus on the use of  $\text{Eu}^{3+}$  and  $\text{Tb}^{3+}$  complexes as luminescent probes.

#### 1.4.1.1 The need for sensitised emission

As a result of the low molar absorption coefficients of the lanthanide ions, the excited energy states will not be efficiently populated by optical irradiation. It is therefore necessary to adopt alternative approaches to populate these states and ensure higher efficiency of fluorescence emission. One possible means of excitation is by the use of high intensity lasers to ensure sufficient population of the excited state, but such a method is not practical for the study of biological systems. Alternatively, efficient excitation can be achieved by sensitisation of the metal ion, in which a sensitizer (usually an organic chromophore) is attached to a lanthanide ion-containing system (Figure 1.10).<sup>62</sup>

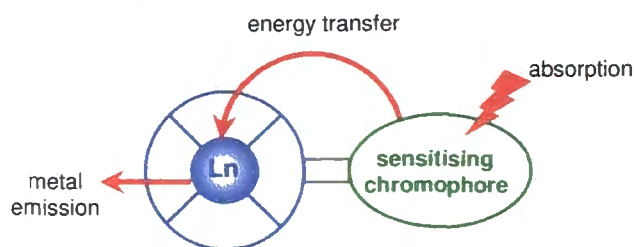


**Figure 1.10:** Schematic diagram showing the energy transfer from the chromophore to the metal ion in a sensitised lanthanide complex

### 1.4.1.2 Energy processes of sensitised emission

The lanthanide excited state is reached after energy transfer from the triplet energy of a sensitising chromophore (Figure 1.11). The sensitizer is first excited to a vibrationally excited level of the  $S_1$  (or  $S_n$ ) band by absorption of a photon. This excited state then relaxes, either by non-radiative vibrational relaxation followed by fluorescence, or by intersystem crossing to the triplet,  $T_1$  manifold. There are then three possible pathways from the  $T_1$  state: back-intersystem crossing to  $S_1$ , phosphorescence, or energy transfer to the lanthanide excited state.<sup>63</sup>

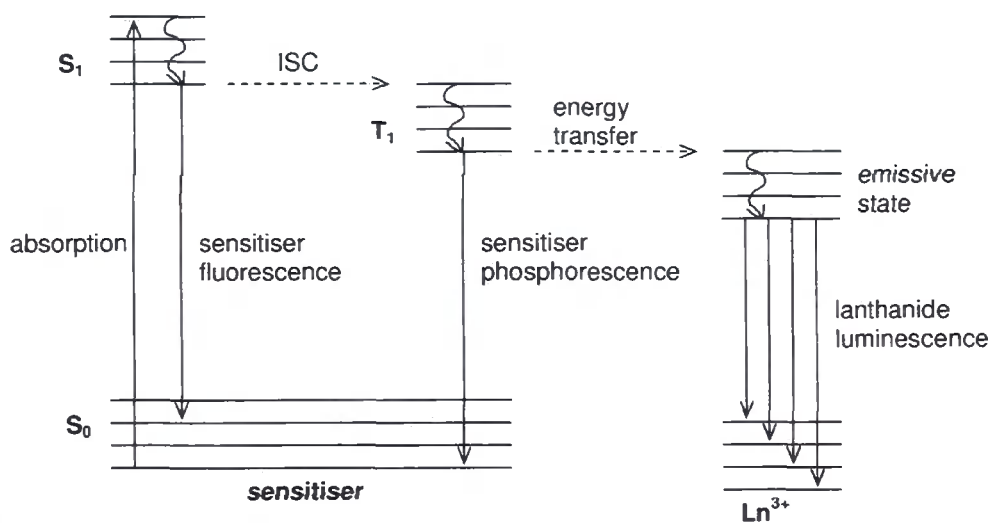


**Figure 1.11:** Jablonski diagram showing the energy processes by which a lanthanide ion is indirectly excited *via* an organic chromophore.

For a system in which the chromophore has a high molar absorption coefficient and efficient intersystem crossing and energy transfer processes, the effective molar absorption coefficient of the metal will be greatly enhanced, allowing for significant

emission following excitation by conventional light sources. For the case of sensitised lanthanide emission, the luminescence quantum yield is defined as the ratio of the number of photons emitted through lanthanide luminescence to the number absorbed by the sample. This value is the product of the efficiencies of each of the individual energy transfer steps involved in reaching the lanthanide emissive state.

#### 1.4.1.3 Mechanisms of energy transfer

Electronic energy transfer may occur either radiatively or non-radiatively. Radiative energy transfer, in which donor-emitted energy is absorbed by the acceptor, is favoured for systems in which donor and acceptor energy levels overlap well, and the emission properties of the donor and absorption by the acceptor are maximised. Despite the good overlap between chromophore and metal energies for sensitised lanthanide emission, radiative energy transfer is unlikely because of the low molar absorption coefficient of Ln(III). Energy transfer therefore occurs by a non-radiative mechanism.<sup>63</sup>

The electronic energy transfer from the sensitiser to the lanthanide (III) can be described by one of three mechanisms of non-radiative electronic energy transfer; the Dexter (exchange) mechanism, Förster (dipole-dipole) or a redox electron exchange mechanism. The Dexter mechanism involves electron exchange between the sensitiser and metal species, with conservation of multiplicity.<sup>64</sup> Such a mechanism requires overlap of the electronic orbitals of the donor and acceptor species. The Förster mechanism involves through-space interactions between the electronic dipole moments of the triplet state of the sensitiser and the 4f orbitals of the lanthanide.<sup>65</sup> In the electron exchange mechanism, the lanthanide ion takes an electron from the excited sensitiser. This electron is then passed back from the Ln(II) ion to the sensitiser, resulting in Ln(III) in its excited state.<sup>66</sup>

#### 1.4.1.4 Basic features of europium(III) and terbium(III) spectra

Much information can be gained from analysis of the well-defined bands that comprise the emission spectra of lanthanide ions. Analysis of the fine structure of these bands and the ratios of intensities, particularly from the emission spectrum of Eu(III) complexes, provides valuable information about the coordination sphere of the lanthanide.

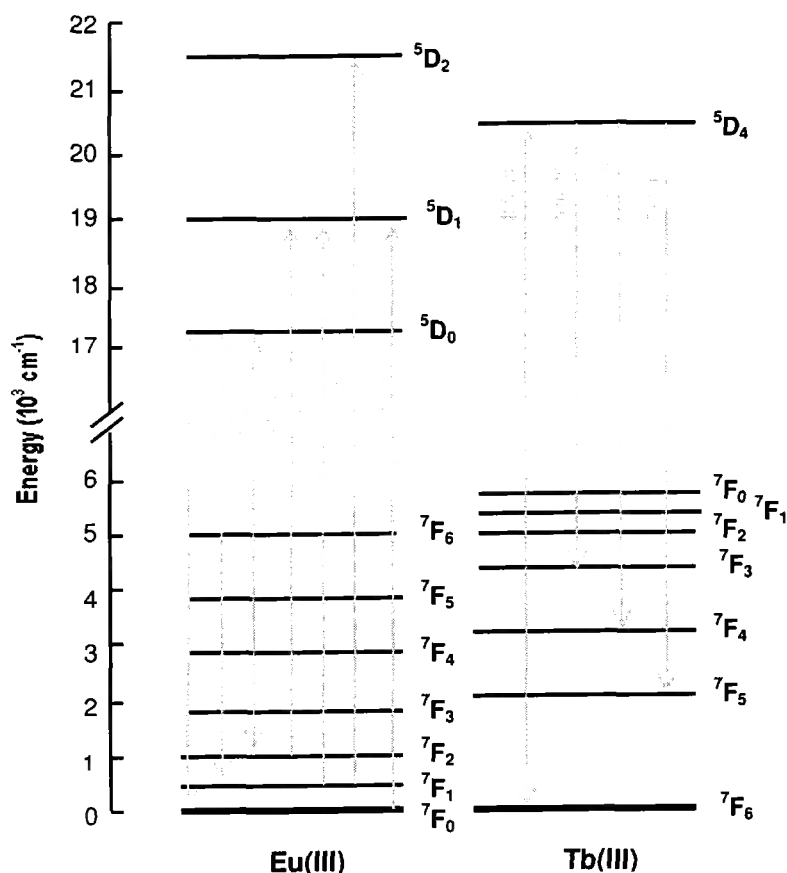


**Figure 1.12:** Partial energy diagrams of Eu(III) and Tb(III)

Examination of the partial energy level diagrams of the ions (Figure 1.12) allows for a correlation with the bands of the emission spectra. The emissive state of Eu(III) complexes is  $^5D_0$ . The two strongest emissions arise from the  $^5D_0 \rightarrow ^7F_1$  ( $\Delta J = 1$ ) transition at 590 nm and the  $^5D_0 \rightarrow ^7F_2$  ( $\Delta J = 2$ ) transition at 612 nm. While the  $\Delta J = 1$  band is magnetic dipole in character and largely independent of the coordination sphere, the  $\Delta J = 2$  band represents an electric-dipole allowed transition and is therefore extremely sensitive to the nature and symmetry of the coordination sphere. The  $\Delta J = 4$  ( $^5D_0 \rightarrow ^7F_4$ ) transition is also relatively intense and sensitive to the ligand field, possessing predominantly electric dipole character.<sup>61</sup>

For Tb(III), emission arises from the  $^5D_4$  level. The  $^5D_4 \rightarrow ^7F_5$  ( $\Delta J = 1$ ) emission band, at 545 nm, is the most intense and sensitive to the ion environment, but less so than the  $\Delta J = 2$  band of  $\text{Eu}^{3+}$ . Since the bands can rarely be fully resolved into component electronic transitions, analysis of  $\text{Tb}^{3+}$  spectra is less informative about the coordination environment of the ion.

## 1.4.2 Ligand design

In designing luminescent lanthanide complexes, it is important to consider factors that will best maximise the stability and photophysical behaviour of the complex. In addition to the selection of lanthanide, as discussed in Section 1.4.1 above, it is important to carefully consider the choice of macrocycle and chromophore.

### 1.4.2.1 The choice of ligand

Selection of an appropriate ligand for a luminescent lanthanide complex requires careful consideration of the coordination chemistry of the lanthanides. Coordination numbers of 7, 8 or 9 are most commonly-observed for lanthanide complexes.<sup>58</sup> The lanthanides are also typically hard Lewis acids, and therefore generally form complexes containing N- and O-donor ligands.<sup>59</sup>

In order to prevent displacement of the lanthanide ion by competing biological molecules, the lanthanide-ligand complex must exhibit high kinetic and thermodynamic stability with respect to metal loss. Many of the early studies of suitable ligands for lanthanide complexes arose from the investigation of gadolinium complexes for use as contrast agents, in which there is a similar need for high stability.<sup>67</sup>

A number of different ligand systems, both linear and macrocyclic, have demonstrated utility for luminescent lanthanide complexes. These include linear polyamino carboxylates such as DTPA (Figure 1.13A)<sup>67</sup> and their macrocyclic analogues, derivatives of DOTA (Figure 1.13B).<sup>68</sup> The latter, cyclen-based ligands, with their very high stabilities (logK values of 23-25) have found widespread use in numerous classes of lanthanide complexes.<sup>62</sup> Other ligand systems include calixarenes (Figure 1.13C)<sup>69</sup> and Schiff-based ligands, formed from the self-condensation of formyl and amine precursors (Figure 1.13D).

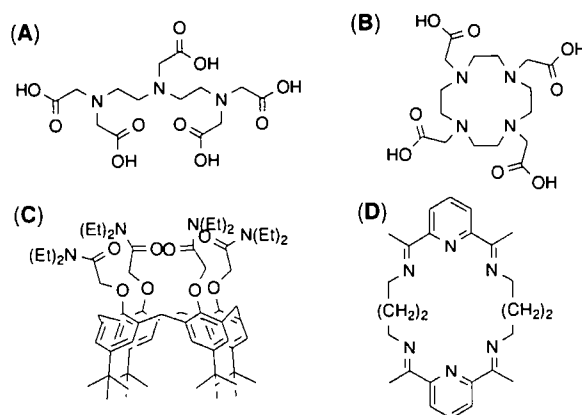


**Figure 1.13:** Examples of suitable ligand systems for luminescent lanthanide complexes.

(A) diethylene triamine pentaacetic acid (DTPA), (B) 1,4,7,10-tetraazacyclododecane-1,4,7,10-tetraacetic acid (DOTA), (C) *p*-tert-butyl calyx[4]arene tetraacetamide and (D) condensation product of 2,6-diacetylpyridine and 1,4-diaminobutane.

### 1.4.2.2 The choice of chromophore

The requirement for a sensitising chromophore is a high molar absorption coefficient at an appropriate excitation wavelength. For single photon microscopy, such excitation should be in the range 337 – 420 nm; higher energy excitation could cause radiation damage to cells, whereas lower energy excitation does not allow intramolecular energy transfer to occur. In order for effective activation of the lanthanide excited state, the chromophore should have a triplet energy which is at least  $1500\text{ cm}^{-1}$  higher than the emissive state of the lanthanide ( $17,240\text{ cm}^{-1}$  and  $20,400\text{ cm}^{-1}$  for Eu and Tb respectively). A smaller energy difference can lead to decreased lifetime and emission intensity due to thermally-accessible back energy transfer, in which energy transfer occurs to the triplet state of the sensitiser.<sup>61</sup>

Selection of a chromophore must take into consideration the efficacy of energy transfer to the lanthanide ion. For efficient transfer, the triplet state of the chromophore should be readily populated; that is, the rate of intersystem crossing must be more rapid than the rates of the fluorescence and non-radiative decay processes. Finally, the quantum efficiency of energy transfer will be maximised when the sensitiser-lanthanide distance is minimised. This can be achieved through direct coordination of the chromophore to the metal centre. Recent work has centred on *m*-terphenyls,<sup>70</sup> phenanthrolines,<sup>71</sup> tetraazatriphenylenes,<sup>72, 73</sup> azaxanthenes and azathioxanthenes (Figure 1.14).<sup>74, 75</sup>

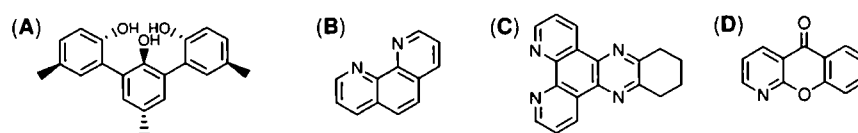


**Figure 1.14:** Examples of suitable chromophores for luminescent lanthanide complexes.

(A) *m*-terphenyl (B) phenanthroline, (C) 10,11,12,13-tetrahydrodipyrido[3,2-*a*:2',3'-*c*]phenazine (dpqc) and (D) azaxanthone

## 1.5 Luminescent lanthanide complexes as cellular probes

The long luminescence lifetime, information-rich emission spectra and large Stokes shifts make luminescent lanthanide complexes ideal candidates for use as cellular probes. As discussed above, the primary requirements for a cellular probe are that it can provide information about its environment and possesses suitable cellular behaviour. Much work in the past has examined one of these two aspects, as will be discussed in the following sections.

### 1.5.1 Examples of responsive systems

A common theme of the study of luminescent lanthanide complexes throughout the world has been the design of systems which can report on their environment. As discussed in Section 1.2.3.1 above, this requires a stable complex which is sensitive to and selective for the analyte, and which exhibits luminescence properties that aid its detectability. A number of promising systems have been developed utilising various detection methods, examples of which are discussed below. This discussion focuses primarily on the detection of species or events which are of cellular relevance, and not on the many systems which have been designed to study other species. In addition, only  $\text{Eu}^{3+}$  and  $\text{Tb}^{3+}$  complexes will be considered, as these are of interest for use as luminescent probes.

### 1.5.1.1 Probes for pH

The detection of pH within a cell is important, as acidic environments have been observed in a number of disease states, including cystic fibrosis<sup>76</sup> and tumour growth.<sup>77</sup> A number of luminescent lanthanide complexes have been developed to probe pH, such as those shown in Figure 1.15.

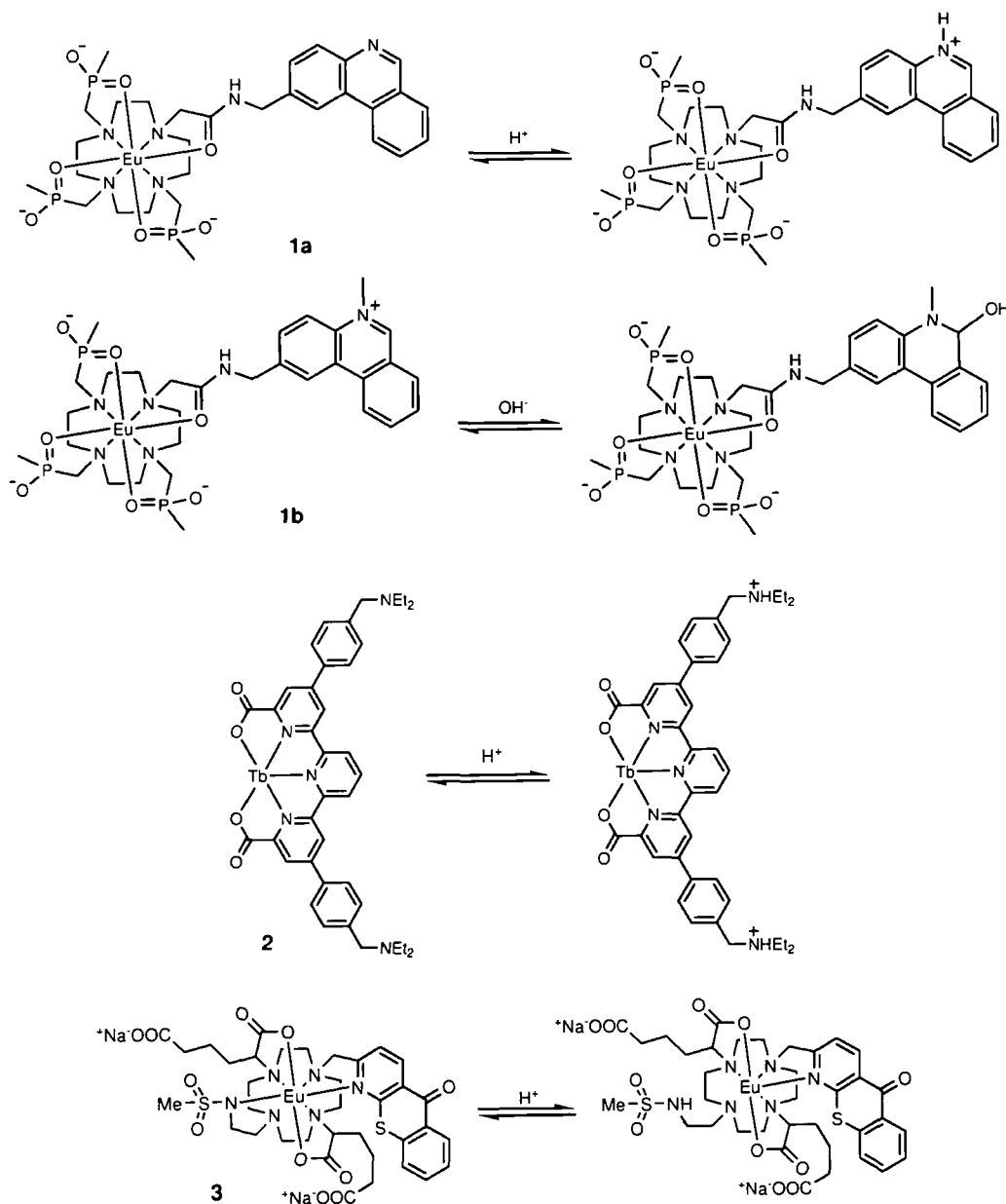


**Figure 1.15:** Examples of luminescent lanthanide systems which report on pH

Complexes **1a** and **1b** contain an unmethylated and methylated phenanthridinium chromophore respectively.<sup>78, 79</sup> Sensitivity of the complexes to pH arises from direct interaction of acid or base with the chromophore, which affects the absorbance

spectrum of the base, and hence the luminescence emission intensity. For complex **1a**, protonation of the phenanthridyl shifts the absorption spectrum of the chromophore to longer wavelengths. Excitation of the complex at these higher wavelengths therefore results in markedly higher europium luminescence for the protonated complex compared to the deprotonated form. The  $pK_a$  of this complex is approximately 4. In a similar manner, hydroxide reacts reversibly with the methylated phenanthridinium in complex **1b**, resulting on loss of the absorption band at 360 nm. Measurement of Eu luminescence upon excitation at 360 nm at varied pH therefore results in a pH titration curve, with a  $pK_a$  of approximately 12. While these complexes exhibit the potential for use as pH sensitive complexes, neither would be directly useful as a cellular probe, as the pH of all biological processes generally lies between 5 and 7 for normal systems, and between 4 and 8 for pathological conditions.<sup>80</sup>

Photoinduced electron transfer (PeT) has been utilised as a mechanism of pH sensing, in the terpyridyl-containing Tb complex, **2**. In the unprotonated form, PeT from the amines to the terpyridyl leads to quenching of the antenna singlet excited state, resulting in poor sensitising of the terbium. Upon protonation of the amines, this quenching pathway is removed, which leads to a 10-16 fold increase in terbium luminescence.<sup>81</sup>

An additional type of pH probe which has been developed, **3**, contains a thioxanthone chromophore and an N-linked methylsulfonamide pendant arm.<sup>82</sup> Protonation of the nitrogen on the methylsulfonamide in acidic pH results in a change in coordination number from 8 to 7, with a resulting change to the form of the Eu spectrum. The ratiometric change of the  $\Delta J=1$  and  $\Delta J=4$  peaks can be calibrated to determine the pH of an unknown solution. The  $pK_a$  for this change is 6.15, and the curve was unchanged in the presence of a mixture of anions. In the presence of protein, a  $pK_a$  value of 7.2 was calculated.

### 1.5.1.2 Probes for endogenous anions

There are numerous endogenous anions whose concentrations must be kept within small windows in order to maintain normal cellular function.<sup>80</sup> As a result, it is important to develop probes to assess the distribution and concentration of these anions *in cellulo*. A number of luminescent lanthanide complexes have been developed to probe the local

concentration of various endogenous anions, some of which are presented below (Figure 1.16).

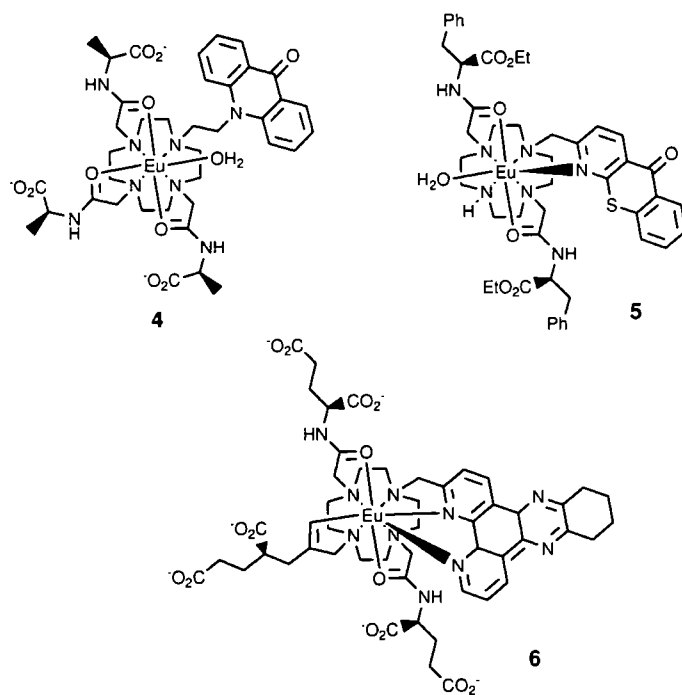


**Figure 1.16:** Examples of luminescent lanthanide systems which report on endogenous anions

Eu acridone complexes such as **4** have found utility as bicarbonate sensors.<sup>83, 84</sup> The complex contains one bound water molecule, but on addition of bicarbonate, the water is displaced and a carbonate chelate formed. This results in a marked change to the Eu emission spectrum, particularly in the  $\Delta J = 2 / \Delta J = 1$  ratio. The complex could be used to determine the bicarbonate concentration in a solution containing other anions such as lactate, citrate and phosphate.

The concept of displacement of a bound water molecule by a chelating anion was also used in the development of a citrate sensor based on a thioxanthone chromophore (**5**).<sup>74</sup> Citrate forms a stable, 1:1 adduct with this complex, with a resulting increase in the  $\Delta J = 2 / \Delta J = 0$ . This behaviour was shown to be independent of pH.

An alternative method of measuring anion concentration is through the measurement of luminescence quenching. One such system is complex **6**, which contains a tetraazatriphenylene chromophore.<sup>85</sup> Lanthanide emission from complexes of this type is quenched by the cellular oxidant urate, most likely by exciplex formation.<sup>86</sup> The Tb complex of **6** is more sensitive to quenching than the Eu analogue, due to its higher

excited energy state. As a result, the ratio of Tb to Eu emission decreases with increasing urate concentration. This enabled the development of a ratiometric assay for the determination of urate concentration in various fluids, including urine and serum.

### 1.5.1.3 Probes for metal ions

Metal ions are essential for a number of biological processes, such as in enzymes and ion channels.<sup>87</sup> Examples of luminescent lanthanide complexes which have been developed to probe for metals in cells are shown in Figure 1.17.

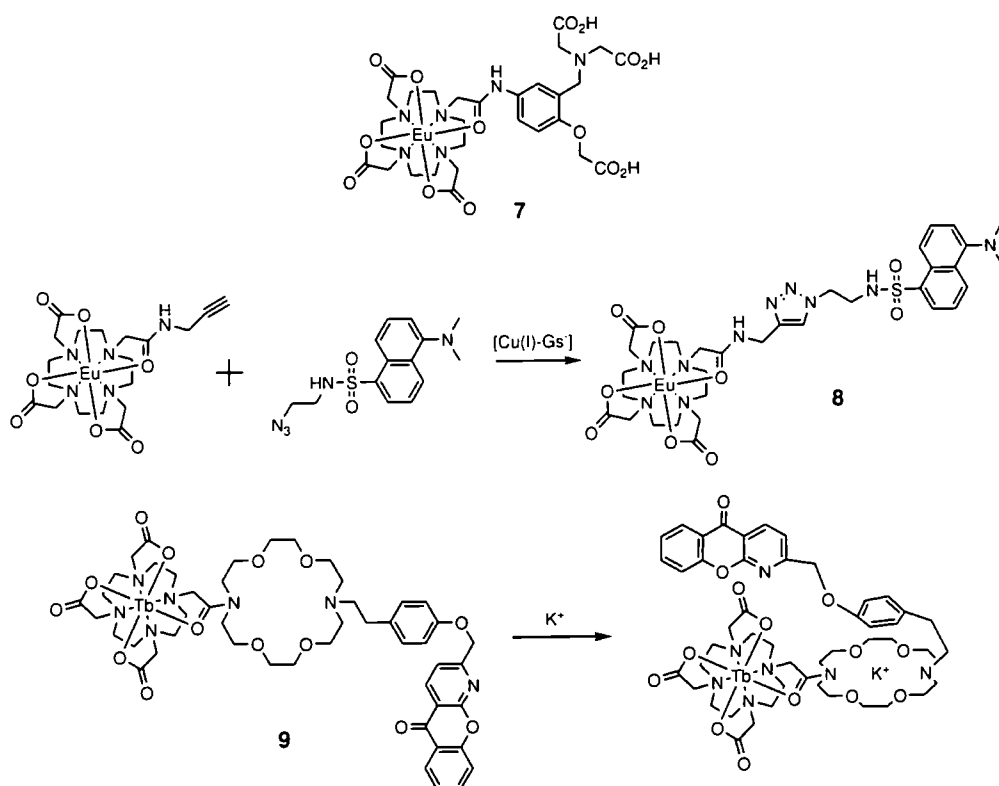


**Figure 1.17:** Examples of luminescent lanthanide systems which report on intracellular metal ions

The incorporation of a substituted aniline in complex **7** gave rise to selectivity for  $\text{Zn}^{2+}$  over  $\text{Mg}^{2+}$  and  $\text{Ca}^{2+}$ .<sup>88, 89</sup> This  $\text{Zn}^{2+}$  binding gave rise to ratiometric changes to the form of both the chromophore and Tb emission spectra which could be used to determine  $\text{Zn}^{2+}$  concentration. The drawbacks of this system are its sensitivity to pH, the moderate (less than 50%) increases in luminescence on  $\text{Zn}^{2+}$  binding and the low excitation wavelengths required (262 nm).

An alternative approach to metal ion sensing involves the use of the metal itself to bring together the lanthanide and the sensitising moiety.<sup>90</sup> The Cu<sup>+</sup>-glutathione complex [Cu<sup>+</sup>-GS<sup>-</sup>], which is the primary intracellular form of Cu<sup>+</sup>, catalyses the reaction of an alkynyl Eu complex with a dansyl azide to produce the sensitised complex **8**. The formation can be monitored by europium emission. This effect is independent of pH for the relevant biological range of 5-8. Although this system is able to report on Cu<sup>+</sup> concentrations, it is unlikely to find use as a cellular probe, as the two components are likely to be endocytosed and compartmentalised in a very different manner; indeed, they may not be in close enough proximity to react within the cell. In addition, it is likely that the azide would react with other cellular species, and could also exert cytotoxic effects on the cell.

Another system in which the metal ion draws together the chromophore and the lanthanide is complex **9**, a K<sup>+</sup> sensor.<sup>91</sup> K<sup>+</sup> ions are complexed in the ether ring, and form cation- $\pi$  interactions with the arene in the chromophore linker. Due to the resulting conformational change, the terbium complex and the azaxanthone chromophore are brought into close enough proximity to facilitate sensitisation, and a concomitant 26-fold increase in Tb luminescence. This system exhibits selectivity for K<sup>+</sup> over Na<sup>+</sup> and other cations, but this selectivity is modest. In addition, the probe is not ratiometric, and intensity changes on binding are strongly pH-dependent.

#### 1.5.1.4 Probes for sub-cellular events

In addition to pH, endogenous anions and metal ions, there are a number of cellular events which can be detected by the use of a cellular probe. For some such events, luminescent lanthanide probes have been developed (Figure 1.18).

The redox environment of the cell is believed to be important in determining the direction of cellular processes.<sup>92</sup> A probe for redox state, **10**, has been developed, containing two cysteine groups.<sup>93</sup> When the probe is in the oxidised form, the formation of an intermolecular disulfide bond brings the chromophore close to the terbium ion, facilitating the energy transfer process. Upon reduction, the peptide adopts a random conformation in which the terbium and the chromophore are spatially separated, resulting in decreased luminescence. The reduction potential of the probe, at -0.243 V, lies near the cytoplasmic potential of many cell lines, giving it great potential use as a

probe for cellular redox environments, however the increase on oxidation is only very modest (3-fold), which may limit its ability to report on *in cellulo* events.

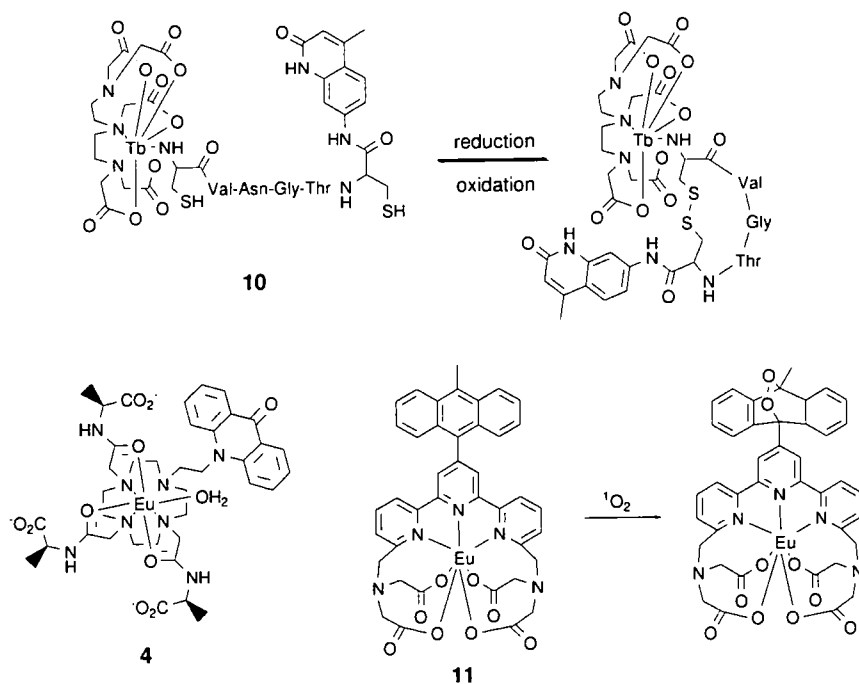


**Figure 1.18:** Examples of luminescent lanthanide systems which report on subcellular events

Many essential biological processes involve phosphorylation and dephosphorylation events. These include the generation of adenosine triphosphate (ATP), and the numerous cellular phosphorylation cascades involved in signal transduction.<sup>94</sup> One method for the detection of phosphorylation events is to use a probe which can signal the presence of a phosphorylated amino acid as distinct from its unphosphorylated form. Complex **4** fulfils this criterion, showing selectivity for phosphotyrosine over tyrosine as well as over other phosphorylated amino acids.<sup>95</sup> Binding of phosphotyrosine gives rise to marked changes in the luminescence emission spectrum due to displacement of the coordinated water molecule. This spectral change was also observed in the presence of short polypeptides containing phosphotyrosine, suggesting the potential of this system to study larger proteins.

The generation of singlet oxygen is an important biochemical process, being implicated in many pathways of cell death, as well as in cell signalling cascades.<sup>96</sup> A lanthanide probe, **11**, has been designed for the detection of singlet oxygen, which is based on a photoinduced electron transfer (PeT) switch.<sup>97</sup> This system comprises a terpyridyl ligand with an attached anthracene group. In its unbound form, the anthracene quenches

the europium luminescence, deactivating the excited state of the terpyridyl moiety by PeT. Singlet oxygen forms an adduct with anthracene, hindering this PeT process, and resulting in increased luminescence. Again, this system is limited in that it is not ratiometric. In addition, the adduct formation is irreversible, such that the emission intensity increases with time as a function of singlet oxygen concentration.

### 1.5.2 Examples of cell-permeating systems

The previous section has described the many and varied complexes which have been designed to report on aspects of the cellular environment. The second criterion for a luminescent lanthanide probe is suitable cellular behaviour; the probe must be cell-permeating, and must be targeted to the particular sub-cellular region of interest. This section outlines examples of cell-permeating lanthanide complexes which have been reported in the literature.

A number of studies have demonstrated the cellular uptake of various luminescent lanthanide complexes (Figure 1.19). Investigations of the triple-stranded [Eu<sub>2</sub>(**12**)<sub>3</sub>] helicate in the human cancer cell line HeLa revealed concentration-dependent luminescence in the cytoplasm, with no loss of cell viability. The emission intensity was greater in cells which were fixed with glutaraldehyde or ice-cold methanol. There was no apparent difference in the emission intensity in cells incubated with the complex at 37 °C and 4 °C, which was interpreted as evidence of an active uptake mechanism.<sup>98</sup> However, active endocytosis is energy-dependent and will be inhibited at low temperatures.<sup>99</sup> It is more likely that these observations signal a passive mechanism of cellular uptake. A later study of related helicates identified greatly reduced uptake at 4 °C, which is consistent with an endocytotic mechanism of cell uptake.<sup>100</sup> In this study, lanthanide uptake was also quantified, allowing for comparison between the behaviour of different complexes. More recently, the subcellular localisation of Eu helicates was investigated by co-localisation studies with commercially available cellular stains.<sup>101</sup> It was concluded that the complexes were localised in the lysosomes, particularly those vesicles which were associated with the endoplasmic reticulum. This localisation was not very well-defined, with the images also indicating a degree of localisation in the Golgi apparatus.

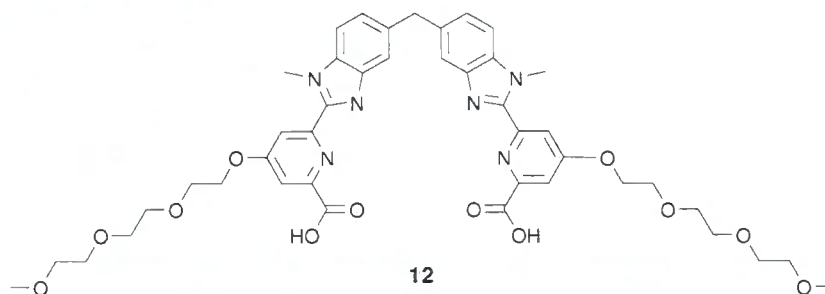


**Figure 1.19:** Ligand employed for formation of bimetallic triple-stranded helicate  $[\text{Eu}_2(\mathbf{12})_3]$

Co-localisation studies have also been utilised for a number of other systems in order to define subcellular localisation profiles (Figure 1.20). The europium complex **13** was demonstrated to localise in the nucleolus of the cell, confirmed by co-staining with the green SYTO RNA-Select stain.<sup>102</sup> This behaviour was observed in a number of cell types and for various dosing concentrations, and luminescence intensity did not appear to change upon incubation at 4 °C.

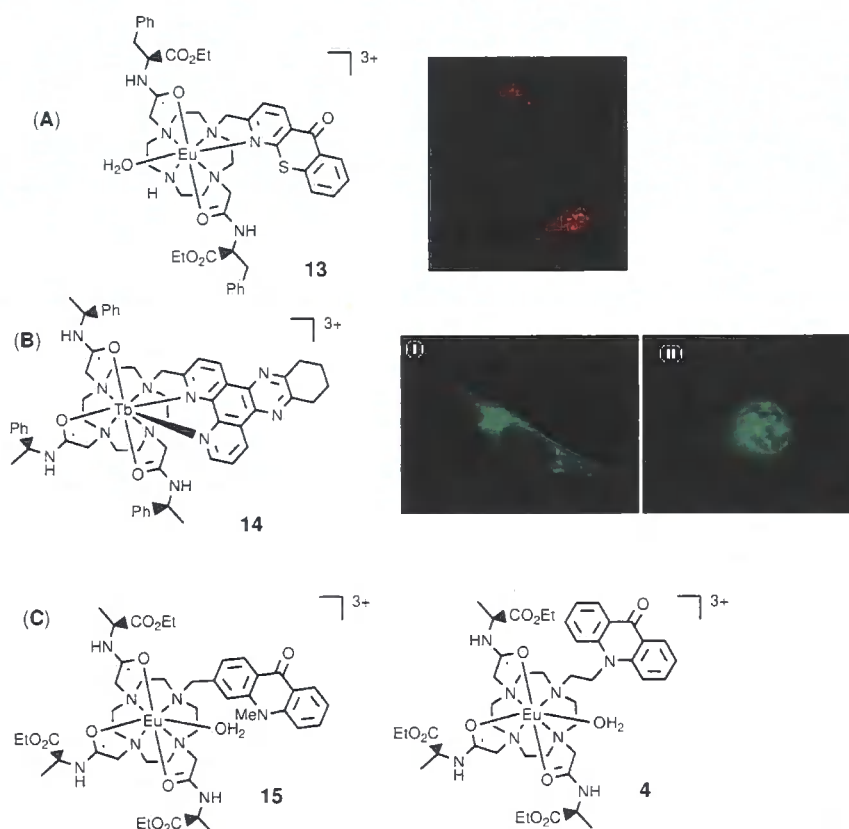


**Figure 1.20:** Cellular localisation profiles of luminescent lanthanide complexes. (A) Luminescence microscope image after incubation of NIH 3T3 cells with **13** (100  $\mu\text{M}$ , 4h);<sup>102</sup> (B) Luminescence microscope images after incubation of NIH 3T3 cells with **14** (i) 0.3 mM, 4h and (ii) 1 mM, 24h;<sup>73</sup> (C) constitutional isomers **15** and **4** which exhibit markedly different cellular localisation.

In contrast, the europium complex **14**, containing the tetraazatriphenylene chromophore, exhibited concentration-dependent localisation. Upon incubation with low concentrations for short periods of time, luminescence was observed in the lysosomes, while dosing at higher concentrations for longer time periods resulted in luminescence in the nucleus, and particularly the nucleolus (Figure 1.20B).<sup>73</sup> A final example of the compartmentalisation of luminescent lanthanide complexes is that of the two constitutionally-isomeric complexes **15** and **4**, which exhibit very different behaviour. While **15** localises to the lysosomes, **4** exhibits a compartmentalisation pattern consistent with the endoplasmic reticulum.<sup>83, 84</sup>

The cellular behaviour of the luminescent lanthanide complexes discussed thus far were neither predicted nor controlled by their structural features. In contrast, a number of studies have been performed in which complexes incorporate moieties designed to influence their cellular behaviour (Figure 1.21). The luminescent europium complex **16** was designed to allow easy conjugation to biological species.<sup>103</sup> Conjugation of the complex to various serum antibodies and the protein streptavidin resulted in sub-cellular localisation, and enabled the probing of a number of antibodies and gene sequences. Another targeted probe is a streptavidin-based macromolecular complex, in which thyroglobulin molecules are used to attach streptavidin to the europium phenanthroline complex **17** to form highly luminescent aggregates, each containing hundreds of  $\text{Eu}^{3+}$  each.<sup>104</sup> Streptavidin has very high affinity for the cofactor biotin, and accordingly the aggregates were observed to localise in regions of the cell with high levels of biotin.

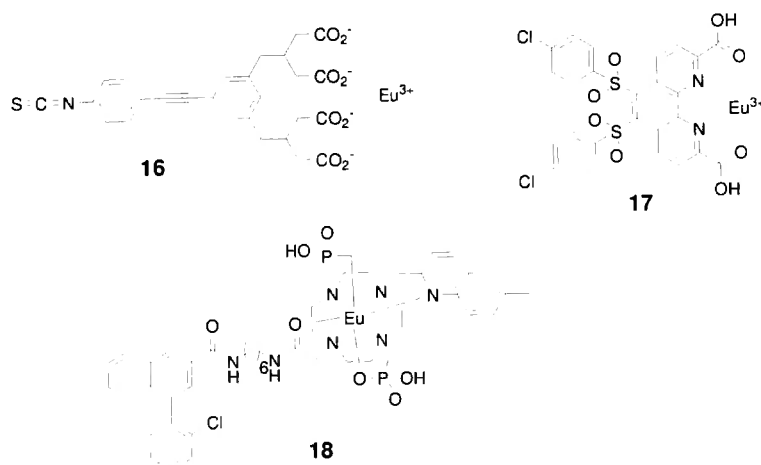


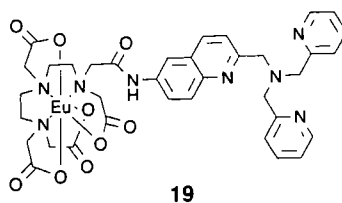
**Figure 1.21:** Examples of luminescent lanthanide complexes which incorporate targeting moieties.

A final example of a targeted luminescent lanthanide probe is **18**, which incorporates a highly specific ligand for the peripheral benzodiazepine receptor (PBR), which is over-expressed in a number of diseases. The luminescence of this complex was readily observed within cells, with increased luminescence from cells which were over-expressing PBR.<sup>105</sup> Preliminary co-localisation studies indicated that the complex was primarily located in the mitochondria, which are the regions of high PBR concentration.

### 1.5.3 The challenge of an informative, cell-permeating probe

Section 1.5.1 demonstrated the great understanding that has been reached into the design and synthesis of responsive luminescent lanthanide systems, which are able to report on specific cellular conditions. However, these studies have all been performed *in vitro*, and in general have not demonstrated *in cellulo* applicability. Cellular studies have been performed on a largely distinct group of luminescent lanthanide complexes, as detailed in Section 1.5.2. These studies revealed the promising cellular behaviour of a number of complexes, and illustrate the issues which must be considered in the design of cellular probes. In particular, most cellular studies identified distinct sub-cellular localisation profiles. It would be useful, then, to combine organelle distribution with probe function to make more informative cellular probes. A pH sensor might therefore be best localised in lysosomes, in which acidity can signify endosome age or health.<sup>106</sup> Similarly, a probe for phosphorylation might be best directed to the mitochondria, where numerous phosphorylation events take place.<sup>80</sup>

However, very few studies have investigated the cellular properties of responsive lanthanide probes. Studies of the  $Zn^{2+}$  sensor **19** in HeLa cells revealed readily-detectable europium luminescence which increased on the addition of  $Zn^{2+}$ , and decreased on treatment with a strong  $Zn^{2+}$  chelator.<sup>107</sup> The complex did not clearly localise within the cell, limiting the utility of the probe as a reporter of the mean intracellular  $Zn^{2+}$  concentration.



There have been cases in which the cellular localisation profiles of responsive probes have been determined. The bicarbonate sensor **4** was found to localise to the endoplasmic reticulum, confirmed by colocalisation with the stain Brefeldin A.<sup>83</sup> This may limit the usefulness of the probe, as there is no evidence that the function of the endoplasmic reticulum is dependent on bicarbonate or related anions. Confocal microscopy studies of cells treated with the pH probe **3** revealed localisation in the nucleolus, as well as more diffuse localisation which was interpreted to correspond to the ribosomes.<sup>82</sup> However, this probe, with an apparent  $pK_a$  of 7.2 in the presence of protein, would have been more useful if it could have been targeted to the lysosomes, or the cytoplasm, for which pH perturbations have greater biological significance.

It is evident, therefore, that greater attention needs to be paid to the combined cellular and responsive behaviour of luminescent lanthanide complexes. Great understanding has been reached as to the design of complexes which are selective and informative about their environment. The challenge remains to harness this understanding in the design and synthesis of complexes which can provide information in a biologically-relevant context. In order to achieve this aim, it is important to understand better the interaction of luminescent lanthanide complexes with biological systems.

## 1.6 Objectives

The aim of the work reported in this thesis is to gain a greater understanding of the cellular behaviour of luminescent lanthanide complexes. This involves the study of the activity of individual complexes, but also the generalisation of trends for larger groups of structurally-related complexes. Importantly, the derivation of structure-activity relationships will allow for the rational design of complexes with desired cellular behaviour.

Research over the past eight years in Durham has yielded a relatively large library of luminescent lanthanide complexes with varying structures and selectivities. As a result, study of the cellular behaviour of this library will allow the determination of general conclusions concerning the structure-activity relationships of luminescent lanthanide probes. This work will therefore focus on complexes which have been synthesised in Durham, in addition to novel complexes reported herein.

Cellular behaviour can be subdivided into a number of important aspects (Figure 1.22). In understanding the interaction of a complex with a cell, it is necessary to consider the mode of cellular uptake and the mechanisms and determinants of sub-cellular localisation. In addition, it is important to establish the cellular fate of the complex, considering factors such as its cellular speciation and protein binding as well as its metabolism and excretion from the cell. Finally, as these complexes are designed as probes of cellular activity, they must cause only minimal perturbation to normal cellular function. It is therefore important to determine the effects of the complexes on the homeostasis of the cell.

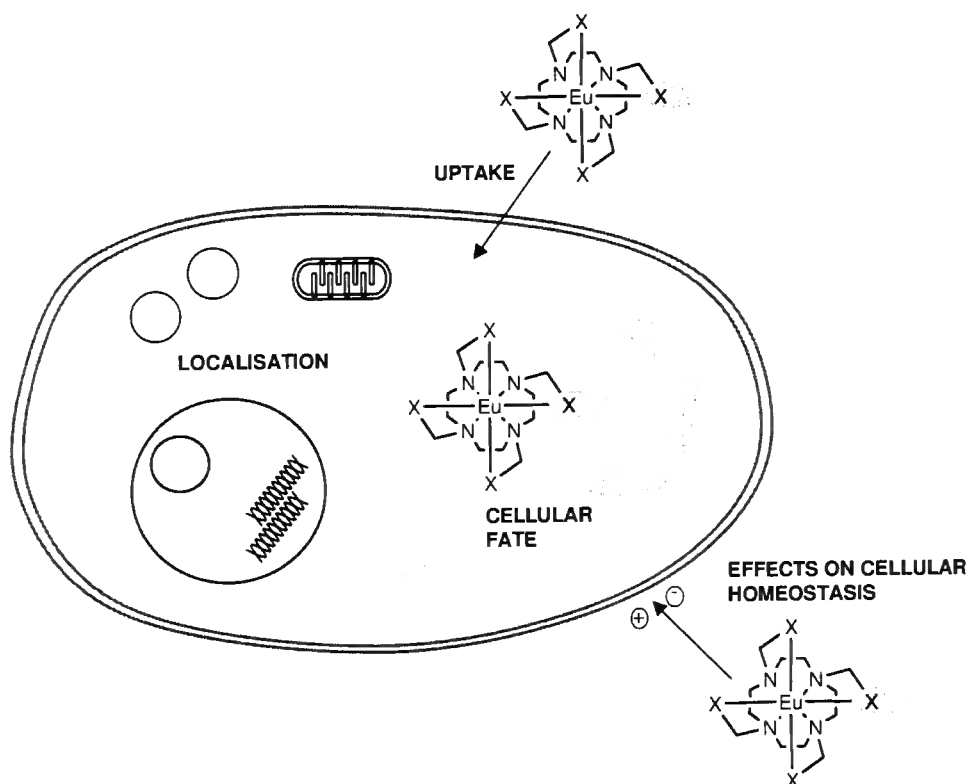


**Figure 1.22:** Important aspects of the cellular behaviour of luminescent lanthanide complexes.

### 1.6.1 Outline

This thesis details the work which has been performed to gain a greater understanding of the cellular behaviour of luminescent lanthanide complexes. Chapter Two describes the synthesis and characterisation of one class of lanthanide complexes, with particular reference to the structure elucidation and studies of cellular behaviour. Chapters Three

to Six in turn explore the four aspects of cellular behaviour outlined in Figure 1.22: Chapter Three describes studies of sub-cellular localisation, Chapter Four details the investigations of cellular uptake, Chapter Five discusses aspects of the cellular fate of luminescent lanthanide complexes, while Chapter Six presents the effects of the complexes on cellular homeostasis.

## CHAPTER TWO

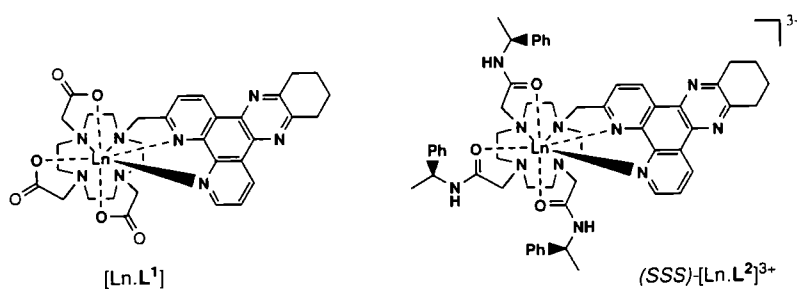
---

# **SYNTHESIS AND CHARACTERISATION OF A SET OF COMPLEXES**

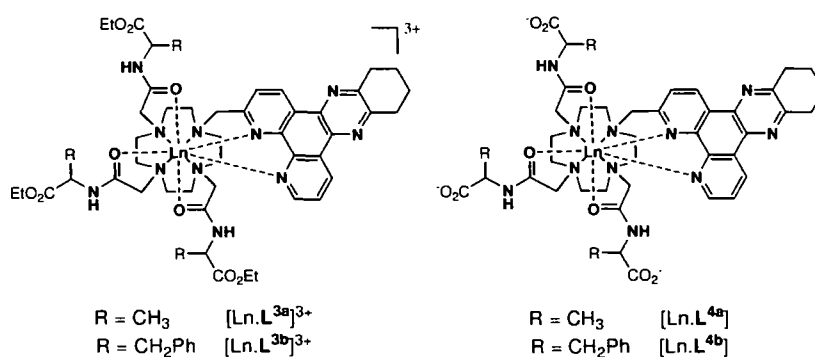
## 2.1 Introduction

In order to study trends in the cellular behaviour of luminescent lanthanide complexes, it is important to establish an understanding of how biological properties relate to probe structure. In striving to establish such structure-activity relationships, it is therefore necessary to study well-defined sub-sets of probes systematically. This chapter details the synthesis, characterisation and subsequent biological studies of a set of related luminescent lanthanide complexes.

The complexes  $[\text{Ln}.\text{L}^1]$  and  $[\text{Ln}.\text{L}^2]^{3+}$ , containing the tetraazatriphenylene chromophore dpqC, have previously been synthesised and described.<sup>73</sup>  $[\text{Ln}.\text{L}^2]^{3+}$  was reported to exhibit readily-detectable luminescence in cell samples, which was localised primarily in the lysosomes. At high concentrations and long dosage times, luminescence was detected in the nucleolus. In contrast, the neutral complex,  $[\text{Ln}.\text{L}^1]$ , was only faintly visible by microscopy.

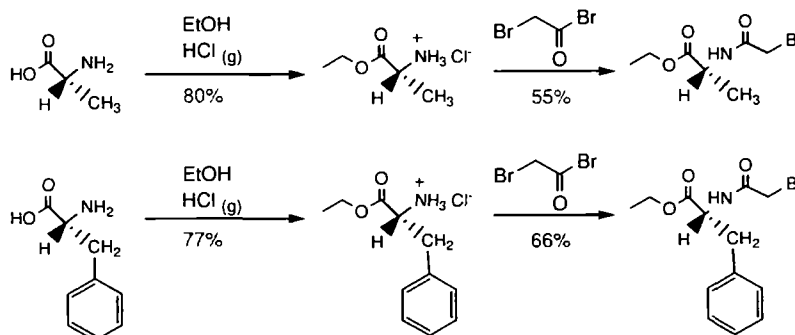


The aim of this section of the work was to synthesise a series of complexes containing the dpqC chromophore, of varying charge and hydrophobicity. This was achieved by substitution of the pendant arms of  $[\text{Ln}.\text{L}^2]^{3+}$  for alanine- and phenylalanine-based arms. Such arms have previously been successfully incorporated into responsive probes.<sup>74, 108</sup> The target complexes were the cationic complexes  $[\text{Ln}.\text{L}^3]^{3+}$ , containing ethyl ester arms, and their neutral analogues  $[\text{Ln}.\text{L}^4]$ , in which the ester has been hydrolysed to the carboxylate form. In order to assess the effects of absolute configuration, both the (*RRR*) and (*SSS*) enantiomers were desired.



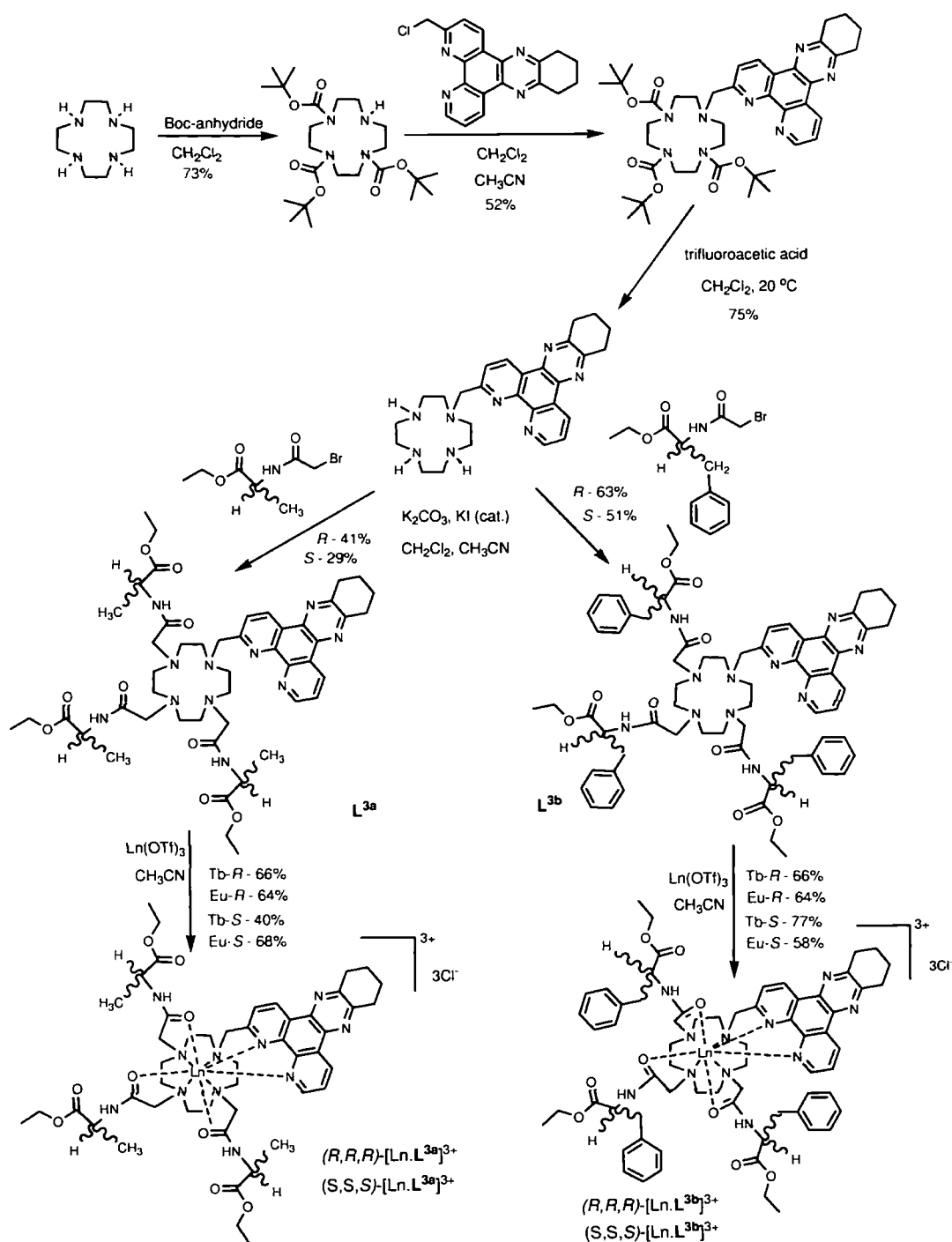
## 2.2 Synthesis

The (*S*)-alanine and (*S*)-phenylalanine haloacetamide precursors were synthesised by Dr Junhua Yu. The corresponding (*R*) compounds was synthesised according to the procedure in Scheme 2.1. Attempts to use chloroacetyl chloride to synthesise the chloramide yielded an oil which proved difficult to purify, and which readily decomposed. The bromamide analogues were therefore prepared for linkage to the cyclen moiety, and were isolated as solids, amenable to recrystallisation.



**Scheme 2.1:** Synthesis of the (*R*)-Ala ester and (*R*)-Phe ester bromamides

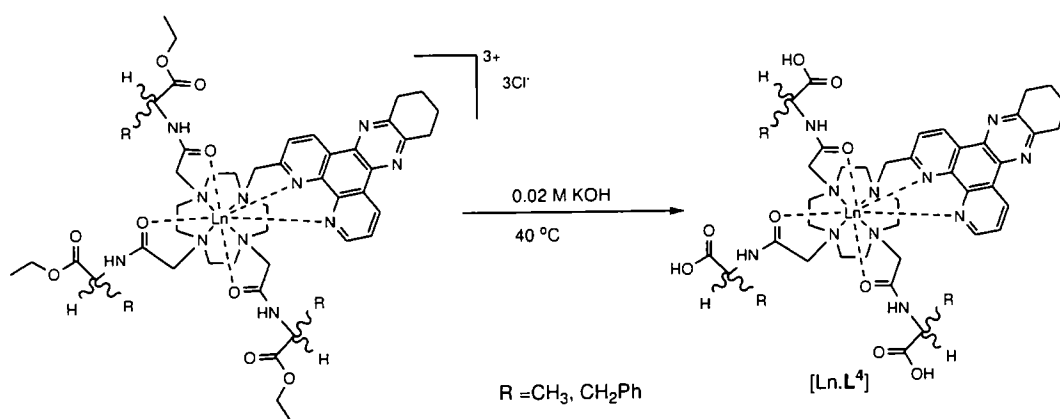
Synthesis of cyclen-dpqc was achieved by Boc-protection of three of the ring nitrogens and subsequent attachment of the dpqc chromophore as a chloromethyl derivative (Scheme 2.2). The Boc groups were removed by using trifluoroacetic acid to yield the macrocycle-chromophore adduct, cyclen-dpqc. The chiral amide arms were introduced under standard conditions (CH<sub>3</sub>CN, K<sub>2</sub>CO<sub>3</sub>) and the ligand purified by column chromatography on neutral alumina. Complexation of the lanthanide (III) salt was undertaken in hot acetonitrile, with the lanthanide added as an anhydrous triflate salt. The triflate anion was subsequently replaced by chloride using anion exchange chromatography to enhance the water solubility of the complex.



Scheme 2.2: Synthesis of lanthanide complexes of  $\text{L}^{3a}$  and  $\text{L}^{3b}$  with Ala and Phe ester arms.

The ester groups in the cationic complexes of  $[\text{Ln}.\text{L}^{3a}]^{3+}$  and  $[\text{Ln}.\text{L}^{3b}]^{3+}$  were hydrolysed to yield the zwitterionic complexes  $[\text{Ln}.\text{L}^{4a}]$  and  $[\text{Ln}.\text{L}^{4b}]$  (Scheme 2.3). Hydrolysis was achieved by treatment with a dilute aqueous KOH solution, ensuring that the pH did not rise above 10 to avoid decomplexation. The progress of hydrolysis was followed by HPLC using a reverse phase column. The column used (Synergi 4 $\mu$  Fusion RP 80Å) has hydrophobic side-chains which aid the separation of relatively hydrophobic species. The hydrolysed complex is more hydrophilic than the parent ester, and hence eluted at shorter retention times. HPLC analyses were performed in the presence of 0.1% formic acid to ensure that the amide-containing complexes did not adhere to the column.

The Tb complexes hydrolysed much more readily than the Eu analogues, requiring only two days at room temperature compared with up to 10 days at 40 °C necessary for hydrolysis of the Eu analogues. For the Eu complexes, it appeared that hydrolysis was in competition with metal decomplexation.



**Scheme 2.3:** Controlled hydrolysis of the ester complexes

## 2.3 Structural analysis

The successful synthesis of complexes  $[\text{Ln}.\text{L}^{3+}]^{3+}$  was confirmed by the use of high resolution mass spectrometry, which revealed accurate masses for the complexes within 1 ppm of the calculated mass. Mass spectrometric analysis of the hydrolysed complexes  $[\text{Ln}.\text{L}^4]$  was less straight-forward, and accurate high resolution mass spectra could not be obtained. In this case, successful hydrolysis was confirmed by monitoring by HPLC. A change in the HPLC retention time could signify hydrolysis or decomplexation; the former was confirmed by observation of the retained sensitised emission of the two samples, through use of the fluorescence channel in HPLC.

### 2.3.1 The method of structural analysis

In order to completely characterise the complexes, it is necessary to determine their absolute configurations. There are a number of possible conformations that complexes may take up, based on a cyclen-based system. The archetypal ligand, 1,4,7,10-tetraazacyclododecanetetraacetic acid (DOTA) will be used as a model for these. In Ln(III) complexes of DOTA there are two elements of chirality to consider (Figure 2.1). The N-C-C-N torsion angle of each five ring chelate within the macrocyclic ring may be  $+60^\circ$  or  $-60^\circ$  ( $\delta$  or  $\lambda$ ), and the N-C-C-O torsion angle of the acetate arms may be  $+30^\circ$  or  $-30^\circ$  ( $\Delta$  or  $\Lambda$ ).<sup>109</sup>

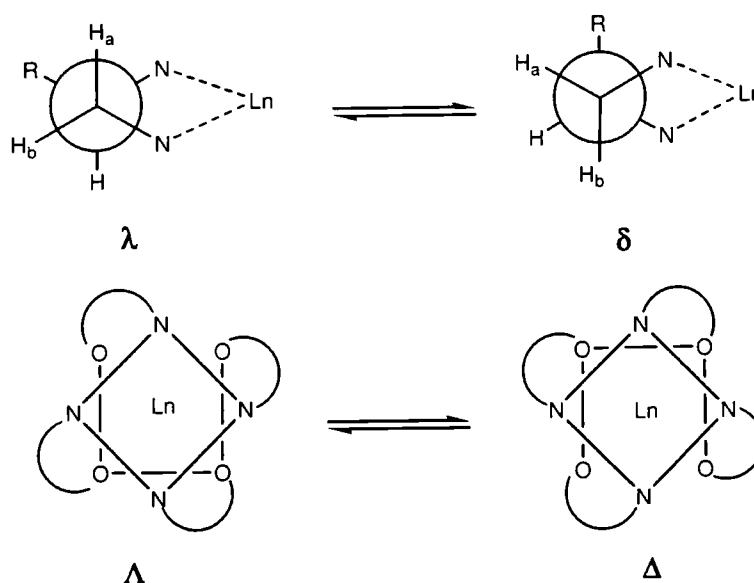


**Figure 2.1:** Conformations of Ln(III) complexes of DOTA showing the limiting orientations of the cyclen ring, and the lay-out of the acetate arms.

These geometries give rise to four stereoisomers that exist as two pairs of enantiomers. The stereoisomers can adopt one of two geometries:  $\Lambda(\delta\delta\delta\delta)$  and  $\Delta(\lambda\lambda\lambda\lambda)$  exhibit a square antiprismatic geometry (SAP) with a twist angle of approximately  $40^\circ$  between the oxygen and nitrogen planes, while  $\Lambda(\lambda\lambda\lambda\lambda)$  and  $\Delta(\delta\delta\delta\delta)$  adopt a twisted square antiprismatic (TSAP) geometry with a twist angle of approximately  $-30^\circ$ . This geometry has been shown to be more favourable for complexes of the larger lanthanides.<sup>110, 111</sup> The four isomers can interconvert in solution by ring inversion or arm rotation (Figure 2.2). Following complexation by Ln(III), the conformation is fixed, since arm rotation is inhibited and the ring inversion process is slow.<sup>112</sup> The Ln(III) complexes of DOTA are 9-coordinate due to the presence of a capping water molecule.<sup>113</sup>

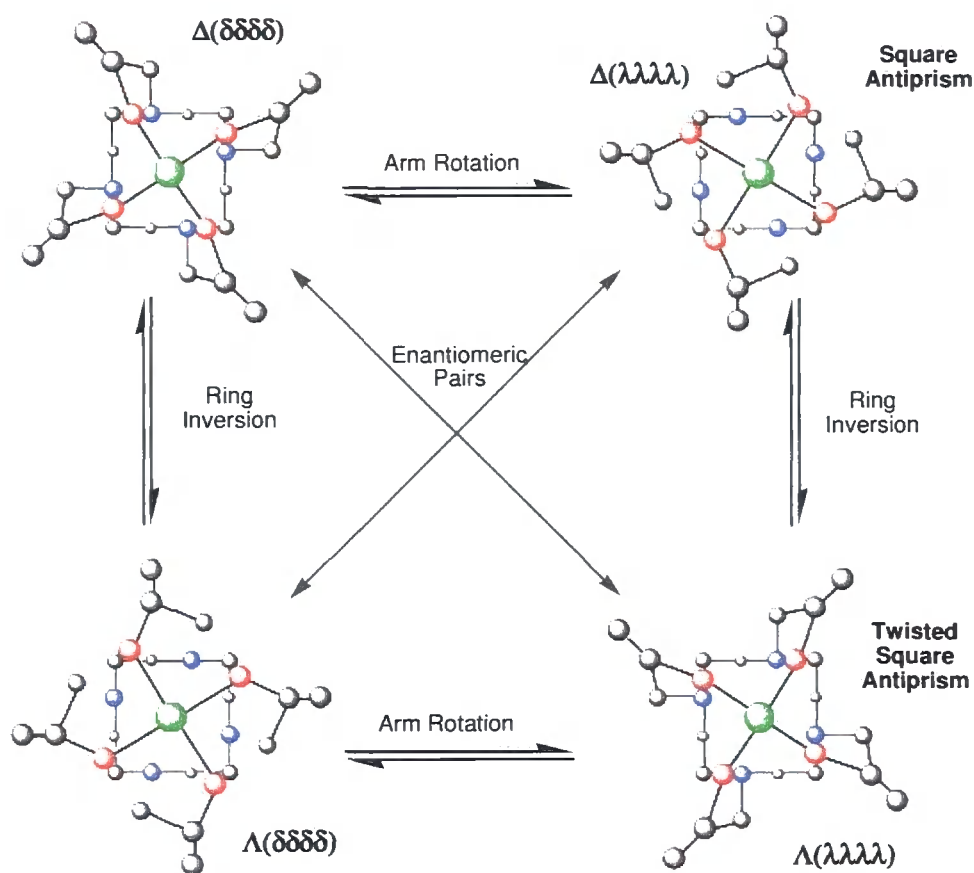
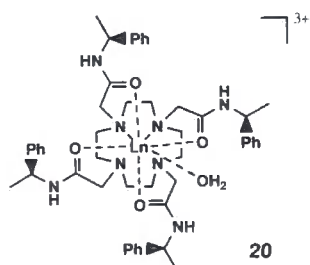


**Figure 2.2:** The four stereoisomers of Ln-DOTA complexes. Interconversion between enantiomeric pairs is possible through successive arm rotation and ring inversion

The most definitive method of structural analysis is X-ray crystallography, but suitable crystals of chromophore-containing complexes have proved to be difficult to cultivate. As a result, the structures of novel complexes must be determined in comparison to known library members by other spectroscopic techniques. The tetraamide **20** has previously been successfully crystallised, and therefore forms the model for comparison with other complexes. Crystallographic analysis of this complex determined a monocapped square-antiprismatic geometry, designated  $\Delta(\lambda\lambda\lambda\lambda)$ .<sup>112</sup>



Previous comparisons of various spectra of **20** with those of  $(SSS)\text{-[Eu.L}^2\text{]}^{3+}$  indicated that the two adopt a similar confirmation. The axial, capping, position, at which the water molecule lies in **20**, is occupied by the second nitrogen of the dpqC chromophore of  $(SSS)\text{-[Eu.L}^2\text{]}^{3+}$ . In this work, therefore, the structure of the complexes  $[\text{Eu.L}^3]^{3+}$  and  $[\text{Eu.L}^4]$  can be determined in comparison to that of  $[\text{Eu.L}^2]^{3+}$  by inspection of spectral similarities and differences between the complexes. A number of different spectroscopic techniques were employed, which will be discussed in the following sections.

### 2.3.2 Emission spectroscopy

Luminescence emission spectra of  $[\text{Eu.L}^{3a}]^{3+}$  and  $[\text{Eu.L}^{3b}]^{3+}$  and their hydrolysed complexes are shown in Figures 2.3 and 2.4 respectively. No ligand fluorescence was observed in any case, as expected for complexes of dpqC, which exhibits highly efficient intersystem crossing.<sup>72</sup> For both Ala- and Phe-based complexes, there are a number of significant changes upon hydrolysis. Notable amongst these changes are the loss of a  $\Delta J = 2$  band at 619 nm and the decreased complexity of the  $\Delta J = 4$  manifold. Since these bands possess electric dipole character, these changes are consistent with the changed local environment, and the resultant change in the oscillator strength, which arises from the altered side-chains. The emission spectrum of the hydrolysed complex  $[\text{Eu.L}^{3a}]^{3+}$  is similar in form to the emission spectrum of the parent triamide,  $[\text{Eu.L}^2]^{3+}$ .<sup>73</sup> There are also notable differences between the Ala- and Phe-derived complexes, particularly in the  $\Delta J = 1$  and  $\Delta J = 2$  bands. In the  $\Delta J = 1$  manifold there are three bands which correspond to the  $A_1\text{-}A_2$ ,  $A_1\text{-}E_1$  and  $A_1\text{-}E_2$  energy transitions. For the Ala-derived  $[\text{Eu.L}^{3a}]^{3+}$  and  $[\text{Eu.L}^{4a}]$ , the splitting between the  $A_1\text{-}A_2$  and  $A_1\text{-}E_{1,2}$  components is approximately  $155\text{ cm}^{-1}$ , whereas for the Phe-based complexes  $[\text{Eu.L}^{3b}]^{3+}$  and  $[\text{Eu.L}^{4b}]$ , the splitting is smaller ( $115\text{ cm}^{-1}$ ). In addition, the relative intensity of the  $\Delta J = 2$  band compared to  $\Delta J = 1$  is greater for the Ala complexes (2.5:1) than for the Phe complexes (1.5:1). These data indicate a change in the Eu coordination environment, which is probably due to a change in the nature of the capping group in the ninth co-ordination site.<sup>114, 115</sup> This is consistent with studies of a range of complexes with varied capping donor atoms, which demonstrated that the polarisability of this group affects the size of the second-order crystal field coefficient,  $B_0^2$ , which in turn influences the splitting of the (A/E) components of the  $\Delta J = 1$  band.<sup>116</sup>

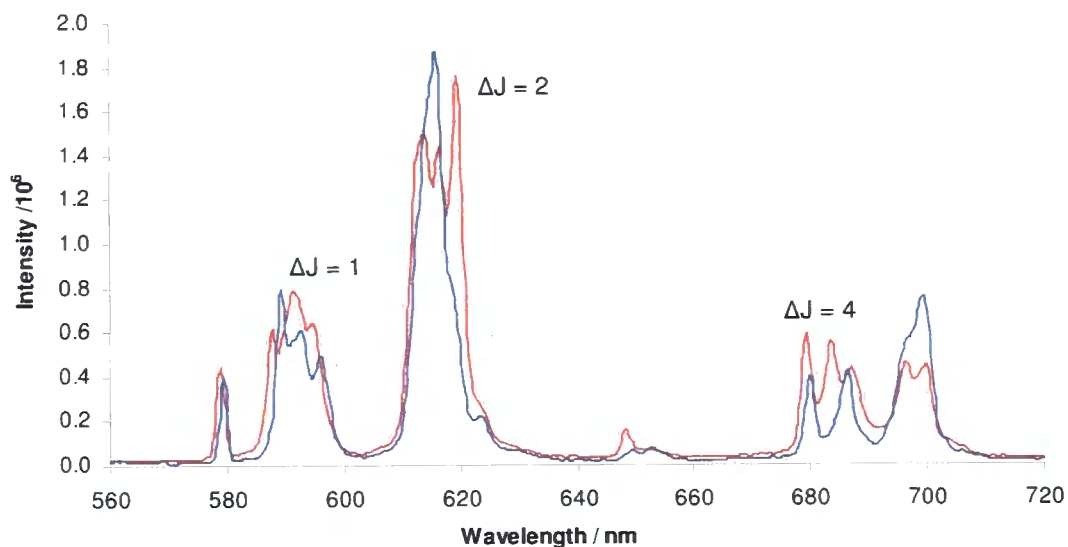


Figure 2.3: Emission spectra of  $[\text{Eu.L}^{3a}]^{3+}$  (red) and  $[\text{Eu.L}^{4a}]$  (blue) solutions ( $\text{D}_2\text{O}$ , 295 K,  $\lambda_{\text{ex}} = 348$  nm)

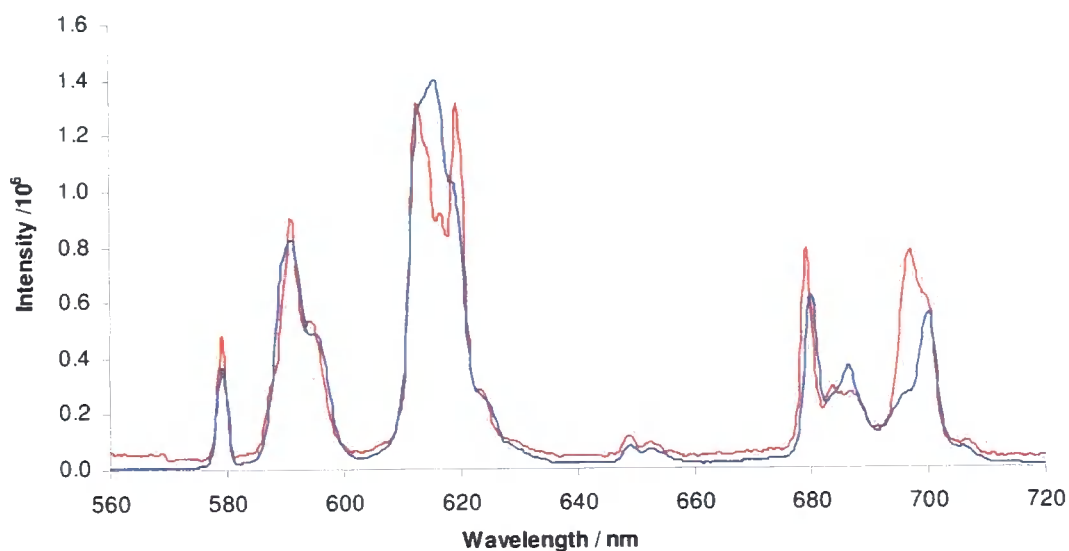
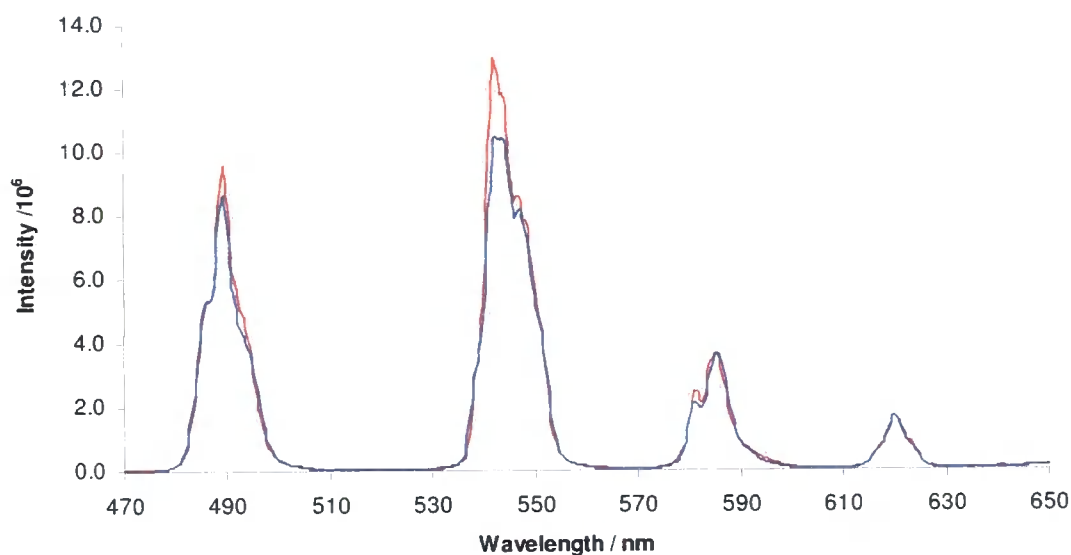
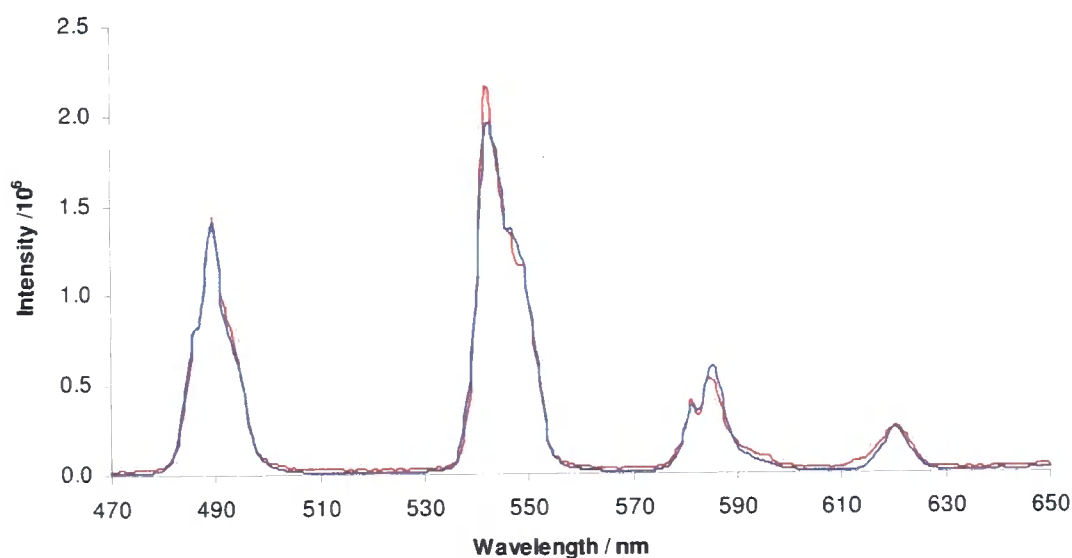


Figure 2.4: Emission spectra of  $[\text{Eu.L}^{3b}]^{3+}$  (red) and  $[\text{Eu.L}^{4b}]$  (blue) solutions ( $\text{D}_2\text{O}$  295 K,  $\lambda_{\text{ex}} = 348$  nm)

The corresponding Tb emission spectra are shown in Figures 2.5 and 2.6. There is very little spectral change on hydrolysis of the esters or following replacement of the Ala ligand for the larger Phe side chain. This is not unexpected, given the relative insensitivity of terbium emission spectra to the coordination environment.



**Figure 2.5:** Emission spectra of  $[\text{Tb.L}^{3\text{a}}]^{3+}$  (red) and  $[\text{Tb.L}^{4\text{a}}]$  (blue) solutions ( $\text{D}_2\text{O}$ , 295 K,  $\lambda_{\text{ex}} = 348 \text{ nm}$ )



**Figure 2.6:** Emission spectra of  $[\text{Tb.L}^{3\text{b}}]^{3+}$  (red) and  $[\text{Tb.L}^{4\text{b}}]$  (blue) solutions ( $\text{D}_2\text{O}$ , 295 K,  $\lambda_{\text{ex}} = 348 \text{ nm}$ )

Emission spectroscopy also allows measurement of the lifetime of the excited state ( $\tau$ ). This can be calculated by exciting the sample, and measuring the emission intensity after various time delays. The luminescence lifetimes for the europium complexes ranged from 0.69 to 1.04 ms, while the values for terbium complexes lay between 1.05 and 1.88 ms (Table 2.1).

**Table 2.1:** Complex luminescence lifetimes in H<sub>2</sub>O and D<sub>2</sub>O, and calculated  $q$  values ( $\lambda_{ex}=348$  nm, 298 K)<sup>a</sup>

Complex	$\tau_{H_2O}$ (ms)	$\tau_{D_2O}$ (ms)	$q$
[TbL <sup>2</sup> ] <sup>3+ b</sup>	1.56	1.72	0.00
[Tb.L <sup>3a</sup> ] <sup>3+</sup>	1.05	1.14	+0.08
[Tb.L <sup>3b</sup> ] <sup>3+</sup>	1.57	1.56	-0.32
[Tb.L <sup>4a</sup> ]	1.58	1.80	+0.09
[Tb.L <sup>4b</sup> ]	1.88	2.07	-0.06
[EuL <sup>2</sup> ] <sup>3+ b</sup>	1.04	1.59	-0.15
[Eu.L <sup>3a</sup> ] <sup>3+</sup>	0.85	1.17	-0.18
[Eu.L <sup>3b</sup> ] <sup>3+</sup>	0.81	1.34	+0.04
[Eu.L <sup>4a</sup> ]	0.69	0.85	-0.24
[Eu.L <sup>4b</sup> ]	0.82	1.22	-0.09

<sup>a</sup> lifetimes have an error of  $\pm 10\%$ ;  $q$  values have an error of  $\pm 20\%$

<sup>b</sup> values previously reported<sup>73</sup>

Lifetime measurements can also be utilised in the measurement of the hydration state of a complex. The number of bound waters,  $q$ , can be determined by a comparison of the radiative relaxation rates of the lanthanide excited state in both H<sub>2</sub>O and D<sub>2</sub>O, defined by the empirically-determined equations 2.1 and 2.2:<sup>117</sup>

$$q_{Eu} = 1.2 \times (k_{H_2O} - k_{D_2O} - 0.25 - 0.075n) \quad [2.1]$$

$$q_{Tb} = 5 \times (k_{H_2O} - k_{D_2O} - 0.06) \quad [2.2]$$

where

$k_{H_2O}$  and  $k_{D_2O}$  are the reciprocals of  $\tau_{H_2O}$  and  $\tau_{D_2O}$  respectively

$n$  is the number of bound amide groups.

The calculated  $q$  values (Table 2.1) have 0 as their closest integral value, which is consistent with complex structures containing no bound water molecules.

### 2.3.3 Circularly polarised luminescence spectroscopy

Circularly polarised luminescence (CPL) spectroscopy is a technique which explores the differential emission of left and right circularly polarised light by emissive chiral luminescent species.<sup>118</sup> Since the excitation is achieved *via* the antenna chromophore, the technique overcomes the limitations experienced in circular dichroism, resulting

from the low molar absorption coefficients of the lanthanide ion. Because complexes of opposite helicity will interact differently with circularly polarised light, CPL can elucidate the helicity about the metal centre, and provide some information about the electronic and magnetic environment of the lanthanide.<sup>119</sup> CPL spectra for the terbium and europium complexes were obtained in Glasgow (with Dr R. D. Peacock), and are shown in Figures 2.7 to 2.10. As expected for the mirror image complexes of  $(SSS)-[Ln.L^3]^{3+}$  and  $(RRR)-[Ln.L^3]^{3+}$ , the terbium and europium CPL spectra are equal and of opposite sign. One representative set of mirror-image spectra is shown in Figure 2.7.

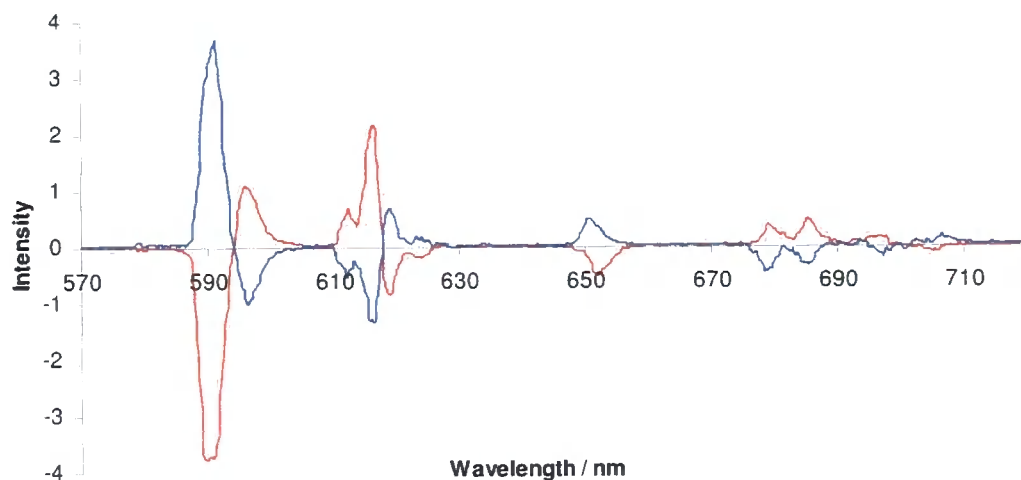


**Figure 2.7:** Mirror image CPL spectra of  $(SSS)-[Eu.L^{3a}]^{3+}$  (blue) and  $(RRR)-[Eu.L^{3a}]^{3+}$  (red) ( $D_2O$ , 295 K,  $\lambda_{ex} = 348$  nm)

Figures 2.8 and 2.9 show the CPL spectra for the four Eu complexes. The spectra for  $(SSS)-[Eu.L^{3a}]^{3+}$  and  $(SSS)-[Eu.L^{4a}]$  (Figure 2.8) are very similar to one another, and to that of  $(SSS)-[Eu.L^2]^{3+}$  in terms of the sign and sequence of the observed bands. On the other hand, the CPL spectra of  $(SSS)-[Eu.L^{3b}]^{3+}$  and  $(SSS)-[Eu.L^{4b}]$  (Figure 2.9) are markedly different from the Ala-derived complexes, and also differ from one another. The CPL spectra of  $(SSS)-[Tb.L^{3a}]^{3+}$  and  $(SSS)-[Tb.L^{3b}]^{3+}$  (Figure 2.10) also exhibit marked spectral differences between the two complexes.

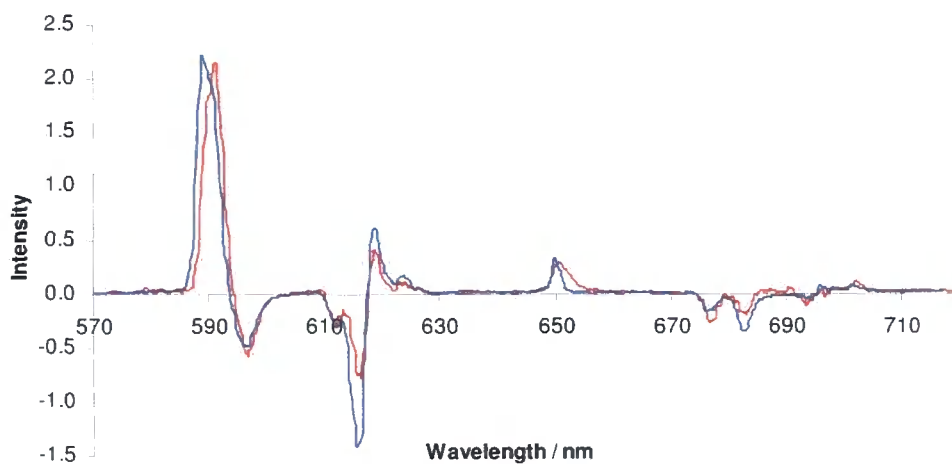


Figure 2.8: CPL spectra for (SSS)-[Eu.L<sup>3a</sup>]<sup>3+</sup> (blue) and (SSS)-[Eu.L<sup>4a</sup>] (red) (D<sub>2</sub>O, 295 K,  $\lambda_{ex}$  = 348 nm)

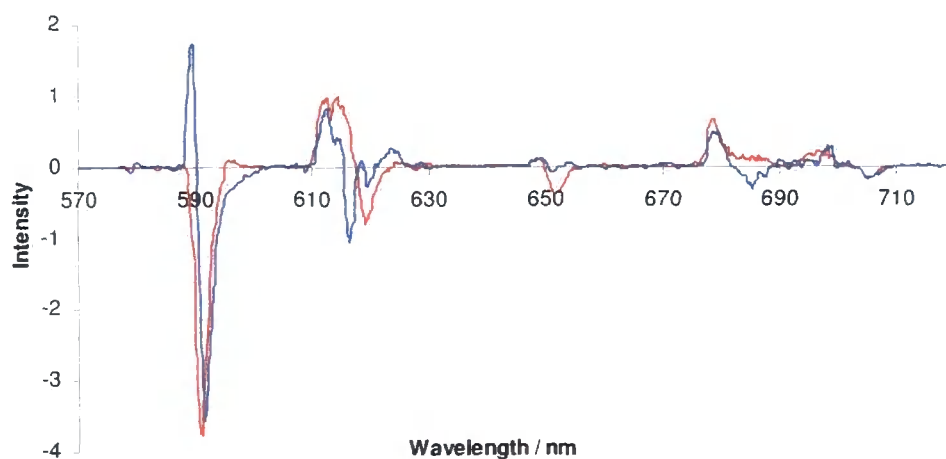


Figure 2.9: CPL spectra for (SSS)-[Eu.L<sup>3b</sup>]<sup>3+</sup> (blue) and (SSS)-[Eu.L<sup>4b</sup>] (red) (D<sub>2</sub>O, 295 K,  $\lambda_{ex}$  = 348 nm)

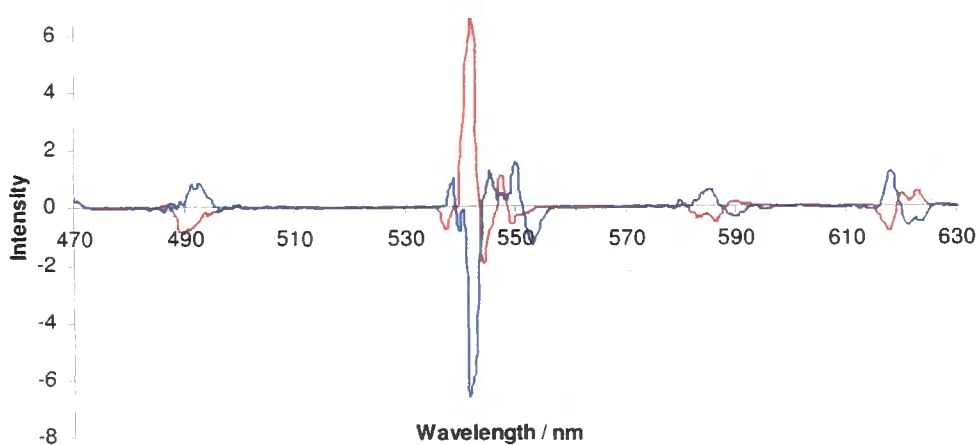


Figure 2.10: CPL spectra for (SSS)-[Tb.L<sup>3a</sup>]<sup>3+</sup> (blue) and (SSS)-[Tb.L<sup>3b</sup>]<sup>3+</sup> (red) (D<sub>2</sub>O, 295 K,  $\lambda_{ex}$  = 348 nm)

Emission dissymmetry factors,  $g_{em}$ , are used to indicate the degree of chirality sensed by an electronic transition.<sup>119</sup> They can be determined by equation 2.3:

$$g_{em} = \frac{2(I_L - I_R)}{(I_L + I_R)} \quad [2.3]$$

where  $I_{L(R)}$  is the intensity of the left (right) circularly polarised component.

The calculated  $g$ -values for the Eu complexes are shown in Table 2.2.

**Table 2.2:** Emission dissymmetry factors for Eu complexes (in D<sub>2</sub>O at 295 K,  $\lambda_{ex} = 348$  nm)

Complex	$g_{em(590)}$	$g_{em(597)}$	$g_{em(612)}$	$g_{em(615)}$	$g_{em(618)}$	$g_{em(651)}$
(SSS)-[Eu.L <sup>2</sup> ] <sup>3+</sup>	+0.23	-0.16	-0.02	-0.05	+0.09	+0.17
(SSS)-[Eu.L <sup>3a</sup> ] <sup>3+</sup>	+0.12	-0.07	-0.01	-0.02	+0.02	+0.18
(SSS)-[Eu.L <sup>3b</sup> ] <sup>3+</sup>	-0.09	+0.03	+0.02	+0.02	+0.01	-0.08
(SSS)-[Eu.L <sup>4a</sup> ]	+0.19	-0.08	-0.01	-0.05	+0.043	+0.26
(SSS)-[Eu.L <sup>4b</sup> ]	+0.05	-0.08	+0.01	-0.02	+0.01	+0.04

The  $g_{em}$  values for the two Ala-derived complexes are very similar, in sign and magnitude, to those of (SSS)-[Eu.L<sup>2</sup>]<sup>3+</sup>. On the other hand, the CPL spectrum of (SSS)-[Eu.L<sup>3b</sup>]<sup>3+</sup> is markedly different, with almost every transition exhibiting the opposite sign. The  $g_{em}$  values for (SSS)-[Eu.L<sup>4b</sup>] differ from those of both the Ala- and Phe-derived ester complexes.

From the CPL spectra and the calculated  $g_{em}$  values, (SSS)-[Eu.L<sup>3a</sup>]<sup>3+</sup> and its hydrolysed derivative exhibit the same helicity. These CPL spectra also exhibit the same sign and sequence of transitions to (SSS)-[Eu.L<sup>2</sup>]<sup>3+</sup>, which has previously been identified to possess a  $\Delta(\lambda\lambda\lambda)$  configuration.<sup>73</sup> These Ala-derived complexes can therefore be assigned a  $\Delta$ -helicity. The Phe-derived complex, (SSS)-[Eu.L<sup>3b</sup>]<sup>3+</sup>, on the other hand, exhibits opposite  $g$  values, suggesting that this complex possesses opposite chirality, consistent with a  $\Lambda(\delta\delta\delta\delta)$  configuration. Assignment of the helicity of [Eu.L<sup>4b</sup>] is less straightforward, as the sign and sequence of transitions appears to be intermediate between those of [Eu.L<sup>3a</sup>]<sup>3+</sup> and [Eu.L<sup>3b</sup>]<sup>3+</sup>. This may be indicative of a more distorted local geometry, and could be a twisted square antiprismatic geometry as distinct from the square antiprismatic forms of the other complexes.

### 2.3.4 $^1\text{H}$ NMR spectroscopy

Due to the paramagnetic nature of most lanthanide(III) ions, the NMR resonances of atoms which are in close proximity to the metal are both broadened and shifted.<sup>120</sup> For well-defined coordination geometries, solution NMR can give precise structural information. For example, for cyclen-based systems, the pseudoaxial macrocyclic ring protons exhibit the greatest shifts in resonance. Of particular interest in NMR analysis is the total observed shift range.<sup>121</sup> The dipolar shift varies with the local magnetic anisotropy, and is related to  $B_0^2$ , the second order crystal field coefficient. As previously discussed,  $B_0^2$  is strongly dependent on the nature of the axial donor.<sup>114, 115</sup>

$^1\text{H}$  NMR spectra were previously measured and compared at 298 K, but under these conditions, spectra were not reproducible and some peaks were very broad. This is likely to be due to the exchange process associated with arm rotation, giving rise to exchange-broadened spectra.  $^1\text{H}$  NMR spectra were therefore recorded at 278 K to freeze out this motion (Figures 2.11 to 2.13). The primary difference between the spectra lies in the range of chemical shifts, as summarised in Table 2.3. The NMR spectrum for  $[\text{Eu.L}^{4b}]$  appears to contain two sets of peaks, one set (the less shifted) corresponding to a major form and the other (which are more shifted) corresponding to a minor form.

**Table 2.3:**  $^1\text{H}$  NMR data for Eu complexes ( $\text{D}_2\text{O}$ , 278 K, 500 MHz)

Complex	Shift range (ppm)
$[\text{Eu.L}^2]^{3+}$	+38 to -24
$[\text{Eu.L}^{3a}]^{3+}$	+43 to -19
$[\text{Eu.L}^{3b}]^{3+}$	+10 to -21
$[\text{Eu.L}^{4a}]$	+37 to -22
$[\text{Eu.L}^{4b}]$ (major peaks)	+14 to -21
(minor peaks)	+38 to -22

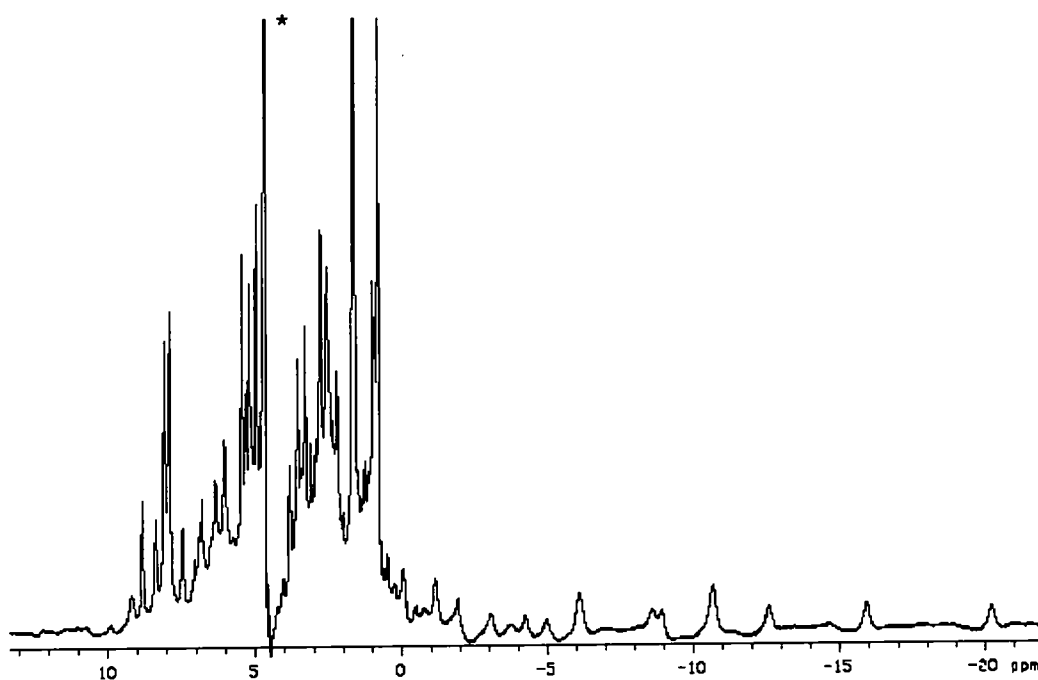


Figure 2.11:  $^1\text{H}$  NMR spectrum of  $[\text{Eu.L}^{3b}]\text{Cl}_3$  ( $\text{D}_2\text{O}$ , 278 K, 500 MHz) \* indicates HOD resonance.

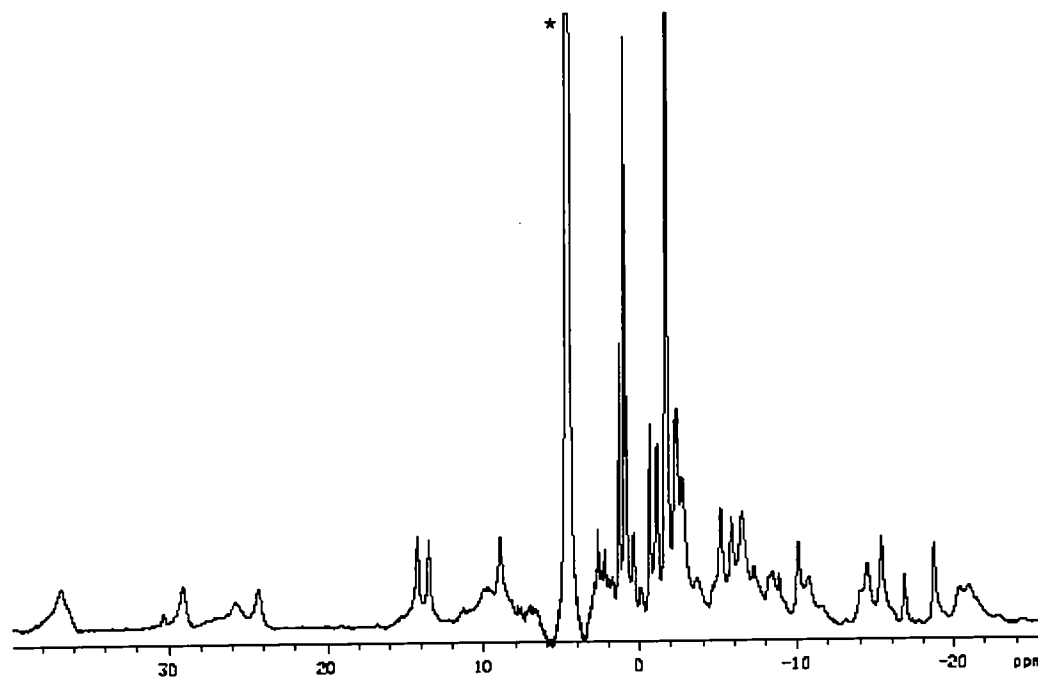


Figure 2.12:  $^1\text{H}$  NMR spectrum of  $[\text{Eu.L}^{4a}]$  ( $\text{D}_2\text{O}$ , 278 K, 500 MHz) \* indicates HOD resonance.

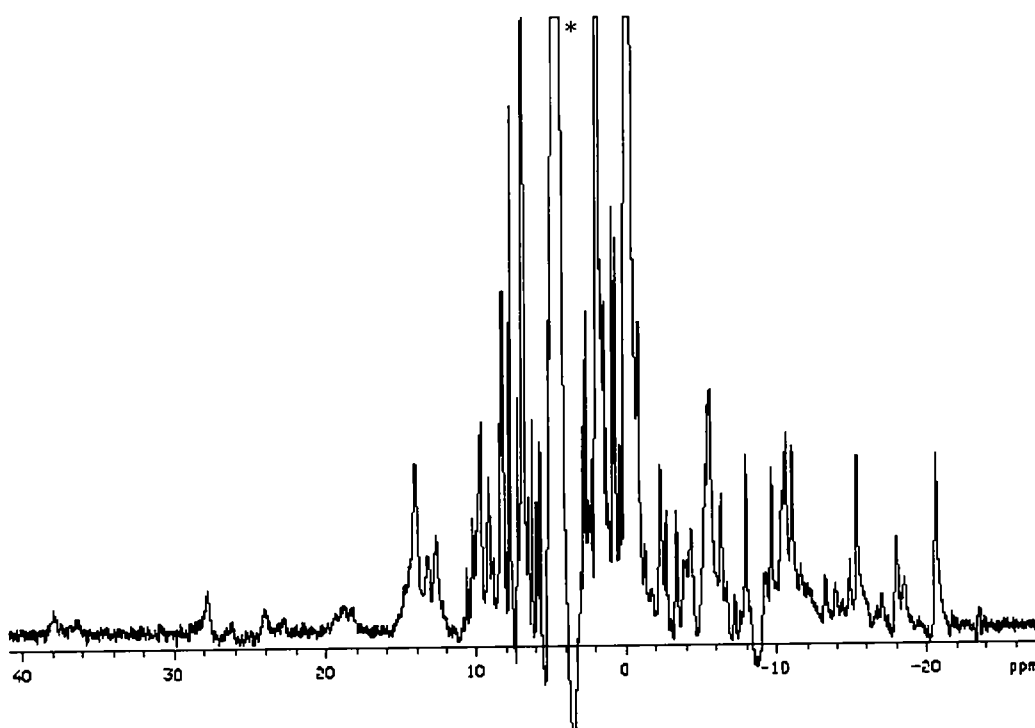


Figure 2.13:  $^1\text{H}$  NMR spectrum of  $[\text{Eu.L}^{4b}]$  ( $\text{D}_2\text{O}$ , 278 K, 500 MHz) \* indicates HOD resonance.

$[\text{Eu.L}^{3a}]^{3+}$  and  $[\text{Eu.L}^{4a}]$  show very similar chemical shift ranges, which are also consistent with those observed for  $[\text{Eu.L}^{2}]^{3+}$ . In comparison, the spectrum of  $[\text{Eu.L}^{3b}]^{3+}$  is much more condensed. This is consistent with a change in the coordination environment, which can result from a number of possible structural changes: the replacement of the capping ligand by water, the rearrangement of the structure so that a different atom is in the ninth coordinate position, or the adoption of an eight-coordinate geometry. The use of other spectroscopy methods allows the possibilities to be distinguished.

The  $^1\text{H}$  NMR spectrum of  $[\text{Eu.L}^{4b}]$  suggests that the complex exists primarily in a form that is similar to that of  $[\text{Eu.L}^{3b}]^{3+}$ , but occurs as a mixture of two isomers, one of which possesses a more expanded range of chemical shifts, like those of  $[\text{Eu.L}^{3a}]^{3+}$  and  $[\text{Eu.L}^{4a}]$ . It is likely that in this complex, the two forms are in slow exchange on the NMR timescale.

### 2.3.5 Infrared spectroscopy

The use of infrared spectroscopy provides further insight regarding the coordination of certain ligand donor groups. In the free ligands  $\text{L}^{3a}$  and  $\text{L}^{3b}$ , the amide and ester carbonyl

stretching bands appear at 1649 and 1732  $\text{cm}^{-1}$  respectively. The IR spectra of both  $[\text{Eu.L}^{3a}]^{3+}$  and  $[\text{Eu.L}^{3b}]^{3+}$  (Figures 2.14 and 2.15) show that these bands have shifted to 1619( $\pm$ 2) and 1733( $\pm$ 2)  $\text{cm}^{-1}$ . This suggests that in each case, each amide carbonyl groups is coordinated to the lanthanide(III) ion.

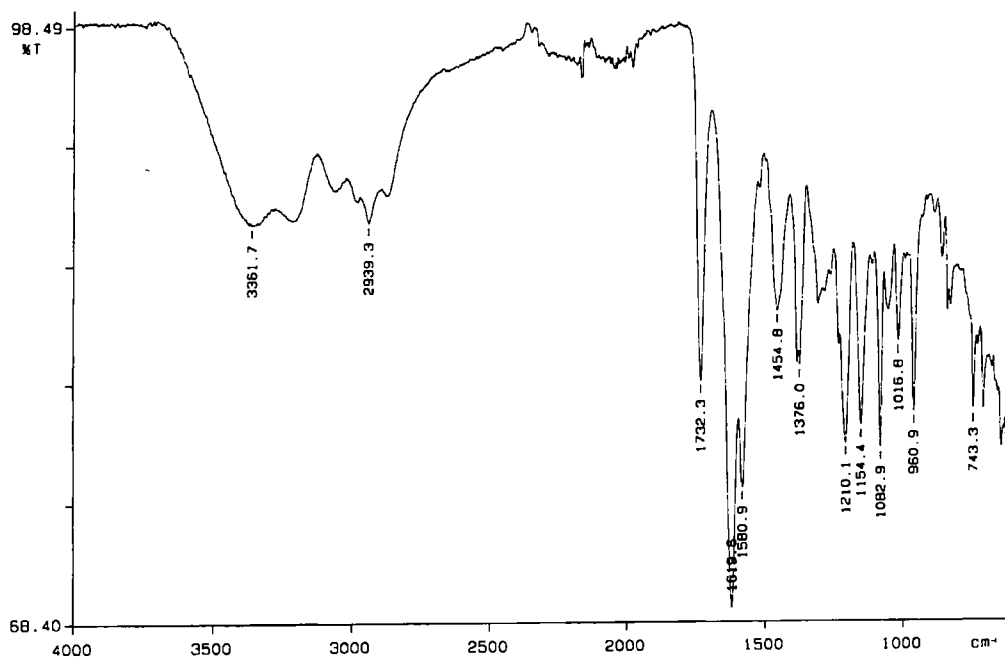


Figure 2.14: Infrared spectrum of  $[\text{Eu.L}^{3a}]^{3+}$  (295 K, solid: golden gate)

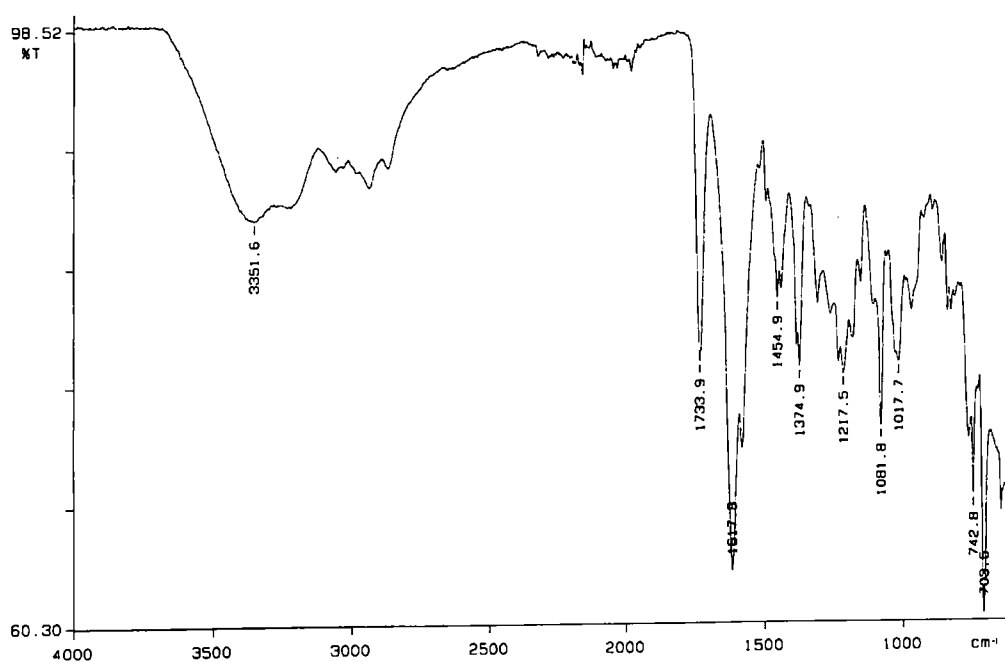


Figure 2.15: Infrared spectrum of  $[\text{Eu.L}^{3b}]^{3+}$  (295 K, solid: golden gate)

### 2.3.6 Conclusions of the structural analyses

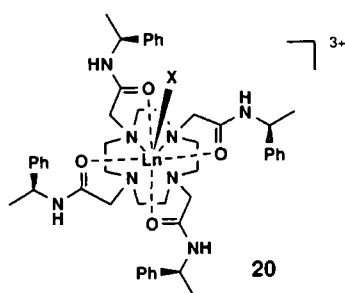
The combined information yielded from the various spectroscopic analyses described above can be utilised in determination of the structure of the Ala- and Phe-derived complexes. The emission, CPL,  $^1\text{H}$  NMR and IR spectra of  $[\text{Eu.L}^{4a}]$  are very similar to those of  $[\text{Eu.L}^2]^{3+}$ . The spectra of  $[\text{Eu.L}^{3a}]^{3+}$  are also very similar, with the emission spectra varying only slightly in the  $\Delta J = 2$  and  $\Delta J = 4$  bands. Since these bands possess electric dipole character, these changes are consistent with the changed local environment and hence oscillator strength resulting from the altered side-chains, with no overall structural change. The two Ala-derived complexes,  $[\text{Eu.L}^{3a}]^{3+}$  and  $[\text{Eu.L}^{4a}]$ , can therefore be assigned the same geometry as  $[\text{Eu.L}^2]^{3+}$ ; a  $\Delta(\lambda\lambda\lambda\lambda)$  square antiprismatic geometry, in which the dpqC nitrogen acts as a capping ligand.

The spectra of  $[\text{Eu.L}^{3b}]^{3+}$  and  $[\text{Eu.L}^{4b}]$ , on the other hand, differ markedly from those of  $[\text{Eu.L}^2]^{3+}$ . The splitting of the  $\Delta J = 1$  manifold of the emission spectra, and the chemical shift range of the  $^1\text{H}$  NMR spectra indicate an altered coordination environment that is most consistent with a change in the nature of the ninth “capping” donor. This may be due to water occupying the ninth coordination site, to the rearrangement of the structure so that a different atom is in the capping position, or could even signify the adoption of an eight-coordinate geometry, with a non-coordinated amide arm. These possibilities were investigated through other spectroscopic methods.

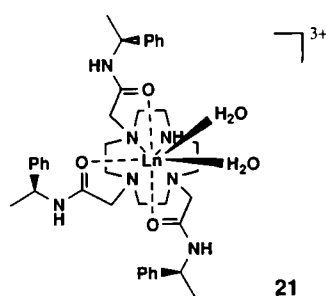
Occupation of the ninth co-ordination site by water would result in a hydration state of one. Determination of the number of bound waters was achieved by comparing the relaxation rates of the lanthanide excited state in both  $\text{H}_2\text{O}$  and  $\text{D}_2\text{O}$ , as discussed above. All complexes had a  $q$  value of close to 0 (Table 2.1), suggesting no bound waters, refuting this hypothesis.

The hypothesis that the complexes adopt an eight-coordinate geometry requires that one of the ligating groups, most likely one of the amide carbonyls, is no longer coordinated. If this were the case, the IR spectrum of  $[\text{Eu.L}^{3b}]^{3+}$  would show two sets of amide resonances, one corresponding to the free amide, at  $1649\text{ cm}^{-1}$ , and the other at the bound amide frequency of  $1618\text{ cm}^{-1}$ . This was not found to be the case, with a single band at  $1618\text{ cm}^{-1}$  being observed (Figure 2.16).

The dismissal of these two hypotheses leaves the remaining possibility that the structure has changed such that a different ligand is in the axial position. The effect of varying the nature of the ninth capping ligand on the emission and  $^1\text{H}$  NMR spectra has previously been explored in detail for the tetraamide **20**. Different solvent molecules in the ninth coordinate site (X) were found to give rise to large changes in  $^1\text{H}$  NMR and emission spectral form.<sup>116</sup> The range of  $^1\text{H}$  NMR values and the  $\Delta J = 2 / \Delta J = 1$  ratio observed for  $[\text{Eu.L}^{3b}]^{3+}$  is similar to that measured for complex **20**, in which DMF is the axial ligand. This lends support to the hypothesis that the  $^1\text{H}$  NMR behaviour can be explained by a structure in which the capping ligand is different from the dpqC nitrogen, but is instead an amide carbonyl nitrogen, that is one of the phenylalanine amide oxygens.



The CPL studies indicate that, in addition to this change in the nature of the capping donor ligand, there is also a marked difference in complex helicity in  $[\text{Ln.L}^{3b}]^{3+}$  compared to  $[\text{Ln.L}^{3a}]^{3+}$ . This change is consistent with the adoption of the opposite,  $\Lambda(\delta\delta\delta\delta)$ , configuration. Such a helicity change has previously been observed in studies of the addition of amino acids to the tris( $\alpha$ -phenylmethyl) complex **21**.<sup>122</sup>



Replacement of the water molecules by (*S*)-Met and (*R*)-Ala yielded a  $\Delta(\lambda\lambda\lambda\lambda)$  structure which was confirmed by X-ray crystallography. This was the opposite chirality to the  $\Lambda(\delta\delta\delta\delta)$  diastereomer observed with (*S*)-Ala and many other natural amino acids. The crystal structures of the two forms are shown in Figure 2.16 and reveal the considerable structural difference between the two square-antiprismatic forms. It is feasible, therefore,

that  $[\text{Eu.L}^{3b}]^{3+}$  adopts the  $\Lambda(\delta\delta\delta\delta)$  structure. This closed structure could be favoured because of the extra steric demand imposed by the benzyl groups of Phe, which preferentially point outwards rather than align in the same direction. The CPL spectrum of  $[\text{Eu.L}^{4b}]$  indicates that it appears to adopt a different geometry still, which is intermediate to the  $\Delta(\lambda\lambda\lambda\lambda)$  configuration of  $[\text{Eu.L}^{3a}]^{3+}$  and the  $\Lambda(\delta\delta\delta\delta)$  configuration of  $[\text{Eu.L}^{3b}]^{3+}$ . This is most consistent with a twisted square antiprismatic geometry.

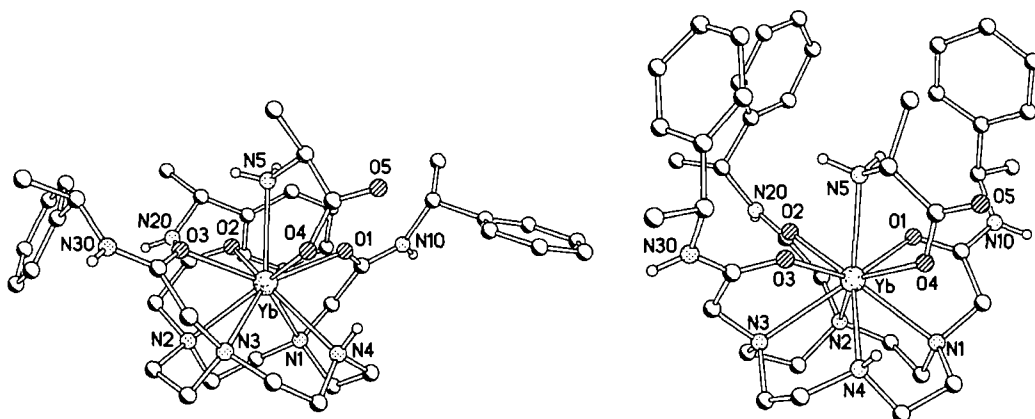


**Figure 2.16:** Crystal structures of the (*S*)-Ala adduct ( $\Delta(\lambda\lambda\lambda\lambda)$ ; left) and (*R*)-Ala adduct ( $\Lambda(\delta\delta\delta\delta)$ ; right) of **21**.<sup>122</sup>

A combination of the structural characteristics identified from the spectral analysis therefore allows assignment of a geometry to each complex.  $[\text{Ln.L}^{3a}]^{3+}$  and  $[\text{Ln.L}^{4a}]$  adopt a  $\Delta(\lambda\lambda\lambda\lambda)$  square antiprismatic geometry, with a dpqC nitrogen in the capping position;  $[\text{Ln.L}^{3b}]^{3+}$  exhibits a  $\Lambda(\delta\delta\delta\delta)$  square antiprismatic geometry with an amide capping group, while  $[\text{Ln.L}^{4b}]$  adopts a  $\Lambda(\lambda\lambda\lambda\lambda)$  twisted square antiprismatic geometry with an amide capping group. It is clear, therefore, that changing the nature of the amide arm can cause considerable changes to the geometry of the complex.

This series of complexes therefore allows the study of the effects of geometry, as well as charge and hydrophobicity, on biological behaviour. The following sections detail the studies which have been performed to explore the effect of complex configuration on excited state quenching, and on cellular behaviour.

## 2.4 Excited state quenching processes

The quantum yield of sensitised lanthanide emission can be decreased by a number of different deactivation pathways. Quenching can occur at any stage of the energy transfer process. The singlet and triplet states of the sensitizer may be quenched by electron or vibrational energy transfer processes.<sup>109, 114, 123</sup> The quantum yield can also be decreased by quenching of the excited state of the lanthanide(III) ion, which is susceptible to deactivation by transfer of vibrational energy to N-H, C-H or O-H oscillators.<sup>117, 124, 125</sup> The  $^5D_0$  and  $^5D_4$  states of  $\text{Eu}^{3+}$  and  $\text{Tb}^{3+}$ , in particular, are quenched by water O-H and amine N-H vibrations in a process that exhibits an  $r^{-6}$  dependence on the Ln/XH separation,  $r$ . The lanthanide excited state can also be quenched by energy transfer to a proximal acceptor group of similar energy.<sup>126</sup> The extent of excited state quenching is therefore an important consideration in the design of luminescent lanthanide complexes for use as cellular probes. For example, a complex with a very high quantum yield will be of less utility if it is very strongly quenched by an endogenous molecule. The following sections detail the investigations of the quenching effects on  $[\text{Ln.L}^3]^{3+}$  and  $[\text{Ln.L}^4]$  of two classes of cellular molecules, biological reductants and proteins.

### 2.4.1 Quenching by urate, ascorbate and iodide

One hypothesis for the quenching of lanthanides by electron rich species is that the free energy of the excited lanthanide ions (Tb and Eu excited states lie at 2.52 and 2.13 eV above the ground state respectively) can be used to drive a charge transfer process. The feasibility of this process is given by the Weller equation (2.4):<sup>127</sup>

$$\Delta G_{ET} = nF[(E_{ox} - E_{red}) - E^{Ln*} - \frac{e^2}{\epsilon r}] Jmol^{-1} \quad [2.4]$$

where

$E_{ox}$  is the oxidation potential of the electron donor (the quencher)

$E_{red}$  is the reduction potential of the acceptor (ligand or metal) in the complex

$E^{Ln*}$  is the energy of the lanthanide excited state

$e^2/\epsilon r$  is the Coulombic attraction correction term associated with the formation of a transient ion pair (or radical/ion pair). This term is typically small (< 0.2 eV).

The electron-rich species which are commonly studied with respect to their quenching effects on lanthanide complexes are halide anions, such as iodide, and low molecular weight anti-oxidants, such as ascorbate and urate. Each of these compounds is common in biological systems, being present in the cell at concentrations between 0.1 and 2 mM.<sup>94</sup> Half equations for the two reductants are shown in Figure 2.17.

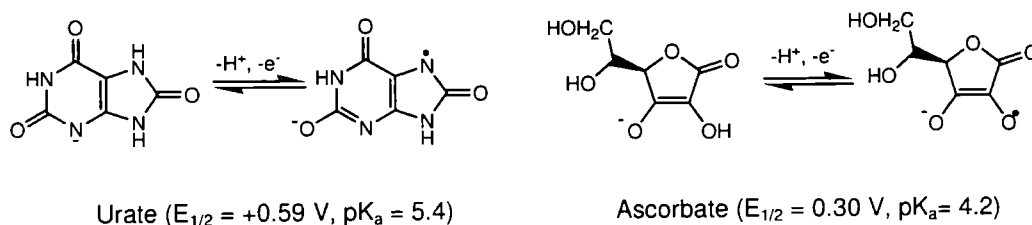


**Figure 2.17:** Half equations for the one electron oxidation of the urate and ascorbate anions.

The sensitivity of a complex to collisional quenching can be described by the Stern-Volmer equation (2.5):<sup>60</sup>

$$\frac{I_0}{I} = 1 + k_q \tau_0 [Q] = 1 + K_{SV} [Q] \quad [2.5]$$

where

$I_0$  and  $I$  are the luminescent intensities in the absence and presence of quencher respectively,

$k_q$  is the rate constant for a bimolecular quenching process

$\tau_0$  is the emissive lifetime of the complex in the absence of quencher

$[Q]$  is the concentration of the quenching species.

The term  $K_{SV}$  is the Stern-Volmer quenching constant, which has units of  $\text{M}^{-1}$ .  $K_{SV}^{-1}$  is commonly quoted for convenience, given in units of mM. This term is equivalent to the concentration of quencher needed to reduce the luminescence intensity to half its initial value. For a dynamic quenching process, the lifetime decreases concomitantly as the luminescence intensity, giving rise to the following equation (2.6):

$$\frac{\tau_0}{\tau} = 1 + k_q \tau_0 [Q] = 1 + K_{SV} [Q] \quad [2.6]$$

$K_{SV}^{-1}$  can therefore be calculated by measuring the change in the luminescence lifetime with the addition of quencher. Stern-Volmer plots were obtained for each of the europium and terbium complexes in pH buffered solution (100 mM HEPES, pH 7.4), in

the presence of sodium chloride (10 mM). Representative plots are shown in Figure 2.18.

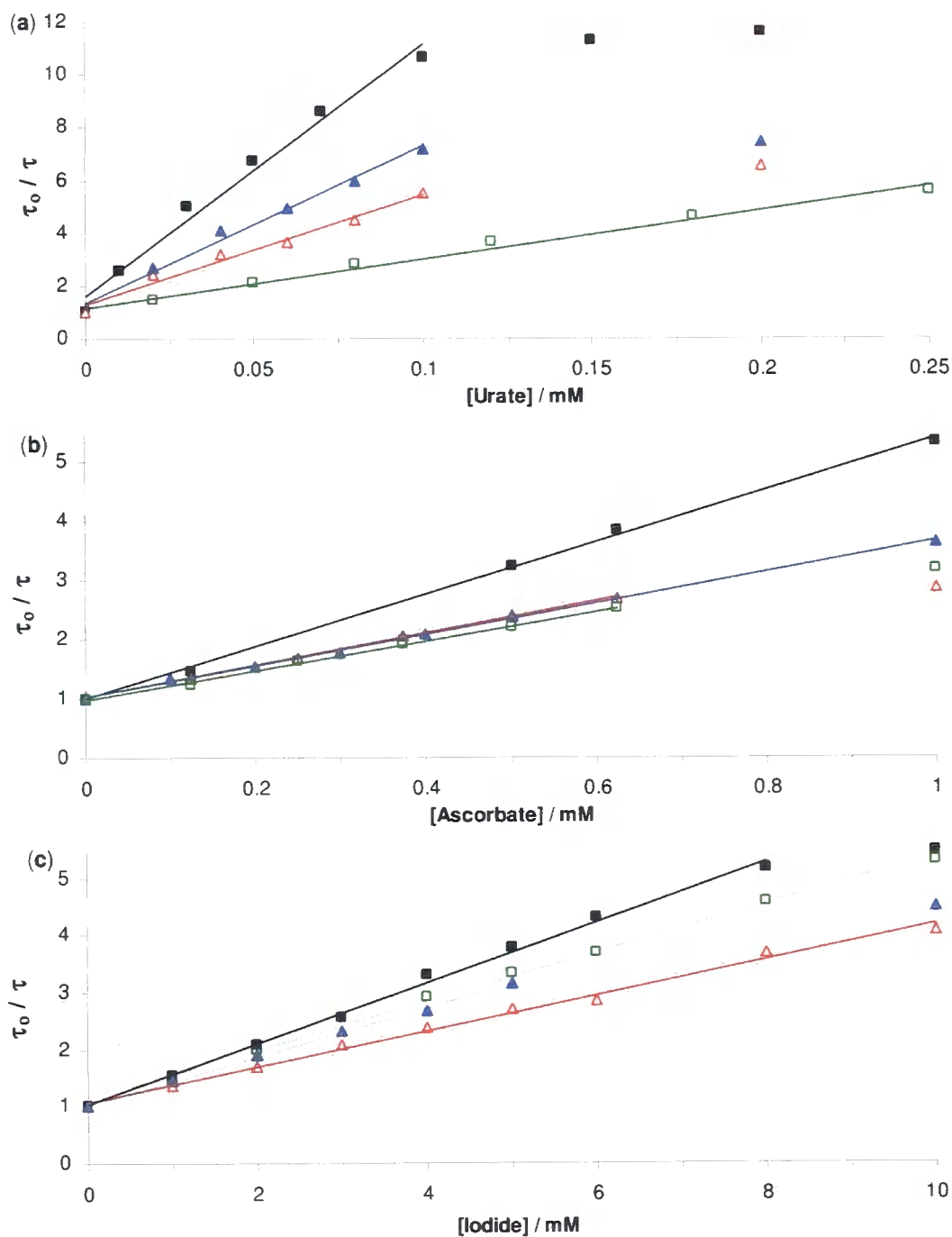


**Figure 2.18:** Stern-Volmer plots for the quenching of [Tb.L<sup>3a</sup>]<sup>3+</sup> (■) [Tb.L<sup>4a</sup>] (□), [Tb.L<sup>3b</sup>]<sup>3+</sup> (▲) and [Tb.L<sup>4b</sup>] (Δ) by (a) urate, (b) ascorbate and (c) iodide (10 μM complex, 100 mM HEPES, 10 mM NaCl, pH 7.4, 298K,  $\lambda_{\text{ex}} = 348$  nm)

The Stern-Volmer plots initially have a constant gradient (Figure 2.18), but at higher concentrations of quencher, the variation reaches a limiting value. This suggests that an upper limit of quencher is reached, above which the rate of change of  $\tau_0/\tau$  with increasing quencher concentration tends to zero. It is not clear why this occurs, but suggests an inefficiency of the quenching mechanism, perhaps due to an intermolecular interaction between the quencher and the complex.  $K_{SV}^{-1}$  values were calculated only by analysis of the linear range.

Stern-Volmer constants,  $K_{SV}^{-1}$ , for quenching with urate, iodide and ascorbate for the series of complexes are presented in Table 2.4.

**Table 2.4:** Stern-Volmer quenching constants for Tb and Eu complexes (10  $\mu$ M complex, 100 mM HEPES, pH 7.4, 10 mM NaCl, 298 K,  $\lambda_{ex} = 348$  nm).

Complex	Urate: $K_{SV}^{-1}$ /mM	Ascorbate: $K_{SV}^{-1}$ /mM	Iodide: $K_{SV}^{-1}$ /mM
[Tb.L <sup>1</sup> ]*	0.006	0.35	2.10
[Eu.L <sup>1</sup> ]*	0.11	2.92	>10 <sup>3</sup>
[TbL <sup>2</sup> ] <sup>3+</sup> *	0.025	0.18	0.92
[EuL <sup>2</sup> ] <sup>3+</sup> *	0.07	0.39	27
[Tb.L <sup>3a</sup> ] <sup>3+</sup>	0.009	0.24	1.64
[Eu.L <sup>3a</sup> ] <sup>3+</sup>	0.049	0.51	8.55
[Tb.L <sup>3b</sup> ] <sup>3+</sup>	0.018	0.47	2.35
[Eu.L <sup>3b</sup> ] <sup>3+</sup>	0.028	0.47	10.8
[Tb.L <sup>4a</sup> ]	0.046	0.55	2.25
[Eu.L <sup>4a</sup> ] <sup>†</sup>	0.048	1.13	>10 <sup>3</sup>
[Tb.L <sup>4b</sup> ]	0.030	0.99	3.22
[Eu.L <sup>4b</sup> ]	0.033	0.96	60

\* values previously reported<sup>85</sup>

† values previously reported<sup>128</sup>

A number of observations and conclusions can be drawn from analysis of the Stern-Volmer constants. The terbium complexes for each ligand are more strongly quenched than their europium analogues, as has been found in previous studies.<sup>85, 129</sup> This is consistent with the predictions of the Weller equation since  $E^{Tb*}$  is higher than  $E^{Eu*}$ . For each complex, the sensitivities to quenching follow the trend urate > ascorbate > I<sup>-</sup>. This is again consistent with previous experimental findings,<sup>85, 129</sup>

but cannot be solely explained by trends in reduction potential, since ascorbate has greater reducing power than urate.

In general, the cationic ester complexes appear to be less sensitive to quenching than the zwitterionic hydrolysed complexes. There is no such clear comparison for the Phe series against the Ala series. Of all the complexes explored in this study, it is the complexes of **L<sup>4a</sup>** and **L<sup>4b</sup>** which exhibit the highest  $K_{SV}^{-1}$  values. Such a property is desired for cellular applications, as a reduced sensitivity to quenching should result in stronger *in cellulo* luminescence.

These measured Stern-Volmer quenching constants have contributed to a more detailed study of quenching mechanisms.<sup>86</sup> A number of pieces of evidence led to the conclusion that iodide quenches by a classical collisional encounter mechanism, fitting traditional Stern-Volmer kinetics (Figure 2.19). Cationic complexes were more sensitive to quenching than neutral or anionic complexes of the same chromophore. For series of complexes with a common donor set but varying chromophore, the trends in quenching mirror the reduction potential of the heterocycle. These results suggest that quenching is sensitive to the local electrostatic environment, which is in keeping with a model of collisional quenching. Increasing the temperature led to increased quenching for quenching by iodide only, consistent with an increased collision rate.

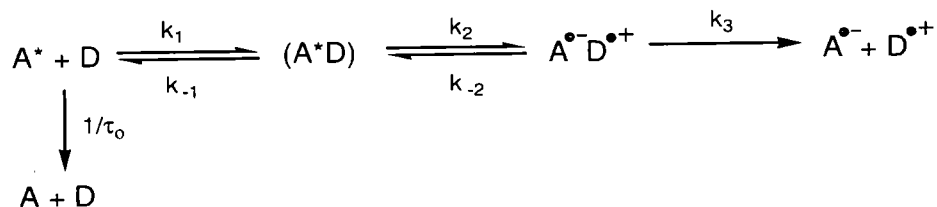


**Figure 2.19:** Rehm-Weller kinetic scheme for quenching via excited state electron transfer

Urate and ascorbate appear to act in a similar manner to each other, with complexes showing greater sensitivity to urate than ascorbate. The electrostatic effects observed for iodide are much less marked for ascorbate and urate. In general, cationic complexes are least sensitive to quenching, suggesting that a quenching mechanism simply involving an electrostatic encounter is unlikely. The linearity of the Stern-Volmer plot is lost at relatively low concentrations for some complexes, suggesting that the Stern-Volmer model cannot be applied. Furthermore, increasing the temperature was shown to result in decreased quenching. Based on these findings, the quenching mechanism was

hypothesised to occur through the formation of an intermediate excited state complex (exciplex; Figure 2.20).

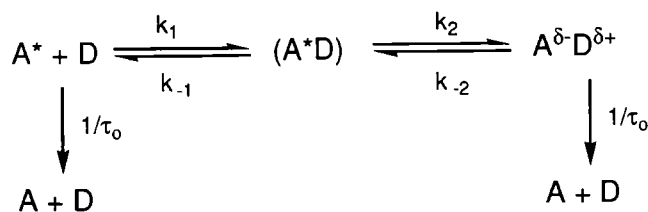


**Figure 2.20:** Suggested kinetic scheme for quenching through exciplex formation

The stronger quenching by urate than ascorbate can be accounted for by structural considerations. Urate incorporates a planar, delocalized electron-rich system, while ascorbate is less conjugated and more hydrophilic. Quenching of complexes by the urate anion might therefore be expected to be enhanced by a  $\pi$ - $\pi$  interaction between the electron-poor chromophore and the electron rich urate anion.

Recent studies have shed further light on the quenching mechanisms of sensitised lanthanide complexes.<sup>130</sup> When the metal was directly excited, no quenching of the luminescence lifetime was observed, suggesting that quenching occurs *via* a charge transfer complex with the triplet excited state of the chromophore. This hypothesis was further supported in studies in  $D_2O$ , where the selective incorporation of deuterium into the chromophore occurred only for complexes containing an intramolecular quenching moiety.

#### 2.4.2 Quenching by serum albumin

Proteins represent another important class of endogenous species that could quench lanthanide luminescence. Serum albumin has been selected for study as it is the most important plasma protein in mammals. Although its intracellular molar concentration is of a similar magnitude to that of urate and ascorbate, due to its bulk (MW ~ 70 kDa) it has a very high effective concentration within cells. For such a system, quenching is likely to result from a ground state binding rather than a transient association of the excited state and the Ln(III) complex. The changes in lifetime as a function of added bovine serum albumin (BSA) are shown in Figure 2.21.

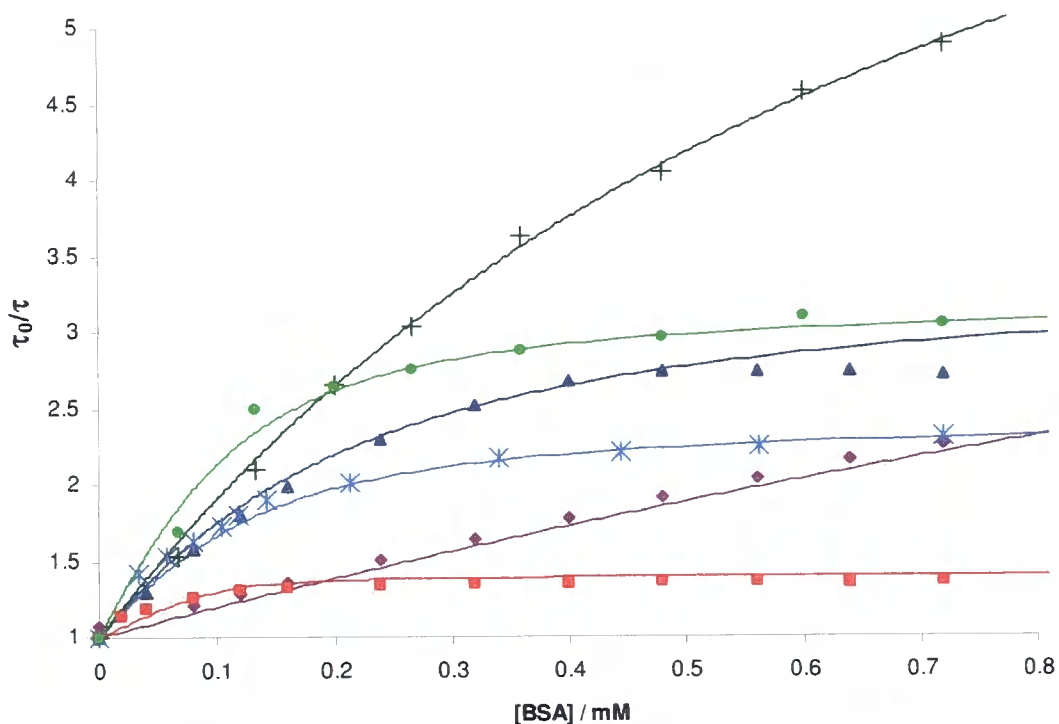


**Figure 2.21:** Quenching of luminescence lifetimes of terbium complexes by bovine serum albumin, showing the fit to a 1:1 apparent binding constant derived by least squares iterative analysis.  $[\text{Tb.L}^1]$  ( $\blacklozenge$ ),  $[\text{Tb.L}^2]$  ( $\blacksquare$ ),  $[\text{Tb.L}^{3a}]^{3+}$  ( $\blacktriangle$ ),  $[\text{Tb.L}^{3b}]^{3+}$  ( $*$ ),  $[\text{Tb.L}^{4a}]$  ( $+$ ) and  $[\text{Tb.L}^{4b}]$  ( $\bullet$ ) (100 mM HEPES, 10 mM NaCl, pH 7.4, 30  $\mu\text{M}$  complex)

Two factors must be considered in analysing these results: the limiting lifetime change observed, which gives information about the quenching properties of BSA, and the form of the curve, which allows calculation of a binding constant,  $K_a$ . The latter is of greater interest towards understanding the cellular behaviour of luminescent lanthanides. The  $K_a$  values for BSA binding were calculated by non-linear least squares fitting of the curve to the observed data points (Table 2.5).

**Table 2.5:**  $K_a$  values for binding of complexes to BSA (100 mM HEPES, 10 mM NaCl, pH 7.4, 30  $\mu$ M complex)

Complex	$K_a$ for protein binding / M	Limiting $\tau_0/\tau$ value
[Tb.L <sup>1</sup> ]	$(3.24 \pm 0.02) \times 10^2$	7.5
[Tb.L <sup>2</sup> ] <sup>3+</sup>	$(1.18 \pm 0.26) \times 10^5$	1.4
[Tb.L <sup>3a</sup> ] <sup>3+</sup>	$(6.60 \pm 0.11) \times 10^3$	3.4
[Tb.L <sup>3b</sup> ] <sup>3+</sup>	$(9.44 \pm 0.10) \times 10^2$	3.2
[Eu.L <sup>3b</sup> ] <sup>3+</sup>	$(2.57 \pm 0.07) \times 10^3$	1.8
[Tb.L <sup>4a</sup> ]	$(1.46 \pm 0.09) \times 10^3$	7.6
[Tb.L <sup>4b</sup> ]	$(2.14 \pm 0.15) \times 10^4$	3.2
[Eu.L <sup>4b</sup> ] <sup>3+</sup>	$(3.58 \pm 0.10) \times 10^3$	1.8

Protein affinities were calculated based on the assumption of a 1:1 binding stoichiometry, using equation 2.7:

$$[BSA] = \frac{\frac{f}{K} + [Eu]f - [Eu]f^2}{1 - f} \quad [2.7]$$

where

$$f = \frac{L - L_i}{L_f - L_i}$$

$$L = \text{luminescence lifetime } \frac{\tau_0}{\tau}$$

$L_i$  = initial luminescence lifetime

$L_f$  = limiting luminescence lifetime

The results show a marked variation in the  $K_a$  values across the range of complexes; from the more weakly-bound [Tb.L<sup>1</sup>] and [Tb.L<sup>3b</sup>] to the very strongly-bound [Tb.L<sup>2</sup>]<sup>3+</sup>. With its more hydrophobic pendant arms leading to a smaller surface area accessible to solvent, the Phe-based complex [Tb.L<sup>3b</sup>]<sup>3+</sup> might be expected to bind more strongly to BSA than the Ala-based [Tb.L<sup>3a</sup>]<sup>3+</sup>. This is not supported by the observed affinity constants (Table 2.5), which could reflect the different solution structure adopted by this complex, as discussed in Section 2.3.

## 2.5 Preliminary studies of cellular behaviour

The aim of the work reported in this thesis is to investigate the cellular behaviour of a large group of luminescent lanthanide complexes, of which these Ala- and Phe-derived complexes comprise one sub-group. The structural changes which result on substituting alanine for phenylalanine in the pendant arms allow an investigation of the effects of geometry on cellular behaviour. The following section details the preliminary microscopy studies which were performed to investigate the uptake and localisation profile of the four complexes.

Two cell lines were selected for preliminary studies; CHO (Chinese Hamster Ovary) cells and NIH 3T3 cells, which are derived from the mouse embryonic fibroblast (connective tissue). Both cell lines are transformed, and comprise adherent cells, which grow in a monolayer. Cells were grown to 60-80% confluence on glass coverslips, and the medium dosed with complex at concentrations ranging from 50 to 200  $\mu\text{M}$  for incubation times from 5 min to 24 h. The coverslips were then mounted onto microscope slides, and the cells visualised using an epifluorescence microscope. Transmitted light was used to obtain a light image, and appropriate filter sets were selected to measure Eu or Tb luminescence following excitation of the chromophore. Representative images of cells treated with Tb complexes are shown in Figure 2.22.

Incubation of both CHO and NIH 3T3 cells with each Tb complex resulted in luminescence that could be readily detected. When optical sections throughout the cell were taken, this luminescence could be observed in most layers, confirming that the complexes were successfully taken up into the cells, and were not merely associating with the cell membrane. As expected, untreated control cells exhibited no luminescence. While only one set of images for each condition is shown here, images were taken at a number of points across the slide, with similar localisation patterns observed at each position.

From these microscope images, there appears to be no luminescence in the nucleus, with luminescence localised in other organelles in the cytoplasm. The appearance of these organelles is most consistent with the size and distribution of late endosomes or lysosomes.

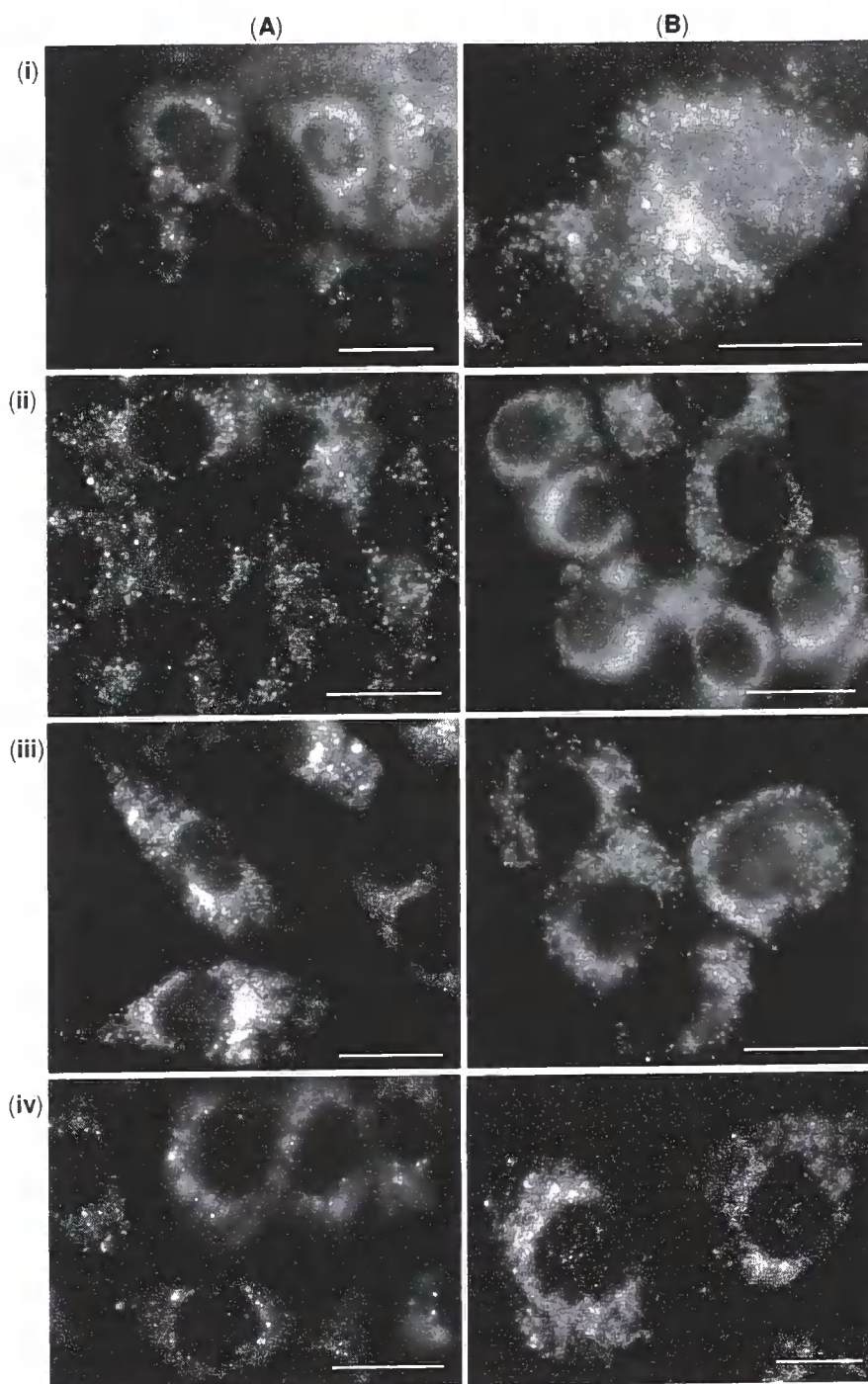


**Figure 2.22:** Microscope images of cells treated for 3 hours with 50  $\mu\text{M}$  complexes. (A) CHO cells and (B) NIH 3T3 cells treated with (i)  $[\text{Tb.L}^{3a}]^{3+}$ , (ii)  $[\text{Tb.L}^{3b}]^{3+}$ , (iii)  $[\text{Tb.L}^{4a}]$  and (iv)  $[\text{Tb.L}^{4b}]$ . G365 ex. filter, BP 546 $\pm$ 12 em. filter. Image brightness and contrast have been altered. Scale bars represent 20  $\mu\text{m}$ .

The observed localisation was confirmed by the use of LysoTracker probes, which are commercially available lysosomal stains.<sup>131</sup> An example of a co-localisation study is

shown in Figure 2.23. The yellow colour in the overlay image confirms co-localisation of the europium luminescence and the LysoTracker green fluorescence.

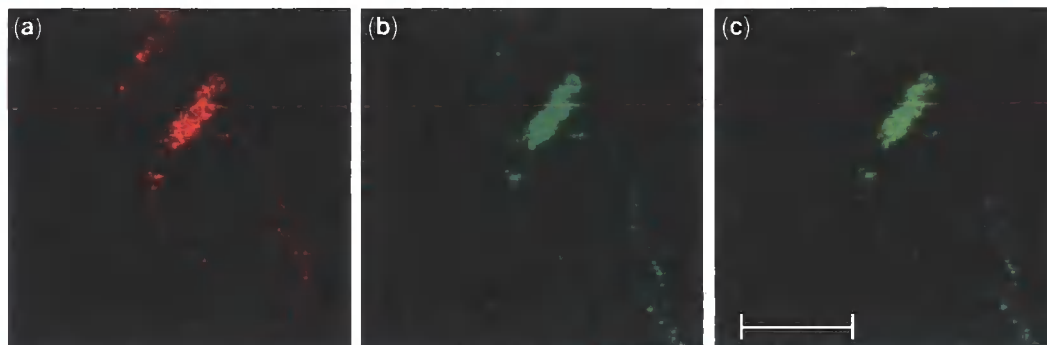


**Figure 2.23:** Fluorescence microscopy images of (a) (SSS)-[Eu.L<sup>3b</sup>]<sup>3+</sup> in NIH-3T3 cells (50 μM complex, 4h incubation), (b) LysoTracker Green<sup>TM</sup> and (c) an overlay of the two channels. Scale bar represents 20 μm.

Cells treated with the (*RRR*)-isomers of these four complexes showed similar, lysosomal localisation under the same conditions. The luminescence was also of similar intensity. There also appeared to be no difference between the intensity and localisation of luminescence from Eu complexes and Tb complexes. While each complex showed a similar localisation pattern, luminescence output varied across the set. It was not possible to gain quantitative measures of the luminescence of the system with the fluorescence microscope set-up, but alterations in the signal contrast required to give approximately equal intensities allowed a rough measure of the absolute intensity. By this method, it could be observed that cells treated with [Ln.L<sup>3a</sup>]<sup>3+</sup> and [Ln.L<sup>4a</sup>] exhibited greater luminescence than those treated with [Ln.L<sup>3b</sup>]<sup>3+</sup> and [Ln.L<sup>4b</sup>]. This could reflect a higher cellular uptake of the Ala-derived complexes, or lesser *in cellulo* quenching. Such effects will be discussed in Chapter Four. Notably, however, these trends follow the quenching data, which show that the Ala-derived complexes are less susceptible to quenching by both common cellular reductants and by BSA.

What can initially be concluded from these microscopy experiments is that changes to the charge and helicity of lanthanide complexes do not appear to affect the localisation, with sequestration of all complexes to the lysosomes or late endosomes.

## 2.6 Conclusions

This thesis investigates the cellular behaviour of a broad range of luminescent lanthanide complexes which have been synthesised recently within the Parker group. This chapter has described the synthesis, characterisation and preliminary cellular studies of one class of such complexes. While the aim of the synthesis was to generate a set of related complexes which differed only in charge and hydrophobicity, the structural analysis also revealed a variation in helicity within the group. A change in the hydrophobicity of the pendant arms, through an additional phenyl group, resulted in an inversion of the helicity, which was also accompanied by a change in the nature of the “capping” donor.

Studies of the changes in the luminescence lifetime with the addition of common cellular anions revealed varying degrees of susceptibility to quenching. Quenching of the luminescence lifetimes by BSA allowed calculation of an apparent binding constant, which varied markedly across the group of complexes. These quenching effects will be discussed in greater detail in Chapters Four and Five.

Preliminary cellular studies using these complexes demonstrated uptake and lysosomal localisation of every complex. This behaviour was independent of complex charge, identity of the lanthanide ion, chirality of the pendant arms, nature of the axial donor atom, and the overall complex helicity. These complexes are therefore examples of luminescent lanthanide complexes which exhibit interesting cellular behaviour, and will be included amongst the wider range of complexes discussed in the following chapters.

## CHAPTER THREE

---

# **SUB-CELLULAR LOCALISATION OF COMPLEXES**

### 3.1 Introduction

Organelle-specific targeting remains a current challenge in biology and medicine alike.<sup>132</sup> From a therapeutic view-point, delivery of a drug to its target organelle can increase efficacy and reduce toxic side-effects. For example, gene therapy drugs act in the nuclei while many cancer therapeutic agents exert their effects in the mitochondria. From an imaging perspective, the conditions within a specific organelle can give the most useful information about a disease state. A number of lysosomal storage diseases are characterised by an elevated lysosomal pH, while the cytoplasmic pH is only minimally perturbed.<sup>133</sup> Similarly, an increase in mitochondrial  $\text{Ca}^{2+}$  levels, but not intracellular  $\text{Ca}^{2+}$  levels, has been implicated in the mitochondrial dysfunction that accompanies aging and ischaemia.<sup>134</sup> An increased understanding of biological function and dysfunction therefore requires the ability to probe the conditions within specific organelles. In order to achieve this, a cellular probe must be delivered to the relevant sub-cellular location about which it is to report.

#### 3.1.1 Mechanisms of sub-cellular trafficking

The factors and processes involved in compartmentalisation of molecules into sub-cellular organelles are not well understood, particularly with respect to exogenous species. Indeed, the current understanding is primarily based on studies of the processing and trafficking of proteins following ribosomal synthesis. In studying trafficking processes, it is important to consider a number of aspects: the signal which triggers a specific localisation, the pathways by which a molecule can enter an organelle, and the mechanical process by which species can be moved within the cell.

The sub-cellular fate of a protein depends on a region of the amino acid sequence, the sorting signal, which directs its delivery to a particular location in the cell.<sup>135, 136</sup> For example, a lysine- and arginine-rich sequence signals import into the nucleus. The sorting signal is recognised by complementary receptor proteins which may be involved in translocation or membrane transport. Such sorting signals occur only on proteins; the structural features which signal compartmentalisation of non-protein species are not understood.

An important aspect of sub-cellular trafficking is transport into an organelle. This can occur by three distinct mechanisms, which vary according to the nature of the organelle (Figure 3.1).<sup>80</sup> Gated transport describes the traffic between the cytosol and the nucleus, which occurs through nuclear pore complexes. Transmembrane transport describes the movement of species through protein translocators from the cytosol to the interior of the mitochondria, peroxisomes, plastids and endoplasmic reticulum. In vesicular transport, species are ferried between compartments by the consecutive budding and fusion of vesicles.<sup>137</sup>

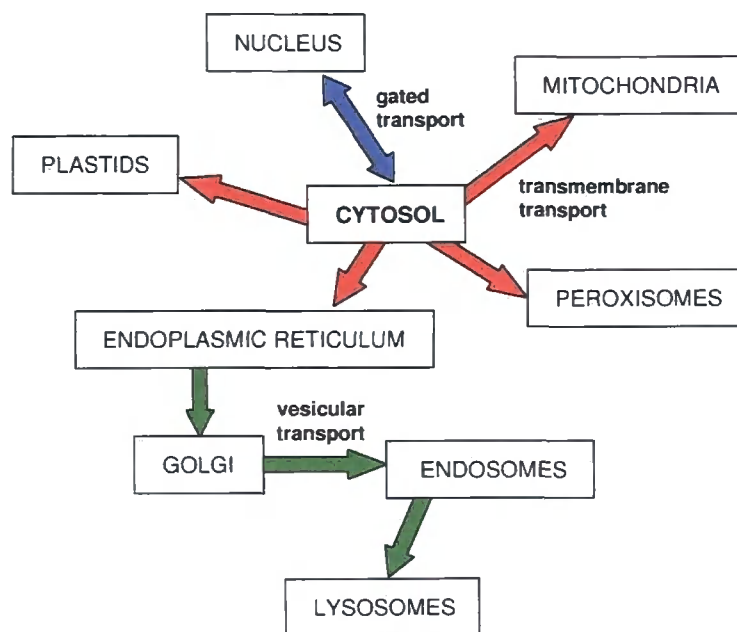


**Figure 3.1:** Schematic diagram showing transport of species between compartments by gated transport (blue), transmembrane transport (red) or vesicular transport (green). Adapted from Alberts *et al.*<sup>80</sup>

Finally, the mechanisms by which a compound can be physically moved within the cell, from one organelle to another, must be considered. The cytoskeleton is the system of filaments with varied roles such as the maintenance of asymmetrical cell shape, the provision of the scaffolding for the development of the cell and the transportation of species within the cell.<sup>80, 138</sup> The primary cytoskeletal elements are microtubules, which are composed chiefly of the protein tubulin, and microfilaments, which are composed of actin.<sup>139</sup> Transportation within the cell requires the coupling of motor proteins to the cytoskeleton. The principal members the family of motor proteins are kinensin and dynein, which bind to microtubules and use the energy from ATP hydrolysis to move

towards the ends of the filament.<sup>140</sup> Kinensins move species towards the cell surface, while dyneins are involved in trafficking towards the interior of the cell.

While these mechanisms relate to proteins and not to exogenous species, they can contribute to an understanding of the factors which affect the localisation of lanthanide complexes. For example, it might be expected that there is some structural signal which determines the final sub-cellular distribution of a complex. It is also feasible that the motor proteins are involved in the trafficking of the complex around the cell.

### 3.1.2 Strategies for controlling localisation

Despite the current paucity of knowledge about sub-cellular trafficking pathways, a number of strategies have been developed to assist the delivery of probes to specific organelles. One strategy for the control of sub-cellular localisation is to encapsulate the compound within a liposome, which usually results in a lysosomal localisation.<sup>132</sup> Liposomes are generally internalised by endocytosis into a vesicle which then fuses with an endosome.<sup>141</sup> Lysosomes are the downstream compartment in this endocytotic pathway, and it is therefore likely that the compound will remain in the lysosome.

Another method by which compounds can be directed to a particular sub-cellular location is through the identification of structural features which affect localisation. This has particular success in achieving mitochondrial localisation. The term mitochondriotropic is used to describe complexes which are rapidly internalised in the mitochondria. In general, these complexes are cationic, as their positive charge is attracted to the negatively charged mitochondrial membrane, and amphiphilic, allowing them to cross both outer and inner mitochondrial membranes.<sup>142</sup> Based on these characteristics, a number of structurally diverse mitochondriotropic compounds have been synthesised, such as rhodamine 123,<sup>143</sup> the gold antitumour complex auranofin<sup>144</sup> and a tetraguanidinium compound<sup>145</sup> (Figure 3.2).

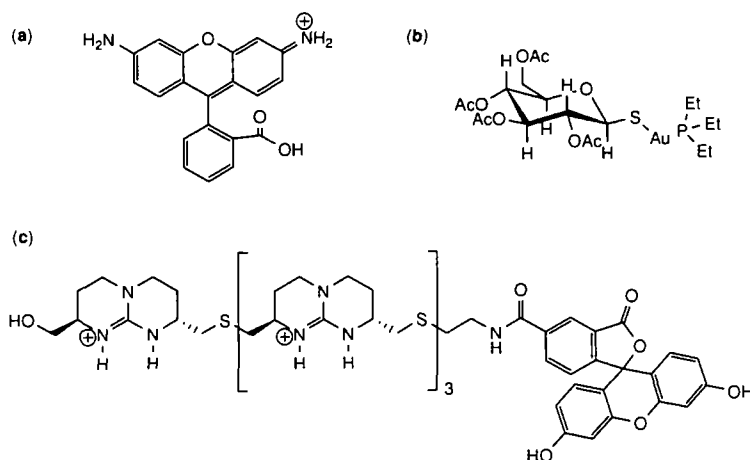


**Figure 3.2:** Compounds which localise in the mitochondria. (a) rhodamine 123, (b) auranofin, (c) tetraguanidinium vector

An additional strategy by which the location of compounds can be controlled is through conjugation to moieties which themselves exert control over localisation. Such groups are commonly peptide-based, and often contain a natural or synthetic signal peptide such as those used in trafficking proteins.<sup>146</sup> For example, the conjugation of a nuclear localisation sequence (NLS) to a platinum complex has been demonstrated to give rise exclusively to nuclear localisation (Figure 3.3).<sup>147</sup>

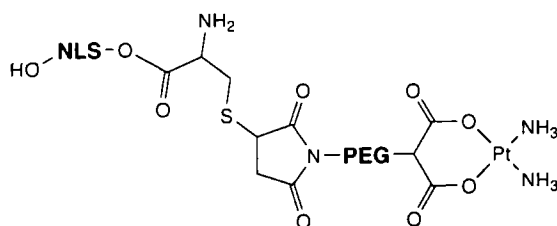


**Figure 3.3:** A carboplatin-based complex which has been modified to localise in the nucleus. NLS = nuclear localisation sequence (Cys-Gly-Gly-Pro-Lys-Lys-Lys-Arg-Lys-Val-Gly-Gly), PEG = polyethylene glycol.

### 3.1.3 Localisation of lanthanide complexes

In order to develop luminescent lanthanide complexes for use as cellular probes, it is essential to gain an understanding of the manner and mechanism of their sub-cellular localisation. To date, such investigations have been limited to preliminary observation of the distribution of some complexes in cells by fluorescence microscopy, as discussed in

Section 1.5.2. In this way, complexes have been observed which localise to the nucleoli,<sup>82, 102</sup> lysosomes<sup>73, 101</sup> and endoplasmic reticulum.<sup>84</sup>

This chapter describes the work which was performed to broaden the understanding of the localisation behaviour of luminescent lanthanide complexes. Complexes will be categorised according to distinctive behaviours and structure-activity relationships described.

### 3.2 Overview

Work at Durham over the past eight years has generated a library of over seventy luminescent lanthanide complexes. This range of complexes allows for the study of structure-activity relationships, and the selection of the most suitable complexes for further mechanistic studies. All complexes are based on the macrocyclic core of cyclen, and have a similar common structure (Figure 3.4) consisting of a heterocyclic sensitising moiety and two or three pendant arms which may be carboxylate, amide or phosphinate based.

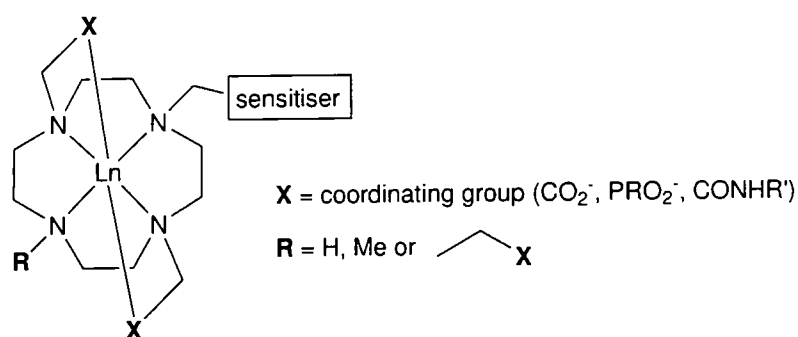
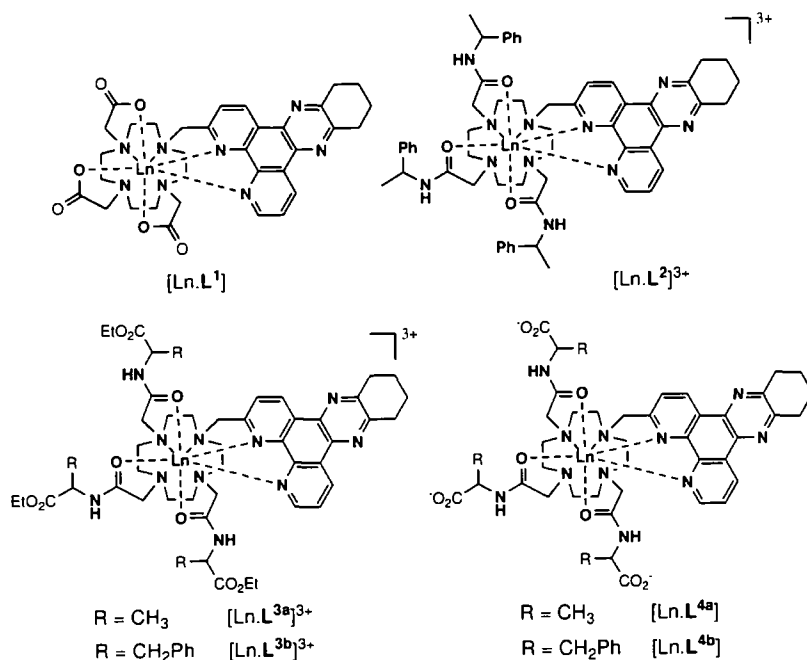


**Figure 3.4:** Generic structure of the luminescent lanthanide complexes under study.

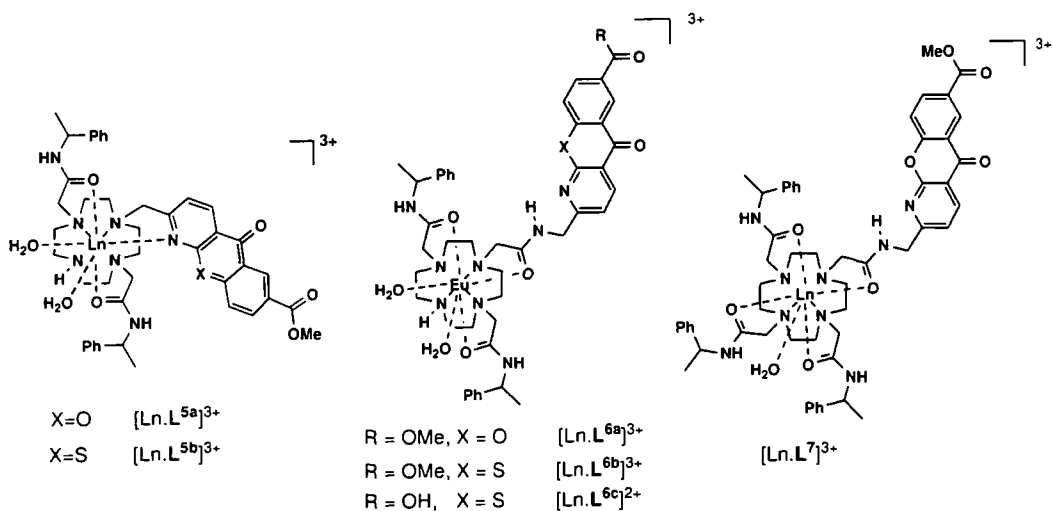
It is not possible to study in detail each member of the library. Accordingly, a subset of complexes has been selected for further study throughout the remainder of this thesis (Appendix 1). The following section gives general details of each complex.

## 3.2.1 Complexes selected for further study

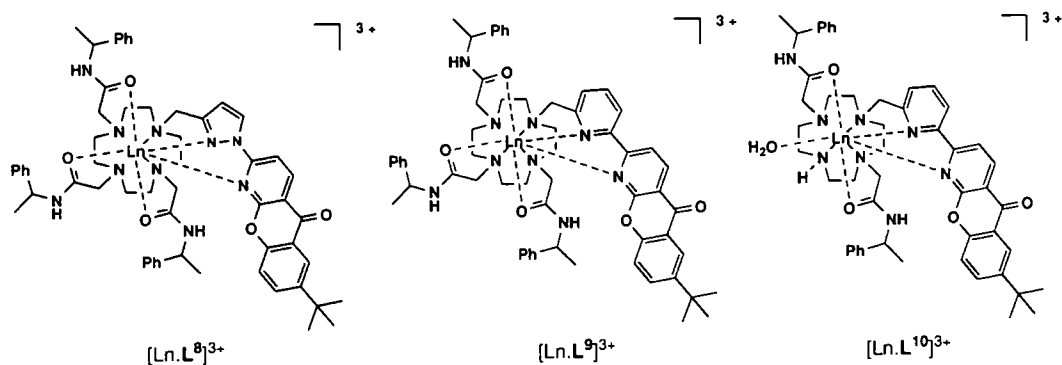
The first set of complexes, containing ligands  $L^1$  to  $L^4$  were described and characterised in Chapter Two.



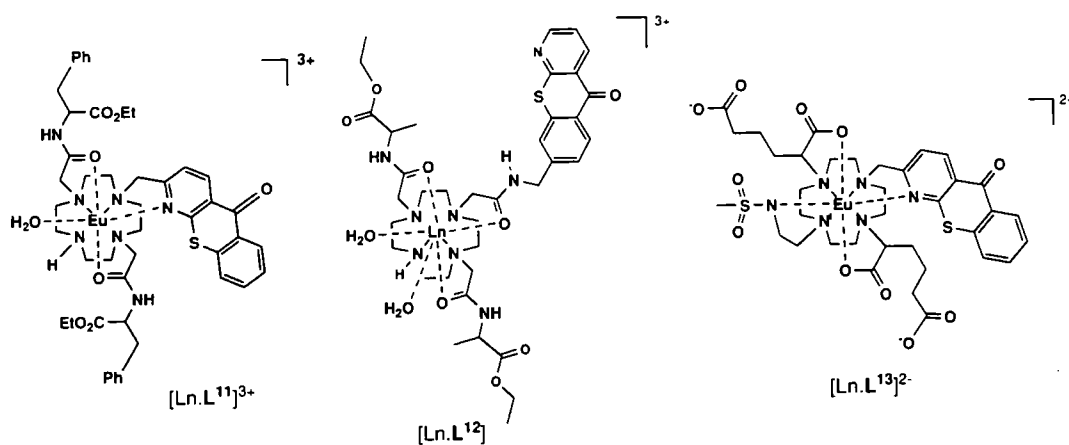
Ligands  $L^5$  to  $L^7$  were synthesised by Benjamin Murray in an investigation of the anion binding properties of luminescent lanthanide complexes.<sup>108, 148</sup> The complexes contain azaxanthone or azathioxanthone chromophores.  $L^5$  and  $L^6$  differ in the nature of the linkage between the chromophore and the cyclen ring.  $L^7$  is the octadentate analogue of  $L^6$ , containing three additional pendant arms rather than two.



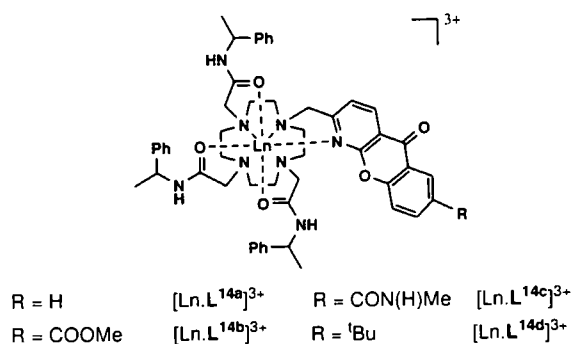
Complexes based on ligands  $L^8$  to  $L^{10}$  were synthesised by Craig Montgomery in his investigations of luminescent lanthanide complexes for FRET applications.<sup>149-151</sup> The pyrazoyl- and pyridylazaxanthone complexes were demonstrated to give rise to very high overall emission quantum yields.



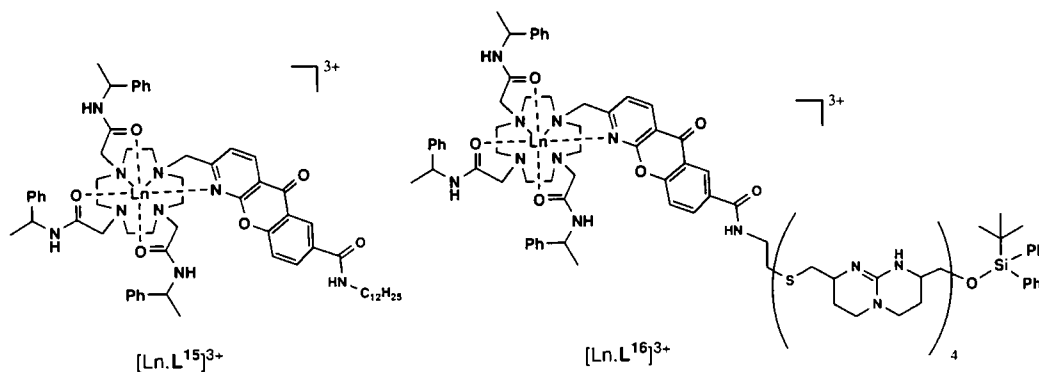
$[Ln.L^{11}]^{3+}$  was synthesised by Junhua Yu as an anion sensor.<sup>152</sup>  $[Ln.L^{12}]^{3+}$  was synthesised by Robert Pal for the same purpose.<sup>108, 153</sup>  $[Ln.L^{13}]^{2-}$  was also synthesised by Robert Pal, for use as a pH probe.<sup>82, 154</sup> All three sets of complexes contain an azathiaxanthone chromophore.



Ligand  $L^{14}$  contains an azaxanthone chromophore with various groups at the 7-position.<sup>75, 155</sup> These complexes were synthesised by Siobhan Richardson, Filip Kielar and Philip Stenson.



Complexes based on ligands  $L^{15}$  and  $L^{16}$  were synthesised by Filip Kielar in an investigation of methods which could be employed to alter biological behaviour.<sup>156, 157</sup>  $[\text{Ln.L}^{15}]^{3+}$  contains a  $C_{12}$  chain, while  $[\text{Ln.L}^{16}]^{3+}$  was synthesised by conjugation to an oligoguanidinium moiety.



### 3.3 Classification of complexes

Cellular localisation behaviour of the luminescent lanthanide complexes presented above was examined by fluorescence microscopy. CHO, NIH 3T3 or HeLa cells were grown as confluent monolayers on a glass coverslip, and were incubated with complexes at varying concentrations (20  $\mu\text{M}$  to 1 mM) for various periods of time (5 min to 1 h). The coverslips were subsequently mounted onto glass slides and the cells visualised on a fluorescence microscope. For all complexes, the G365 excitation filter (Zeiss) was used, which allowed the passage of light between 300 and 400 nm. For terbium complexes, a  $546 \pm 12$  nm band pass filter (Comar) was employed, while europium complexes were visualised with a 575–625 nm band pass filter (Zeiss). In this way, the distribution of the emissive lanthanide species in the cell could be observed. Localisation was confirmed by use of commercially available cellular stains (Invitrogen). Red stains were used for

terbium, and green stains for europium to ensure minimal overlap between the complex luminescence and the excitation of the fluorophore. The complexes studied could be classified into four groups according to their sub-cellular localisation. While the complexes in each group were found to have remarkably similar biological properties, each class exhibited distinct behaviour. The four classes and their principal characteristics will be discussed briefly.

### 3.3.1 Lysosomally-localising complexes

The largest group of complexes are those which are observed to localise to the lysosomes. A single cell contains an average of 300 lysosomes, which are membrane-bound organelles of variable size. They contain powerful hydrolytic enzymes which digest waste material, whether ingested foreign bodies, worn-out organelles or engulfed viruses.<sup>139</sup> Lysosomes are characterised by their low luminal pH, of between 4 and 5. In general, internalisation into the lysosomes seems to be the default pathway for ingested particles, which may arise from one of two main mechanisms. If the particle has been taken into the cell by receptor-mediated endocytosis, it will reside in an endosome which will age to become a lysosomal compartment, unless it can escape in some manner.<sup>158</sup> If a particle which is not located in the lysosomes is recognised as being foreign, it is likely to be ubiquitinated and transported to the lysosome for subsequent degradation.<sup>80</sup>

It appears that in the case of the range of luminescent lanthanide complexes studied, localisation in the lysosomes is the default situation. Complexes with all manner of structure were observed to be distributed throughout lysosomal or late endosomal bodies. This localisation was confirmed by co-staining with LysoTracker probes (Invitrogen). Example fluorescence microscopy images of luminescence from complexes which have localised in the lysosomes are shown in Figure 3.5.

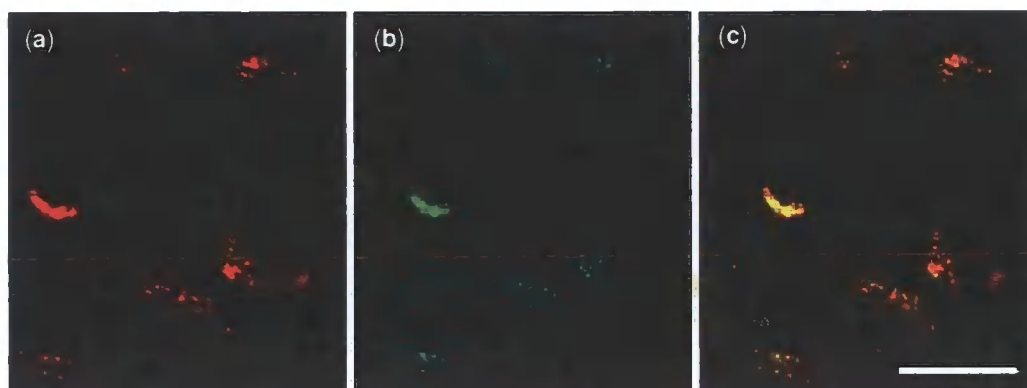
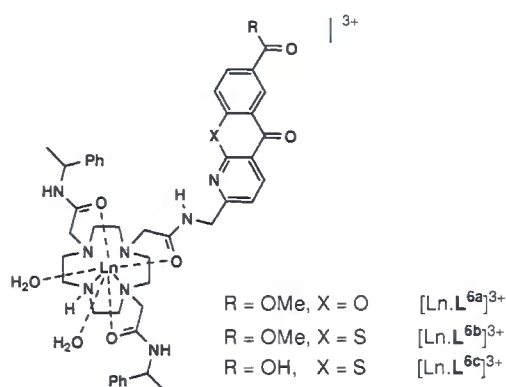


**Figure 3.5:** Fluorescence microscopy images of CHO cells treated with  $[\text{Eu.L}^2]\text{Cl}_3$  ( $50 \mu\text{M}$ , 4h) and LysoTracker Green (LTG;  $100 \text{ nM}$ , 15 min). (a) Europium luminescence, (b) LTG fluorescence, (c) image overlay. Scale bar represents  $20 \mu\text{m}$ . Image brightness and contrast have been adjusted.

### 3.3.2 Mitochondrially-localising complexes

In contrast to the lysosomally-localising complexes, a much smaller group of complexes was observed to localise to the mitochondria. Mitochondria are centres of aerobic respiration through the electron-transport chain and oxidative phosphorylation.<sup>159</sup> Most importantly, they are involved in the generation of adenosine triphosphate (ATP), which is an essential energy source for many cellular processes.<sup>160</sup>



The europium and terbium complexes of three related ligands,  $\text{L}^6$ , exhibited mitochondrial localisation following incubation times of 5 min to 12 h.<sup>108</sup> Localisation was confirmed by co-staining with MitoTracker probes (Invitrogen; Figure 3.6a). After 24 h incubation, the luminescence pattern was no longer consistent with a mitochondrial distribution, but instead co-localised with LysoTracker probes (Figure 3.6b). After a further 12 h incubation, very little luminescence could be observed within the cell. This

suggests that after longer periods of time, the complexes are being transported to the lysosomes for degradation and removal from the cell.

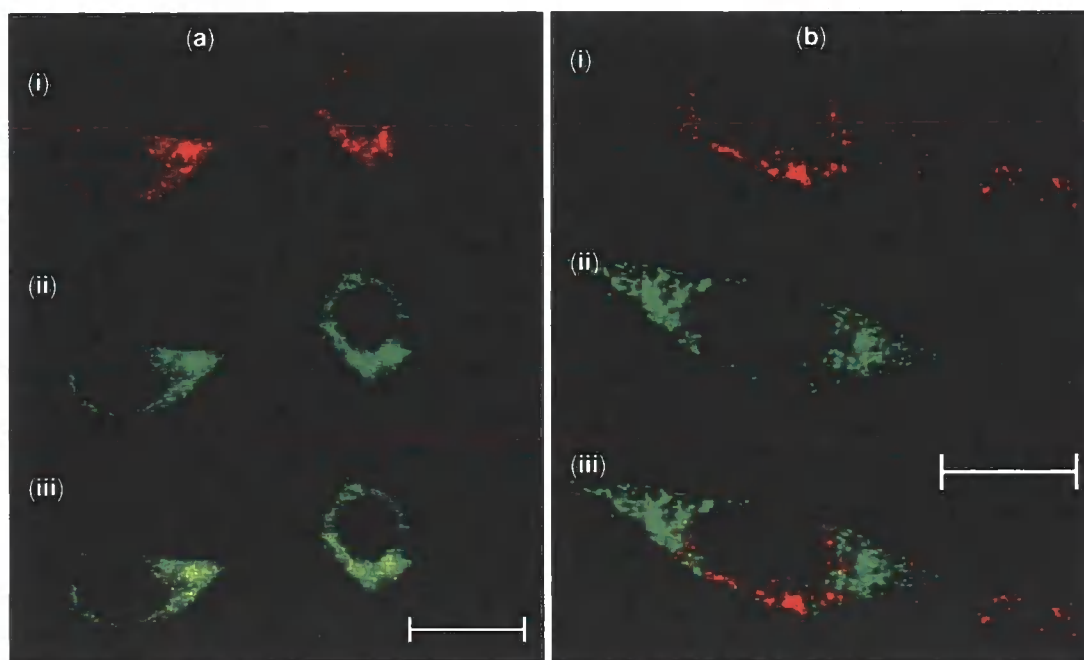
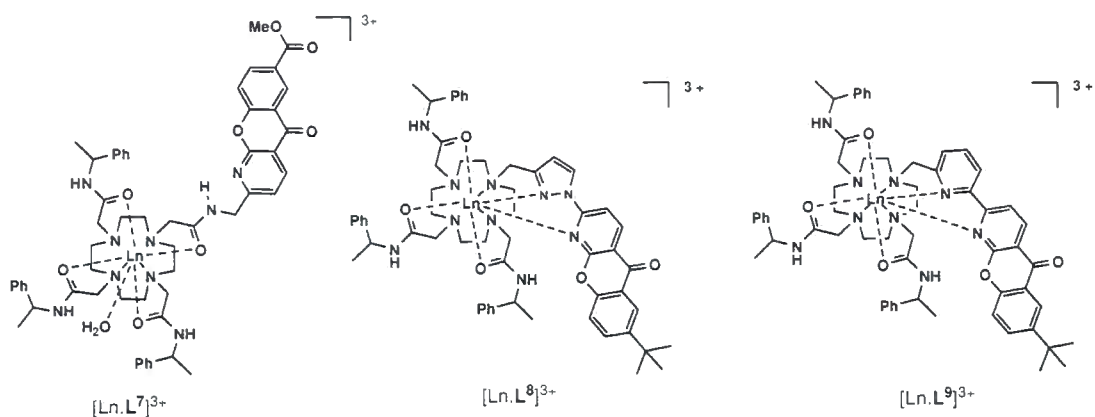


**Figure 3.6:** Fluorescence microscopy images of CHO cells treated with  $[\text{Eu.L}^{6\text{c}}]^{2+}$  ( $50 \mu\text{M}$ ) and MitoTracker Green (MTG;  $200 \text{ nM}$ ,  $15 \text{ min}$ ) for (a)  $4 \text{ h}$  and (b)  $24 \text{ h}$  showing (i) Eu luminescence, (ii) MTG fluorescence and (iii) overlay image. Scale bar represents  $20 \mu\text{m}$ . Image brightness and contrast have been altered.

### 3.3.3 Complexes which localise to the mitochondria and lysosomes

The complexes described above exhibit distinct distribution patterns, with observed localisation in only one organelle. An additional class of complexes appear to be simultaneously localised in both the lysosomes and the mitochondria.<sup>151</sup> These complexes;  $[\text{Ln.L}^7]^{3+}$ ,  $[\text{Ln.L}^8]^{3+}$  and  $[\text{Ln.L}^9]^{3+}$ , contain azaxanthone chromophores which are coupled to the cyclen ring through a pyrazole, pyridine and amide group respectively.



The localisation profile was confirmed by co-staining with LysoTracker and MitoTracker probes, in which both probes showed overlapping fluorescence with the lanthanide luminescence profile. For example, the localisation of Eu luminescence from  $[Eu.L^9]Cl_3$  does not completely overlap with either LTG or MTG fluorescence (Figure 3.7). Both the bright spots consistent with lysosomal staining, and the more diffuse pattern characteristic of mitochondrial localisation can be observed.

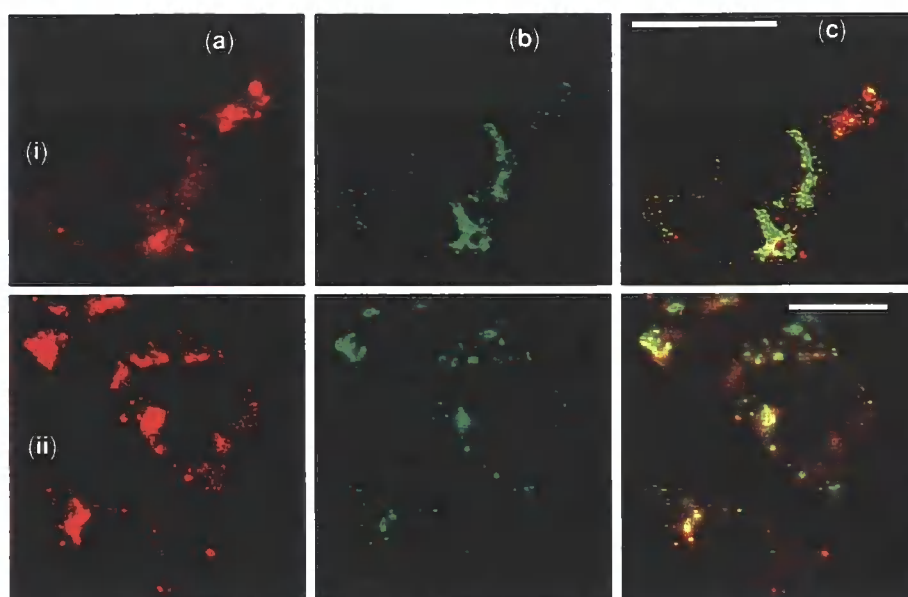


**Figure 3.7:** Fluorescence microscopy images of CHO cells treated with  $[Eu.L^9]Cl_3$  (50  $\mu$ M, 4h) and (i) MitoTracker green or (ii) LysoTracker green. (a) Eu luminescence, (b) tracker luminescence, (c) overlay image. Scale bar represents 20  $\mu$ m. Image brightness and contrast have been altered.

### 3.3.4 Complexes which localise to the nucleoli

The nucleolus is a sub-nuclear, protein-rich structure which is primarily involved in ribosome assembly.<sup>161</sup> The first complex which was observed to show nuclear localisation was  $[\text{Eu.2}]^{3+}$ , when administered to cells at relatively high concentrations and for long incubation times.<sup>73</sup> Subsequently,  $[\text{Eu.L}^{11}]^{3+}$ , which was synthesised as a citrate sensor, was observed to localise to the nucleolus.<sup>102</sup> This sub-cellular distribution was confirmed by co-localisation studies with SYTO-RNA (Figure 3.8). The yellow colour visible in the overlay image is evidence of overlap between the red Eu luminescence and the green SYTO fluorescence. The microscope images also reveal luminescence in regions of the cytoplasm. These were interpreted as corresponding to the ribosomes, because of their close functional relationship with the nucleoli.<sup>161</sup> This could not be confirmed, however, as no ribosomal stain is available.

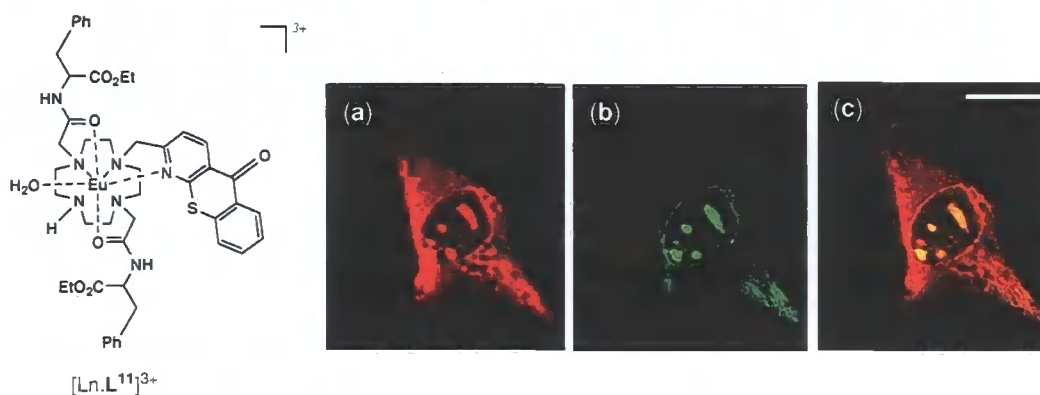
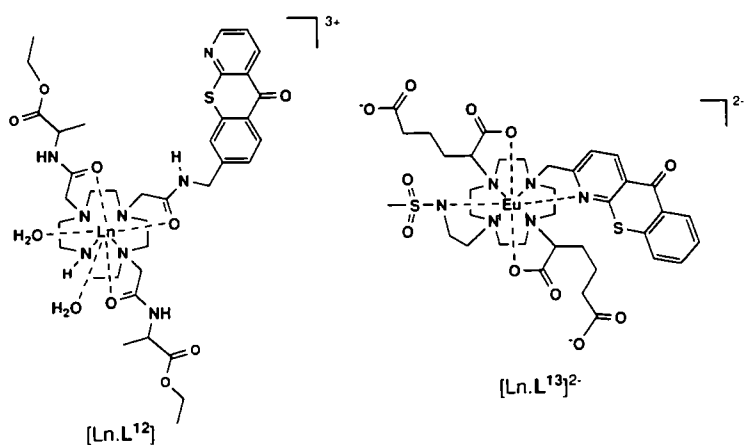


**Figure 3.8:** Confocal microscopy images of NIH 3T3 cells treated with  $[\text{Eu.L}^{11}]$ triflate (100  $\mu\text{M}$ , 4h) and sytoRNA (500 nM, 30 min). (a) Eu luminescence, (b) SYTO fluorescence, (c) overlaid image.<sup>102</sup>

Scale bar represents 10  $\mu\text{m}$ .

Subsequently, a number of complexes have been observed to localise in the nucleolus.<sup>82, 154, 162</sup> These complexes were synthesised as anion or pH sensors, and have structural similarities to  $[\text{Ln.L}^{11}]^{3+}$ , bearing an azathioxanthone chromophore, two amide-based pendant arms and a different group (which may be a free NH, a sulfonamide or a methyl group) on the fourth cyclen nitrogen. For example,  $[\text{Ln.L}^{12}]$  and  $[\text{Ln.L}^{13}]^{2-}$  exhibit nucleolar localisation.



When these localisation experiments described in previous studies were repeated, variable results were found. In particular, the nucleolar distribution of luminescence was not reproducible. Accordingly, the observed nucleolar localisation was studied in more detail.

### 3.4 Understanding nucleolar localisation

Based on the results of previous studies, it was initially believed that the complexes which showed nucleolar localisation belonged to a fourth, distinct group from those exhibiting other localisation behaviours. Attempts to repeat the experiments performed in these studies, however, were unsuccessful, and did not yield reproducible results. Indeed, there were a number of pieces of evidence that nucleolar localisation represented abnormal behaviour.

#### 3.4.1 Evidence for altered behaviour

The first piece of evidence was that attempts to repeat the microscopy studies reported previously failed to show nucleolar localisation in most cases. Instead, localisation appeared to be lysosomal. Figure 3.9 shows the fluorescence microscope image of CHO cells treated with  $[Eu.L^{11}]^{3+}$ , in which there is clearly no luminescence within the nucleus. In cases where nucleolar localisation could be observed, it was in cells which appeared to be detaching from the glass coverslip, and losing membrane integrity. This behaviour is consistent with a loss of viability.



**Figure 3.9:** Fluorescence microscopy images of CHO cells treated with  $[\text{Eu.L}^{11}]\text{Cl}_3$  (100  $\mu\text{M}$ , 4h). Scale bar represents 20  $\mu\text{m}$ . Image brightness and contrast have been altered.

The second piece of evidence was that other complexes which demonstrated clearly lysosomal or mitochondrial localisation, were found to show distribution consistent with the nucleolus when administered at high concentrations.

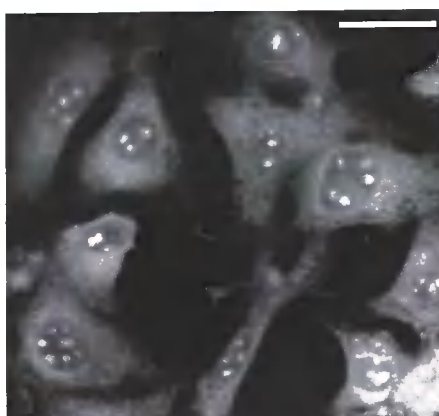


**Figure 3.10:** Fluorescence microscopy images of CHO cells treated with  $[\text{Eu.L}^{4a}]\text{Cl}_3$  (1 mM, 4h). Scale bar represents 20  $\mu\text{m}$ . Image brightness and contrast have been altered.

The final piece of evidence was obtained through the assessment of the cytotoxicity of the complexes. These cytotoxicity measurements and their results will be discussed in detail in Chapter Six. Importantly,  $[\text{Eu.L}^2]\text{Cl}_3$  was found to have an  $\text{IC}_{50}$  value of 110  $\mu\text{M}$ , indicating that only 50% of a cell population is viable after 24 h incubation at this concentration. This indicates that at 1 mM concentrations, the conditions under which nucleolar localisation was observed, most of the cell population would be expected to be non-viable. This was not true, however, of all complexes with demonstrated nucleolar localisation: for other complexes, luminescence had been observed in the nucleolus at concentrations below the  $\text{IC}_{50}$  value. This observation gave

rise to the hypothesis that nucleolar localisation might arise in conditions under which the cell is stressed, and in which the cell membrane has therefore become more permeable. Further studies were therefore performed to test this hypothesis.

### 3.4.2 Studies of a permeabilised membrane

In order to test the hypothesis that nucleolar localisation of lanthanide complexes could be attributed to an increased cellular permeability, the cell membrane was permeabilised according to the method of Johnson *et al.*,<sup>163</sup> in which cells were cooled to 0 °C by incubation with sequentially colder solutions of phosphate-buffered saline (PBS), followed by a 15 min incubation with the permeabilising solution. Cells were then brought back to 37 °C by a series of PBS washes prior to incubation with the complex. Initially, three different permeabilising solutions were used: the surfactant Triton X-100 (1%), the glycoside saponin (0.5 mg/mL) and a 70% ethanol solution. It was found that 70 % ethanol caused cells to become detached from the glass coverslips, so subsequent studies used only Triton X-100 and saponin.

Propidium iodide (PI) was used to confirm successful permeabilisation of the cell membrane. PI is a common DNA stain which is membrane impermeant, and is therefore excluded from viable cells.<sup>164</sup> Examples of complexes which localised in the lysosomes, mitochondria and in both organelles were studied by this method, and gave identical results. Cells treated with both saponin and Triton X-100 also gave similar microscopy images. One set of microscopy images is shown in Figure 3.11. In the absence of the permeabilising agent, the expected luminescence distribution was observed. No PI fluorescence could be seen, which is consistent with an intact cell membrane. Permeabilisation of the cell membrane by saponin or Triton X-100 was confirmed by the PI fluorescence in the nucleus. In the same cells, lanthanide luminescence was now also observed in the nucleolus.

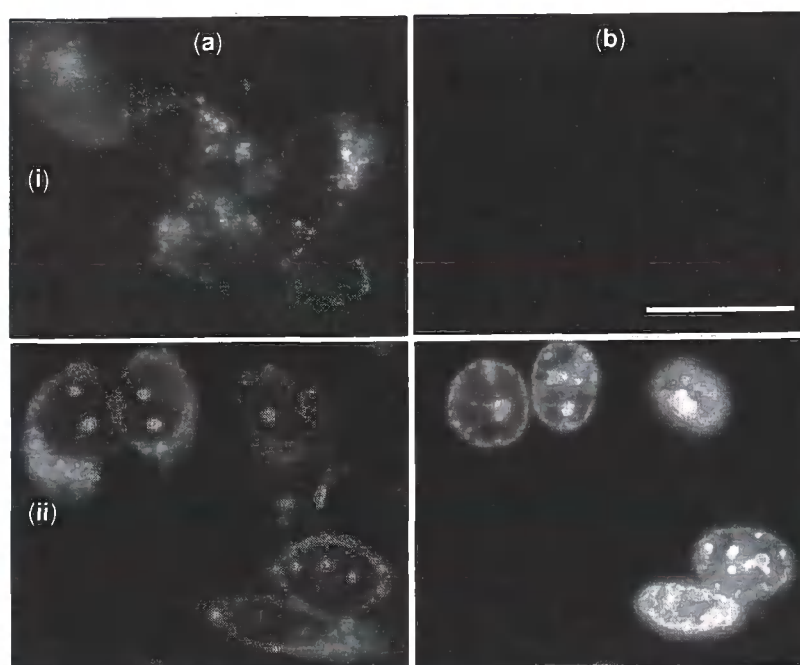


**Figure 3.11:** Fluorescence microscopy of CHO cells treated with  $[\text{Tb.L}^8]\text{Cl}_3$  ( $50 \mu\text{M}$ , 4h) and propidium iodide ( $1 \mu\text{M}$ , 5 min) without (i) and with (ii) saponin treatment ( $0.5 \text{ mg/mL}$ , 15 min). (a) Eu luminescence and (b) propidium fluorescence. Scale bar represents  $20 \mu\text{m}$ .

This experiment provides confirmation of the hypothesis that luminescence in the nucleolus could be attributed to an increased permeability of the cell membrane. This explains why complexes were visualised in the nucleolus when administered to cells at concentrations far above their  $\text{IC}_{50}$  values, as loss of membrane integrity is one of the first events in necrosis.<sup>80</sup> For complexes which were sometimes observed in the nucleoli at lower concentrations, however, this explanation is insufficient. Instead, the complexes themselves must induce permeability in the cell membrane.

One possible explanation for the increased permeability of the cell membrane is the presence of free lanthanide ion in the complex samples. It has previously been demonstrated that low concentrations of lanthanide ions can enhance the permeability of the cell membrane.<sup>165</sup> For example, the addition of  $100 \mu\text{M}$   $\text{TbCl}_3$  to ovarian carcinoma cells led to an eight-fold increase in the uptake of cisplatin.<sup>166</sup> Atomic force microscopy studies revealed that  $\text{Ln}^{3+}$  bound to the cell surface, and induced the formation of pores in the membrane.<sup>167</sup> The optimal  $\text{Ln}^{3+}$  concentration for this effect was found to be  $10 \mu\text{M}$ . It was possible, therefore, that the presence of free  $\text{Ln}^{3+}$  in the complex solution could be causing increased permeability of the cell, leading to nucleolar localisation. This possibility was investigated by performing microscopy studies of CHO cells treated

with 1, 10 or 100  $\mu\text{M}$   $\text{TbCl}_3$  in addition to  $[\text{Tb.L}^8]^{3+}$  or  $[\text{Tb.L}^{14a}]^{3+}$ . In each case, the expected, lysosomal/mitochondrial or lysosomal distribution was observed rather than a nucleolar pattern. In addition, cells were treated with propidium iodide in the presence of  $\text{TbCl}_3$ , but no PI fluorescence was visible in the nucleus. These results indicate that  $\text{Tb}^{3+}$  has not induced sufficient pore formation for the transport of either lanthanide complexes or PI. This suggests that  $\text{Ln}^{3+}$ -induced permeability is unlikely to account for the observed nucleolar localisation.

Another possible reason for this permeabilising effect is that the complexes reported to localise in the nucleolus were administered as triflate salts,<sup>82, 102, 154</sup> while all other experiments reported here involve chloride salts. It is possible, therefore, that the triflate itself is causing the cell membrane to become more permeable. This hypothesis was tested by performing a similar study to that described above, but by pre-treating with sodium triflate (10 mM) rather than saponin. In this study, neither propidium iodide fluorescence nor complex luminescence could be observed in the cell, suggesting that triflate does not induce cell membrane permeability. An alternative explanation is that the cationic complex is able to cross the membrane in the form of an ion pair with the triflate anion. It has previously been shown that triflate anions associate more closely with lanthanide complexes than other anions.<sup>168</sup> The very hydrophobic nature of the triflate anion could contribute to the membrane permeability towards this ion pair.<sup>169</sup>

### 3.4.3 Understanding transport across the nuclear membrane

To this point, the studies which have been described have focussed on the movement of complexes into the cell. It is important to also consider how the complexes reach the nucleoli. In order for complexes to localise in the nucleoli, they must be transported across the nuclear membrane. Small molecules, like PI, can freely diffuse across the nuclear membrane, but most compounds are trafficked through nuclear pore complexes which selectively allow passage of complexes into the nucleus.<sup>170</sup>

Nuclear transport was studied by extracting the nuclei and investigating the processes of trafficking across the membrane of the isolated organelles. Nuclei were extracted using the Nuclei EZ Prep Kit (Sigma). Cells were treated with trypsin to detach them from the flask and incubated on ice with the provided lysis buffer. The resulting contents of the lysed cell were then centrifuged at 500g to pellet the nuclei, which are the most dense of

the sub-cellular components.<sup>171</sup> The pellet was resuspended in lysis buffer, and the mixture centrifuged once again to yield a cleaner nuclear fraction (Figure 3.12).

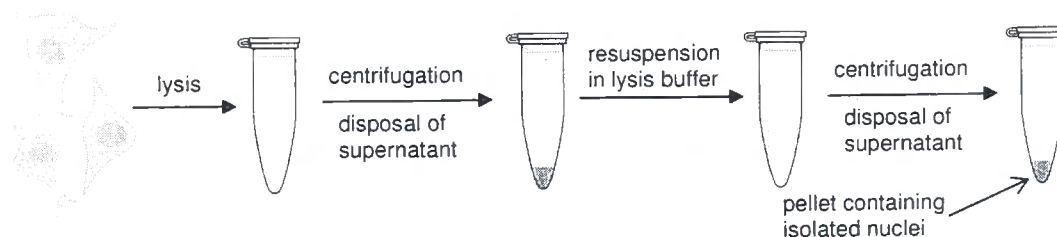


**Figure 3.12:** Schematic diagram showing the process of nuclear extraction.

The nuclei thus obtained could be mounted onto a microscope slide and visualised by fluorescence microscopy, but because of their small size it was difficult to locate individual nuclei by transmission light. Nuclei were therefore stained with trypan blue, a nuclear stain which absorbs strongly in the blue spectral region but is not fluorescent.<sup>172</sup>

In order to study nuclear transport, extracted nuclei were incubated with 50  $\mu\text{M}$  complex for 1 h prior to visualisation by fluorescence microscopy. In addition, some nuclei were treated with PI as a control. Prior to incubation with complex, nuclei were treated for 15 min with one of four substances. Saponin and Triton X-100 were used at dosages similar to the whole cell experiments, in order to assess whether they enhanced complex uptake to the nucleus. The third treatment was lysolecithin (5  $\mu\text{g}/\text{mL}$ ), which inserts itself into lipid membranes and induces permeability.<sup>173</sup> Lysolecithin has been used in a number of studies to permeabilise the nuclear membrane.<sup>174, 175</sup> The final treatment was with sodium triflate (10 mM), to assess the effect of the triflate ion on the nuclear membrane. All complexes studied behaved in nuclei in a similar manner. A representative set of results of the nuclei extraction experiments is shown in Figure 3.13.

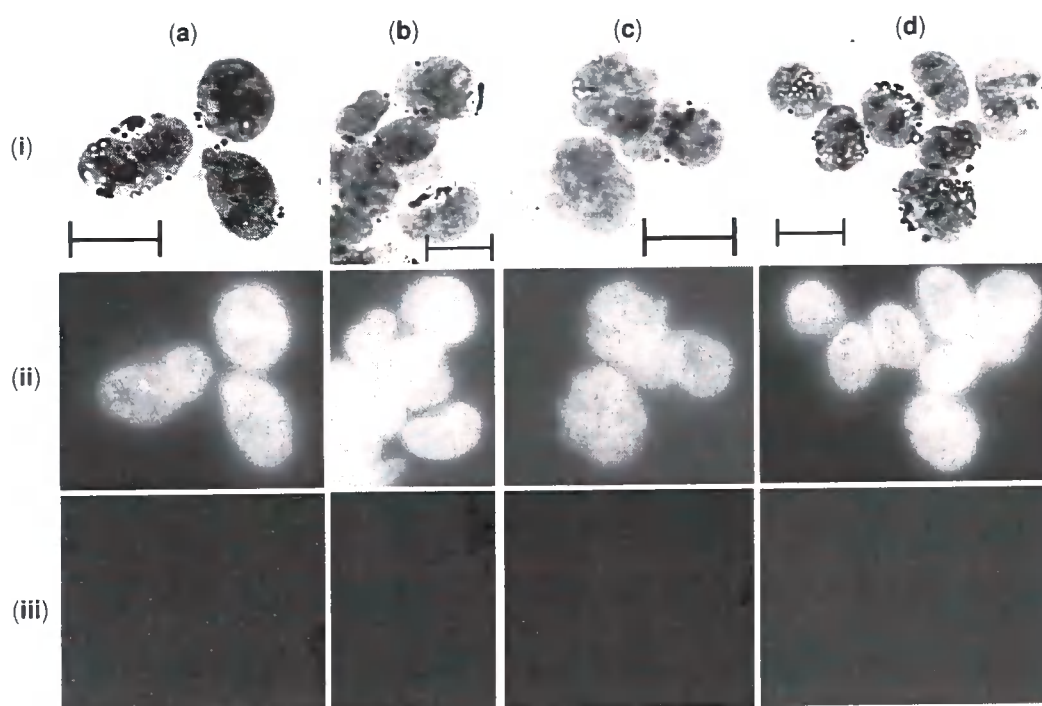


**Figure 3.13:** Fluorescence microscope images of extracted nuclei treated with  $[\text{Tb.L}^8]\text{Cl}_3$  ( $50 \mu\text{M}$ , 1h) and propidium iodide ( $1 \mu\text{M}$ , 5 min) (a) with no pre-treatment and after 15 min pre-treatment with (b) saponin ( $0.5 \text{ mg/mL}$ ), (c) lysolecithin ( $5 \mu\text{g/mL}$ ) and (d) sodium triflate ( $10 \text{ mM}$ ). (i) transmitted light images, (ii) propidium fluorescence, (iii) Tb luminescence. Scale bars represent  $20 \mu\text{m}$ .

The results confirm that the nuclear membrane is permeable to propidium iodide, as it is visible even in nuclei which have not been pre-treated with any permeabilising agent. Unlike PI, however, lanthanide complexes do not passively cross the cell membrane, nor can they be induced to do so by the addition of saponin, Triton X-100 or lysolecithin. This suggests that complex uptake into the nucleus occurs *via* an active transport pathway, which cannot occur in extracted nuclei in the absence of specific cytoplasmic species. The treatment of the nuclei with sodium triflate also failed to induce permeability towards the complexes, indicating that it is not by this means that nucleolar uptake is achieved.

#### 3.4.4 Conclusions regarding nucleolar localisation

These studies have partially elucidated the factors which effect the observed distribution of some complexes in the nucleoli. Complex luminescence in the nucleolus is consistent with systems in which the permeability of the cell membrane has been enhanced. In

some cases, this may be due to the cytotoxic effects of the complexes. For other complexes, which at lower concentrations localise to the nucleoli, the presence of the triflate counterion could contribute to the localisation.

What is clear, however, is that nucleolar localisation only occurs in cells in which some biological processes have been perturbed. These complexes are therefore less promising candidates for use as probes of normal cellular function.

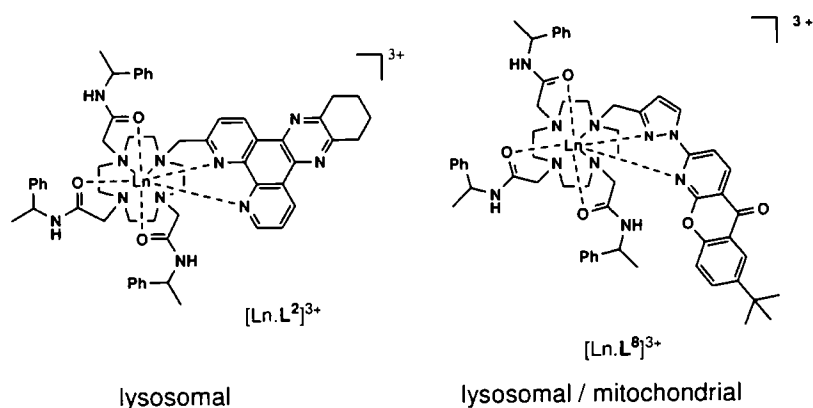
### 3.5 Structural factors affecting localisation

In addition to this group of complexes which show nucleolar localisation under some conditions, the localisation of complexes appears to fall into one of three categories: lysosomal, mitochondrial and a lysosomal-mitochondrial shuttling behaviour. In order to understand these distributions further, it was important to establish any relationships between the structure of a complex and its localisation profile. There are a number of structural aspects which could affect the *in cellulo* distribution pattern of the complex. In order to assess the importance of each structural component, series of complexes were studied in which only one feature was varied. In many cases, more than one series from the total library available was studied in order to confirm the conclusions reached. Only one example for each structural feature is provided here.

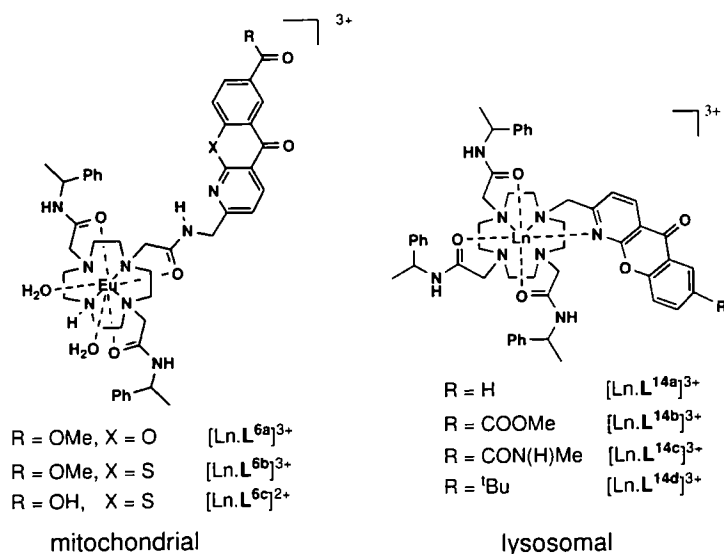
#### 3.5.1 Effect of chromophore

There are a number of ways in which the chromophore can be altered in the synthesis of luminescent lanthanide complexes. The nature of the chromophore itself may vary, or remote substituents altered. In addition, the point of attachment to the cyclen ring, or the linking moiety, can be changed. Each variation will be considered in turn.

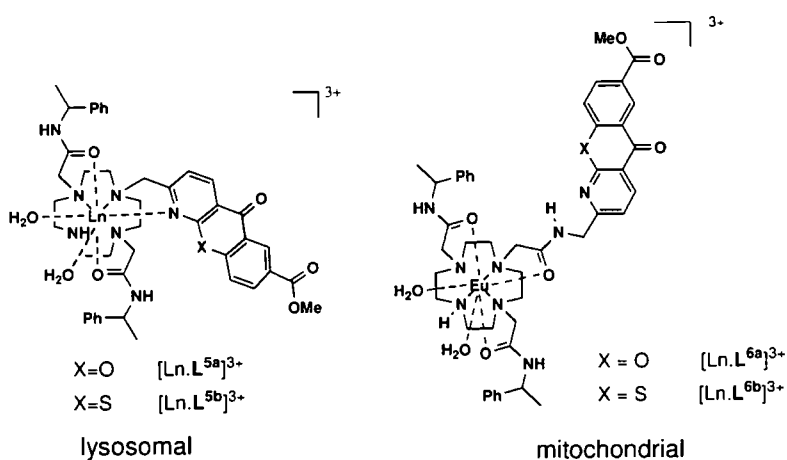
The nature of the chromophore itself does appear to have an effect on the localisation of the complex. Replacement of the dpqC chromophore of  $[\text{Ln.L}^2]^{3+}$  for the pyrazole-linked azaxanthone of  $[\text{Ln.L}^8]^{3+}$ , for example, resulted in a changed localisation from lysosomal to a lysosomal-mitochondrial distribution.



Small modifications to the chromophore structure, on the other hand, do not appear to influence the complex localisation. All forms of  $[\text{Tb.L}^{14}]^{3+}$ , in which the group attached to the 7-position of the chromophore is varied, exhibited lysosomal localisation. Likewise, hydrolysis of the ester group in  $[\text{Eu.L}^{6a}]^{3+}$  to the acid form in  $[\text{Eu.L}^{6c}]^{2+}$ , as well as conversion of the azaxanthone chromophore to an azathioxanthone, in  $[\text{Eu.L}^{6b}]^{3+}$ , did not change the mitochondrial localisation of the complexes.

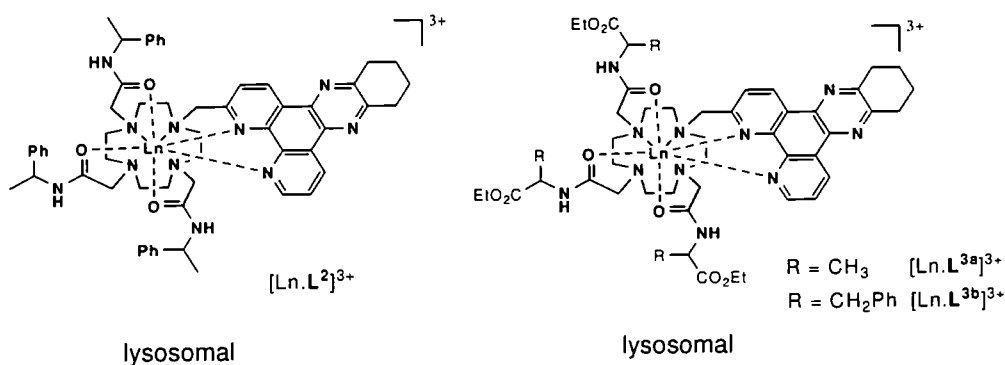


A marked change in localisation occurred on alteration of the linkage between the chromophore and the cyclen ring. This had previously been observed for constitutionally-isomeric complexes in which an acridone chromophore was linked to cyclen in different manners.<sup>83, 84</sup> In this study, a similar observation was made regarding the lysosomally-localising  $[\text{Ln.L}^5]^{3+}$ , containing a methylene linkage, and the mitochondrially-localising  $[\text{Ln.L}^6]^{3+}$ , in which linkage occurs through an amide moiety.

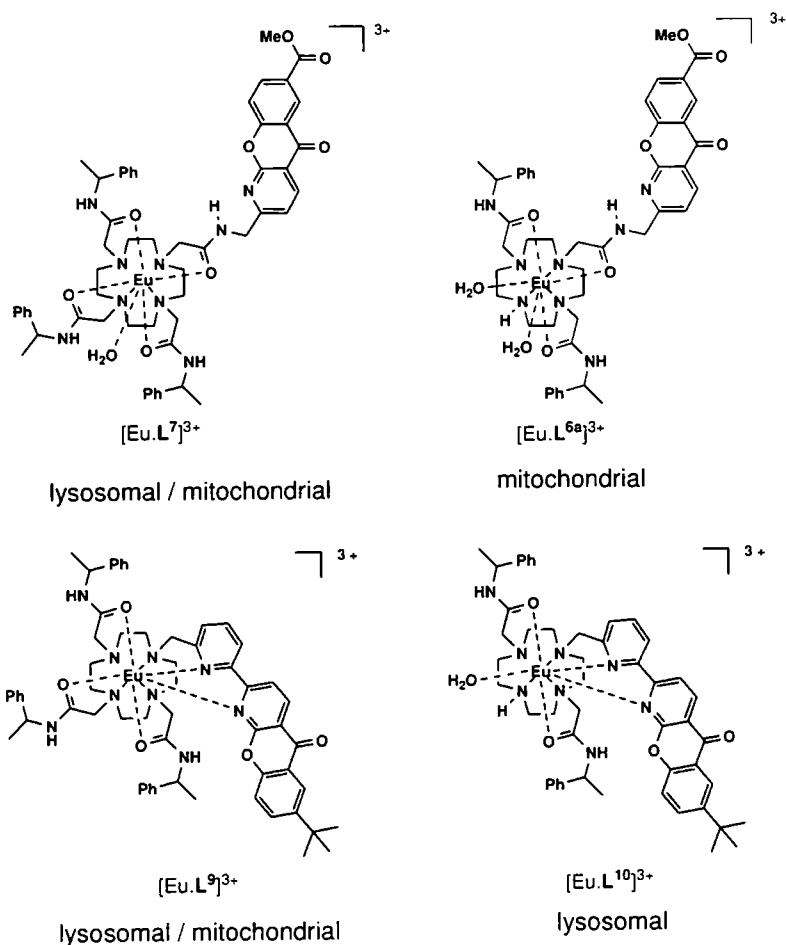


### 3.5.2 Effect of pendant arms

In considering the effect of the pendant arms on the localisation of complexes, it is important to consider both the nature and number of pendant arms. The series of complexes of ligands  $L^1$  to  $L^4$  contain pendant arms which differ considerably in hydrophobicity and charge, as discussed in Chapter Two. All complexes, however, exhibit identical localisation patterns in the lysosomes. It appears, therefore, that the nature of the pendant arms does not affect the sub-cellular localisation.



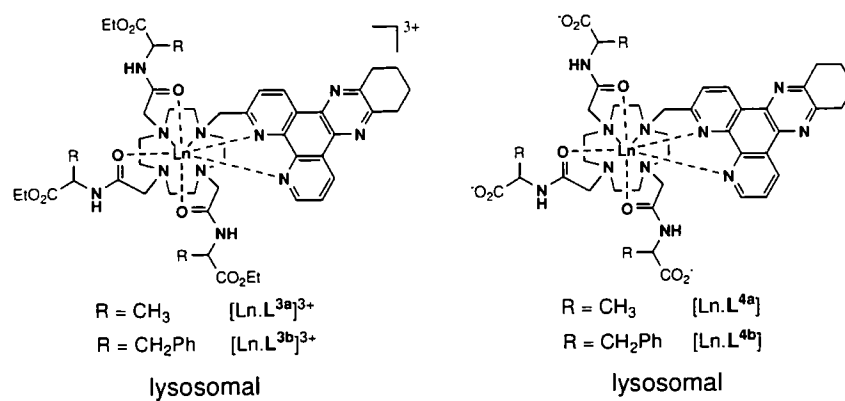
In contrast, the number of pendant arms, or ligand denticity, does appear to influence the distribution of the complex *in cellulo*. Complexes [Eu.L<sup>7</sup>]<sup>3+</sup> and [Eu.L<sup>9</sup>]<sup>3+</sup> contain three identical, chiral amide pendant arms, and localise similarly, to the lysosomes and mitochondria. Removal of the pendant arm opposite the chromophore, giving complexes [Eu.L<sup>6a</sup>]<sup>3+</sup> and [Eu.L<sup>10</sup>]<sup>3+</sup> respectively, resulted in a change of distribution.



### 3.5.3 Effect of charge and counterion

Most of the ligands synthesised for use in luminescent lanthanide complexes are neutral, giving rise to a complex with an overall charge of 3+. Some neutral and anionic complexes have also been synthesised, and it is therefore important to consider the effect of charge on the localisation of the complex. Cationic and anionic complexes must be administered to the cells with a counter-ion, so the influence of this ion must also be considered.

There is no evidence to suggest that complex charge has an effect on sub-cellular localisation. The cationic [Ln.L<sup>3</sup>]<sup>3+</sup> complexes and their neutral analogues, [Ln.L<sup>4</sup>], for example, all exhibit lysosomal distributions.



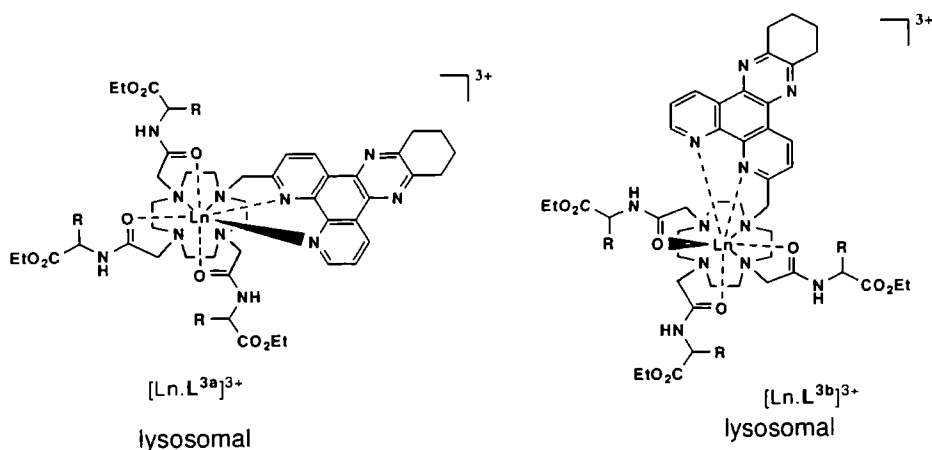
The counterion which is most commonly employed for cationic complexes is chloride. Cellular studies were also performed in which acetate, nitrate and triflate complexes were administered to cells. These did not reveal any change in the sub-cellular localisation, except in the case of the nucleolarly-localising complexes, for which the triflate counterion could act to promote cellular permeability.

### 3.5.4 Effect of geometry

Geometry in biological systems is very important due to the chiral environment of the cell, and the specific shape of the protein binding sites. It is therefore important to consider the geometry of the complexes, and how this affects their sub-cellular trafficking behaviour.

For a number of ligands, synthesis was performed using both *S* and *R* enantiomers of the pendant arms, giving rise to opposite complex configurations. In all cases, no difference in sub-cellular localisation was observed between the two enantiomers.

[Ln.L<sup>3a</sup>]<sup>3+</sup> and [Ln.L<sup>3b</sup>]<sup>3+</sup> not only exhibit different configurations, but the arrangement of the ligands around the mono-capped square antiprism is also varied, as discussed in Chapter Two. Despite these dramatic changes to the complex geometry, there was no resultant change to the localisation.



### 3.5.5 Effect of lanthanide ion

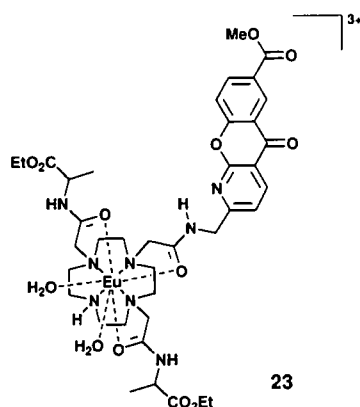
The final structural feature which must be considered is the lanthanide ion itself. It is not expected that the lanthanide should affect the cellular behaviour of the complex, as it is buried within the ligand structure. For most ligands, both Eu and Tb complexes were synthesised and their sub-cellular localisation analysed. These studies confirmed that the nature of the lanthanide ion had no effect on the cellular distribution, or indeed, on any other aspect of cellular behaviour.

### 3.5.6 Deriving structure-localisation relationships

These investigations reveal that the localisation of a complex is affected by the nature of the chromophore and, more significantly, its point of attachment to the macrocycle, as well as by the ligand denticity. At this stage, it is important to consider whether it is possible to predict the sub-cellular localisation of a novel complex. The complexes which have been investigated comprise a relatively small library of chromophores and pendant arms. The information which has been gained from this structural study allows the prediction of the localisation of a complex composed of elements from this library. For entirely new complexes, however, which contain different chromophores or pendant arms, such prediction is less straight-forward.

For example, an analogue of  $[Eu.L^{6a}]^{3+}$  bearing amino acid-based pendant arms, such as **23** might be expected to localise to the mitochondria since modification of pendant arms was not found to affect localisation, but the amide-linkage on the chromophore

determined mitochondrial localisation. In this way, the selectivity of the complex could be optimised without altering the sub-cellular distribution.



### 3.6 Assessing for nuclear localisation

The discussion in this chapter has relied on the fluorescence microscopy evidence of sub-cellular localisation. It is important to consider whether this reveals the complete picture. For example, it is possible that the complex is localised elsewhere in the cell, but its luminescence quenched. This is most likely to be the case for a nucleary-localised complex whose luminescence is quenched by DNA. It was therefore important to test for any such DNA quenching.

#### 3.6.1 DNA quenching studies

The interaction of complexes with DNA has previously been extensively studied.<sup>176</sup> This study was therefore primarily concerned with observation of possible quenching of the total luminescence, or the luminescence lifetime, of complexes upon addition of DNA. For this study, calf thymus DNA was utilised, and was prepared as a 1 mg/mL solution in HEPES buffer (pH 7.4). This DNA solution was added incrementally to solutions of complex (30  $\mu$ M), and the emission spectrum collected and luminescence lifetime measured. For every complex, the luminescence lifetime remained unchanged upon titration of DNA.

For some complexes, there was marked quenching of the emission intensity on addition of DNA. The titration curves for selected Eu and Tb complexes are shown in Figures 3.14 and 3.15 respectively.  $[\text{Eu.L}^2]^{3+}$  and  $[\text{Tb.L}^2]^{3+}$  show the most dramatic changes on

addition of DNA, with the emission intensity rapidly dropping ten-fold. This quenching effect does not appear to be stereospecific: the intensities of  $(RRR)$ -[Tb.L<sup>8</sup>] and  $(SSS)$ -[Tb.L<sup>8</sup>] decrease in a very similar fashion. While a number of complexes are clearly quenched by DNA, the emission intensities of many complexes remained unchanged. It is interesting to note that those complexes whose emission was quenched by DNA bore the same chiral phenylmethyl amide pendant arms. These groups may be mediating this interaction with DNA.

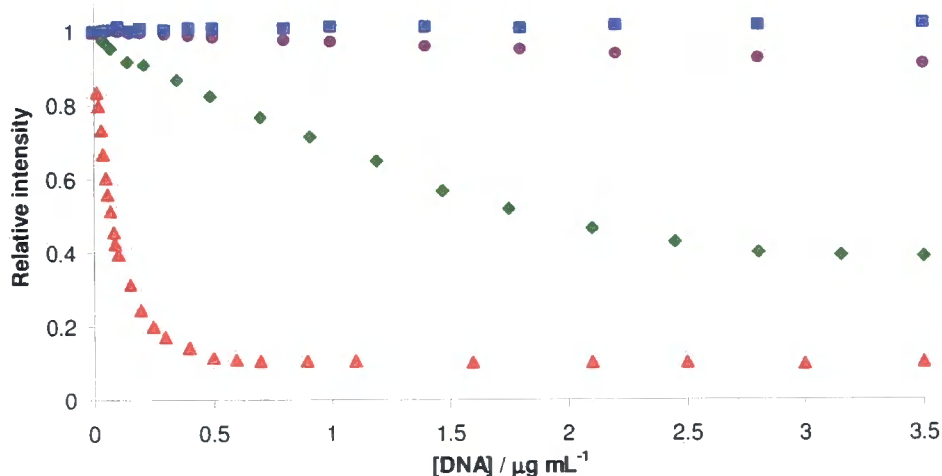


**Figure 3.14:** Changes in the relative emission intensity of [Eu.L<sup>2</sup>]Cl<sub>3</sub> (▲), [Eu.L<sup>4</sup>] (●), [Eu.L<sup>6</sup>]Cl<sub>3</sub> (■) and [Eu.L<sup>10</sup>]Cl<sub>3</sub> (◆) on incremental addition of DNA. (100 mM HEPES, 10 mM NaCl, pH 7.4, 30 μM complex, λ<sub>em</sub> = 615 nm)

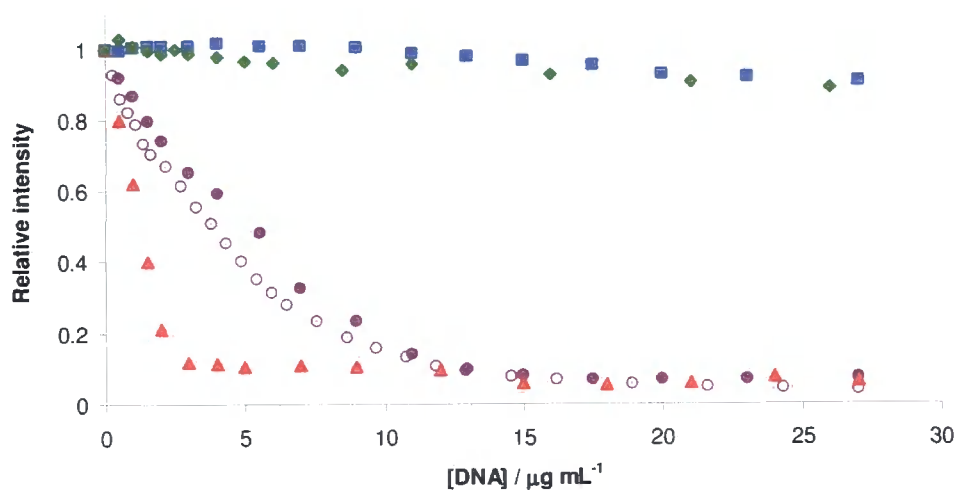


**Figure 3.15:** Changes in the relative emission intensity of [Tb.L<sup>1</sup>] (○), [Tb.L<sup>2</sup>]Cl<sub>3</sub> (▲), [Tb.L<sup>3b</sup>]Cl<sub>3</sub> (■),  $(SSS)$ -[Tb.L<sup>8</sup>]Cl<sub>3</sub> (●) and  $(RRR)$ -[Tb.L<sup>8</sup>]Cl<sub>3</sub> (○) on incremental addition of DNA. (100 mM HEPES, 10 mM NaCl, pH 7.4, 30 μM complex, λ<sub>em</sub> = 543 nm)

It is possible, therefore, that those complexes whose emission was dramatically quenched by DNA may be present in the nucleus, but not visible. It was important to perform further studies to explore this hypothesis.

### 3.6.2 Nuclear extraction experiments

In order to test for the presence of complex in the nucleus, nuclear extractions were performed as described in Section 3.4.3, and the lanthanide content determined by inductively coupled plasma – mass spectrometry (ICP-MS). This value was then compared to the lanthanide content of the whole cell, and of the mitochondria, which were extracted in a similar manner, using a mitochondria isolation kit (Pierce Bioscience).

Inductively coupled plasma mass spectrometry (ICP-MS) is an important technique for the analysis of trace elements, allowing determination of the concentration of an element in a sample with detection limits of the order of ppb.<sup>177</sup> The sample is atomised and ionised by injection into an argon plasma, and the resulting ions are passed through a series of cones to a quadrupole mass spectrometer. The observed ion signal is proportional to the concentration, which can be determined by calibration with elemental standards. In this way, ICP-MS can be used to give an indication of the total amount of lanthanide within a sample.

Cells were grown in cell culture flasks, and treated with 50  $\mu\text{M}$  complex for 4 h. (SSS)-[Tb.L<sup>8</sup>]Cl<sub>3</sub> was used as an example of a complex whose emission was quenched by DNA, while [Eu.L<sup>6a</sup>] was selected for comparison, as it was not quenched by DNA. Cells were either analysed as whole cells, or their nuclei or mitochondria extracted. All experiments were performed in triplicate. The calculated lanthanide uptake values are shown in Figure 3.16. The results indicate very similar behaviour for each complex, with approximately 30% of the total intracellular lanthanide measured in the nuclear fraction. This fraction is similar to the amount of lanthanide in the mitochondria. There is some doubt cast on the results of this experiment, however, as it might be expected that since the luminescence of [Eu.L<sup>6a</sup>]Cl<sub>3</sub> is not quenched by DNA, its presence in the nucleus should be observable by fluorescence microscopy. This is not the case, as no luminescence is visible in the nucleus of cells treated with [Eu.L<sup>6a</sup>]Cl<sub>3</sub>. This large measured uptake into the nucleus could instead result from the experimental procedure.

The nuclear isolation process relies solely on separation according to density (Figure 3.12). It is possible that some large cytoplasmic proteins, or even portions of the lysed cell membrane, have a similar density to nuclei, and are therefore collected with this fraction. The complexes could be non-covalently bound to these fragments, and therefore be measured among the nuclear fraction.

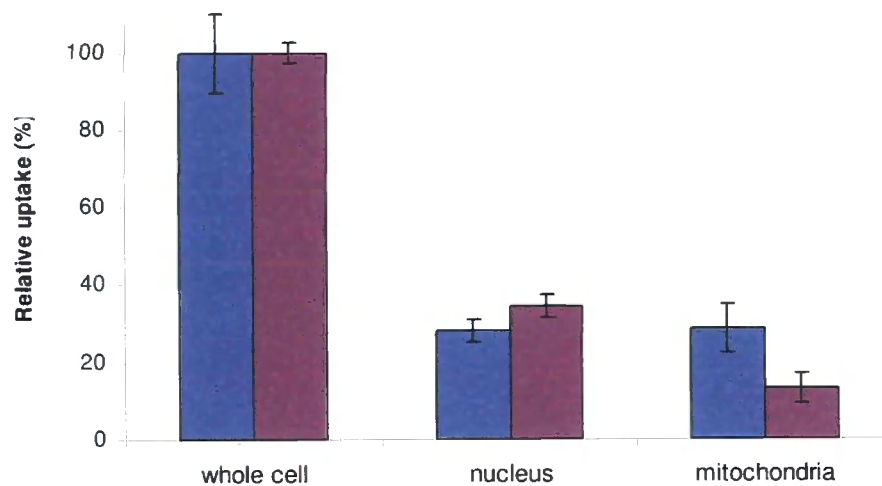


**Figure 3.16:** Measured concentration of lanthanide in the nucleus and mitochondria relative to the amount in the whole cell for CHO cells treated with [Eu.L<sup>6a</sup>]Cl<sub>3</sub> (blue) and [Tb.L<sup>8</sup>]Cl<sub>3</sub> (purple) (4h incubation, 50 $\mu$ M complex).

### 3.6.3 Further experiments

Since the nuclear extraction studies do not clearly indicate the presence or absence of complex in the nucleus, it is important to perform further studies. This could be achieved by using another method to gain a cellular localisation profile to supplement the information gained from fluorescence microscopy. For example, transmission electron microscopy or X-ray fluorescence spectroscopy, have been successfully used to study sub-cellular distributions of other metal complexes.<sup>178, 179</sup> This would enable a determination of whether fluorescence microscopy studies provide an accurate reflection of the true localisation of the complex.

## 3.7 Understanding trafficking

The sequestration of complexes into specific sub-cellular compartments, and the movement of complexes between organelles, requires complex trafficking processes

within the cell. This is of particular importance for the class of complexes which have been simultaneously observed in both the lysosomes and the mitochondria. A preliminary investigation of these trafficking mechanisms was performed using FRET techniques.

Förster resonance energy transfer (FRET) is based on the principle that if two fluorescent moieties are in close proximity (usually 2 – 10 nm), there can be a non-radiative energy transfer from one to the other. This will be observed as a decreased fluorescence intensity of one (the donor) and increased intensity of the other (the acceptor). In order for FRET to occur, the emission spectrum of the donor and the excitation spectrum of the acceptor must overlap.<sup>11</sup> From a biological perspective, FRET studies can be useful in giving information about the proximity of two species within the cell.<sup>180</sup>

This study aimed to investigate the interaction between lanthanide complexes and tubulin and actin, which are the main components of the microtubules and microfilaments respectively. In this way, the role of the cytoskeleton in sub-cellular trafficking can be investigated. This was achieved by using forms of tubulin and actin which were tagged with red fluorescent protein (RFP). Luminescent terbium complexes can act as good donors for RFP fluorescence (Figure 3.17).

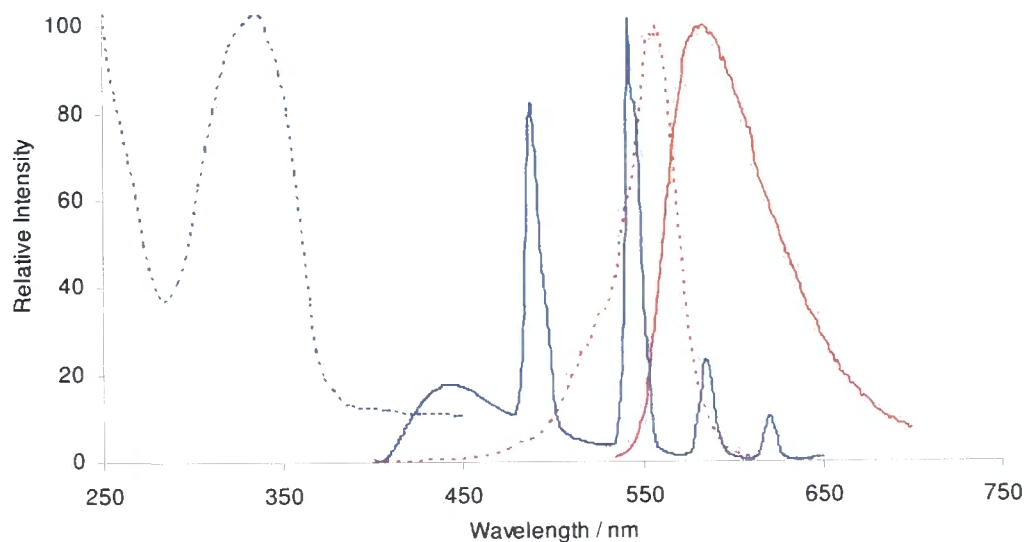


**Figure 3.17:** Excitation (---) and emission (—) spectra of  $[\text{Tb.L}^8]^{3+}$  (blue) and RFP (red). RFP spectral data obtained from Evrogen.<sup>181</sup>

The RFP-labelled tubulin and actin were sourced from Invitrogen in the form of protein expression constructs utilising an insect virus (baculovirus) to promote cellular delivery and expression.<sup>182</sup> CHO cells were treated with the construct for four hours, after which time the cells were incubated for twenty-four hours to allow protein expression. The cells were then incubated with [Tb.L<sup>8</sup>]Cl<sub>3</sub> (4h, 50 µM). It is likely that any FRET which occurs will do so with only very low emission intensities. For this purpose, the fluorescence microscope system utilised for other experiments may not be sufficiently sensitive. The cells were therefore visualised using a confocal microscope system. Three channels were set up, as shown in Table 3.1, to measure the Tb luminescence, the RFP fluorescence, and FRET.

**Table 3.1:** Microscope channels employed for study of cells treated with [Tb.L<sup>8</sup>]Cl<sub>3</sub> and RFP-labelled protein. LP = long pass filter

Channel	Purpose	Laser excitation wavelength	Emission filter
1	Tb luminescence	405 nm	505-550
2	RFP fluorescence	543 nm	LP 650
3	FRET	405 nm	LP 650

The results of this experiment are shown in Figure 3.18. The RFP fluorescence channel confirms successful transfection, although only approximately half of the cells showed staining for RFP. This is likely to be due to the fact that not all cells had completed a full cell cycle, and were not expressing the recombinant protein. There was no detectable fluorescence in the FRET channel for either protein, indicating that the complex is not close enough in space to actin or tubulin. There is, however, co-localisation of the Tb luminescence and the RFP fluorescence for the RFP-labelled actin, indicated by the yellow colour in the overlap images. This suggests that, although the complex is not associating directly with actin, it is still relatively close. This might indicate that the microfilaments play a role in transporting the complex within the cell.

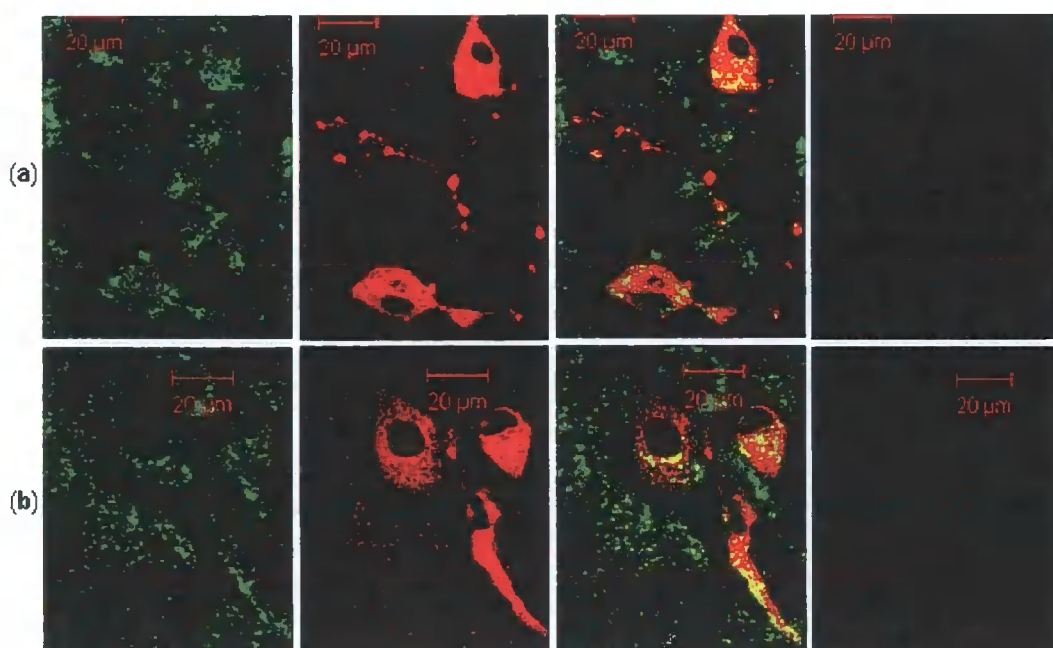


**Figure 3.18:** Confocal microscopy images of CHO cells treated with  $[\text{Tb.L}^8]^{3+}$  ( $50 \mu\text{M}$ , 4h) and (a) tubulin-RFP or (b) actin-RFP. (i) Tb luminescence, (ii) RFP fluorescence, (iii) overlay of Tb luminescence and RFP fluorescence, (iv) FRET channel.

### 3.8 Conclusions

The range of complexes synthesised in Durham exhibit various sub-cellular localisations which can be divided into four main categories. Two distinct groups rapidly localise to the mitochondria and to the lysosomes, while a third appears to be distributed between both types of organelle. From a molecular imaging perspective, it is generally desirable for a probe to localise in only one organelle type, in order to provide specific information about the environment of that particular region of the cell. Future design of luminescent lanthanide complexes might therefore attempt to avoid such localisation behaviour. Structural studies indicated that it was complexes with three identical pendant arms which exhibited this intermediate localisation. By removing one pendant arm, the complex should localise in a single organelle type. This is unlikely to be a hindrance to complex design, as many responsive complexes contain a free amine at the fourth cyclen nitrogen.

The fourth class of complexes exhibited nucleolar localisation under certain conditions. Further studies of this behaviour showed it to be due to increased membrane permeability, induced by necrotic conditions or other effects of the complexes

themselves. Trafficking across the nuclear membrane was found to require active transport processes, evidenced by the fact that complexes could not be induced to enter extracted nuclei.

This work has demonstrated that it is not necessary to employ complex strategies to effect mitochondrial, lysosomal or even nucleolar localisation. If other sub-cellular organelles were to be targeted, however, other approaches might be necessary. These might involve more drastic structural modifications, or incorporation of peptides which target different sub-cellular locations.

While this study has focussed on sixteen different ligand types, it is not possible to continue all other investigations of cellular behaviour on such a large set of complexes. The classification of complexes into four groups of distinct types of behaviour will assist in the rational selection of examples of each type for the further studies which are described in subsequent chapters.

## CHAPTER FOUR

---

# CELLULAR UPTAKE OF COMPLEXES

## 4.1 Introduction

In order for a probe to report on sub-cellular conditions, it must be able to enter the cell by crossing the cell membrane. This chapter explores the studies which have been performed to understand the permeability of the cell membrane towards the luminescent lanthanide complexes, and the manner in which they are taken up into cells.

The design of cell-permeating compounds is a key challenge in many fields, most notably in the pharmaceutical industry, in which it is essential to ensure that drugs reach their intracellular targets.<sup>132</sup> In some cases, compounds utilise endogenous mechanisms of internalisation, but for non-permeating cases, it might be necessary to perform modifications to ensure cellular uptake. The following section explores modes of cellular uptake.

### 4.1.1 Cellular uptake pathways

The mechanisms by which species can be transported across the cell membrane can be divided into a number of classes (Figure 4.1).<sup>139</sup> The term passive transport encompasses those pathways which do not require energy input: the driving force for the transport is instead the movement of molecules down their concentration gradient. Osmosis is the movement of water from a region of low solute concentration to a region of higher concentration, while diffusion describes the movement of any molecule down its concentration gradient. Oxygen and carbon dioxide, for example, readily diffuse across the cell membrane. Facilitated diffusion describes the movement of species through protein channels in the cell membrane. While this process is primarily involved in the internalisation of small ions and molecules such as  $\text{Na}^+$ ,  $\text{Ca}^{2+}$  and glucose, some metal complexes have been observed to enter cells through ion channels. For example, cisplatin is thought to enter cells through the copper transporter Ctr1.<sup>183</sup>



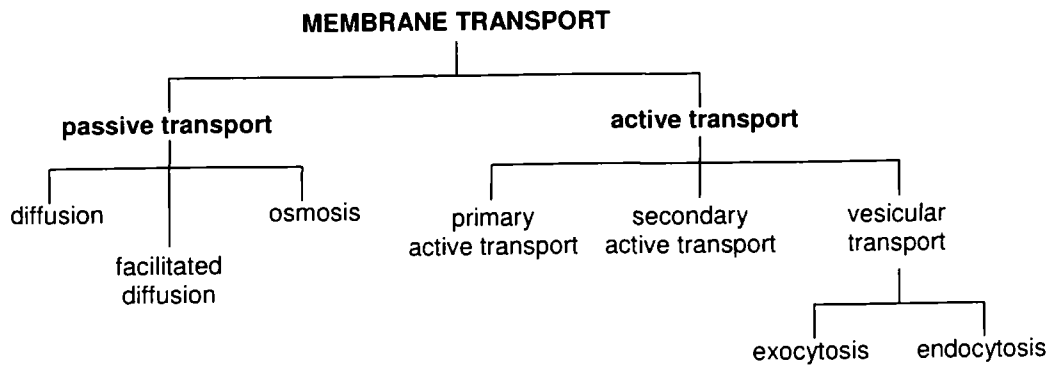


**Figure 4.1:** Methods of membrane transport

Active transport pathways, on the other hand, are those which require the input of energy. Primary active transport involves the use of specific membrane-bound carriers or channels to move species across the cell membrane. For example, the  $\text{Na}^+/\text{K}^+$ -ATPase uses the energy from ATP to simultaneously move three sodium ions out of the cell and two potassium ions into the cell. In contrast, secondary active transport uses an ion gradient which is established by the simultaneous transport of a second species. An example is the glucose symporter, SGLT1, which co-transport one glucose molecule into the cell with every two sodium ions which are imported.<sup>184</sup>

The third major class of active transport is vesicular transport, which is the least understood mechanism of membrane transport.<sup>185</sup> Endocytosis and exocytosis are essentially reverse processes, enabling the movement of species into and out of the cell respectively. For the purposes of this study, therefore, cellular uptake, or endocytosis, is of primary interest. Endocytosis describes the process by which the membrane encapsulates an extracellular particle into a vesicle which is subsequently internalised. The process can occur *via* one of a number of mechanisms (Figure 4.2).

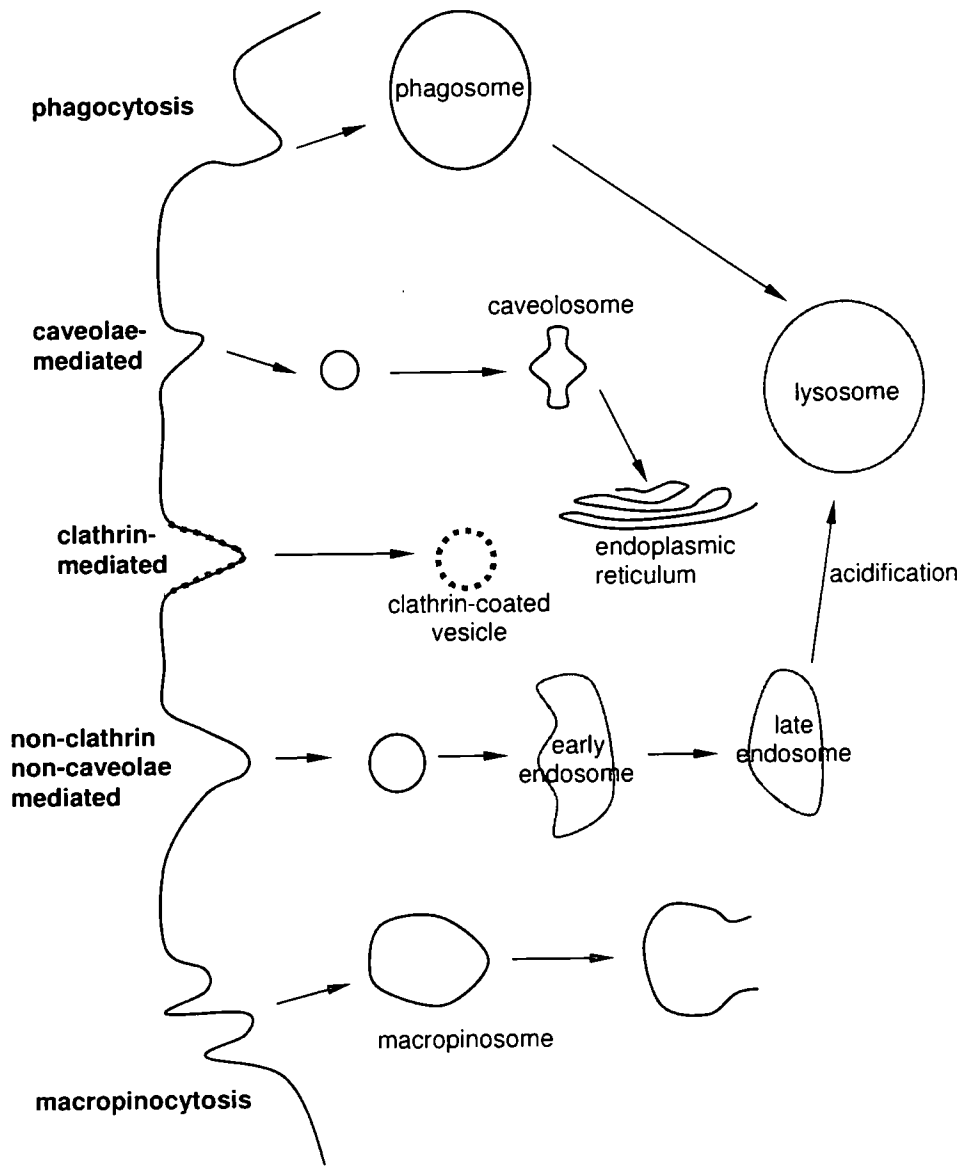


**Figure 4.2:** Putative mechanisms of membrane transport by endocytosis

Endocytosis can be divided into two broad categories: pinocytosis involves the uptake of extracellular fluid and any particles it may contain, while phagocytosis describes the transport of large multimolecular particles such as dead cells, bacteria and viruses.<sup>94</sup> Phagocytosis is performed by specialised white blood cells, phagocytes, on materials which have been identified as foreign or diseased. The cell membrane engulfs the solid particle to form a phagosome, which is delivered to the lysosome for degradation. The products are released intracellularly for further processing, or extracellularly *via* exocytosis.<sup>172</sup>

Pinocytosis can be further divided into classes according to mechanism. The best understood endocytotic route is clathrin-mediated endocytosis, which occurs at specific regions of the cell membrane called coated pits, which have high concentrations of specific proteins such as clathrin and the adaptor protein AP-2.<sup>186</sup> These proteins facilitate the invagination, constriction and fission of the cell membrane to form a vesicle. The membrane proteins are then recycled to form a new coated pit. Clathrin-mediated endocytosis is the principal mechanism of internalisation for proteins, membrane-localised receptors and ion channels.

It was initially believed that clathrin-coated pits were the only form of specific pinocytosis. However, studies of the uptake of the virus SV40 revealed an alternative mechanism, *via* caveolae.<sup>187, 188</sup> Caveolae are flask-shaped invaginations of the cell membrane,<sup>189</sup> which are coated with a number of lipids and proteins, notable among which is the integral membrane protein caveolin.<sup>190</sup> Caveolae internalise species by potocytosis, a term which specifically describes the sequestration and transport of small molecules by caveolae.<sup>191</sup> Invagination of a caveola results in the formation of a caveolosome, which then delivers its contents to one of a number of locations: the cytoplasm, endoplasmic reticulum or other organelles, or the cell membrane for re-release or repositioning in the plasma membrane.

Clathrin- and caveolae-dependent endocytosis rely on ligand-binding to a receptor to signal vesicular formation. In contrast, macropinocytosis is a non-specific mechanism for internalisation, for which ligand binding is not required.<sup>192</sup> Instead, vesicles are formed by ruffling of the membrane in response to cell stimulation. This ruffling results in the formation of large, irregular vesicles called macropinosomes. This process is driven by actin, and the mechanism of membrane invagination is similar to that of phagocytosis. It is not understood how the contents of the macropinosome are processed. Macropinosomes can fuse with one another, and can reassociate with the cell membrane, but in most cell lines do not seem to associate with early or late endosomes.<sup>193</sup>

Observation of persistent endocytosis even in the presence of drugs blocking the clathrin- and caveolae-dependent pathways has led to the hypothesis of an additional pathway, non-clathrin non-caveolae dependent endocytosis.<sup>158</sup> This process is not well understood, but has been observed for the internalisation of the cholera toxin in some cell lines.<sup>194</sup>

### 4.1.2 Strategies for cellular delivery

While many exogenous molecules have been observed to enter cells by the above mechanisms, in a number of cases it is necessary to assist the transport of drugs or probes across the cell membrane. There are a number of means of achieving such cellular uptake.

A common challenge for drug delivery is to facilitate a hydrophilic drug molecule to cross the lipophilic cell membrane. This can be achieved by encapsulating the drug in a liposome or micelle which will carry it into the interior of the cell.<sup>132</sup> In a similar manner, viral vectors can be generated in which the protein coat of the virus can encapsulate a molecule, usually comprising nucleic acids.<sup>195</sup> The vector then harnesses the mechanisms by which viruses efficiently transport their genomes into infected cells.

An additional mechanism for enhancing cellular uptake is to incorporate a peptide domain which will be recognised and internalised by the cell. This may be a ligand domain which can bind to a receptor involved in endocytosis, or a signal peptide which enhances membrane translocation. Such peptides, which are called cell-penetrating peptides (CPPs), have recently gained popularity as drug delivery vehicles.<sup>146</sup> For example, the conjugation of synthetic import peptides to oligonucleotides has been demonstrated to increase the cellular transport of the oligonucleotide.<sup>196</sup>

### 4.1.3 Uptake of lanthanide complexes

While there has been no comprehensive study of the cellular transport of lanthanide complexes, the uptake behaviour of a number of example complexes has previously been reported. One important consideration is whether structural characteristics determine the ability of a complex to enter the cell. Previous studies of  $[\text{Ln.L}^2]^{3+}$  demonstrated clear *in cellulo* luminescence, consistent with good cellular uptake. In contrast, microscopic investigations of cells treated with its neutral and anionic analogues (Figure 4.3) showed no readily-detectable luminescence, with the conclusion that cell uptake is very low for these cases.<sup>197</sup> This led to the hypothesis that for efficient membrane transport, a complex should be relatively lipophilic, have an overall positive charge and contain one or more planar aromatic heterocycles.<sup>128</sup> However, this same work also reported inductively coupled plasma – mass spectrometry (ICP-MS)

measurements of cells treated with  $[\text{Ln.L}^2]^{3+}$  and its analogues which indicated comparable intracellular concentrations of each complex. This suggests that the poor visibility of the neutral and anionic complexes *in vivo* might be due to a mechanism other than reduced uptake.

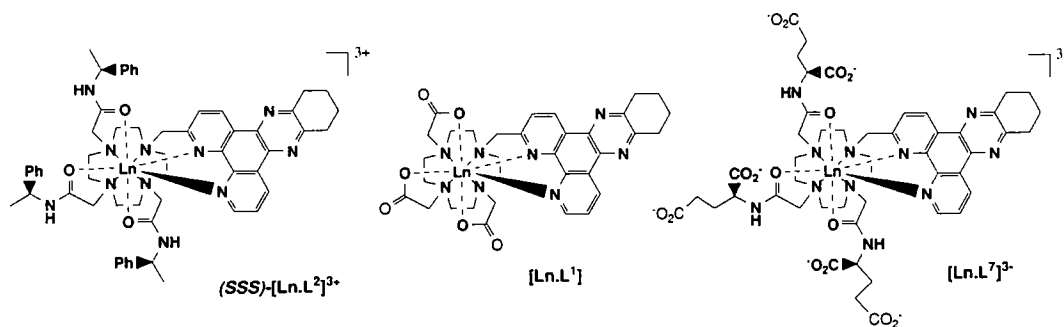
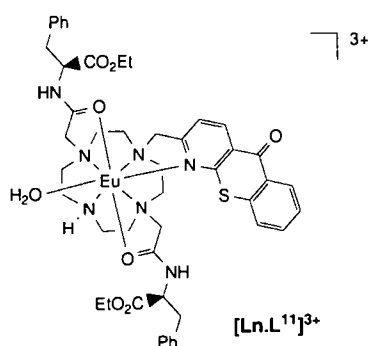


**Figure 4.3:** Structures of  $[\text{Ln.L}^2]^{3+}$  and its neutral and anionic analogues.

Microscopy studies of Eu and Tb complexes of  $\text{L}^2$  at various timepoints and concentrations revealed that the Eu complex could be more readily observed at early timepoints than the Tb analogue. This was initially interpreted as being due to faster uptake of the Eu complex. In contrast, there was no significant difference between the uptake of the  $\Delta$  and  $\Lambda$  enantiomeric forms.<sup>198</sup>

A number of studies have drawn preliminary conclusions regarding the mechanism of cellular uptake of various lanthanide complexes. The size and charge of  $[\text{Ln.L}^2]^{3+}$  was believed to preclude its passive entry to the cell, while the lack of vesicular structures in the fluorescence microscopy images were at variance with an endocytotic mechanism.<sup>198</sup> This was further supported by the observation that microscopy images collected at 4 °C appeared to be similar to those collected at 37 °C.<sup>73</sup> At low temperatures, energy dependent processes such as endocytosis are inhibited. As a result,  $[\text{Ln.L}^2]^{3+}$  was believed to enter cells through a transporter or pore in the cell membrane. Such a mechanism was also hypothesised for the citrate sensor  $[\text{Ln.L}^{11}]^{3+}$ , for which considerable uptake at 4 °C was again identified.<sup>102</sup>



In contrast, studies of a range of other lanthanide complexes have identified minimal cellular uptake upon incubation at 4 °C. This led to the conclusion that, in these cases, uptake is likely to be due to an endocytotic mechanism.<sup>100, 105</sup>

It is evident, therefore, that conclusive studies must be performed in which the cellular uptake of a broad range of complexes is assessed with reference to the structure of the complex, and that more detailed mechanistic studies are required to elucidate the mode of cellular uptake. The following sections describe the work which has been performed to that end.

## 4.2 Exploring effects of structure on cellular uptake

An understanding of the structure-uptake relationship is important in the study of luminescent lanthanide complexes, as it enables the design of probes which are most likely to exhibit sufficient cellular uptake. Previous studies of the uptake of various complexes led to the conclusion that poorly visible neutral and anionic complexes were not able to efficiently cross the cell membrane. These observations served as a starting point for this investigation.

Earlier microscopy examinations noted that while  $[\text{Ln.L}^2]^{3+}$  was visible by fluorescence microscopy,  $[\text{Ln.L}^1]$  could not readily be observed.<sup>128</sup> These two complexes were therefore selected as examples of readily and poorly visible complexes respectively. Microscopy studies were performed to repeat these experiments. Representative microscope images for Tb complexes in CHO cells are shown in Figure 4.4.

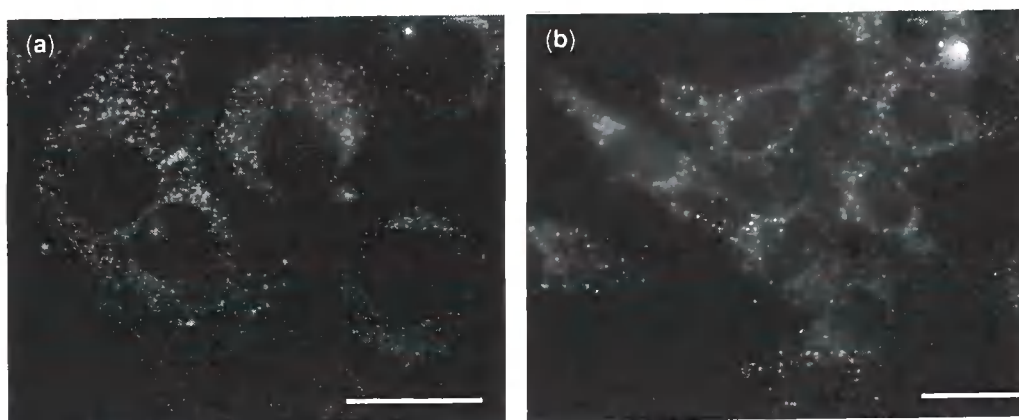


**Figure 4.4:** Luminescence microscopy images showing terbium luminescence of CHO cells treated for 3 h with 50  $\mu\text{M}$  (a)  $[\text{Tb.L}^1]$  and  $[\text{Tb.L}^2]\text{Cl}_3$ . Scale bar represents 20  $\mu\text{m}$ . Image brightness and contrast have been altered.

It is evident that both  $[\text{Tb.L}^1]$  and  $[\text{Tb.L}^2]\text{Cl}_3$  give rise to *in cellulo* luminescence, confirming that both are able to cross the cell membrane. The fact that previous studies were unable to observe  $[\text{Tb.L}^1]$  by microscopy could be due to the use of emission filters which were not optimal. However, as previously observed, repeated experiments in both CHO and NIH 3T3 cells, and for both Tb and Eu complexes, showed that the luminescence of  $[\text{Ln.L}^1]$  was considerably weaker than that of  $[\text{Ln.L}^2]^{3+}$ . It was not possible to quantify the luminescence output with the microscope system employed. Such a measurement would require the use of a laser scanning confocal microscope, in which the laser power could be accurately measured.

The challenge remains, therefore, to explain this varying *in cellulo* visibility. Such a difference could result from two primary causes: a decrease in the permeability of the cell membrane to some complexes compared to others, or a quenching of the luminescence in the cell. Each possibility will be explored in turn.

#### 4.2.1 Comparing the absolute cellular uptake

Determination of the amount of complex which has been internalised by the cell requires a method other than luminescence microscopy, which can be biased by factors such as quenching. In order to achieve this, the intracellular concentration of lanthanide was determined by ICP-MS. In order to compare the uptake of different samples, however, it is necessary to measure the number of cells in the sample to allow calculation of an

intracellular lanthanide concentration. In previous investigations, this was achieved by the use of flow cytometry.<sup>128, 129</sup>

Flow cytometry is a technique which uses fluorescence to count and sort populations of cells (Figure 4.5).<sup>199</sup> The cell suspension is inserted into the flow chamber and focused to a stream of droplets, each containing a single cell. The stream of cells is then interrogated with a laser which excites the fluorophore with which the cells have been treated. The emitted light is collected and the droplets are given an electrical charge that varies depending on their fluorescence profile. This allows them to be separated into different populations according to their charge.

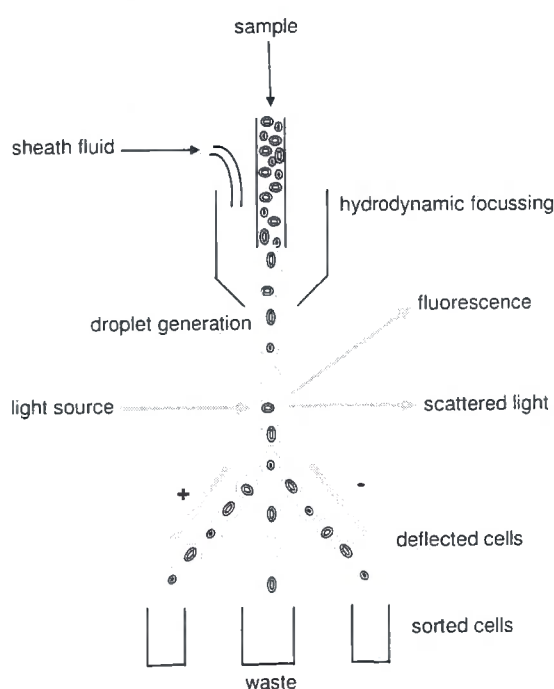


**Figure 4.5:** Schematic diagram showing the process of flow cytometry.

Cells typically move through the flow chamber at a speed of 1 to 25  $\text{ms}^{-1}$ , so they are only very briefly illuminated by the laser. Indeed, this interrogation time is shorter than the luminescence lifetime of lanthanide complexes, so they are not practical for use as fluorophores in flow cytometry. As a result, a second fluorophore must be added. In this case, live cells were labelled with the acetylmethoxy ester, calcein AM, a dye which is used to assess cell viability and cytotoxicity of eukaryotic cells. Calcein AM is retained in cells that have intact membranes, but not in dead cells, and is rapidly lost under conditions that cause cell lysis.<sup>200</sup> While calcein AM is not fluorescent, it is hydrolysed

by the intracellular esterases present in viable cells to calcein, which exhibits green fluorescence detectable in flow cytometry.

In this investigation, cells were treated with both calcein AM and the lanthanide complex, allowing live cells containing the lanthanide complex to be selectively sorted and dead cells to be discarded. It has previously been demonstrated that in more than 97 % of cells examined by microscopy, both the green fluorescence of calcein and the red fluorescence of various europium complexes could be observed.<sup>128</sup>

NIH 3T3 cells were treated with 50  $\mu\text{M}$  complex for varying time periods. For the last half hour of incubation, calcein AM was added to the medium. After incubation, the complex-containing medium was removed and the cells rinsed with phosphate-buffered saline (PBS). Cells were immediately harvested and subjected to flow cytometry, in which calcein-positive cells were collected. The cell samples were then submitted for analysis by ICP-MS. Prior to injection of the sample into the mass spectrometer, samples were treated with nitric acid to digest the cell membrane and to ensure that the complex did not adhere to the sample vial. The results of these uptake studies are shown in Figure 4.6a.

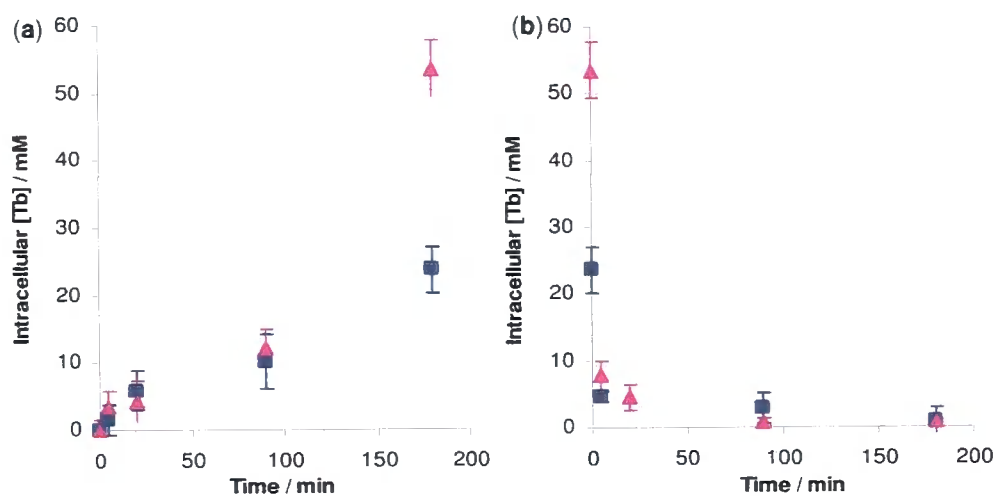


**Figure 4.6:** Uptake (a) and egress (b) of  $[\text{Tb.L}^1]$  (■) and  $[\text{Tb.L}^2]\text{Cl}_3$  (▲) (50  $\mu\text{M}$ ) in NIH 3T3 cells over a period of 3 h. A mean cell volume of 4000  $\mu\text{m}^3$  is assumed.

It can be seen that  $[\text{Tb.L}^1]$  and  $[\text{Tb.L}^2]\text{Cl}_3$  are initially transported across the cell membrane at a very similar rate. At the 90 min time-point, both complexes have accumulated to a concentration of approximately 10  $\mu\text{M}$ . The values have diverged by

180 min, with approximately twice as much  $[\text{Tb.L}^2]\text{Cl}_3$  as  $[\text{Tb.L}^1]$  within the cell. This could result from decreased uptake, or increased excretion of  $[\text{Tb.L}^1]$ . The results clearly show that, despite its poor visibility,  $[\text{Tb.L}^1]$  does show appreciable cellular uptake. A previous study of the uptake of  $[\text{Eu.L}^1]$  and  $[\text{Eu.L}^2]\text{Cl}_3$  in CHO cells gave intracellular concentrations of 12  $\mu\text{M}$  and 26  $\mu\text{M}$  respectively.<sup>129</sup> While the values obtained in this experiment cannot be directly compared due to the different cell line and lanthanide ion that were used, they show similar magnitude and relative difference.

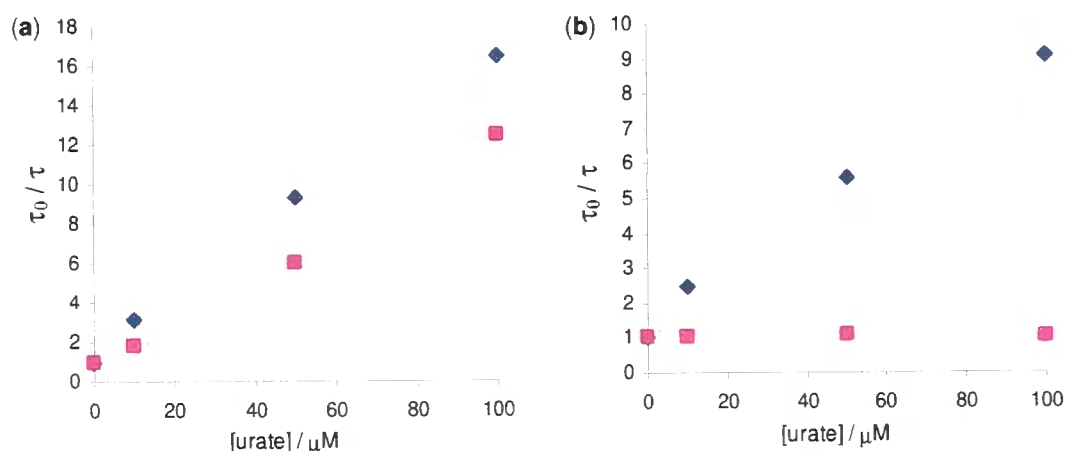
A concurrent experiment was performed to study the egress of the complexes from the cells. The experimental procedure was similar to that described above for the uptake studies, and differed only in the incubation procedure. All cells were incubated with 50  $\mu\text{M}$  complex for 3 h, after which the medium was removed and replaced with PBS. The cells were then harvested at various time-points over the subsequent 3 h (Figure 4.6b). The aim of this experiment was to study the transport of the complex across the cell membrane under conditions of high intracellular concentration, and low extracellular concentration.

Figure 4.6b highlights the very rapid egress of the complexes, with over 80% of both complexes being lost from the cells in the first five minutes. However, the entire process of harvesting the cells and performing flow cytometry takes at least twenty minutes, during which time it would be expected that complex would be rapidly leaving the cells. This means that the actual intracellular concentrations throughout this experiment are likely to be higher than those measured. It was therefore necessary to use a different method for subsequent quantification of intracellular lanthanide concentrations, as will be discussed in Section 4.4.1 below. The conclusions of this uptake experiment are, nevertheless, valid, as all cells were treated in an identical manner and meaningful comparisons of the intracellular concentrations of the two complexes can be drawn. It appears, therefore, that the poor visibility of  $[\text{Tb.L}^1]$  cannot be attributed to its poor uptake.

It is also important to note that the intracellular concentrations of both  $[\text{Tb.L}^1]$  and  $[\text{Tb.L}^2]\text{Cl}_3$  are of a similar magnitude to the dosage concentration of 50  $\mu\text{M}$ . This indicates good transport of complexes across the cell membrane; it is not necessary to dose the cells with very high concentrations of complex to force only small amounts to enter. This is a particularly valuable property for complexes which may be cytotoxic at higher concentrations.

### 4.2.2 Comparing *in cellulo* quenching

The second hypothesised explanation for the lower visibility of  $[\text{Ln.L}^1]$  compared with that of  $[\text{Ln.L}^2]^{3+}$  is that the former is more susceptible to quenching *in cellulo*. Stern-Volmer quenching constants are shown in Table 2.4 in the Chapter Two (page 58), and illustrate no marked differences between the two sets of complexes in terms of their sensitivity to quenching by urate, ascorbate or iodide. These values were, however, calculated from measurements made in a buffer system which bears little resemblance to cellular conditions. In order to more closely mimic a cellular environment, the urate quenching experiment was repeated in the presence of BSA (Figure 4.7).



**Figure 4.7:** Urate quenching curves for (a)  $[\text{Tb.L}^1]$  and (b)  $[\text{Tb.L}^2]^{3+}$  in the absence (♦) and presence (■) of 0.4 mM BSA. (100 mM HEPES, 10 mM NaCl, pH 7.4)

These quenching curves show a marked difference between the behaviour of the two complexes. The presence of BSA completely suppresses the quenching of  $[\text{Tb.L}^2]^{3+}$ .  $[\text{Tb.L}^1]$ , on the other hand, is still quenched in the presence of BSA, although the value of  $K_{sv}^{-1}$  has increased from 0.0058 mM to 0.0095 mM. It might be expected, therefore, that  $[\text{Tb.L}^1]$  experiences considerable luminescence quenching *in cellulo*, even in the presence of proteins such as BSA. This could therefore contribute to its poorer visibility. Similar results were observed for the Eu complexes, and for quenching by ascorbate in the presence of BSA. This difference between the two complexes can be attributed to two factors. Firstly, the structure of  $[\text{Ln.L}^1]$  is more open than that of  $[\text{Ln.L}^2]^{3+}$ , and is therefore more accessible to quenching. Secondly,  $[\text{Ln.L}^1]$  binds more weakly to protein,

as illustrated in Figure 2.21 (page 61), and will therefore be less shielded from approach by urate and ascorbate than  $[\text{Ln.L}^2]$ .<sup>86, 129</sup>

### 4.2.3 Conclusions regarding poorly visible complexes

These studies of  $[\text{Ln.L}^1]$  and  $[\text{Ln.L}^2]^{3+}$  have indicated that it is quenching which caused poor visibility within cells, rather than a reduced uptake as previously thought. This could explain the earlier observation that the *in cellulo* luminescence of Tb complexes increases more slowly with time than that of their Eu analogues. While this was attributed to a slower rate of uptake,<sup>198</sup> it is in fact more likely to reflect the greater susceptibility to quenching of Tb complexes than Eu complexes.

This section has demonstrated that cellular uptake cannot be assessed on the luminescence output observable by microscopy alone. Microscopy is still, however, a valuable tool to survey a broad array of complexes, since even the strongly quenched  $[\text{Tb.L}^1]$  could be observed after increasing the gain and contrast. The following section describes the general observations which have been made regarding the uptake of a broad array of complexes.

### 4.2.4 General observations of cellular uptake

At Durham, a set of more than seventy luminescent lanthanide complexes has been synthesised. These complexes differ in geometry, charge, chromophore, pendant arm and lanthanide ion. The cellular uptake behaviour of a large proportion of these complexes has been determined by luminescence microscopy. CHO or NIH 3T3 cells were treated with 50  $\mu\text{M}$  complex for time periods between 5 min and 24 h. While the absolute emission intensity varied across the range of complexes, as discussed above, all complexes exhibited a similar rate of uptake – luminescence could be observed within the cell after 5 min. This luminescence intensity increased over the first hour, and then generally remained constant for the subsequent hours. After 24 h incubation, luminescence was again lower, which is likely to reflect degradation or efflux of the complex.

These initial studies therefore indicate that all complexes, regardless of their structural features, exhibit similar uptake behaviour. The following sections detail more rigorous

studies which were performed on selected complexes to gain a better understanding of the nature of the cellular uptake.

### 4.3 Determining the energy dependence of uptake

As discussed in Section 4.1.1, cellular transport mechanisms can be divided into passive and active pathways according to their need for energy input. In order to determine the mode of cellular uptake for lanthanide complexes, it is therefore necessary to first categorise the mechanism as active or passive. This was achieved by studying the lipophilicities of the complexes, and performing preliminary low-temperature experiments.

#### 4.3.1 Correlating lipophilicity with uptake

The ability of a compound to partition between lipophilic and hydrophilic substances greatly affects its cellular behaviour. In order for a compound to diffuse through a cell or organelle membrane, it must be sufficiently hydrophobic to partition into the lipid bilayer, but hydrophilic enough to ensure that it will be able to leave the bilayer again.<sup>201</sup> This partitioning ability is of particular importance in the absorption of drugs.<sup>202</sup>

The standard model for the assessment of lipophilicity is the partition coefficient  $\log P_{oct}$ , which can be calculated by equation 4.1.

$$\log P_{oct} = \log \left( \frac{[solute]_{octanol}}{[solute]_{water}} \right) \quad [4.1]$$

The measurement or calculation of  $\log P$  is important in pharmacokinetics, where a high  $\log P$  correlates with poor permeation into cells.<sup>203</sup>  $\log P$  is of interest in this study, as it has been shown that the rate of passive diffusion correlates with  $\log P$ .<sup>204</sup>

In order to measure  $\log P$ , it is necessary to have some method of measuring the concentration of complex in octanol and water. This has been achieved in the past in various ways, such as scintillation counting of radio-labelled complexes<sup>205</sup> and flame atomic absorption spectroscopy.<sup>206</sup> In this study, lanthanide luminescence was used to calculate concentrations. For all complexes, standard curves were constructed over

appropriate concentration ranges for solutions in both 1-octanol and water. For all studies, water was saturated with 1-octanol and *vice versa* to ensure that any miscibility effects were constant throughout the experiment. 100  $\mu\text{M}$  aqueous solutions of the complexes were used to prepare mixtures containing various water : 1-octanol solvent ratios. A concentration of 100  $\mu\text{M}$  was selected after preliminary trials, as it ensured measurable luminescence in 1-octanol even for the most hydrophilic complexes. In total, three replicates of three different water : 1-octanol ratios were prepared, and shaken overnight to ensure complete partitioning. The luminescence of both the water and 1-octanol layers was then measured and the calibrations curves used to calculate concentrations of complex in each solvent. This allowed calculation of average  $\log P$  values, shown in Table 4.1. A range of complexes was studied which represented various structures and localisation behaviours.

**Table 4.1:**  $\log P_{oct}$  values for various lanthanide complexes, with standard deviations (SD)

	$\log P_{oct}$	SD
$[\text{Eu.L}^2]\text{Cl}_3$	-1.34	0.10
$[\text{Eu.L}^{3a}]\text{Cl}_3$	-2.10	0.40
$[\text{Tb.L}^{3a}]\text{Cl}_3$	-2.06	0.09
$[\text{Eu.L}^{3b}]\text{Cl}_3$	-1.15	0.20
$[\text{Eu.L}^{4a}]$	-1.74	0.37
$[\text{Tb.L}^{4a}]$	-1.56	0.25
$[\text{Eu.L}^{4b}]$	-0.16	0.03
$[\text{Eu.L}^{6b}]\text{Cl}_3$	-1.36	0.18
$[\text{Eu.L}^{6a}]\text{Cl}_3$	-1.56	0.09
$[\text{Tb.L}^8]\text{Cl}_3$	0.05	0.04
$[\text{Eu.L}^9]\text{Cl}_3$	-0.06	0.03
$[\text{Eu.L}^{11}](\text{OTf})_3$	1.06	0.13
$[\text{Eu.L}^{11}]\text{Cl}_3$	0.49	0.11
$[\text{Eu.L}^{12}]$	-1.52	0.05
$\text{Na}_2[\text{Gd.L}^{13}]$	-0.28	0.06

The measured partition coefficients range from hydrophilic (-2.10) to lipophilic (+1.06). The nature of the lanthanide ion does not appear to affect the  $\log P$  value, but variation of the counterion does have a significant effect, with the triflate complex being more lipophilic than the chloride form. This is consistent with previous observations of the

hydrophobicity of triflate.<sup>169</sup> Charged complexes have more negative  $\log P$  values than their neutral analogues, consistent with a greater aqueous solubility.

Importantly, the results reveal that complexes with very similar cellular behaviour, such as the lysosomally-localising  $[\text{Ln.L}^3]^{3+}$  and  $[\text{Ln.L}^4]$ , exhibit very different  $\log P$  values, from -0.16 to -2.10. Indeed, while all the complexes had been observed to cross the cell membrane at a similar rate, they vary greatly in partitioning behaviour. This suggests that cell uptake does not occur by passive diffusion, as in such a case diffusion rates would mirror trends in  $\log P$ .

#### 4.3.2 Preliminary low-temperature experiments

A common method which has been used to study the uptake of lanthanide complexes in the past is the incubation of cells at 4 °C. Lowering the incubation temperature for cells results in blocking of all endocytotic, energy-dependent processes.<sup>99, 207</sup> Similar uptake at 4 °C compared with that at 37 °C would therefore be evidence of a passive diffusion mechanism. In this preliminary study, microscopy was used as a means to observe changes in the uptake caused by incubation at low temperature. Cells were treated with various complexes, and incubated at either 4 °C or 37 °C. They were then visualised by fluorescence microscopy as previously described. It was important to rapidly view the cells, as at room temperature any endocytotic processes would be again switched on.

Representative microscopy images for two complexes are shown in Figure 4.8. The luminescence from the cells treated at 37 °C is readily observable, showing lysosomal and mitochondrial distribution for  $[\text{Eu.L}^2]^{3+}$  and  $[\text{Eu.L}^{6b}]^{3+}$  respectively. In cells treated at 4 °C, the luminescence is much weaker, and does not show clear localisation. Indeed, the luminescence intensity is not significantly greater than that observed for background, untreated cells. The cellular uptake is therefore greatly decreased at low temperatures, suggesting that uptake occurs by an active, energy-dependent process. More quantitative confirmation of these findings was obtained by ICP-MS studies, as will be presented in Section 4.5.3.

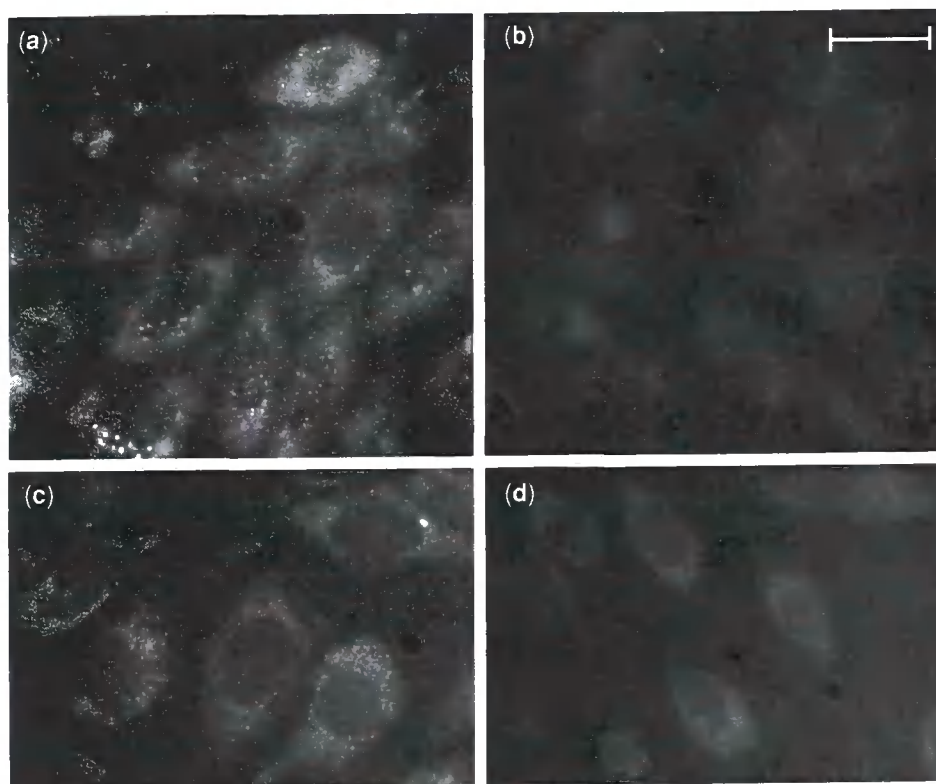


**Figure 4.8:** Fluorescence microscopy images showing CHO cells treated with  $[\text{Eu.L}^2]\text{Cl}_3$  (50  $\mu\text{M}$ , 4h) at (a) 37 °C and (b) 4 °C, and with  $[\text{Eu.L}^{6b}]\text{Cl}_3$  (50  $\mu\text{M}$ , 4h) at (c) 37 °C and (d) 4 °C. Scale bar represents 20  $\mu\text{m}$ .

### 4.3.3 Further evidence for active transport

The partitioning and low-temperature studies provide good evidence that uptake occurs *via* an active transport mechanism. This is further supported by the large size of the complexes – most have molecular weights exceeding 1 kDa – which has previously been shown to greatly hinder passive diffusion.<sup>203</sup>

Another effective method which could be adopted to assess for passive transport is the use of synthetic liposomes. Such liposomes, comprised of lipids such as phosphocholines, are good models for the lipid bilayer of the cell membrane in the absence of any proteins. Observation of the movement of a complex in or out of the liposome would therefore be evidence of its ability to passively diffuse across the cell membrane.<sup>208</sup> Preliminary attempts to use this method were unsuccessful, as the complex adhered to dialysis tubing which was used in the preparation and separation of the dosed liposomes. There was, nevertheless, sufficient evidence to assume that the lanthanide complexes were not passively diffusing across the cell membrane.

Investigations were therefore directed towards the determination of a possible active mechanism for cellular uptake. Before this could be achieved, however, it was necessary to refine the methods for measuring uptake.

## 4.4 Refining uptake measurements

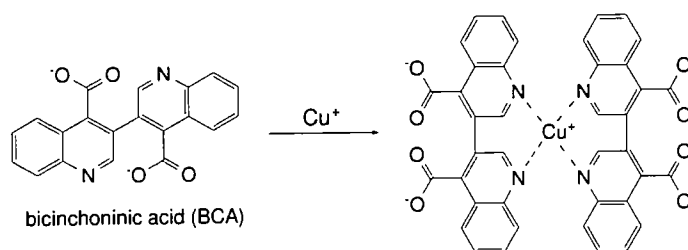
### 4.4.1 A new method for quantifying uptake

The flow cytometry process necessitates a relatively long time period between harvesting and collecting the cells, as discussed in Section 4.2.1. Over this time period, complex could leave the cells, and would not be measured by ICP-MS. It was therefore necessary to use a different method to count the number of cells.

One possible solution was to count the number of cells using a haemocytometer, as in previous studies of the uptake of metal complexes.<sup>209</sup> This could be performed immediately before plating, or on an aliquot of the sample to be submitted for ICP-MS. A number of trials were performed in which cells were counted and the cell count confirmed by flow cytometry, but the results proved neither sufficiently accurate nor precise.

Another method which is commonly adopted in cell uptake studies is the use of a protein assay kit to determine total protein content.<sup>210, 211</sup> While this method does not give a total number of cells, the protein content is proportional to the number of cells, and allows for calculation of a relative concentration, which can be used to compare samples.

The protein assay kit which was selected for use is the BCA Protein Assay Kit (Sigma). It is based on the reduction of  $\text{Cu}^{2+}$  to  $\text{Cu}^+$  by protein in alkaline conditions. The  $\text{Cu}^+$  then forms a complex with bicinchoninic acid (BCA) to form a complex which absorbs strongly at 562 nm (Scheme 4.1).<sup>212</sup>



Scheme 4.1

#### 4.4.2 Testing the uptake method

In order to test this alternative method for assessing cellular uptake, a similar experiment to that described in Section 4.2.1 was performed, again using  $[\text{Tb.L}^2]\text{Cl}_3$  in NIH 3T3 cells. In this case, however, the relative cell number was determined using the BCA protein assay kit. The values obtained were then compared to those previously determined by the flow cytometric method (Figure 4.9). The two methods give different units of intracellular concentration, and the values themselves cannot be compared, but the trends can be examined. Most notably, the egress of the complex from the cells (Figure 4.9b) appears to be less rapid by the BCA method. This is likely to be due to the very high rate of complex loss which could occur during the processes of harvesting and flow cytometry. Similarly, the intracellular concentration appears to increase more rapidly according to the BCA protein assay method, which again is likely to result from greater retention of complex prior to analysis. It appears that this modified method does circumvent the problems experienced in early experiments, and was therefore used for all subsequent studies.

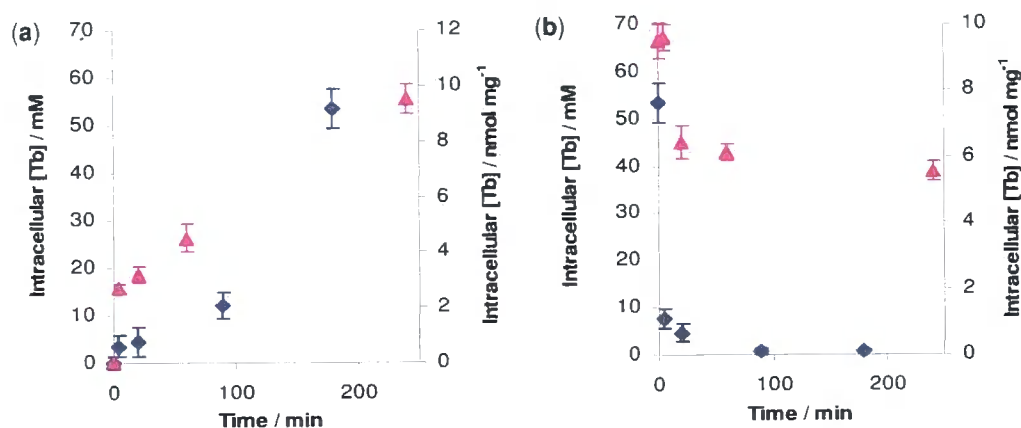


**Figure 4.9:** Uptake (a) and egress (b) of  $[\text{Tb.L}^2]\text{Cl}_3$  over a period of 4 h, measured by flow cytometric method (♦) and BCA protein assay (▲) ( $50 \mu\text{M}$  complex, NIH 3T3 cells).

#### 4.4.3 Determining the optimum incubation time

In order to further study the cellular transport of lanthanide complexes, it is necessary to compare the relative uptake under different conditions. It is therefore important to establish the optimum incubation time which will allow for the greatest cellular uptake

but avoiding any metabolism or excretion which might occur at longer time-points. To determine this, the uptake of two complexes was monitored over a 24 h period (Figure 4.10). For both complexes, the intracellular concentration increases rapidly over the first four hours. For the subsequent twenty hour period, there is only a very moderate further increase. An incubation time of 4 h was therefore chosen for all subsequent uptake experiments.

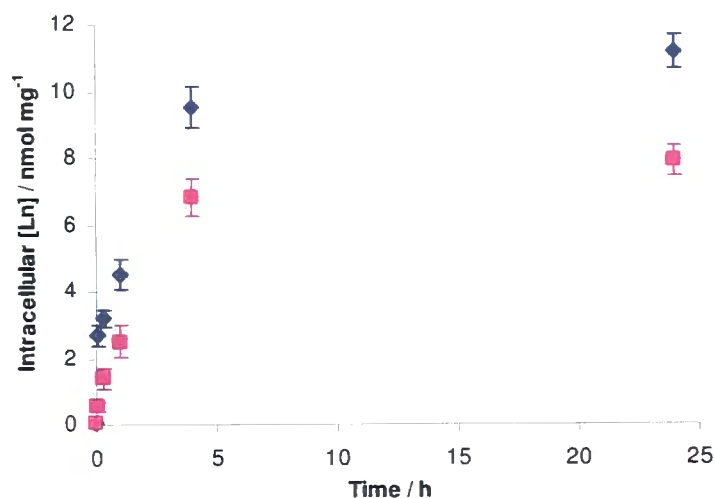


**Figure 4.10:** Uptake of  $[\text{Tb.L}^2]\text{Cl}_3$  ( $\blacklozenge$ ) and  $[\text{Eu.L}^{6a}]\text{Cl}_3$  ( $\blacktriangle$ ) over a period of 24 h (50  $\mu\text{M}$  complex, NIH 3T3 cells).

## 4.5 Determining the mode of endocytosis

The experiments described in Section 4.3 indicate an active uptake mechanism. Investigations therefore turned to the exploration of a possible endocytotic pathway for cellular uptake.

### 4.5.1 Selection of inhibitors and activators

A common method which has been employed to determine uptake mechanisms for various molecules such as cell-penetrating peptides,<sup>213</sup> modified RNA<sup>214</sup> and liposomes,<sup>141</sup> is the treatment of cells to selectively block or enhance different pathways. A number of treatments were selected from the literature, shown in Figure 4.11 and Table 4.1. Literature concentrations of all substances were used as a guideline, with non-toxicity confirmed by examining cells by microscopy.

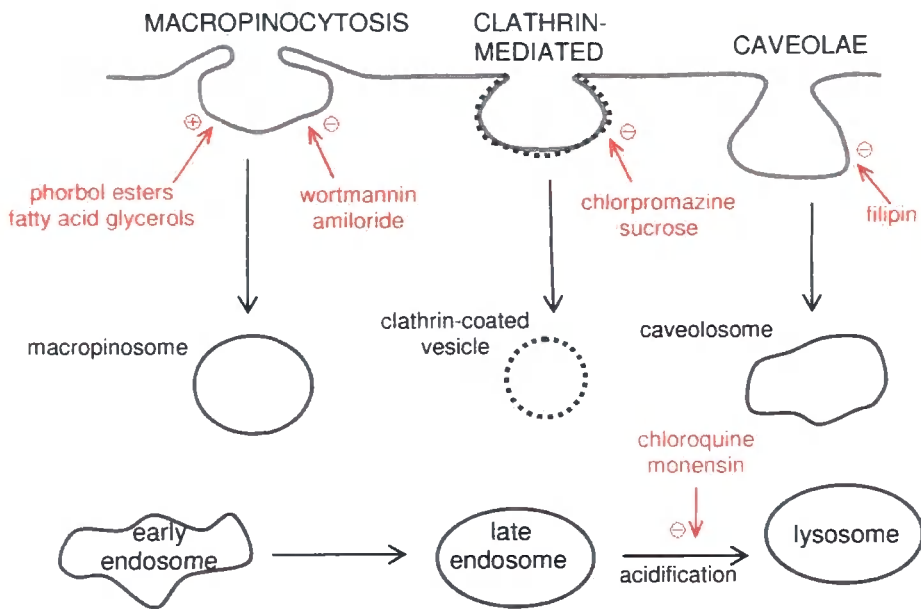


**Figure 4.11:** Schematic diagram illustrating the three endocytotic pathways in addition to the intracellular maturation of endosomes to lysosomes. Inhibitors (-) and activators (+) of each pathway are indicated.

**Table 4.2:** Inhibitors and activators for different endocytotic pathways

Treatment	Dosage	Effect	Mechanism
Sucrose	50 mM	Inhibitor of clathrin-mediated endocytosis	Unselective inhibition of clathrin-coated pit <sup>214</sup>
Chlorpromazine	50 $\mu$ M	Inhibitor of clathrin-mediated endocytosis	Dissociates the clathrin lattice <sup>215</sup>
Filipin	1 mg/mL	Inhibitor of caveolae	Binds to cholesterol <sup>216, 217</sup>
Wortmannin	300 nM	Inhibitor of macropinocytosis	Inhibitor of phosphatidyl inositol-3-phosphate <sup>218</sup>
Amiloride	3 mM	Inhibitor of macropinocytosis	Inhibits $\text{Na}^+/\text{H}^+$ pump <sup>219</sup>
Phorbol 12-myristate-13-acetate	50 ng/mL	Stimulator of macropinocytosis	Protein kinase C activator <sup>193, 220</sup>
1,2-Dipalmitoyl- <i>rac</i> -diacylglycerol	500 ng/mL	Stimulator of macropinocytosis	Protein kinase C activator <sup>220</sup>
Monensin	2 $\mu$ M	Inhibitor of endosome maturation	Prevents acidification of endosomes <sup>221</sup>
Chloroquine	10 $\mu$ M	Disruption of lysosomes	Prevents acidification of endosomes; causes lysosome swelling <sup>222</sup>
Poly-L-lysine	0.01%	Disrupts interaction with cell membrane	Non-specifically binds to cell membrane <sup>213</sup>
4 °C	-	General inhibitor of endocytosis	Depletion of energy <sup>99, 207</sup>

In order to determine the mode of uptake, it is important to compare the uptake of complex by control cells with the uptake by cells which have been treated with one of the drugs. CHO, NIH 3T3 and HeLa cells were grown to confluence in 12-well plates. The cells were pre-treated for 30 min with the drugs at concentrations shown in Table 4.2. Lanthanide complexes were then added (50  $\mu\text{M}$ ) and the cells incubated for a further 4 h. Uptake was then measured by one of two experiments. Microscopy studies were performed to give a visual indication of uptake changes. The second experiment involved quantification of the intracellular lanthanide concentration by using ICP-MS.

#### 4.5.2 Microscopy studies of uptake

Microscopy studies using inhibitors and activators were performed using complexes  $[\text{Eu.L}^2]\text{Cl}_3$ ,  $[\text{Eu.L}^{3b}]\text{Cl}_3$ ,  $[\text{Eu.L}^{6a}]\text{Cl}_3$ ,  $[\text{Eu.L}^{6b}]\text{Cl}_3$ ,  $[\text{Tb.L}^8]\text{Cl}_3$ ,  $[\text{Eu.L}^9]\text{Cl}_3$  and  $[\text{Eu.L}^{11}]\text{Cl}_3$ . All complexes were studied in CHO, HeLa and NIH 3T3 cells. Some representative images, of CHO cells treated with  $[\text{Tb.L}^8]\text{Cl}_3$ , are shown in Figure 4.12.

The control cells (Figure 4.12a) show the lysosomal distribution typical of  $[\text{Tb.L}^8]\text{Cl}_3$  after 4 h incubation. Upon treatment with chloroquine (b), the lysosomes appear to be larger. This is likely to be due to the inhibition by chloroquine of the maturation of the endosomes to lysosomes.<sup>222</sup> The relative luminescence intensity, however, remains unchanged. Cells which had been pre-treated with chlorpromazine (c) and filipin (d) show a similar luminescence pattern and intensity to the control cells. In contrast, treatment with wortmannin (e) results in a marked reduction in the luminescence intensity, while cells treated with the diacylglycerol (f) exhibited a higher level of luminescence, which was evident in the requirement for a shortened image acquisition time.

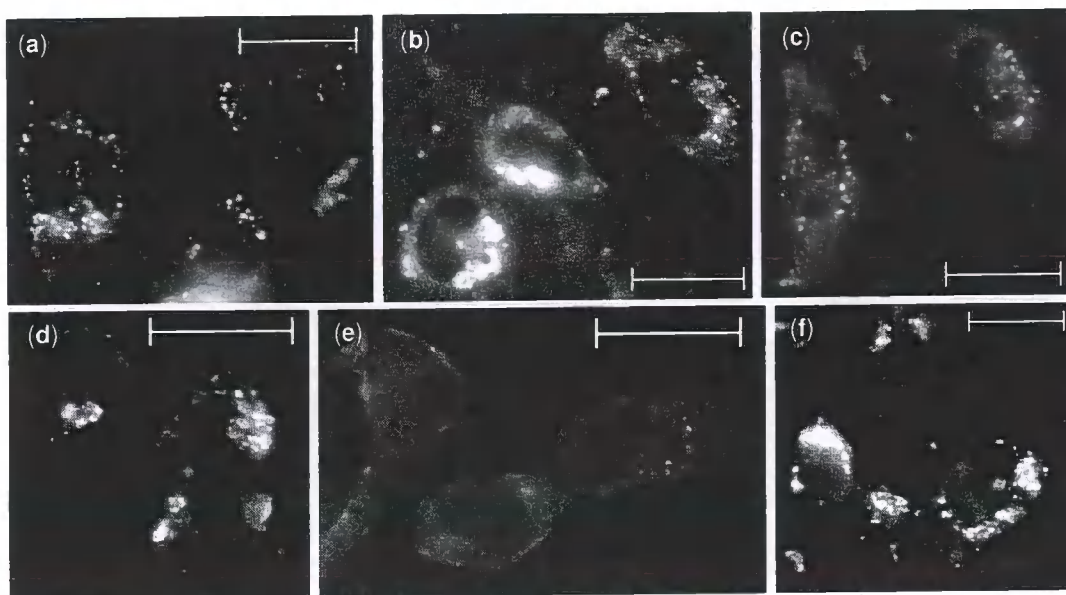


**Figure 4.12:** Fluorescence microscopy images showing luminescence of (a)  $[\text{Tb.L}^8]\text{Cl}_3$  (50  $\mu\text{M}$ , 4h) in CHO cells (a) without pre-incubation and following 30 min pre-incubation with (b) 10  $\mu\text{M}$  chloroquine, (c) 50  $\mu\text{M}$  chlorpromazine, (d) 1 mg/mL filipin, (e) 300 nM wortmannin and (f) 500 ng/mL 1,2-dipalmitoyl-*rac*-diacylglycerol.

For all the complexes and cell types studied, a comparison could be made of the luminescence intensity relative to that of the control. A summary of results is shown in Table 4.3. While the assessments of the relative luminescence intensity are somewhat arbitrary, they nonetheless demonstrate clear trends in the behaviour. Treatment with sucrose, chlorpromazine, filipin, monensin, chloroquine and poly-L-lysine did not result in significant luminescent changes. Treatment with wortmannin and amiloride, on the other hand, generally resulted in decreased luminescence intensity, while treatment with phorbol 12-myristate-13-acetate and 1,2-dipalmitoyl-*rac*-diacylglycerol gave rise to increased luminescence intensity. Since these are inhibitors and activators of macropinocytosis respectively, the microscopy results provide evidence for this endocytotic mechanism.

**Table 4.3:** Summary of microscopy results for various lanthanide complexes in (a) CHO, (b) NIH 3T3 and (c) HeLa cells.

Symbols indicate the strength of the effect ranging from (--- much weaker to +++ much stronger luminescence than from control cells), O denotes luminescence intensity approximately equivalent to the control.

Treatment	Complex																				
	[Eu.L <sup>2</sup> ]Cl <sub>3</sub>			[Eu.L <sup>3b</sup> ]Cl <sub>3</sub>			[Eu.L <sup>6a</sup> ]Cl <sub>3</sub>			[Eu.L <sup>6b</sup> ]Cl <sub>3</sub>			[Tb.L <sup>8</sup> ]Cl <sub>3</sub>			[Eu.L <sup>9</sup> ]Cl <sub>3</sub>			[Eu.L <sup>11</sup> ]Cl <sub>3</sub>		
	a	b	c	a	b	c	a	b	c	a	b	c	a	b	c	a	b	c	a	b	c
Sucrose	O	O	+	O	+	O	O	O	O	-	-	O	+	O	O	-	O	+	O	O	O
Chlorpromazine	O	+	O	O	++	O	O	O	O	O	-	O	O	O	O	-	-	O	+	O	O
Filipin	-	-	O	--	O	O	O	--	O	-	O	O	O	-	O	O	-	O	-	O	O
Wortmannin	--	---	--	---	--	-	--	--	-	---	--	--	---	---	-	---	---	-	--	---	-
Amiloride	---	---	--	--	---	--	--	---	---	---	---	-	--	---	--	--	---	--	---	--	-
Phorbol 12-myristate-13-acetate	++	++	+	++	+++	++	+++	++	+	+++	+	++	+	+++	O	++	+++	+	+++	++	++
1,2-Dipalmitoyl- <i>rac</i> -diacylglycerol	++	++	O	+++	++	+	+++	O	++	++	+++	+	+++	++	+	+	++	++	++	O	+
Monensin	O	O	+	+	O	O	O	O	-	--	-	O	O	+	O	+	O	O	O	O	-
Chloroquine	O	--	O	-	O	+	O	O	+	O	-	+	O	O	++	O	O	+	O	-	-
Poly-L-lysine	+	O	O	O	-	+	O	+	+	O	O	O	+	O	O	O	O	O	++	+	O

While this method did not provide quantitative results, it allowed study of a broad range of complexes and cell types. Examination of the morphology of the cells also enabled confirmation that the drugs were not being administered at cytotoxic concentrations. It was necessary, however, to confirm the conclusions drawn from these observations by a quantitative method.

### 4.5.3 Results of ICP-MS analysis

The intracellular concentration of lanthanide was therefore determined by a combination of the BCA assay and ICP-MS. Immediately after incubation with complex, cells were lysed with 500  $\mu\text{L}$  lysis buffer. Three 25  $\mu\text{L}$  aliquots were taken for analysis by the BCA assay, and a 400  $\mu\text{L}$  aliquot submitted for ICP-MS. In this way, any lanthanide that was within the cell at the end of the incubation time was measured by ICP-MS. In this method, it was important to thoroughly rinse the cells with PBS prior to lysis to ensure that only intracellular complex was being measured.

Initial studies of the BCA assay using both CHO and NIH 3T3 cells revealed that CHO cells gave more consistent results. This cell line was therefore used for all subsequent uptake studies. A range of complexes was tested by this method, which exhibited varying lipophilicities and localisation behaviour.

The uptake results are shown in Figure 4.13, and demonstrate a behaviour that is consistent with macropinocytosis. Both wortmannin and amiloride result in decreased uptake of all complexes, while the phorbol ester and fatty acid glycerol enhance uptake. The other drug treatments did not result in significant variations from the control.

The strongest inhibitory effect on uptake was observed when cells were incubated at 4  $^{\circ}\text{C}$ . This indicates that an energy-driven cellular process is responsible for cellular transport, which provides further support for the conclusions drawn in Section 4.3.

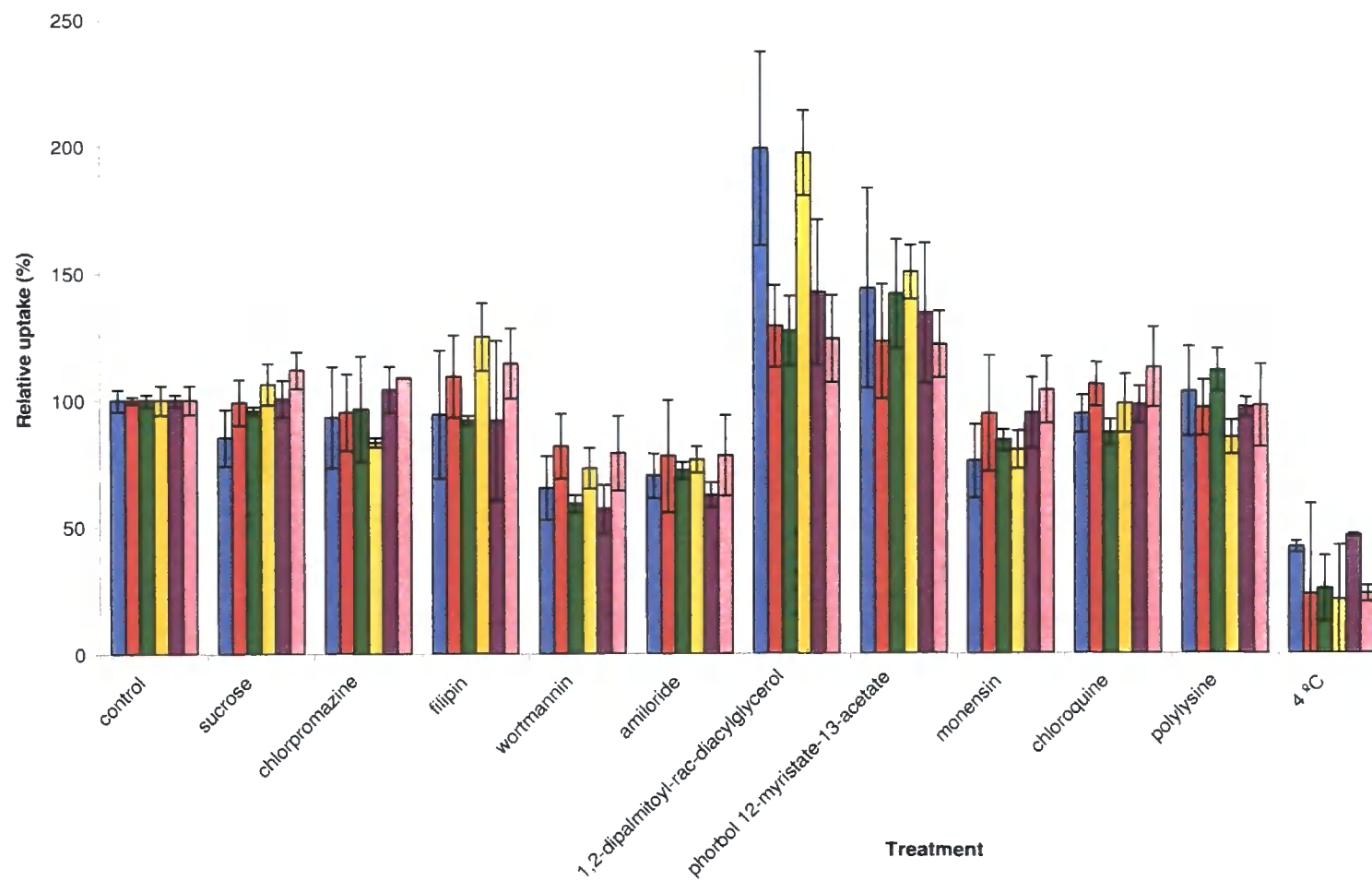


**Figure 4.13:** Relative changes in uptake of [Eu.L<sup>2</sup>]Cl<sub>3</sub> (blue), [Tb.L<sup>4a</sup>] (red), [Eu.L<sup>6a</sup>]Cl<sub>3</sub> (green), [Tb.L<sup>8</sup>]Cl<sub>3</sub> (yellow), [Eu.L<sup>9</sup>]Cl<sub>3</sub> (purple) and [Eu.L<sup>11</sup>](OTf)<sub>3</sub> (pink) following drug treatments (CHO cells, 50 μM complex, 4h incubation). n=4

While Figure 4.13 shows all intracellular concentrations relative the control case, it is valuable to compare their magnitudes. Table 4.4 shows the intracellular concentrations measured for CHO cells treated with each complex alone. The values are all of a similar order of magnitude, and do not appear to vary according to structure. For example,  $[\text{Tb.L}^8]\text{Cl}_3$  and  $[\text{Eu.L}^9]\text{Cl}_3$ , which are the most structurally similar exhibit the greatest difference in intracellular concentration.

**Table 4.4:** Intracellular lanthanide concentration after 4 h incubation (CHO cells, 50  $\mu\text{M}$  complex)

Complex	[Ln]; (nmol / mg protein)
$[\text{Eu.L}^2]\text{Cl}_3$	4.13
$[\text{Tb.L}^{4a}]$	2.87
$[\text{Eu.L}^{6a}]\text{Cl}_3$	5.15
$[\text{Tb.L}^8]\text{Cl}_3$	10.7
$[\text{Eu.L}^9]\text{Cl}_3$	0.95
$[\text{Eu.L}^{11}]\text{Cl}_3$	7.42

## 4.6 Exploring the macropinocytotic pathway

### 4.6.1 Confirmation of macropinocytosis

The microscopy and ICP-MS studies therefore indicate that endocytosis occurs *via* macropinocytosis. An uptake mechanism of macropinocytosis suggests that the lanthanide complexes should be localised within the macropinosomes at early time-points. A co-localisation study was therefore performed to confirm this hypothetical transport pathway. The fluorescein-labelled dextran conjugate (MW 70 kD) has been shown to be internalised by macropinocytosis, and can therefore be successfully used as a marker for the macropinosomes in fluorescence microscopy studies.<sup>223, 224</sup>

CHO and NIH 3T3 cells were incubated with 100  $\mu\text{M}$   $[\text{Eu.L}^1]\text{Cl}_3$ ,  $[\text{Eu.L}^{6a}]\text{Cl}_3$  or  $[\text{Eu.L}^9]\text{Cl}_3$  for 15 min in the presence of FITC-dextran (2.5 mg/mL), after which time the cells were visualised by microscopy. In every case the europium luminescence showed good co-localisation with the fluorescein fluorescence. An example set of images is shown in Figure 4.14. This study confirms the hypothesised endocytotic mechanism established above.

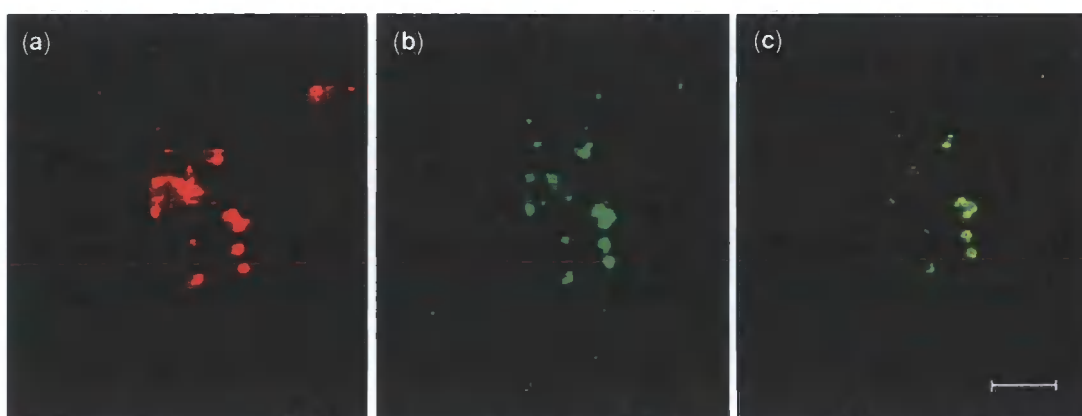


**Figure 4.14:** Fluorescence microscopy images of CHO cells treated with  $[\text{Eu.L}^{6a}]\text{Cl}_3$  (100  $\mu\text{M}$ ) and FITC-dextran (70 kDa, 2.5 mg/mL) for 15 min. (a) Eu luminescence, (b) fluorescein fluorescence and (c) colocalisation image. Scale bar represents 20  $\mu\text{m}$ .

#### 4.6.2 Implications of uptake by macropinocytosis

There is very strong evidence, therefore, for an uptake mechanism of macropinocytosis. It is important to consider whether the observed behaviour of the complexes is consistent with the current understanding of this pathway.

Both clathrin-coated pits and caveolae contain receptors to which a ligand must bind to induce endocytosis.<sup>158</sup> This binding event has a high structural specificity. It is unlikely therefore, that the broad array of complexes, which differ so markedly in geometry, charge and lipophilicity, should all bind to these receptors. Macropinocytosis, on the other hand is not a receptor-mediated process; macropinosomes do not concentrate receptors,<sup>225</sup> and the internalisation process is relatively non-specific.<sup>226</sup> The observation that the broad range of lanthanide complexes studied are all internalised by macropinocytosis is consistent with its lack of specificity.

While macropinocytosis is not a receptor-mediated process, it does require a number of signalling factors. Ruffling of the cell membrane is mediated by various GTPases belonging to the Ras superfamily,<sup>227</sup> while closure of the ruffles to form the macropinosomes requires different signals including phosphatidylinositol 3-kinase.<sup>228</sup> Further work would be required to determine what triggers such signalling pathways in the case of the lanthanide complexes.

A second important consideration in examining endocytotic pathway is the fate of the generated vesicles. The downstream route of the macropinosome has not been fully elucidated, and appears to differ between cell types.<sup>229, 230</sup> While macropinosomes in macrophages have been observed to fuse with endosomes,<sup>225</sup> in fibroblasts they appear not to transfer their contents to the endosomal pathway.<sup>193</sup> The large size of the macropinosomes compared to other vesicles is believed to render them more leaky, readily releasing their contents into the cytoplasm.<sup>225</sup> It is possible that, from there, they are then trafficked to different locations within the cell. The fact that the macropinosomes do not deliver their contents to a single location is consistent with the observation that all lanthanide complexes studied are endocytosed by the same mechanism, despite their very different subsequent sub-cellular localisations.

## 4.7 Conclusions

In designing luminescent lanthanide complexes for use as cellular probes, it is important to assess whether the cell membrane is permeable towards these complexes. If, for example, only certain complexes were transported across the cell membrane, then their structural features would need to be conserved in future complex design. If no complexes showed sufficient cellular uptake, it would be necessary to make structural modifications, such as the conjugation of a cell-penetrating peptide or encapsulation into a liposome.

The results of this study have shown that all lanthanide complexes investigated are able to cross the cell membrane. Cases in which complexes are only poorly visible by microscopy can be attributed to higher *in cellulo* quenching rather than to decreased uptake. Each lanthanide complex studied seems to enter cells by the mechanism of macropinocytosis. It is likely that this pathway contributes to the fact that such a broad range of complexes is internalised, and that complexes show diverse distribution patterns within the cell.

## CHAPTER FIVE

---

# **SUB-CELLULAR SPECIATION OF COMPLEXES**

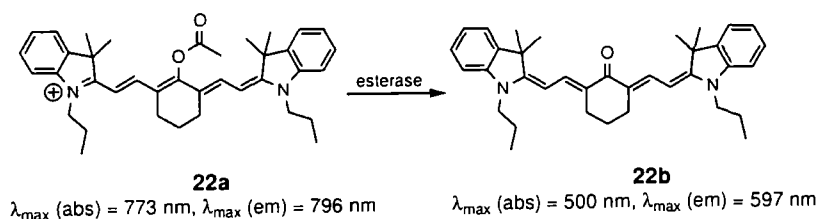
## 5.1 Introduction

Chapters Three and Four have discussed the localisation and uptake behaviour respectively of the luminescent lanthanide complexes. Another important aspect of cellular behaviour is the fate of the complexes in cells, and the form which those complexes will take *in cellulo* – that is, their sub-cellular speciation.

The cell contains many species which can interact with an exogenous compound and alter its function. For example, complexes may be oxidised, reduced, methylated or hydrolysed by various enzymes. In addition, they may be conjugated to amino acids, sugars or thiols, or they may bind to proteins.<sup>231</sup> These interactions may exert negative or positive effects on the function of a probe or drug.

There are many examples of drugs which are inactivated by metabolic events. The main challenge in the design of orally-active drugs, for example, is to prevent any such inactivation from occurring before the drug reaches its target.<sup>231</sup> Furthermore, drug metabolism to toxic forms has been implicated as the principal source of hepatotoxicity in clinical drug trials.<sup>232, 233</sup> While considerably less work has been performed concerning the inactivation of probes by cellular events, it can be assumed that the same principles apply.

In contrast, many drugs and probes are activated by sub-cellular events. In order to overcome the toxicity effects which drugs may exert as they travel from the point of administration to the point of activity, much drug design utilises pro-drugs, which are activated by metabolic events in the cell.<sup>234</sup> This principle has also been applied to the design of molecular imaging probes. There are many examples of probes which are administered as cell-permeable, but less fluorescent, esters, and are then hydrolysed by esterases within the cell to a fluorescent form.<sup>15</sup> For example, hydrolysis of the ester **22a** to the ketone **22b** results in dramatic changes in the fluorescence emission and excitation spectra (Scheme 5.1).<sup>235</sup>



Scheme 5.1

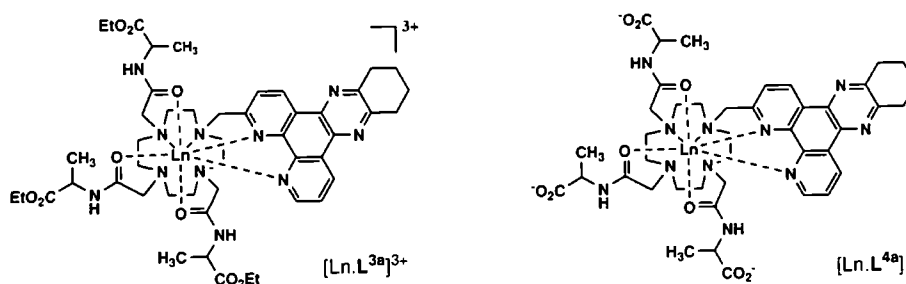
Another example of an activatable probe is an avidin-rhodamine X complex, which is self-quenching. The avidin has an affinity for the lectin expressed on cancer cells, and the complex is therefore endocytosed by cancer cells, before being transferred to the lysosomes. Here, the protein is hydrolysed, resulting in release of the rhodamine X, and a concomitant return of fluorescence. In this way, the complex can act as a selective marker for cancer cells.<sup>236</sup>

In assessing the suitability of a cellular probe, therefore, it is important to consider its speciation, and whether it affects the intended purpose. This chapter describes work which has been performed to study sub-cellular speciation of certain complexes, by presenting examples of four specific cellular interactions: hydrolysis, dissociation, anion binding and protein binding.

## 5.2 Sub-cellular speciation

### 5.2.1 Enzyme hydrolysis

The observation of enzyme hydrolysis requires that the hydrolysed and non-hydrolysed form of the complex have different spectral properties. This is the case for the series of complexes  $[\text{Eu.L}^3]^{3+}$  and  $[\text{Eu.L}^4]$ , in which hydrolysis of the ethyl ester arms results in a marked change in the luminescence emission profiles. This change is most evident for the alanine system,  $[\text{Eu.L}^{3a}]^{3+}$ , for which there are large changes in the  $\Delta J = 2$  and  $\Delta J = 4$  bands (Figure 5.1).



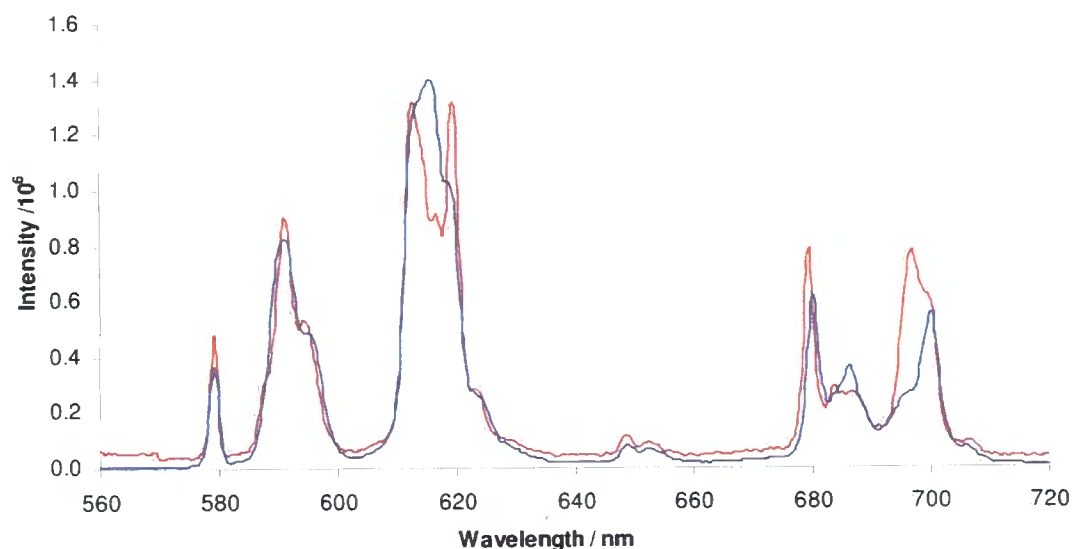


**Figure 5.1:** Emission spectra of  $[\text{Eu.L}^{3\text{a}}]^{3+}$  (red) and  $[\text{Eu.L}^{4\text{a}}]$  (blue) solutions ( $\text{D}_2\text{O}$ , 295 K,  $\lambda_{\text{ex}} = 348 \text{ nm}$ )

In order for this hydrolysis event to be observable in cells, the complex must be a substrate for hydrolytic enzymes. To study this, an aqueous solution of  $[\text{Eu.L}^{3\text{a}}]^{3+}$  was treated with two different hydrolytic enzymes, and the emission spectrum monitored over time. The two enzymes selected were chymotrypsin and pig liver esterase (PLE). Chymotrypsin is a proteolytic enzyme which cleaves on the C-terminal side of the aromatic amino acids tyrosine, tryptophan and phenylalanine.<sup>237</sup> PLE is a carboxylesterase which is commonly employed in organic synthesis.<sup>238</sup> The complex solution was prepared using phosphate buffered saline (pH 7.4), and the experiment performed at 37 °C to mimic biological conditions.

Treatment of  $[\text{Eu.L}^{3\text{a}}]^{3+}$  with PLE did not give rise to any changes in the emission spectrum over a two week period. Treatment with chymotrypsin, on the other hand, resulted in a very rapid decrease in the band at 620 nm (Figure 5.2). In addition, an overall quenching of luminescence was observed. This is consistent with the findings presented in Chapter Two (page 58), which showed that  $[\text{Eu.L}^{4\text{a}}]$  is more susceptible to quenching by endogenous anions than  $[\text{Eu.L}^{3\text{a}}]^{3+}$ . The change in the ratio of intensities at 614 nm and 620 nm over time indicates that the hydrolysis occurs over the first ten minutes, and then remains constant (Figure 5.2 inset). The  $I_{614 \text{ nm}}/I_{620 \text{ nm}}$  ratio for  $[\text{Eu.L}^{4\text{a}}]$  and  $[\text{Eu.L}^{3\text{a}}]^{3+}$  are 3.2 and 1.0 respectively, while the value reached on enzyme treatment is 2.2. This indicates that enzyme hydrolysis has not gone to completion.

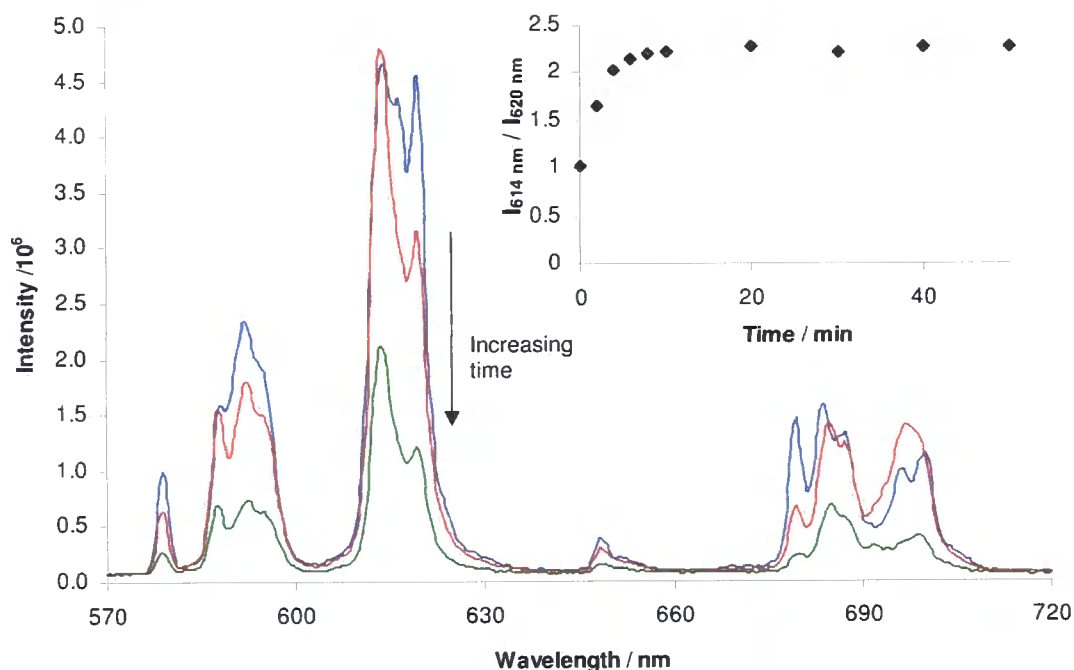
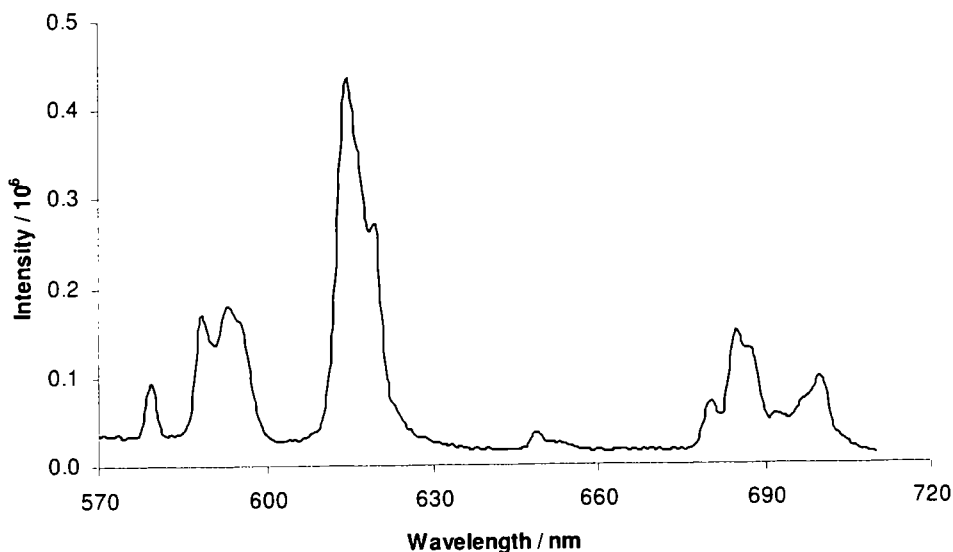


Figure 5.2: Emission spectra ( $\lambda_{\text{ex}} = 348 \text{ nm}$ ) of  $[\text{Eu.L}^{3a}]\text{Cl}_3$  (blue) and 10 min (red) and 4 h (green) after treatment with chymotrypsin (37 °C, pH 7.4). Inset: Change in the luminescence intensity ratio  $I_{614 \text{ nm}} / I_{620 \text{ nm}}$  with time after treatment with chymotrypsin

These results indicate that  $[\text{Eu.L}^{3a}]^{3+}$  is susceptible to hydrolysis by biologically-occurring enzymes. It was therefore of interest to assess the *in cellulo* speciation of the complex, by collecting an emission spectrum of the complex in whole cells. This was achieved by incubating cells with the complex (50  $\mu\text{M}$ , 4h), washing the cells thoroughly with PBS to ensure only complex in the cell would be measured, and rapidly harvesting the cells. The cell pellet was resuspended in 1 mL PBS and an emission spectrum collected. It was important that all steps were performed as quickly as possible to minimise complex egress from the cell. Over the time required to collect the emission spectrum, the cells began to settle to the bottom of the cuvette, resulting in decreased signal at higher wavelengths as the cells were no longer in the path of the beam. Multiple spectra were therefore obtained at a faster scan rate, and averaged to minimise noise. The mixture was shaken well between each data collection to ensure that the maximum amount of signal could be measured.

The emission spectrum recorded from CHO cells treated with  $[\text{Eu.L}^{3a}]^{3+}$  is shown in Figure 5.3. The spectral profile is very similar to that of the enzyme-treated complex in Figure 5.2. The  $I_{614 \text{ nm}} / I_{620 \text{ nm}}$  ratio, of 1.8, indicates that reaction has not gone to

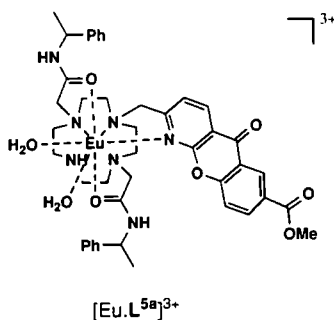
completion. This result is consistent with expectation, as the cell contains a large range of esterases which would be expected to hydrolyse the complex.



**Figure 5.3:** Emission spectrum ( $\lambda_{\text{ex}} = 348 \text{ nm}$ , PBS, pH 7.4) of CHO cells treated with  $[\text{Eu.L}^{3a}]\text{Cl}_3$  ( $50 \mu\text{M}$ , 4h)

### 5.2.2 Complex dissociation

As discussed in Section 1.4.2.1 (page 19), the luminescent lanthanide design was based on the cyclen macrocycle in order to afford stable complexes. It is possible, however, that decomplexation may occur in cells. This was found to be the case for  $[\text{Eu.L}^{5a}]^{3+}$ .



Previous studies of  $[\text{Eu.L}^{5a}]^{3+}$  described the formation of precipitate in solutions of  $\text{NaHCO}_3$  or  $\text{NaHPO}_4$ , which was attributed to decomplexation of Eu(III) from the ligand.<sup>148</sup> It was therefore expected that such an event should be observable *in cellulo*.

CHO cells were treated with  $[\text{Eu.L}^{5a}]\text{Cl}_3$  ( $50\ \mu\text{M}$ ), and prepared for microscopy as previously described. In addition to the standard filter set designed to measure Eu luminescence, a filter set was also selected to capture ligand fluorescence. A set of microscopy images obtained after 1 h incubation are shown in Figure 5.4. There is an observable difference between the distribution of Eu luminescence and ligand fluorescence, suggesting that dissociation has indeed occurred. The complex luminescence and ligand fluorescence for a number of other systems were visualised, but for no other complex was this phenomenon observed.

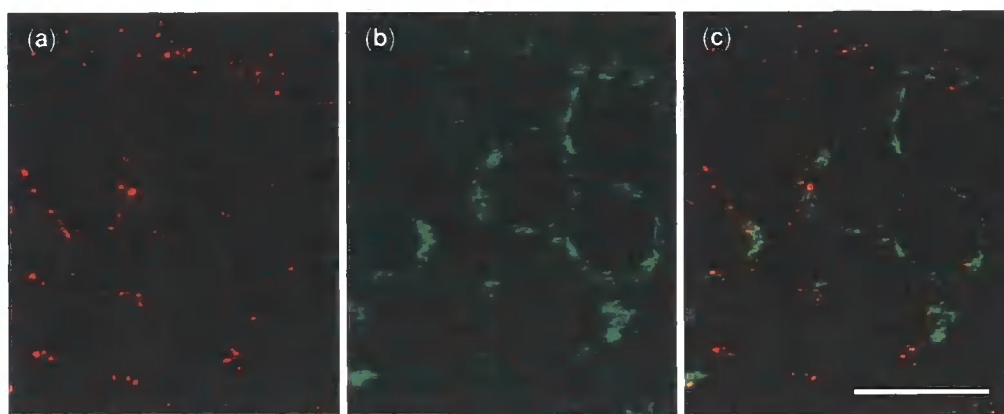


**Figure 5.4:** Fluorescence microscopy images of CHO cells treated with  $[\text{Eu.L}^{5a}]\text{Cl}_3$  ( $50\ \mu\text{M}$ , 1h), (a) Eu luminescence, (b) ligand fluorescence and (c) image overlay. Scale bar represents  $20\ \mu\text{m}$ . Image brightness and contrast have been altered.

### 5.2.3 Anion binding

Many of the luminescent lanthanide complexes that have been synthesised in Durham bind selectively to anions such as carbonate or phosphate. It is possible, therefore, that in cells, these complexes are bound to anions.  $[\text{Eu.L}^{6a}]^{3+}$  was studied for this purpose. Previous studies had identified selectivity for citrate and bicarbonate, and a marked change in the emission spectrum in the presence of a number of anions such as bicarbonate and phosphate.<sup>148</sup> An emission spectrum of CHO cells treated with  $[\text{Eu.L}^{6a}]\text{Cl}_3$  ( $50\ \mu\text{M}$ , 4h) was therefore obtained (Figure 5.5).

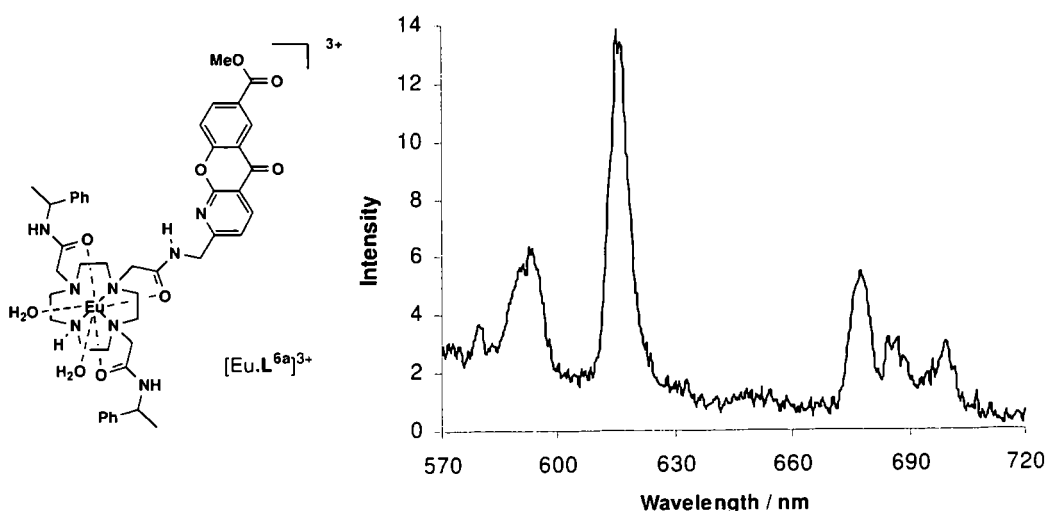


**Figure 5.5:** Emission spectrum ( $\lambda_{\text{ex}} = 335$  nm, PBS, pH 7.4) of CHO cells treated with  $[\text{Eu.L}^{6a}]\text{Cl}_3$  (50  $\mu\text{M}$ , 4h).

While the emission profile collected from cells is not sufficiently well resolved to allow accurate calculation of intensity ratios, it does reveal valuable information about the relative intensity of transitions, which can be used to determine the species which are bound to the complex. Taking into account the tail of the protein fluorescence (from approximately 400 to 600 nm),  $\Delta J = 2 / \Delta J = 1$  and  $\Delta J = 2 / \Delta J = 0$  ratios can be calculated and compared to that of the complex alone, and in its various bound forms (Table 5.1).

**Table 5.1:** Relative peak intensities for  $[\text{Eu.L}^{6a}]^{3+}$  after various treatments.

Treatment	$\Delta J = 2 / \Delta J = 1$	$\Delta J = 2 / \Delta J = 0$
Complex alone <sup>†</sup>	2.2	3.3
$\text{HCO}_3^-$ (0.5 mM) <sup>†</sup>	2.2	7.2
$\text{HPO}_4^{2-}$ (0.5 mM) <sup>†</sup>	2.3	9.0
HSA (0.35 mM) <sup>†</sup>	2.3	5.4
HSA (0.35 mM) + $\text{HCO}_3^-$ (30 mM) <sup>†</sup>	3.3	15
CHO cells	3.1	14

<sup>†</sup> Values previously reported<sup>148</sup>

The  $\Delta J = 2 / \Delta J = 1$  and  $\Delta J = 2 / \Delta J = 0$  ratios observed from the complex in cells are most similar to the complex in the presence of both bicarbonate and HSA. This suggests that, in addition to being associated with protein *in cellulo*, the complex is also binding to intracellular bicarbonate. These results indicate that  $[\text{Eu.L}^{6a}]^{3+}$  has potential utility as

a probe of bicarbonate concentration, but that calibration would need to be performed in the presence of protein.

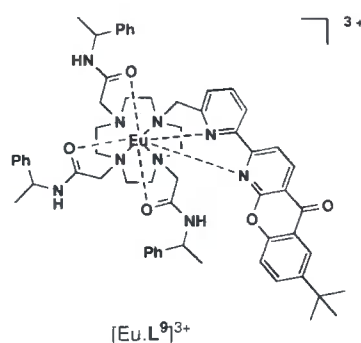
### 5.2.4 Protein binding

Due to the high intracellular concentration of protein, a number of studies have investigated the effect of protein binding on the *in vitro* properties of luminescent lanthanide complexes.<sup>129, 154, 239</sup> The studies reported in Section 2.4.2 (page 60) of the variation of luminescence lifetime with the addition of BSA revealed a range of affinities, which span a 2-log range. These association affinities do not appear to correlate with lipophilicities (Table 5.2). In addition, these complexes, despite their vastly different protein association behaviour, exhibited identical lysosomal localisation.

**Table 5.2:** Comparison of protein binding data to logP values for complexes with common ligands

Ligand	$K_a$ for protein binding (Tb complex)	Limiting $\tau_0/\tau$ value (Tb complex)	LogP (Eu complex)
$L^2$	$1.18 \times 10^5$	1.4	-1.34
$L^{3a}$	$6.60 \times 10^3$	3.4	-2.06
$L^{3b}$	$9.44 \times 10^2$	3.2	-1.15
$L^{4a}$	$1.46 \times 10^3$	7.6	-1.56
$L^{4b}$	$2.14 \times 10^4$	3.2	-0.16

To date, these studies have assumed that this association of lanthanide complexes with protein observed *in vitro* also occurs *in cellulo*. It is important, however, to demonstrate that complexes do interact with protein in a cellular environment. Analysis of the emission spectrum of  $[\text{Eu.L}^{6a}]^{3+}$  described above (Figure 5.5) provides evidence for intracellular protein binding. Further evidence was obtained from the study of  $[\text{Eu.L}^9]^{3+}$ .<sup>151</sup>



Addition of aqueous solutions of citrate (0.13 mM) or HSA (0.4 mM) to  $[Eu.L^9]^{3+}$  led to a reduction in the intensity of the europium emission, in addition to changes in spectral form (Figure 5.6). In each case, the europium emission lifetime changed by less than 10%. These spectral changes are consistent with dissociation of the chelating nitrogens of the sensitizer.

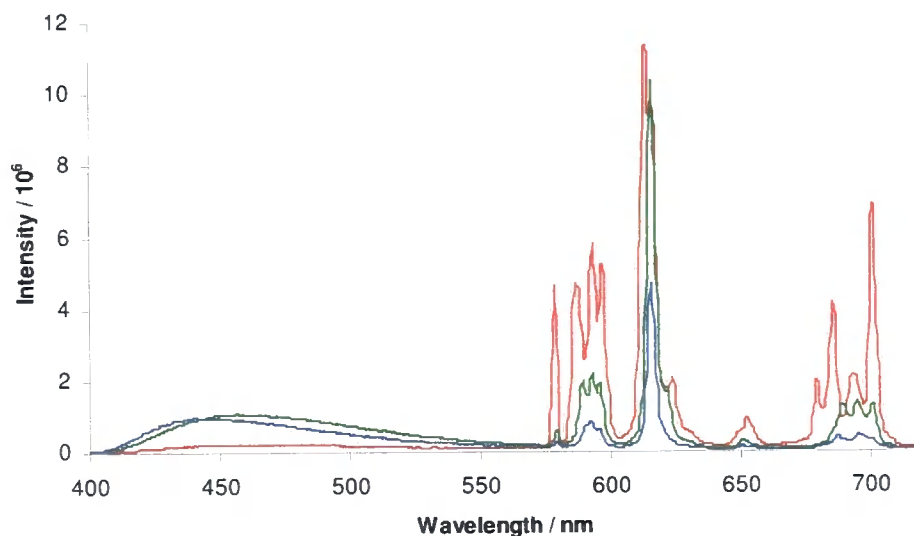


**Figure 5.6:** Emission spectra ( $\lambda_{ex} = 355$  nm) of  $[Eu.L^9]Cl_3$  (red) and in the presence of 0.13 mM citrate (green) and 0.4 mM HSA (blue).

CHO cells were treated with  $[Eu.L^9]Cl_3$  (50  $\mu$ M, 6h) and an emission spectrum recorded, as described above (Figure 5.7). Cells treated in an identical manner were also visualised by fluorescence microscopy, and at this time-point a predominant lysosomal localisation was observed. This confirmed that the emission spectrum obtained corresponded to intracellularly localised complex. The spectral form collected in this manner is very similar to that of the spectrum of complex in the presence of HSA (Figure 5.6). This suggests that the *in cellulo* form of  $[Eu.L^9]Cl_3$  is protein-bound.

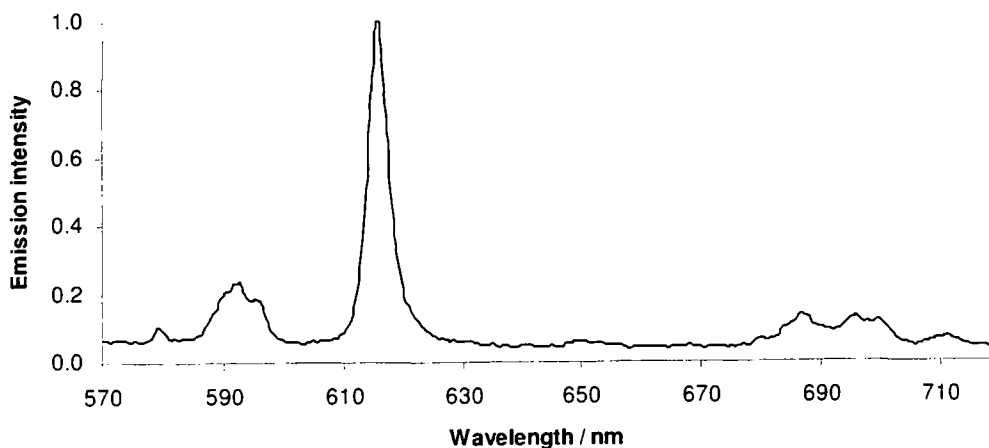
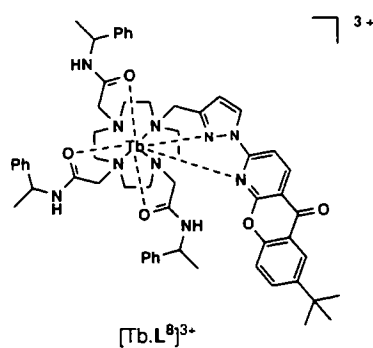


**Figure 5.7:** Emission spectrum ( $\lambda_{\text{ex}} = 355 \text{ nm}$ , PBS, pH 7.4) of CHO cells treated with  $[\text{Eu.L}^9]\text{Cl}_3$  ( $50 \mu\text{M}$ , 6h)

These results have demonstrated that protein binding is an important aspect of sub-cellular speciation. It is therefore important to consider the effect of protein binding on other aspects of probe behaviour. One species for which this is relevant is  $[\text{Tb.L}^8]^{3+}$ , which was demonstrated to have a clear and reversible variation of intensity on changing pH.<sup>151</sup> It was therefore postulated that  $[\text{Tb.L}^8]^{3+}$  may have potential utility as an *in cellulo* pH probe. In order to test this behaviour, the pH titration was repeated in the presence of HSA ( $0.4 \text{ mM}$ ; Figure 5.8 overleaf).



The resulting titration curve indicates very different behaviour to that observed in the absence of protein. This could be due to the fact that in the presence of protein, the chelating nitrogens of the sensitiser are dissociated at all pH values, while in the absence of protein this dissociation event only takes place at relatively high pH. The altered spectral properties may also be due to the fact that the intensity ratio utilised measures the ratio of  $\text{Tb}^{3+}$  emission intensity against the residual ligand fluorescence. The HSA itself, however, fluoresces in the same region as the ligand fluorescence, thus interfering

with the measurement. As a result of this investigation, it was concluded that  $[\text{Tb.L}^8]^{3+}$  is not a suitable candidate for use as an intracellular pH probe. This work highlights the importance of testing probe behaviour in a biologically-relevant context.

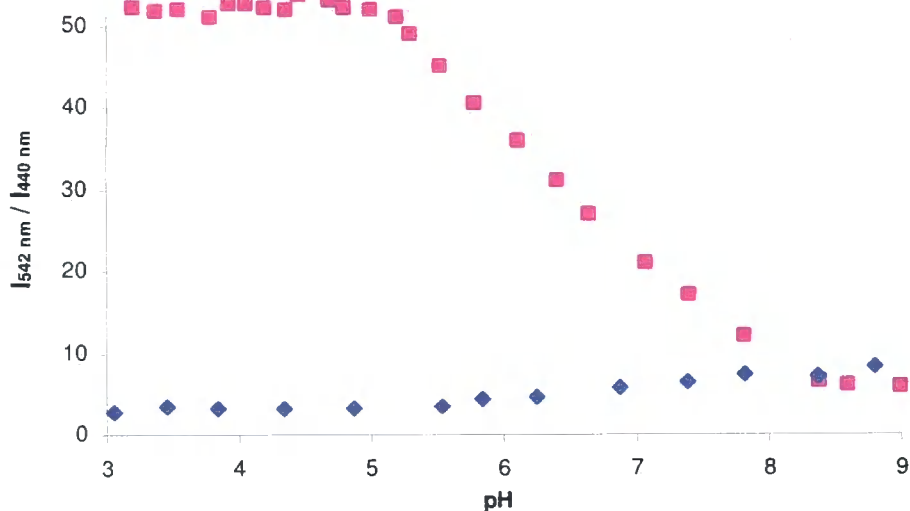


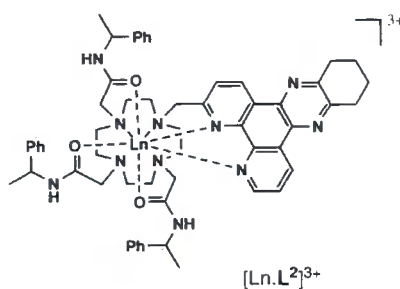
**Figure 5.8:** Variation of the ratio of  $\text{Tb}^{3+}$  emission intensity versus residual ligand fluorescence with pH for  $[\text{Tb.L}^8]^{3+}$  in the absence (■) and presence (◆) of HSA (0.4 mM) (295 K, 0.1M NaCl)

This pH study of  $[\text{Tb.L}^8]^{3+}$  provides an example of how protein binding can strongly perturb probe behaviour. However, protein interaction can also have positive effects on such activity. The clearest example of this is the alleviation of quenching which has been observed in the presence of protein, as discussed in Section 4.2.2 (page 112) and elsewhere.<sup>86, 148</sup> This behaviour ensures that, even in the presence of intracellular quenchers, the probe has sufficient *in cellulo* luminescence to be visible by microscopy. It is therefore important to assess the effects of protein binding on the behaviour of each potential probe. The following section discusses one specific case of protein binding, which was found to exhibit unprecedented behaviour.

### 5.3 Stereoselectivity of protein interactions

As discussed in Section 2.4.2 (page 60), the binding of complexes to protein can be studied by measurement of the emission lifetime. This enabled comparison of the binding associations of a range of complexes with BSA. Complexes such as  $[\text{Tb.1}]$

exhibited only weak, non-specific interactions, while  $[\text{Tb.L}^2]^{3+}$  showed apparently strong 1:1 binding.



The stereospecificity of the association was investigated by comparing the binding isotherm for  $(SSS)\text{-}[\text{Tb.L}^2]^{3+}$  to that of the enantiomer,  $(RRR)\text{-}[\text{Tb.L}^2]^{3+}$  (Figure 5.9). Incremental addition of BSA to  $(SSS)\text{-}[\text{Tb.L}^2]^{3+}$  gave rise to a well-defined binding curve reaching a limiting-value, consistent with an interaction with one major protein binding site. The corresponding curve for  $(RRR)\text{-}[\text{Tb.L}^2]^{3+}$  was more complex in form, suggesting that the complex is interacting with up to three protein binding sites of different affinities, which have different effects on the emission lifetime. This suggests that the two enantiomers interact differently with BSA.

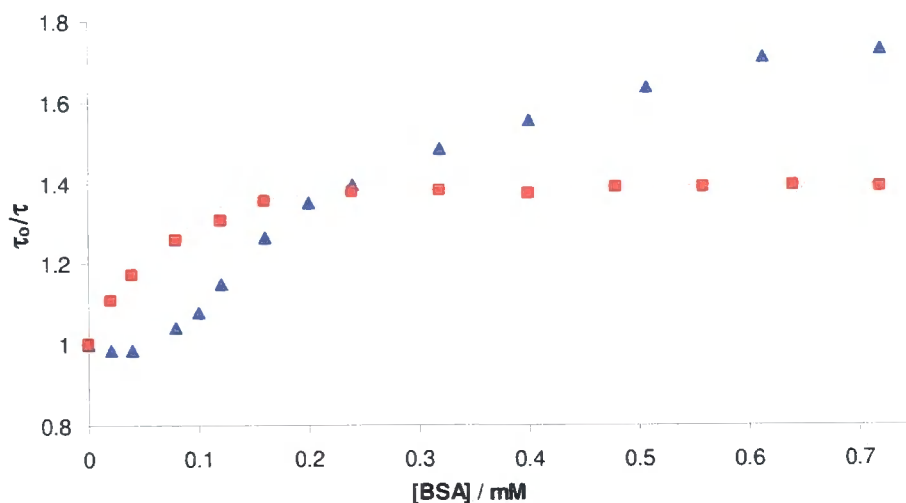


**Figure 5.9:** Quenching of the luminescence lifetime,  $\tau$ , upon addition of BSA to  $(SSS)\text{-}[\text{Tb.L}^2]^{3+}$  (■), showing the fit to the observed data for a 1:1 complex,  $\log K = 5.1$  and  $(RRR)\text{-}[\text{Tb.L}^2]^{3+}$  (▲) (295 K, pH 7.4, 0.1 M HEPES, 10  $\mu\text{M}$  NaCl, 30  $\mu\text{M}$  complex,  $\lambda_{\text{ex}} = 348$  nm)

### 5.3.1 CPL studies in the presence of protein

In order to study these enantiospecific effects in more detail, CPL spectroscopy studies were performed in the presence of BSA, and the resulting spectra compared to the spectra of the complexes alone. Addition of BSA to  $(SSS)\text{-[Eu.L}^2\text{]}^{3+}$  resulted in a marked change in the CPL spectrum (Figure 5.10). Most transitions are inverted in sign, in addition to the decreased overall emission resulting from quenching by the protein.<sup>240</sup>

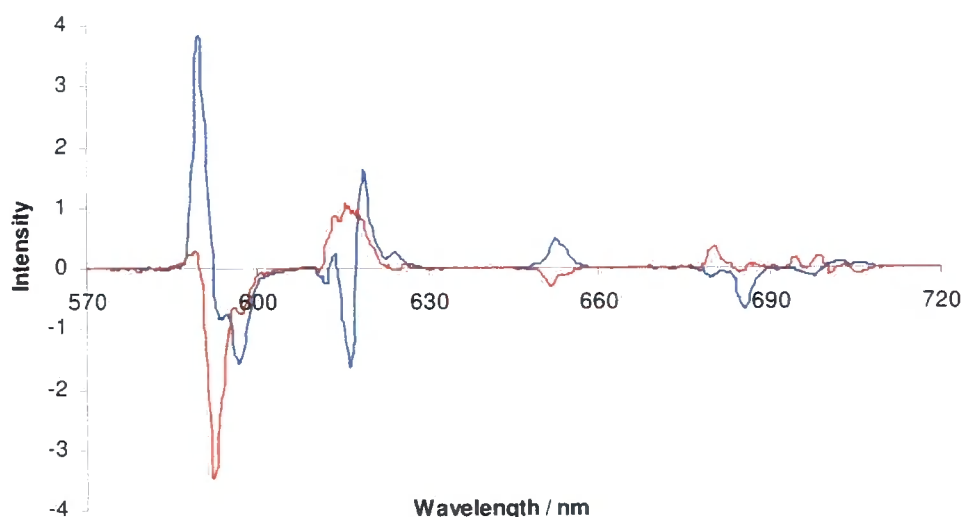


**Figure 5.10:** CPL spectra for  $(SSS)\text{-[Eu.L}^2\text{]}^{3+}$  in the absence (blue) and presence (red) of 15  $\mu\text{M}$  BSA ( $\text{D}_2\text{O}$ , 295 K,  $\lambda_{\text{ex}} = 348 \text{ nm}$ )

The same experiment was performed with the enantiomer,  $(RRR)\text{-[Eu.L}^2\text{]}^{3+}$  (Figure 5.11). While the CPL spectrum of the complex alone is the mirror image of that of its enantiomer, the spectrum of the BSA-treated sample is markedly different; in this case, it follows the same form as the untreated sample. This suggests that the complexes interact with BSA in a stereospecific manner, in agreement with the observed differences in the quenching behaviour (Figure 5.9).

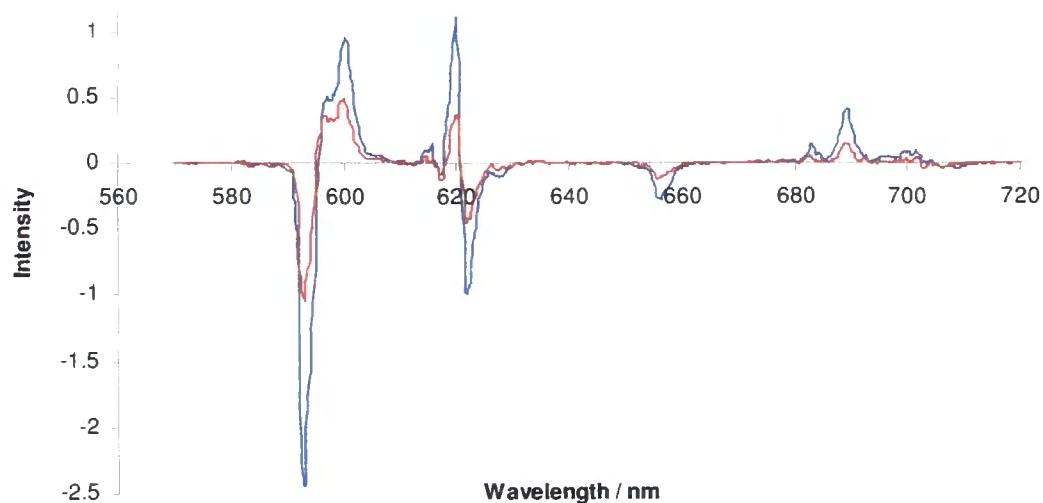


**Figure 5.11:** CPL spectra for  $(RRR)\text{-[Eu.L}^2\text{]}^{3+}$  in the absence (blue) and presence (red) of 15  $\mu\text{M}$  BSA ( $\text{D}_2\text{O}$ , 295 K,  $\lambda_{\text{ex}} = 348$  nm)

The same effect was observed for  $\text{Tb}^{3+}$  complexes: there was a marked change in the spectral form for  $(SSS)\text{-[Tb.L}^2\text{]}^{3+}$  (Figure 5.12) but not for  $(RRR)\text{-[Tb.L}^2\text{]}^{3+}$ .

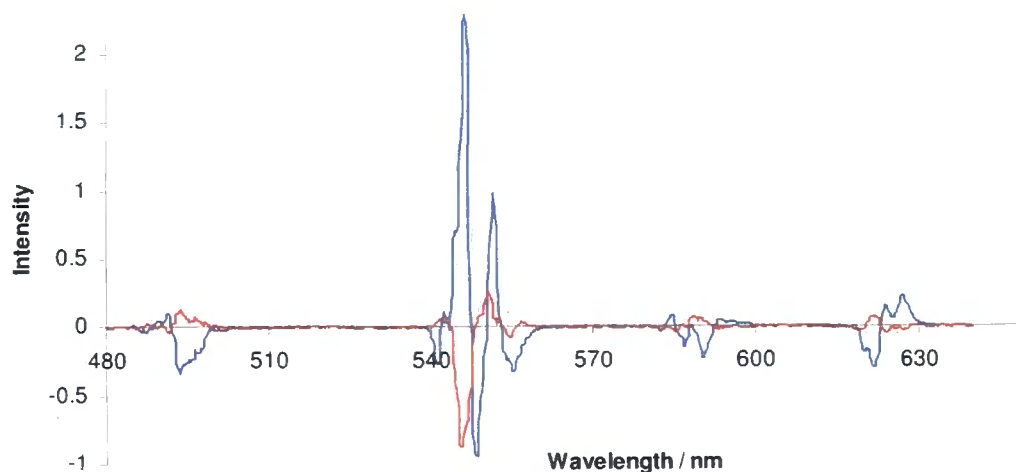


**Figure 5.12:** CPL spectra for  $(SSS)\text{-[Tb.L}^2\text{]}^{3+}$  in the absence (blue) and presence (red) of 15  $\mu\text{M}$  BSA ( $\text{D}_2\text{O}$ , 295 K,  $\lambda_{\text{ex}} = 348$  nm)

Attempts were then made to identify any other complexes which behaved in a similar fashion. The only complex for which similar behaviour was observed was the activated form of  $[\text{Ln.L}^2]^{3+}$ , in which the pendant arm opposite the chromophore was converted

into an ester form for conjugation to other groups. The CPL spectra of a number of other complexes, including  $[\text{Ln.L}^3]^{3+}$ ,  $[\text{Ln.L}^4]$ ,  $[\text{Ln.L}^{6a}]$  and  $[\text{Ln.L}^{14a}]$ , were obtained in the presence of BSA. In no case did the addition of protein change the form of the CPL spectrum. The spectra of  $(SSS)\text{-}[\text{Eu.L}^{3a}]^{3+}$  before and after BSA addition are shown as an example (Figure 5.13).  $[\text{Ln.L}^3]^{3+}$  and  $[\text{Ln.L}^4]$  possess the same chromophore as  $[\text{Ln.L}^2]^{3+}$ , while  $[\text{Ln.L}^{6a}]^{3+}$  and  $[\text{Ln.L}^{14a}]^{3+}$  bear the same pendant arms, and yet neither set of complexes exhibits this enantiospecific behaviour. It appears, therefore, that it is the specific structure of  $[\text{Ln.L}^2]^{3+}$ , and not any one component of its structure, which interacts with BSA in this peculiar fashion.

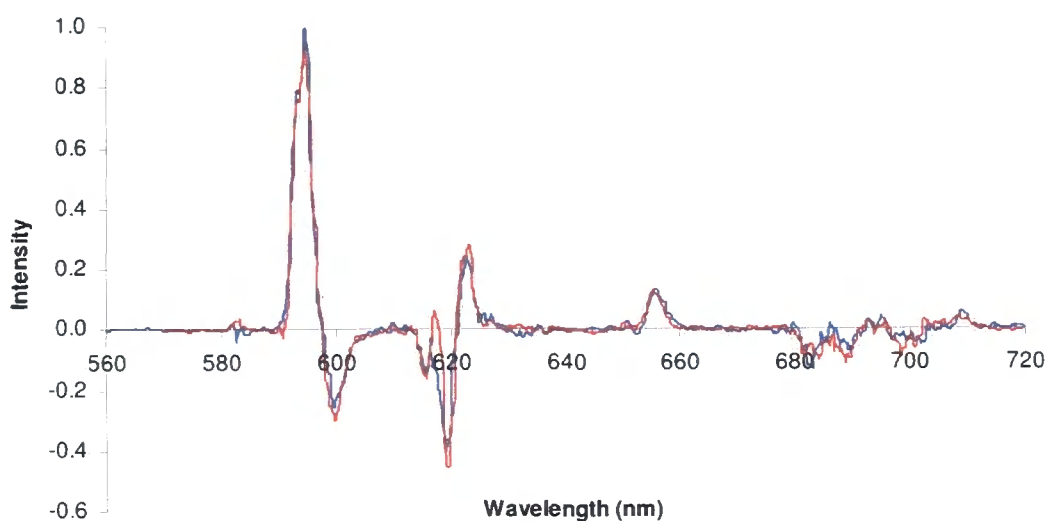


**Figure 5.13:** CPL spectra for  $(SSS)\text{-}[\text{Eu.L}^{3a}]^{3+}$  in the absence (blue) and presence (red) of 15  $\mu\text{M}$  BSA ( $\text{D}_2\text{O}$ , 295 K,  $\lambda_{\text{ex}} = 348 \text{ nm}$ )

The CPL profile of  $(SSS)\text{-}[\text{Eu.L}^2]^{3+}$  in the presence of BSA is similar to the spectrum of  $(SSS)\text{-}[\text{Eu.L}^{3b}]^{3+}$  (Figure 5.14). The characterisation described in Chapter Two concluded that  $(SSS)\text{-}[\text{Eu.L}^{3b}]^{3+}$  adopted a  $\Lambda(\delta\delta\delta\delta)$  configuration, in contrast to the  $\Delta(\lambda\lambda\lambda\lambda)$  configuration observed for  $(SSS)\text{-}[\text{Eu.L}^2]^{3+}$ . It appears, therefore, that binding to BSA induces a helicity change in the complex.

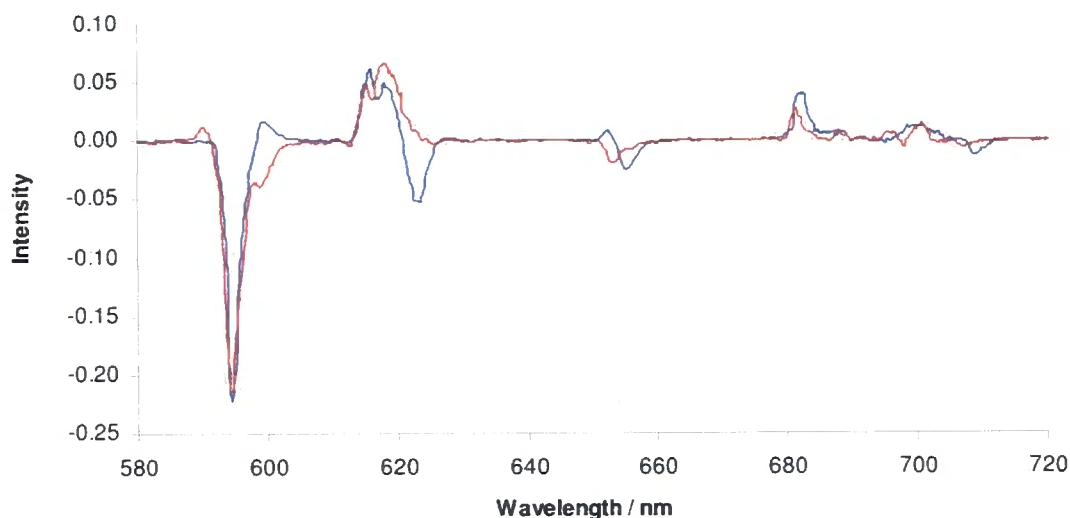


**Figure 5.14:** Comparison of the CPL spectrum for  $(SSS)\text{-[Eu.L}^{3b}\text{]}^{3+}$  (blue) with that of  $(SSS)\text{-[Eu.L}^2\text{]}^{3+}$  in the presence of 15  $\mu\text{M}$  BSA (295 K,  $\lambda_{\text{ex}} = 348$  nm)

The effect of HSA on the CPL spectra was also studied, with spectra showing a similar form to BSA-treated spectra, as can be seen from the calculated emission dissymmetry factors ( $g_{\text{em}}$ ; Table 5.3). This is consistent with findings that HSA and BSA display approximately 76% sequence homology, with strict conservation of the disulfides which maintain the overall structure.<sup>241</sup> Furthermore, studies of the binding sites of the two proteins have indicated similarities in these regions.<sup>242</sup>

**Table 5.3:** Emission dissymmetry factors for Eu complexes (in  $\text{D}_2\text{O}$  at 295 K,  $\lambda_{\text{ex}} = 348$  nm)

Complex	$g_{\text{em}}(590)$	$g_{\text{em}}(597)$	$g_{\text{em}}(616)$	$g_{\text{em}}(620)$	$g_{\text{em}}(624)$	$g_{\text{em}}(651)$
$(SSS)\text{-[Eu.L}^2\text{]}^{3+}$	+0.22	-0.31	-0.048	+0.10	+0.048	+0.27
$(SSS)\text{-[Eu.L}^2\text{]}^{3+}$ + BSA	+0.018	-0.14	+0.020	+0.017	-0.023	-0.066
$(SSS)\text{-[Eu.L}^2\text{]}^{3+}$ + HSA	+0.051	-0.25	+0.040	+0.042	-0.023	-0.21
$(SSS)\text{-[Eu.L}^2\text{]}^{3+}$ + AAG	+0.083	-0.11	-0.021	+0.032	+0.027	+0.035
$(RRR)\text{-[Eu.L}^2\text{]}^{3+}$	-0.17	+0.22	+0.041	-0.071	-0.042	-0.23
$(RRR)\text{-[Eu.L}^2\text{]}^{3+}$ + BSA	-0.14	+0.19	+0.043	-0.085	-0.061	-0.17
$(RRR)\text{-[Eu.L}^2\text{]}^{3+}$ + HSA	-0.095	+0.13	+0.12	-0.036	-0.020	-0.082
$(RRR)\text{-[Eu.L}^2\text{]}^{3+}$ + AAG	-0.14	+0.16	+0.024	-0.032	-0.035	-0.10

In order to further study this phenomenon, the effect on CPL behaviour of another common protein was studied.  $\alpha_1$ -Acid glycoprotein (AAG) is a major serum

carbohydrate-containing protein which has been isolated and characterised from many mammals.<sup>243, 244</sup> Addition of AAG to each enantiomer of  $[\text{Eu.L}^2]^{3+}$  resulted in a reduction in the  $g_{\text{cm}}$  values, but no change in the sign of the transitions (Table 5.3), suggesting that the change observed for the serum albumins is not typical of all proteins. The effect of the interaction of the two complexes with a chiral anion was studied by addition of *R* and *S* enantiomers of phenylsuccinate. This salt was selected due to its negative charge, which will encourage ion-pairing with the cationic complex. There was no change in the CPL spectra on addition of these salts.

In order to better understand the changes in the helicity, a series of CPL spectra were obtained with increasing concentrations of BSA (Figure 5.15). The spectra changed considerably on addition of BSA up to 10  $\mu\text{M}$ , and then remained constant. Monitoring the CPL intensity at individual wavelengths confirmed these observations.

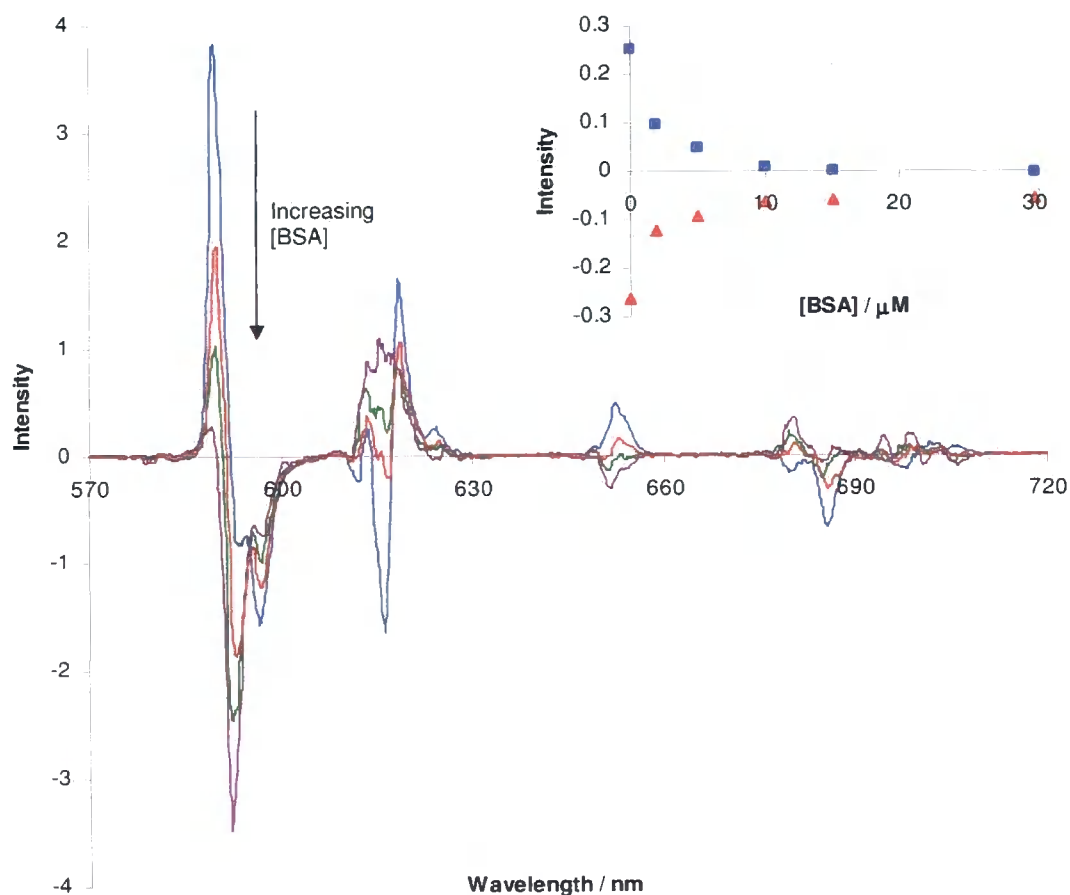


**Figure 5.15:** CPL spectra for  $(SSS)\text{-}[\text{Eu.L}^2]^{3+}$  in the absence (blue) and presence 2  $\mu\text{M}$  (red), 5  $\mu\text{M}$  (green), 10  $\mu\text{M}$  (purple) BSA ( $\text{D}_2\text{O}$ , 295 K,  $\lambda_{\text{ex}} = 348$  nm). Inset: Change in the CPL intensity at 590 nm ( $\blacktriangle$ ) and 616 nm ( $\blacksquare$ ) with increasing BSA.

A final experiment which was performed using CPL spectroscopy was the study of the spectrum obtained from cells treated with  $(SSS)\text{-[Eu.L}^2\text{]}^{3+}$ . CHO cells were treated and prepared as described in Section 5.2.1 above, and a CPL spectrum recorded (Figure 5.16). A CPL spectrum of untreated cells was also obtained, which shows only background noise. The CPL spectrum of the complex in CHO cells is most similar in form to the spectrum obtained in the presence of 2 or 5  $\mu\text{M}$  BSA. Since the intracellular concentration of albumin is likely to be of the order of 10 to 100 times higher, it appears that only a fraction of the complex is bound to albumin. It is possible that the complex is more strongly bound by other proteins in the cell.

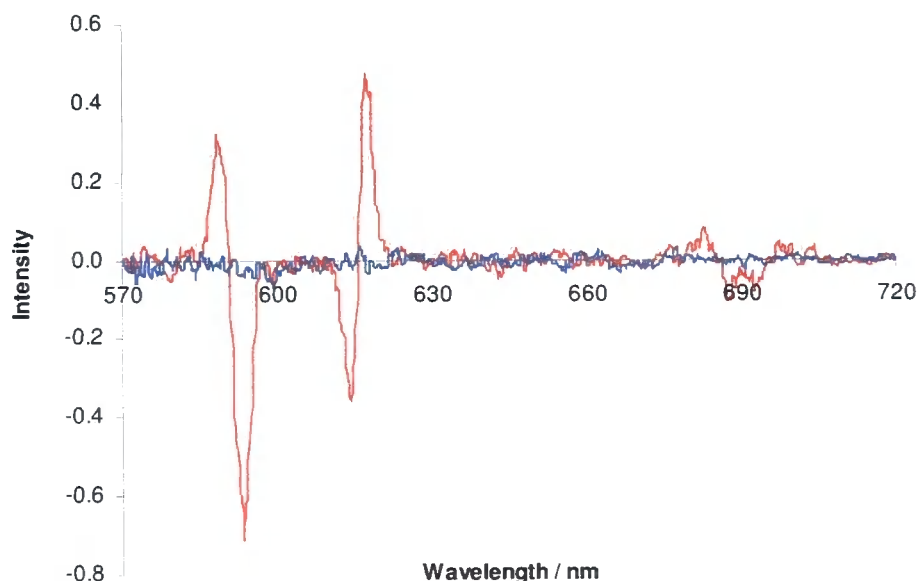


**Figure 5.16:** CPL spectra of CHO cells alone (blue) and cells treated with  $(SSS)\text{-[Eu.L}^2\text{]}^{3+}$  (red; 50  $\mu\text{M}$ , 4h; spectra collected in  $\text{H}_2\text{O}$ , 295 K,  $\lambda_{\text{ex}} = 348 \text{ nm}$ )

### 5.3.2 Probing the protein binding site

The quenching and CPL studies suggest that  $(SSS)\text{-[Eu.L}^2\text{]}^{3+}$  binds to serum albumin in a different manner to the binding of other lanthanide complexes. This aspect was studied further by seeking to identify the binding site of serum albumin with which the complex interacts. Since most previous experiments of serum albumin behaviour concentrate on HSA, further experiments were conducted with this isoform alone. HSA contains two major binding sites, named site I and site II (Figure 5.17).<sup>245</sup> Early investigations of the binding sites of HSA revealed a number of fluorescent probes which bind to each site and are non-fluorescent in solution, but fluoresce in the ultraviolet-blue on HSA

binding.<sup>246</sup> These studies established the commonly-employed fluorescence method for determining the binding site targeted by a particular compound, in which the displacement of these fluorescent probes is monitored by measuring emission changes. This technique has been successfully utilised for the study of lanthanide complexes in examining the interactions of various gadolinium complexes, used as contrast agents for MRI.<sup>247, 248</sup>

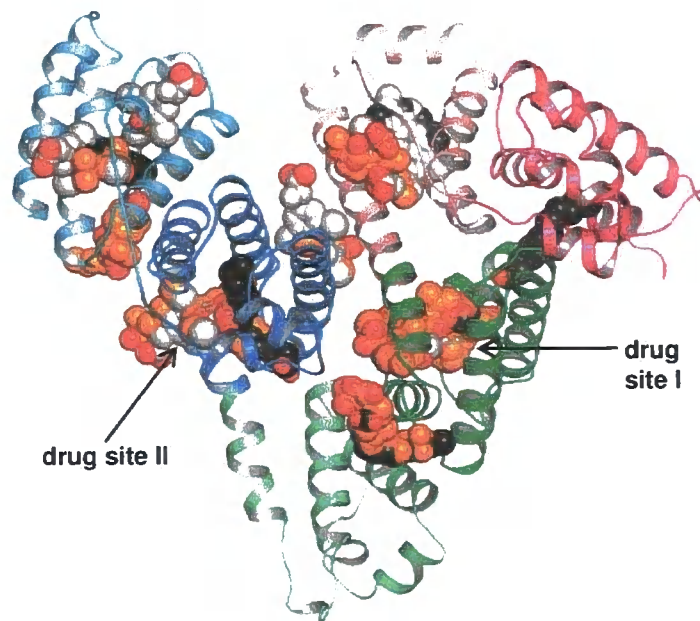
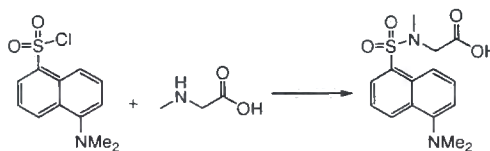


**Figure 5.17:** Structure of HSA as defined by crystallographic studies, showing the two drug binding sites. Adapted from Ghuman *et al.*<sup>249</sup>

In order to perform binding site studies, dansyl sarcosine, a marker for drug site II, was synthesised by condensation of dansyl chloride with sarcosine in aqueous acetone (Scheme 5.2).



**Scheme 5.2**

Attempts were made to study the displacement of the site I markers warfarin and dansyl-L-asparagine, and the site II probes, dansyl sarcosine and dansyl proline, by both Eu and

Tb complexes of  $L^2$ , using the fluorescence methods reported in the literature. This proved to be unsuccessful as the complexes themselves perturbed the fluorescence of the dansyl group. Titration of the complex into a solution of the probe (in the absence of HSA) led to a linear increase in the fluorescence. For example, addition of one equivalent of  $(SSS)-[Tb.L^2]^{3+}$  to dansyl sarcosine led to a 37% increase in fluorescence, while addition to dansyl proline led to a 230% increase. As a result, the probes would still fluoresce, even on displacement from the protein. These results indicated that this method could not be utilised for the study of the binding of these complexes to HSA. An alternative method was therefore required.

Previous studies had revealed marked changes in the relaxivity of  $(SSS)-[Gd.L^2]^{3+}$  on protein binding, with a greater than four-fold change in relaxivity on binding of HSA.<sup>73</sup> It was therefore postulated that changes in the relaxivity could be utilised to study binding site interactions. Experiments were performed in 5% MeOH to overcome the insolubility of warfarin, which was used as a probe of drug site I. Addition of HSA to  $(RRR)-[Gd.L^2]^{3+}$  resulted in a very similar relaxivity curve to that of its enantiomer (Figure 5.18). Based on these titration curves, an HSA concentration of 0.4 mM was selected for subsequent studies to ensure complete binding of the complex to the protein.

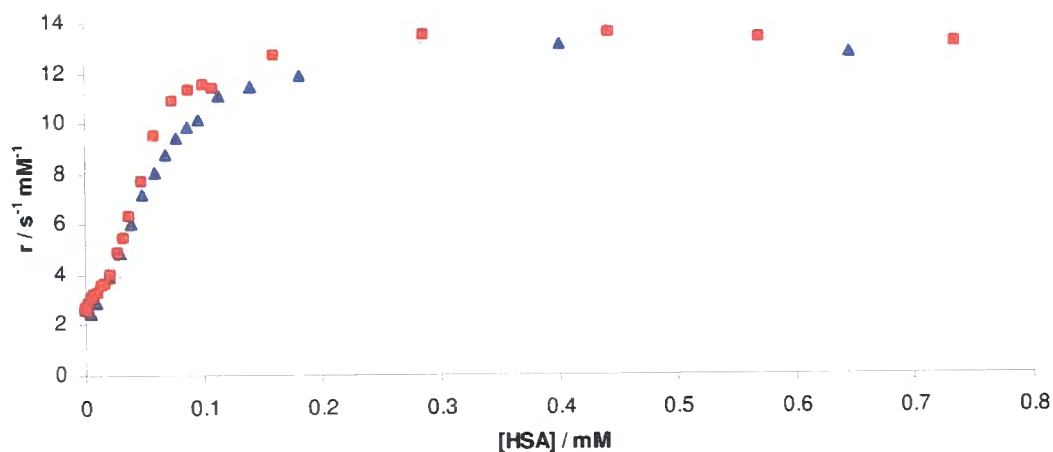


**Figure 5.18:** Variation of the proton relaxivity (310 K, 60 MHz) of  $(SSS)-[Gd.L^2]^{3+}$  ( $\blacktriangle$ ) and  $(RRR)-[Gd.L^2]^{3+}$  ( $\blacksquare$ ) with added HSA.

Dansyl sarcosine and warfarin were titrated into the  $[Gd.L^2]^{3+}$ : HSA mixture for both  $(SSS)$  and  $(RRR)$  isomers, and the relaxivity monitored. The relaxivity of  $(SSS)-[Gd.L^2]^{3+}$  rapidly decreased on addition of dansyl sarcosine, reaching a limiting value of approximately  $3 \text{ mM}^{-1} \text{ s}^{-1}$ , which is similar to the relaxivity of the free complex (Figure

5.19). This suggests that dansyl sarcosine is able to displace the complex from drug site II. In contrast, the identical experiment with  $(RRR)\text{-[Gd.L}^2\text{]}^{3+}$  resulted in no such decrease in the relaxivity. The limiting relaxivity value is reached after addition of approximately 1.2 equivalents of dansyl sarcosine. This suggests that both  $(SSS)\text{-[Gd.L}^2\text{]}^{3+}$  and dansyl sarcosine have very similar affinities for HSA. This is consistent with the reported  $\log K$  for dansyl sarcosine of 5.2,<sup>246</sup> which is similar to the measured value for  $(SSS)\text{-[Gd.L}^2\text{]}^{3+}$  of 5.1, reported here (Table 2.5, page 62).

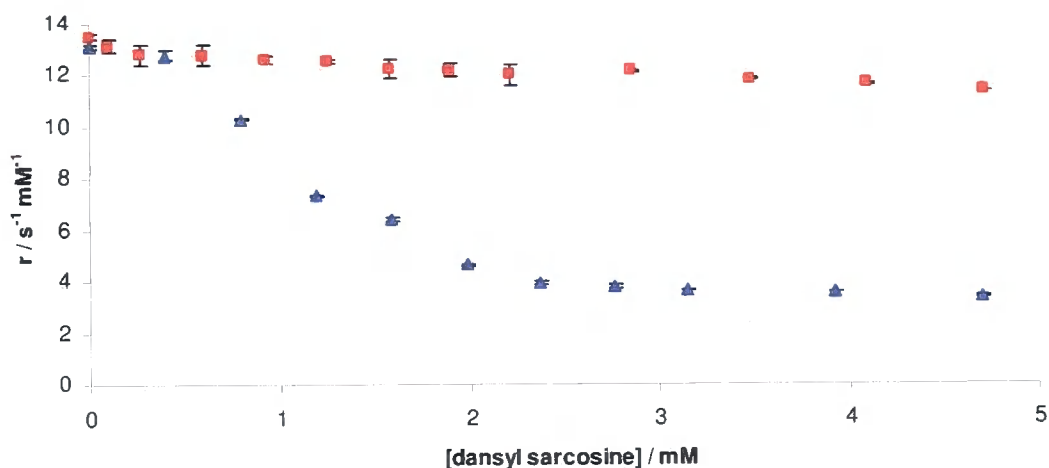


**Figure 5.19:** Variation of the proton relaxivity (310 K, 60 MHz) of a mixture of HSA (0.4 mM) and 1.7 mM  $(SSS)\text{-[Gd.L}^2\text{]}^{3+}$  ( $\blacktriangle$ ) or  $(RRR)\text{-[Gd.L}^2\text{]}^{3+}$  ( $\blacksquare$ ) with added dansyl sarcosine.

The same experiment was performed with warfarin, a marker for drug site I (Figure 5.20). For neither  $(SSS)\text{-[Gd.L}^2\text{]}^{3+}$  nor  $(RRR)\text{-[Gd.L}^2\text{]}^{3+}$  was there a large decrease in the relaxivity, suggesting that neither complex binds to drug site I.

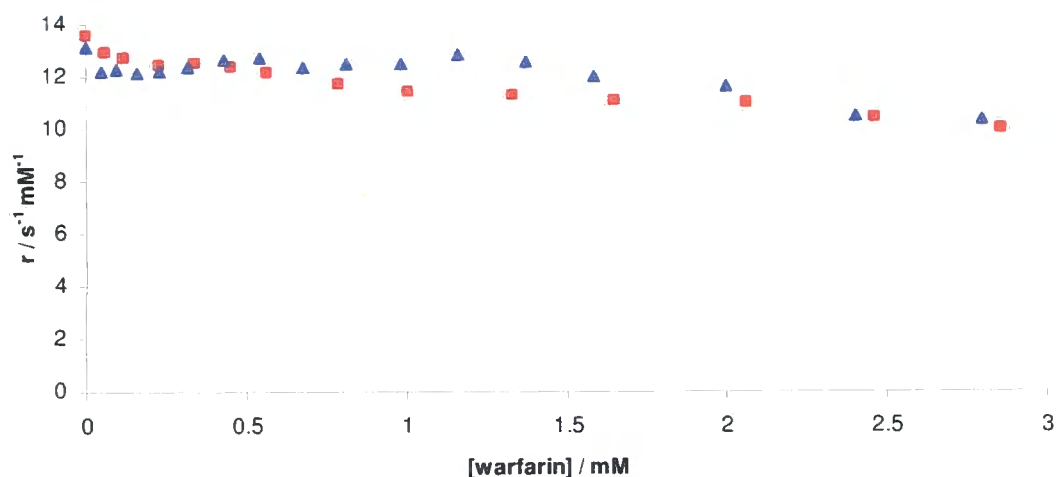


**Figure 5.20:** Variation of the proton relaxivity (310 K, 60 MHz) of a mixture of HSA (0.4 mM) and 1.7 mM [(SSS)-Gd.L<sup>2</sup>]<sup>3+</sup> (▲) or [(RRR)-Gd.L<sup>2</sup>]<sup>3+</sup> (■) with added warfarin.

It appears, therefore, that (SSS)-[Gd.L<sup>2</sup>]<sup>3+</sup> binds to drug site II of HSA, and that (RRR)-[Gd.L<sup>2</sup>]<sup>3+</sup> binds to neither drug site. This differential binding between the two isomers is consistent with previously-reported findings that drug site II is stereospecific.<sup>247</sup> The change in the CPL spectrum on interaction with HSA suggests that not only is (SSS)-[Gd.L<sup>2</sup>]<sup>3+</sup> binding to the protein, but its structure and helicity is also being altered on binding.

For the (SSS)-[Gd.L<sup>2</sup>]<sup>3+</sup> curve (Figure 5.18), saturation is reached at a protein concentration that is approximately one tenth of the complex concentration, suggesting that several complexes are binding per protein. This is likely to correspond to one complex in drug site II, and the others associated with but not bound to protein. The relaxivity titration curve was obtained with an excess of complex, so reflects the relaxivity of a large proportion of associated complex, and a smaller proportion of bound complex. This explains the similarity with the relaxivity curve obtained for (RRR)-[Gd.L<sup>2</sup>]<sup>3+</sup>, for which all complex is associated. On the other hand, CPL spectra were obtained with an excess of HSA. The complete change in the helicity observed in the CPL spectrum of (SSS)-[Gd.L<sup>2</sup>]<sup>3+</sup> in the presence of HSA indicates that only bound complex is present. This indicates that the complex preferentially binds to drug site II of HSA, rather than associating with multiple sites, which occurs only in cases of excess complex.

### 5.3.3 NMR studies of protein binding

A further study designed to understand the complex binding properties involved saturation transfer difference (STD) NMR spectroscopy experiments, which were performed by Prof. Carlos Geraldes, João Teixeira and David Dias at the University of Coimbra (Portugal). Saturation transfer NMR spectroscopy is a technique which is commonly used to characterise the binding in ligand-receptor complexes.<sup>250</sup> The method involves saturation of the protein by selective irradiation. Any ligand protons that interact with the protein will also be saturated. Due to the equilibrium between bound and free form, the partially-saturated bound ligand will at some times be in solution. An NMR spectrum of this saturated form can therefore be collected (Figure 5.21). A spectrum of the non-saturated protein and ligand is also acquired, and the spectra subtracted, to give a saturation transfer difference spectrum. Only those ligand protons which were saturated (that is, which were bound to the protein) will appear in this difference spectrum. In this way, STD NMR can give information about the mode of binding of a ligand.

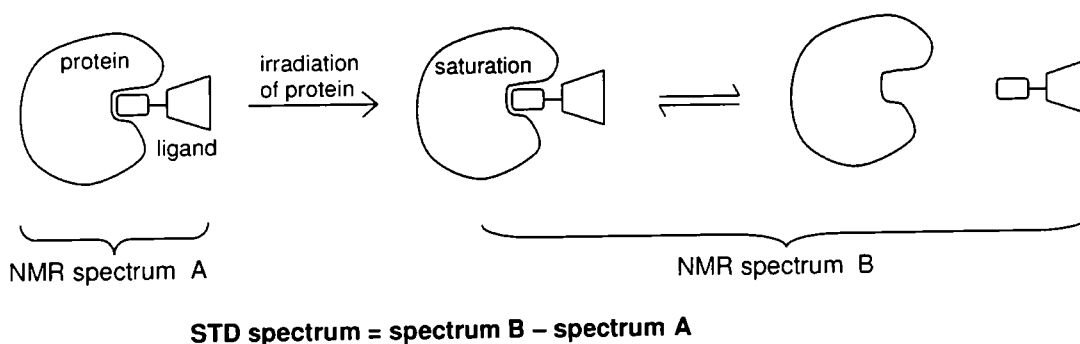


**Figure 5.21:** Schematic diagram summarising the process of STD NMR

In order to use the STD NMR technique, it was necessary to select a diamagnetic metal, which does not induce a shift in the  $^1\text{H}$  NMR spectrum of the complex. Yttrium(III), which is diamagnetic, is a good model for europium and terbium, with an ionic radius that is only  $0.02\text{\AA}$  smaller than terbium(III) in nine-coordinate systems. As a result, the yttrium complex was synthesised from  $\text{L}^2$  using yttrium acetate. In the past, it was not possible to fully assign the  $^1\text{H}$  NMR spectra of  $\text{L}^2$  or  $[\text{Eu.L}^2]^{3+}$  because of the conformation flexibility of the ligand, and the broad peaks observed in the Eu complex. As a result, only the aromatic protons could be clearly identified.  $[\text{Y.L}^2]\text{Cl}_3$ , on the other

hand, was found to exist primarily as only one isomer which gave rise to sharp peaks. In addition, because of the close coupling of the protons, it was possible to obtain a well-defined COSY spectrum (Figure 5.22), which aided the characterisation process. This enabled the assignment of most protons of the complex (see Section 8.2 for complete analysis). It was observed that while the protons of the aromatic regions of two pendant arms lay at approximately 7.3, the other set of protons lay more upfield, near 6.3. This suggests a deshielding ring current effect due to a through-space interaction with another aromatic system. Due to structural constraints, it was determined that such an interaction would arise between the chromophore and an adjacent pendant arm.

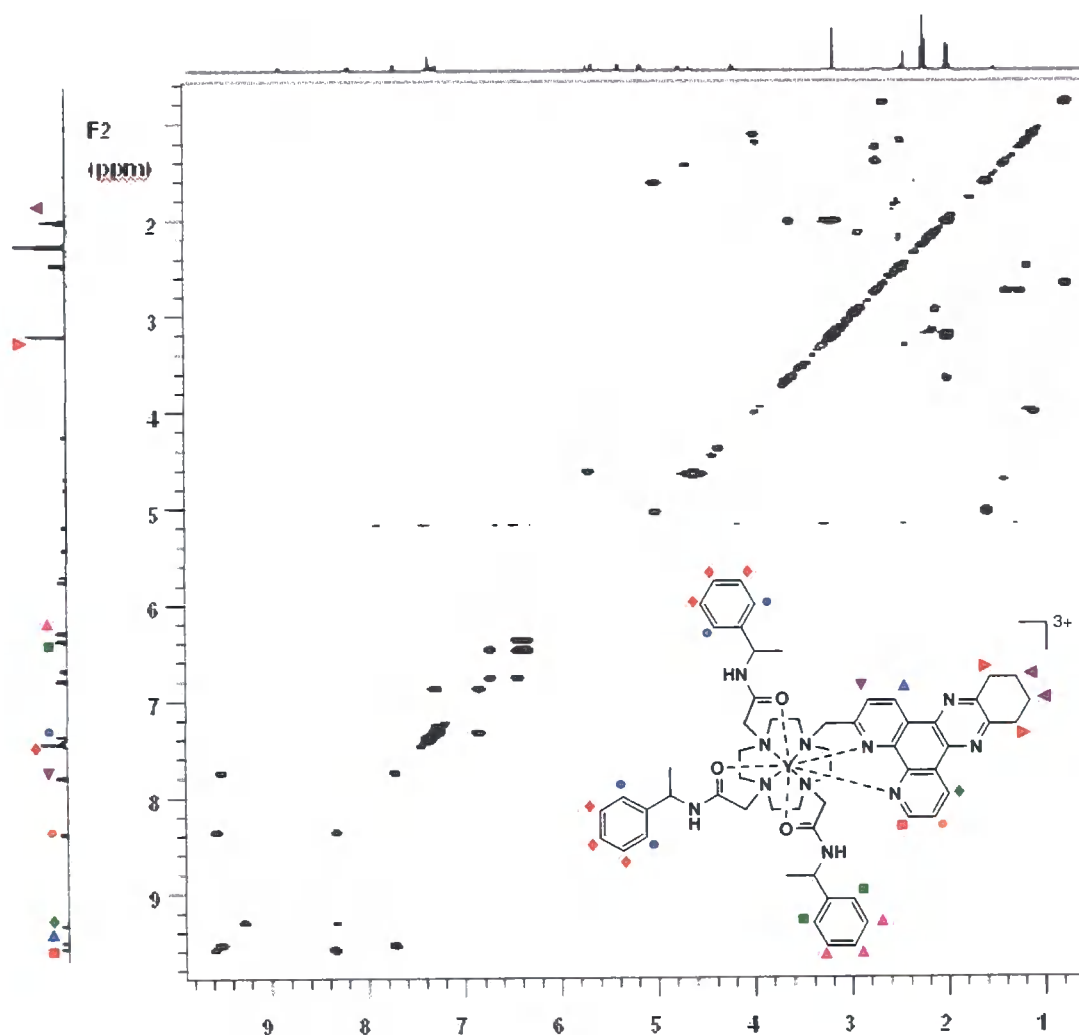


**Figure 5.22:** COSY NMR spectrum of  $(SSS)\text{-}[\text{Y.L}^2]\text{Cl}_3$  (600 MHz, 295 K) showing partial assignments

The aims of the STD NMR studies were to test for any difference between the behaviour of the  $(RRR)$  and  $(SSS)$  enantiomers, and to define the regions of the complex which bind

to HSA. STD NMR spectra were acquired with pre-saturation of the protein at -0.5 ppm. The resulting spectra are shown in Figure 5.23.

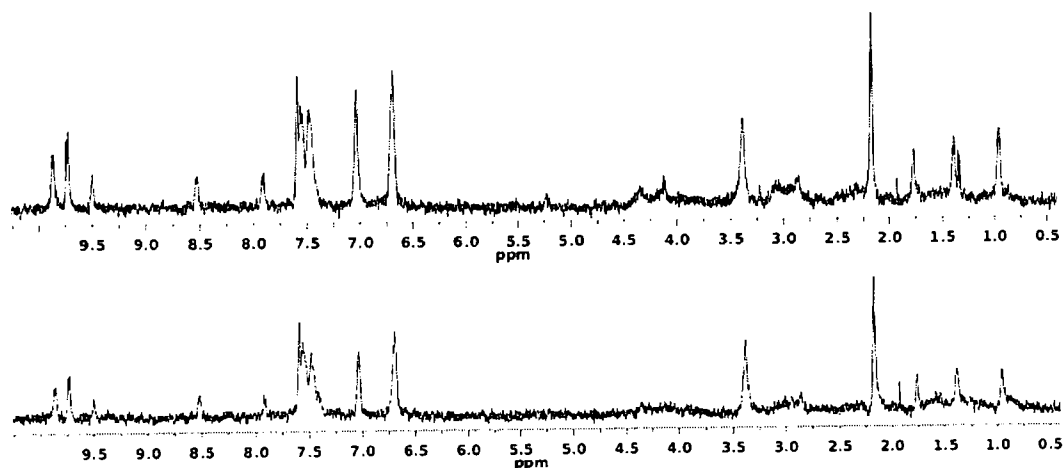


**Figure 5.23:**  $^1\text{H}$  STD NMR spectra of (*SSS*)- (upper) and (*RRR*)- $[\text{Y.L}^2]\text{Cl}_3$  (lower) in the presence of  $30\ \mu\text{M}$  HSA (1 mM complex,  $25\ ^\circ\text{C}$ ,  $\text{D}_2\text{O}$ , 600 MHz, -0.5 ppm saturation)

On first inspection, the spectra of the two enantiomers seem very similar. As a result, the STD amplification factor was calculated in order to better compare the spectra. The STD amplification factor is the relative intensity of the STD signal compared to that of a signal of the protein.<sup>251</sup> STD amplification factors for the two complexes are shown in Table 5.4. For all but three peaks, the difference in the relative amplified STD intensities is greater than 10%, indicating a significant difference between the  $^1\text{H}$  NMR STD spectra of the (*RRR*)- and (*SSS*)- enantiomers. This confirms that the two enantiomers interact differently with HSA, as was observed by CPL and binding site studies.

**Table 5.4:** STD amplification factors and relative STD (to the most shifted proton) for (*SSS*)- and (*RRR*)-[*Y.L*<sup>2</sup>]Cl<sub>3</sub> in the presence of HSA

ppm	( <i>RRR</i> ) STD amplification	Rel. STD (%)	( <i>SSS</i> ) STD amplification	Rel. STD (%)	%( <i>SSS</i> ) - %( <i>RRR</i> )
9.86	3.51	100	4.08	100	-
9.72	2.50	71.2	3.86	94.6	23.4
9.50	1.46	41.5	2.41	59.0	17.5
8.53	2.63	75.0	3.24	79.5	4.5
7.91	1.40	39.9	2.27	55.6	15.8
7.59	1.94	55.3	2.69	65.9	10.6
7.04	1.88	53.6	3.19	78.1	24.5
6.69	2.48	70.8	3.75	91.8	21.1
3.38	1.65	47.1	2.67	65.4	18.2
2.18	1.74	49.6	2.86	70.0	18.5
1.93	2.54	72.5	2.79	68.3	-4.2
1.77	0.62	17.6	1.03	25.2	7.6
1.39	1.34	38.2	2.07	50.8	12.5
0.96	1.21	34.6	2.11	51.7	17.1

In order to determine the region of the complex which interacts with HSA, the <sup>1</sup>H STD NMR spectrum of (*SSS*)-[*Y.L*<sup>2</sup>]<sup>3+</sup> was compared to that of the standard <sup>1</sup>H NMR spectrum. By this method, the protons which appear in the standard NMR but not the STD NMR can be identified, and classified as protons which do not bind to HSA. In addition, the peaks which were shown from the amplification analysis to vary least between (*RRR*) and (*SSS*) enantiomers are also likely to correspond to non-binding protons. The classification of peaks is shown in Figure 5.24. The cyclen ring and amide methylene protons do not appear to interact with protein, which is consistent with their structural location towards the centre of the complex, shielded by the pendant arms and chromophore. In addition, while the pendant arm which interacts with the chromophore, and the cyclohexyl ring of the chromophore do not appear to interact with HSA, the phenanthrene region of dpqC may be involved in binding. These results suggest that it is the two other phenylmethyl pendant arms and the aromatic region of the chromophore which lie in the binding site of the protein. This is consistent with findings that complexes with the same dpqC chromophore but different pendant arms do not exhibit the same HSA-binding behaviour.

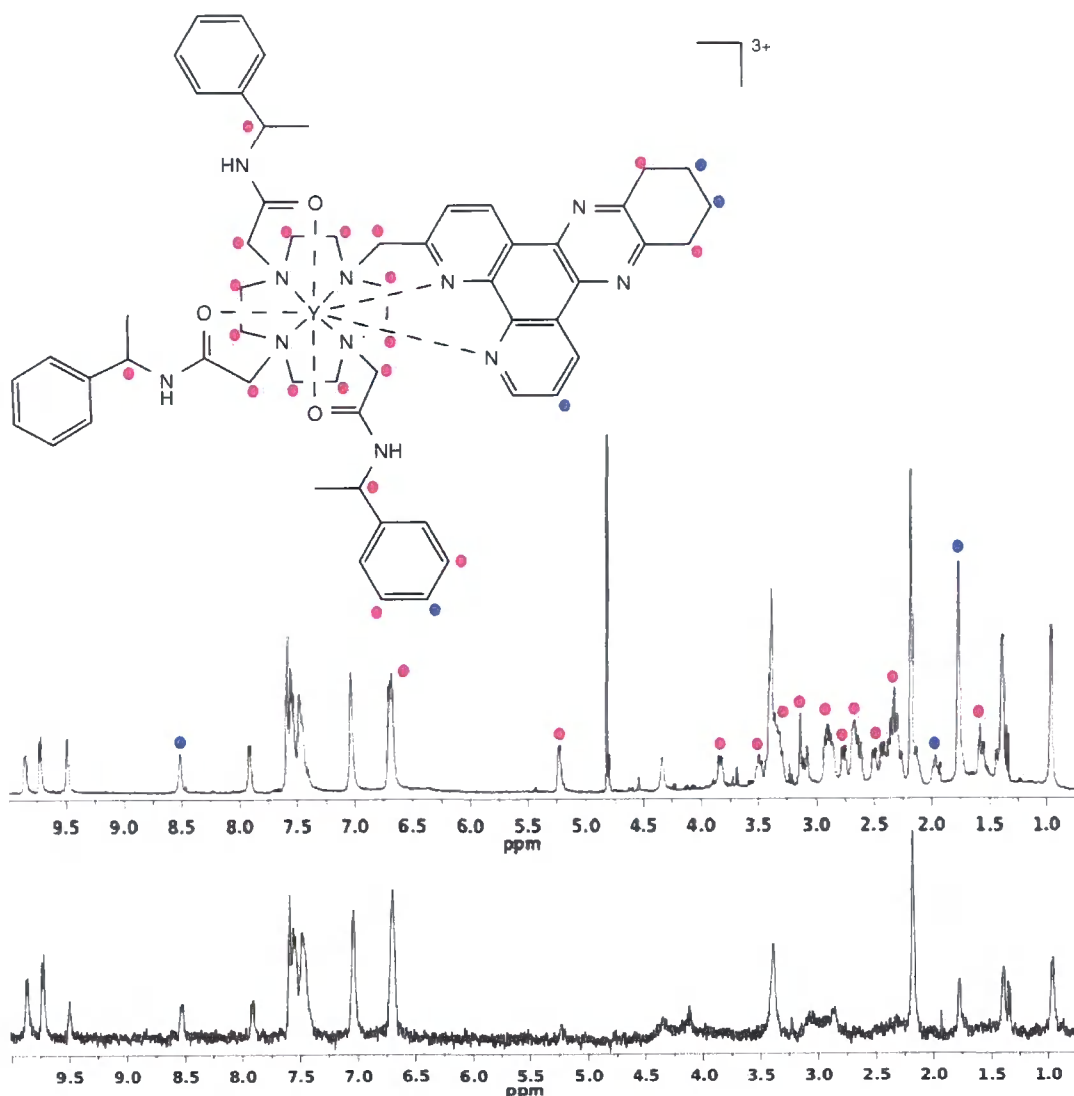


**Figure 5.24:** Comparison of the  $^1\text{H}$  NMR spectrum of  $(SSS)\text{-}[\text{Y.L}^2]\text{Cl}_3$  (upper) with the STD NMR spectrum of the same complex, and the structural conclusions, indicating protons which exist in the  $^1\text{H}$  NMR but not the STD NMR spectrum (●) and protons for which there is only a modest difference between the STD behaviour of  $(SSS)$  and  $(RRR)$  enantiomers (◆).

An additional STD NMR experiment was performed using dansyl sarcosine as a competitive binder, to supplement the information obtained from the competition studies. Dansyl sarcosine (2 mM) was added to the mixtures of HSA and  $(RRR)\text{-}$  or  $(SSS)\text{-}[\text{Y.L}^2]^{3+}$ , and STD NMR spectra obtained as described above. STD amplification factors were calculated for each peak, and compared to those measured in the absence of dansyl sarcosine (Table 5.5). For the  $(RRR)\text{-}$  isomer, the difference between the relative STD in the presence and absence of dansyl sarcosine ranges from -17 to +24%, with an average change of +1.5%; the corresponding changes for the  $(SSS)\text{-}$  enantiomer range

from -63 to -15%, with an average of -33%. This indicates that the spectrum of the (*SSS*)-isomer is more dramatically perturbed than that of the (*RRR*)-enantiomer upon addition of dansyl sarcosine. This is consistent with release of the (*SSS*) complex from drug site II by dansyl sarcosine, as observed in the relaxivity studies.

**Table 5.5:** Changes in the relative STD (to the most shifted proton) for (*SSS*)- and (*RRR*)-[ $Y.L^2$ ]Cl<sub>3</sub> upon the addition of dansyl sarcosine (2 mM)

ppm	<i>(RRR)</i> Rel. STD (%)			<i>(SSS)</i> Rel. STD (%)		
	Without dansyl sarcosine	With dansyl sarcosine	Change	Without dansyl sarcosine	With dansyl sarcosine	Change
9.86	100	100	-	100	100	-
9.72	71.2	80.0	<b>8.8</b>	94.6	64.1	<b>-30.5</b>
9.50	41.5	53.5	<b>12.0</b>	59.0	22.2	<b>-36.8</b>
7.91	39.9	63.8	<b>23.9</b>	55.6	30.9	<b>-24.7</b>
7.04	53.6	54.1	<b>0.5</b>	78.1	15.3	<b>-62.8</b>
6.69	70.8	86.2	<b>15.4</b>	91.8	54.1	<b>-37.7</b>
3.38	47.1	30.6	<b>-16.5</b>	65.4	24.3	<b>-41.1</b>
2.18	49.6	36.5	<b>-13.1</b>	70.0	36.2	<b>-33.8</b>
1.77	17.6	12.7	<b>-4.9</b>	25.2	10.6	<b>-14.6</b>
1.39	38.2	27.4	<b>-10.8</b>	50.8	20.2	<b>-30.6</b>
0.96	34.6	34.1	<b>-0.5</b>	51.7	35.8	<b>-15.9</b>

### 5.3.4 A unique example of dynamic helicity inversion

Molecular recognition of a substrate by a protein binding site often involves “induced fit”, in which the conformation of one or both species changes to enable binding.<sup>252</sup> Very few cases have been observed in which binding of a chiral system induces inversion of helicity, although such an event is believed to be of importance in gene expression as well as other cellular processes.<sup>253, 254</sup> For example, binding of right-handed *B*-DNA to spermine and phenanthrolines can lead to alteration in its conformation to left-handed *Z*-DNA.<sup>255, 256</sup> A number of synthetic systems have been observed to undergo helicity inversion upon interaction with an external stimulus, including helical organic compounds<sup>257, 258</sup> and metal coordination complexes.<sup>259, 260</sup> For example, a slowly epimerising complex has been observed to switch configuration at the Ru and N stereogenic centres on binding to *N*-ethylguanine and *B*-DNA.<sup>261</sup>

While biological systems are commonly enantioselective, there appear to be no previous examples where this is accompanied by selective inversion of one enantiomeric form. Studies of  $(SSS)\text{-[Ln.L}^2\text{]}^{3+}$  have revealed that it binds enantioselectively to drug site II of serum albumin, and that this binding is accompanied by helicity inversion. In this behaviour, this complex is a unique example of dynamic helicity inversion.

## 5.4 Conclusions

The studies of cellular fate have identified complexes which exhibit a range of sub-cellular speciation states. *In cellulo* hydrolysis of ester-containing pendant arms was observed by changes in the relative emission intensities of a Eu(III) complex with Ala pendant arms. Cellular demetallation of a different complex, which had been observed in previous *in vitro* studies, was visualised by microscopy. Analysis of the intracellular anion binding of a complex by luminescence spectroscopy indicated that the complex was bound competitively by serum albumin and bicarbonate, and serum albumin-binding was observed for another complex, highlighting the need to assess the effect of protein binding or association on probe behaviour.

This work has highlighted the importance of investigating the *in cellulo* behaviour of a probe early in the design process. In some cases, the effects of sub-cellular speciation can enhance the ability of a probe to report on its environment, but in other cases they can be a hindrance.

One case of protein binding which was studied in more detail revealed that  $[(SSS)\text{-Ln.L}^2]^{3+}$  binds in an enantioselective fashion to drug site II of serum albumins. This binding is likely to involve the phenyl rings of two of the pendant arms and the chromophore itself, and is signalled by a change in the helicity as demonstrated by the change the circularly polarised emission. This complex is therefore a unique chiroptical probe for albumin binding, and could find use in the tracking of protein association *in vitro* and *in cellulo*. This could be best achieved by construction of a CPL microscope, which would give information about the circularly polarised emission of a complex at defined positions in a cell.

## CHAPTER SIX

---

# **EFFECTS OF COMPLEXES ON CELLULAR HOMEOSTASIS**

## 6.1 Introduction

The function of a cellular probe is to report on the physiological conditions of a cell. It is important, therefore, that the probe reports on these conditions without interfering with cellular processes. In assessing the suitability of a probe, its effect on cellular homeostasis is an essential consideration. The primary indicator of this is the toxicity of the probe. In considering the cellular behaviour of the luminescent lanthanide complexes, it is important to assess the effects of the probe itself as well as those of its metabolites.

Very few studies have assessed the effect of luminescent lanthanide complexes on the homeostasis of the cell. The cellular toxicity of a set of acridone-containing luminescent lanthanide complexes was assessed by addition of Trypan Blue, which stains only non-viable cells. By counting the ratio of dead to live cells, it was determined that the complexes were non-toxic at concentrations of 1 mM.<sup>83</sup> This method does not, however, allow for the generation of quantitative data by which to compare a range of complexes. No reported study has addressed any other aspect of the effect of complexes on cellular homeostasis.

This chapter explores the effects of luminescent lanthanide complexes on the physiological conditions of the cell. Two principal aspects will be considered: the cytotoxicity of the complexes, and their effect on the mitochondrial membrane potential.

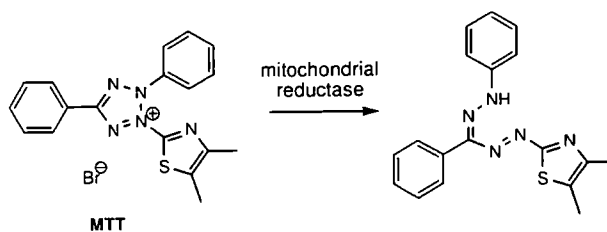
## 6.2 Cytotoxicity

The cytotoxicity of a compound refers to ability to effect cell death. In order for a complex to act as a cellular probe, it is essential that it is non-toxic at the concentrations at which it will be used. The cytotoxicities of the luminescent lanthanide complexes under study were therefore measured.

### 6.2.1 Measuring cytotoxicity

The method selected for the assessment of cytotoxicity was the MTT assay. This test makes use of the conversion of MTT (3-(4,5-dimethylthiazol-2-yl)-2,5-diphenyltetrazolium bromide) into a purple formazan product by the mitochondrial

reductase present in viable cells (Scheme 6.1).<sup>262</sup> The amount of formazan is therefore proportional to the number of viable cells. The insoluble formazan can be dissolved in DMSO, and quantified spectrophotometrically.



**Scheme 6.1**

Cells were grown overnight in a 96-well plate to allow them to adhere to the base of each well. After this time, cells were dosed with varying concentrations of complex and incubated at 37 °C. For the final 4 h of incubation, MTT was added to the medium. Following incubation, the medium containing MTT was decanted and DMSO added. It was found that the process of decanting the medium resulted in loss of cells which were poorly adherent to the base of the wells. This was particularly noticeable in cells which had been incubated for shorter time periods. For these studies, therefore, an incubation time of 24 h was selected as this was the longest incubation time used in any microscopy study. In addition, CHO cells did not appear to adhere sufficiently well to the base of the wells. All reported cytotoxicity values were therefore measured in NIH 3T3 cells.

The data points derived from the MTT assay of  $L^{5b}$  are shown in Figure 6.1. The percentage viability was calculated from the relative absorbance of a well compared to that of untreated cells. In many cases, the cells treated with the lowest concentration were more viable than untreated cells. This is likely to be due to hormesis, the phenomenon that defines how low doses of toxic substances can stimulate biological systems.<sup>263</sup> After this point, the viability of the cells decreased exponentially with increasing concentrations of compound. When the concentrations were plotted on a logarithmic scale, a linear relationship could be observed. This allowed calculation of the concentration which inhibits viability by 50%, termed the  $IC_{50}$  value.

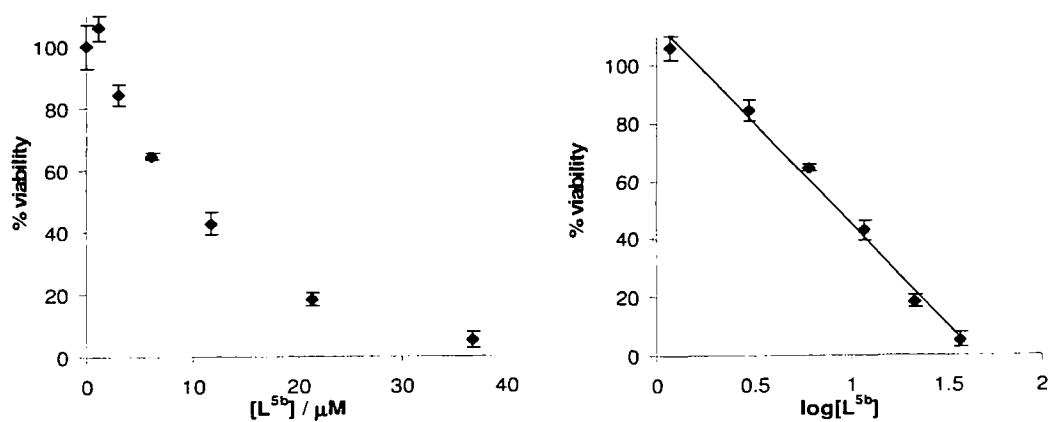


**Figure 6.1:** Example data for  $L^{5b}$ , showing variation of cell viability with concentration on (a) a linear scale and (b) a logarithmic scale (NIH 3T3 cells, 24h incubation). Data-points represent the average of three separate measurements.

By this method, the  $IC_{50}$  values for a range of complexes and ligands were calculated (Table 6.1).

**Table 6.1:** Cytotoxicity data for selected complexes and ligands in NIH 3T3 cells following 24 h incubation, showing standard deviations (SD)

Complex / ligand	$IC_{50}$ ( $\mu M$ ) <sup>†</sup>	SD ( $\mu M$ )	Complex / ligand	$IC_{50}$ ( $\mu M$ ) <sup>†</sup>	SD
[Tb. $L^1$ ]	393	42	[Eu. $L^7$ ]Cl <sub>3</sub>	>240	-
[Tb. $L^2$ ]Cl <sub>3</sub>	131	27	$L^7$	173	15
[Eu. $L^2$ ]Cl <sub>3</sub>	109	20	[Tb. $L^8$ ]Cl <sub>3</sub>	40.9	8.9
[Eu. $L^{3a}$ ]Cl <sub>3</sub>	144	12	[Eu. $L^9$ ]Cl <sub>3</sub>	72.9	4.1
[Eu. $L^{3b}$ ]Cl <sub>3</sub>	121	17	[Eu. $L^{11}$ ]Cl <sub>3</sub>	120	10
[Eu. $L^{4a}$ ]	>240	-	[Eu. $L^{11}$ ](OTf) <sub>3</sub>	79.0	9.4
[Eu. $L^{4b}$ ]	>240	-	[Eu. $L^{12}$ ](OTf) <sub>3</sub>	>100	-
[Eu. $L^{5a}$ ]Cl <sub>3</sub>	173	34	$L^{12}$	>150	-
$L^{5a}$	180	15	[Eu. $L^{13}$ ]	55.9	19.1
[Eu. $L^{5b}$ ]Cl <sub>3</sub>	5.6	0.3	[Tb. $L^{14a}$ ]Cl <sub>3</sub>	>240	-
$L^{5b}$	4.9	1.3	[Tb. $L^{14b}$ ]Cl <sub>3</sub>	77	33
[Eu. $L^{6a}$ ]Cl <sub>3</sub>	164	31	[Tb. $L^{14c}$ ]Cl <sub>3</sub>	131	33
$L^{6a}$	99.3	11.8	[Eu. $L^{14d}$ ]Cl <sub>3</sub>	57.4	1.5
[Eu. $L^{6b}$ ]Cl <sub>3</sub>	>270	-	[Eu. $L^{15}$ ]Cl <sub>3</sub>	7.2	0.5
$L^{6b}$	>350	-	[Eu. $L^{16}$ ]Cl <sub>3</sub>	13	5
[Eu. $L^{6c}$ ]Cl <sub>2</sub>	109	13			

<sup>†</sup> Values are mean for data from three independent experiments with quadruplicate readings in each experiment.

### 6.2.2 General comments about cytotoxicity

The results show that most complexes have  $IC_{50}$  values of greater than  $100\ \mu\text{M}$ ; many greater than  $200\ \mu\text{M}$ . Since cellular studies are generally performed in this work at  $50\ \mu\text{M}$ , the complexes can be considered to be non-toxic for the purposes of these investigations. However, there are isolated examples of complexes which exhibit much higher cytotoxicity. In order to understand the mechanisms by which they kill cells, these cases were investigated further and are discussed in Section 6.2.4.

These cytotoxicity measurements demonstrate the importance of carefully considering dosages. A number of studies in the past used concentrations as high as  $1\ \text{mM}$ ,<sup>83, 197</sup> which for most complexes are toxic. For  $[\text{Eu.L}^2]^{3+}$ , for example, dosing cells at  $1\ \text{mM}$ , nine times above the  $IC_{50}$  value, resulted in permeabilisation of the cell membrane.<sup>102</sup>

Other general comments can be made from the cytotoxicities observed. The replacement of Eu for Tb does not appear to greatly alter the cellular toxicity;  $[\text{Eu.L}^2]^{3+}$  and  $[\text{Tb.L}^2]^{2+}$ , for example, exhibit similar  $IC_{50}$  values, within the range of error. It appears that neutral complexes are generally less cytotoxic than cationic complexes;  $[\text{Tb.L}^1]$  is three times less toxic than  $[\text{Tb.L}^2]^{3+}$ , while the hydrolysed complexes  $[\text{Eu.L}^4]$  were not toxic over the range tested, in contrast to their ester forms,  $[\text{Eu.L}^3]^{3+}$ . This could be due to the decreased interaction of neutral complexes with the mitochondria, important players in apoptosis, or due to the lower protein association observed for these neutral complexes.

It can be noted that changing the groups appended to the chromophore has some effect on the  $IC_{50}$  of the complex. For the series  $[\text{Eu.L}^5]^{3+}$  and  $[\text{Tb.L}^{14}]^{3+}$ , in which the moiety at the 7-position of the chromophore is changed, there is significant variation in the cytotoxicity. This could indicate that the appended group is interacting with cellular species and inducing toxic effects in some cases. Notably, complexes containing an appended <sup>t</sup>Bu group appear to exhibit higher cytotoxicity:  $[\text{Tb.L}^8]\text{Cl}_3$ ,  $[\text{Eu.L}^9]\text{Cl}_3$  and  $[\text{Tb.L}^{14d}]$  have  $IC_{50}$  values of  $41$ ,  $73$  and  $57\ \mu\text{M}$  respectively. It was hypothesised that this was due to interaction with the mitochondrial membrane, and was further investigated, as discussed in Section 6.3 below.

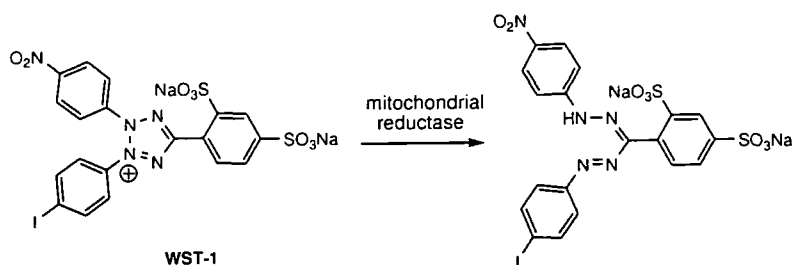
All ligands studied follow similar toxicity trends to their complexes: non-toxic ligands appear to give rise to non-toxic complexes, while the toxic ligand  $\text{L}^{5b}$  forms the toxic

complex  $[\text{Eu.L}^{5b}]\text{Cl}_3$ . This suggests that the metal ion itself is either not exerting any additional toxic effects, or that in this case, the complex is prone to dissociation

Most complexes were tested with chloride as the counterion, as this was the form commonly synthesised and studied. Investigation of the chloride and triflate salts of  $[\text{Eu.L}^{11}]^{3+}$  gave  $\text{IC}_{50}$  values of 120 and 79  $\mu\text{M}$  respectively. This suggests that the counterion may have an effect on the toxicity of a complex. In addition to the considerably lower solubility of triflate complexes, this provides further evidence that triflate salts are not the most ideal form for administration of complexes.

### 6.2.3 An alternative method for assessing cytotoxicity

In order to confirm the cytotoxicity data derived from the MTT assay, a different method was investigated. This assay utilised WST-1 ((4-[3-(4-iodophenyl)-2-(4-nitrophenyl)-2H-5-tetrazolio]-1,3-benzene disulfonate) which, like MTT, is a tetrazolium ion that is cleaved by mitochondrial reductase (Scheme 6.2). The principal difference between MTT and WST-1 is that the reduced product of WST-1 is water soluble, and the DMSO solubilisation step is therefore no longer required.<sup>264</sup>



Scheme 6.2

NIH 3T3 cells were prepared in an identical manner to that described for the MTT assay. WST-1 was added to the wells for the final 30 min, 1 h, 2 h or 4 h of incubation in order to determine the minimum time required for good readings. After incubation, the trays were immediately processed in the plate reader. It was found that cells incubated with WST-1 for 30 min gave very similar readings to cells treated for longer times. A 30 min incubation with this reagent was therefore adopted for subsequent studies. It was also necessary to select the appropriate blank to use for the photometric measurements. For MTT assays, DMSO was used as a blank. Initial WST-1 assays were performed using growth medium as a blank, but a number of wells gave negative readings. It was

therefore necessary to add WST-1 to the medium (in the absence of cells) for the blank. This is likely to be due to the fact that the tetrazolium form of WST-1 absorbs weakly in the spectral region of interest, and this must be taken into account.

In order to study the WST-1 assay in comparison to the MTT assay,  $IC_{50}$  values of four complexes were assessed using each method in parallel (Table 6.2). The results for the two assays were very similar. This confirms the validity of the results presented in Table 6.1. The advantages of WST-1 over MTT are its solubility, and the short time for which the cells must be incubated with the dye. Both properties are particularly advantageous for the measurement of  $IC_{50}$  values at shorter time points. WST-1 would therefore be the reagent of choice for future studies, particularly those which monitor changes in toxicity over time.

**Table 6.2:** Comparison of  $IC_{50}$  values derived from parallel measurements using the WST-1 and MTT assays following 24 h incubation

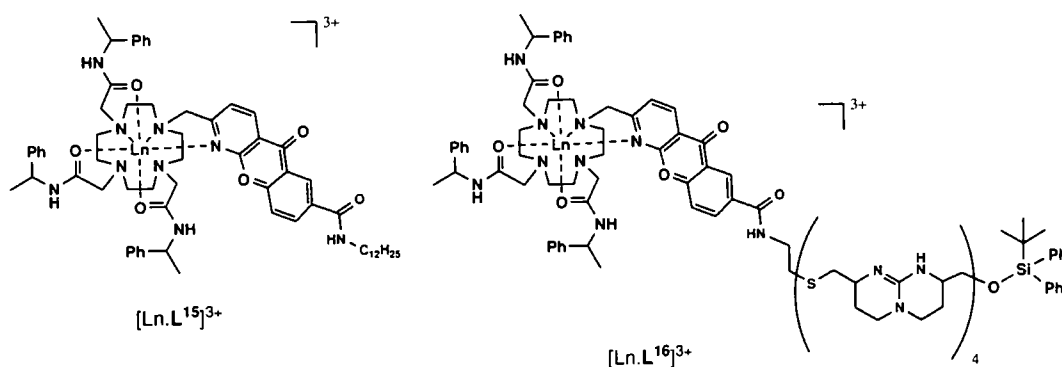
Complex / ligand	$IC_{50}$ ( $\mu$ M)	$IC_{50}$ ( $\mu$ M)
	MTT	WST-1
[Eu.L <sup>5a</sup> ]Cl <sub>3</sub>	>200 $\mu$ M	>200 $\mu$ M
[Eu.L <sup>5b</sup> ]Cl <sub>3</sub>	9 $\mu$ M	11 $\mu$ M
[Tb.L <sup>8</sup> ]Cl <sub>3</sub>	45 $\mu$ M	40 $\mu$ M
[Eu.L <sup>11</sup> ](OTf) <sub>3</sub>	70 $\mu$ M	59 $\mu$ M

#### 6.2.4 Understanding cytotoxicity of selected lanthanide complexes

While most complexes have  $IC_{50}$  values of greater than 100  $\mu$ M, there are isolated examples which are more cytotoxic (Table 6.1). Notably, complexes [Eu.L<sup>5b</sup>]<sup>3+</sup>, [Eu.L<sup>15</sup>]<sup>3+</sup> and [Eu.L<sup>16</sup>]<sup>3+</sup> had  $IC_{50}$  values of 5.6, 7.2 and 13  $\mu$ M respectively. It is important to understand how these complexes are causing cell death, in order to avoid such features in future probe design.

Complexes [Eu.L<sup>15</sup>]<sup>3+</sup> and [Eu.L<sup>16</sup>]<sup>3+</sup> were synthesised amongst a series of different conjugates linked to emissive terbium complexes in an investigation of the compartmentalisation of such complexes.<sup>156, 157</sup> [Eu.L<sup>15</sup>]<sup>3+</sup> incorporates a C<sub>12</sub> chain, while [Eu.L<sup>16</sup>]<sup>3+</sup> was synthesised by conjugation to an oligoguanidinium moiety which itself was designed to localise in the mitochondria.<sup>145</sup> Attempts to observe the cellular

behaviour of these two complexes, however, were marred by their high cytotoxicities, as evidenced by their low  $IC_{50}$  values (Table 6.1). These cytotoxicities can be compared to relatively lower toxicities of other complexes bearing the same chromophore and pendant arms,  $[Tb.L^{14}]^{3+}$ . In order to understand the mechanisms by which these complexes kill cells, an apoptosis-necrosis flow cytometry assay was performed.



The apoptosis-necrosis assay utilises the different properties of cells which are undergoing apoptosis and necrosis.<sup>265</sup> Propidium iodide (PI) is a cell impermeable salt whose fluorescence is enhanced 30-fold on binding to DNA. As it can only enter necrotic cells, which have compromised membrane integrity, the presence of propidium iodide fluorescence indicates necrosis. Annexin V is a phospholipid-binding protein which has a high affinity for the phospholipid phosphatidyl serine (PS), which is presented on the membrane of cells in early apoptosis.<sup>266</sup> This binding event is signalled by induced fluorescence of the fluorescein which is conjugated to the Annexin V in the form of fluorescein isothiocyanate (FITC).<sup>267</sup> As well as presenting PS, late apoptotic cells experience some loss of membrane integrity, and can therefore be distinguished from early apoptotic cells which show no PI fluorescence.

Both CHO and NIH 3T3 cells were treated with complexes  $[Eu.L^{15}]^{3+}$  and  $[Eu.L^{16}]^{3+}$  and stained with PI and the annexin V-FITC conjugate. As controls, cells were treated with ethanol to induce necrosis, and staurosporine, which induces apoptosis.<sup>268</sup> Example flow cytometry dot plots for complex-treated cells are shown in Figure 6.2.

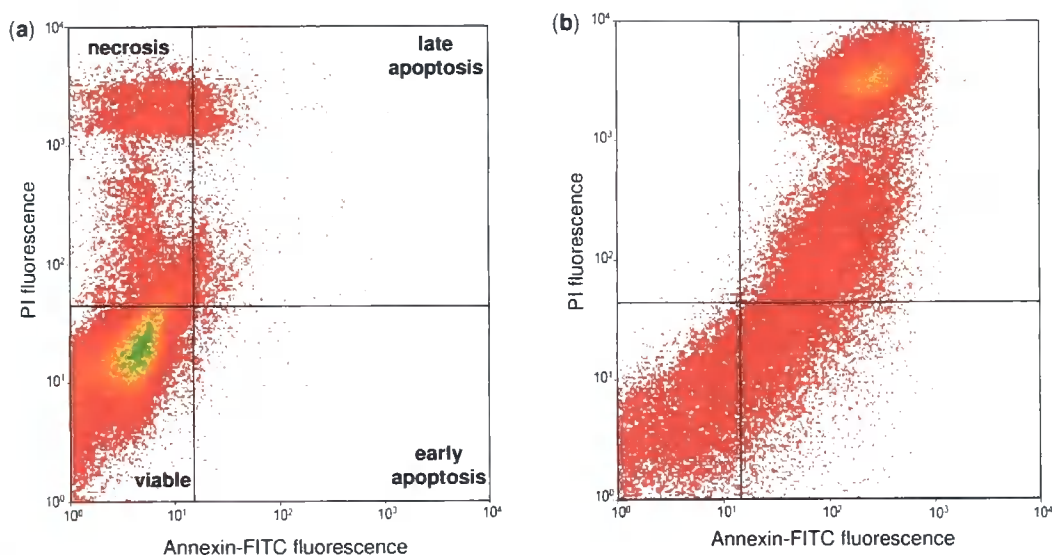


**Figure 6.2:** Flow cytometry plots following staining with propidium iodide and Annexin V-FITC of (a) CHO cells after 24 h incubation with  $[\text{Eu.L}^{15}]^{3+}$  and (b) NIH 3T3 cells after 4 h incubation with  $[\text{Eu.L}^{16}]^{3+}$ .

Cells treated with  $[\text{Eu.L}^{15}]^{3+}$  do not exhibit significant annexin-FITC fluorescence, but a population are stained by PI, suggesting that they are undergoing necrosis. This is consistent with the expectation that the long hydrophobic chain lodges in the lipid bilayer, disrupting the cell membrane. This indicates that future probe design should avoid such hydrophobic moieties. Cells treated with  $[\text{Eu.L}^{16}]^{3+}$ , on the other hand, do show FITC fluorescence, and a path can be seen from viable cells through early apoptosis, with the largest population lying in the quadrant corresponding to late apoptosis. An explanation for this observation is that the polyguanidinium vector transports the conjugate to the mitochondria, which are heavily involved in the induction of apoptosis.<sup>269</sup> While it is desirable to design complexes which are trafficked to the mitochondria, it is important to ensure that they do not adversely affect mitochondrial function. This will be considered further in Section 6.3.

The other cytotoxic complex identified from the MTT assays is  $[\text{Eu.L}^{5b}]^{3+}$ , which exhibited an  $\text{IC}_{50}$  value of  $5.6 \mu\text{M}$ .<sup>108</sup> Interestingly, the oxygen analogue,  $[\text{Eu.L}^{5a}]^{3+}$  is 30-fold less cytotoxic. As demetallation of the complexes had been observed in carbonate-binding studies, as described in Chapter Five (page 134), the *in cellulo* speciation is likely to be that of the dissociated complex. The cytotoxicities of the ligands alone are very similar to those of the complexes (Table 6.1). In order to

understand better the difference in toxicity between the oxygen- and sulfur-containing compounds,  $IC_{50}$  values of the chromophores alone were evaluated (Table 6.3). Again, it can be noted that the azaxanthone (**24**) is less cytotoxic than the azathioxanthone (**25**). The azathioxanthone is, however, ten times less toxic than the related ligand and complex. Further studies were performed of the sulfoxide (**26**) and sulfone (**27**) derivatives of this azathioxanthone, as they are likely to be the products of *in cellulo* oxidative metabolism. The sulfone derivative has an  $IC_{50}$  value of 21  $\mu\text{M}$ , and is therefore likely to contribute to the toxicity of the complex and its ligand. It is not the presence of this sensitiser alone which causes this cytotoxicity, as other azathioxanthone-containing complexes such as  $[\text{Eu.L}^{6b}]^{3+}$  and  $[\text{Eu.L}^{11}]^{3+}$  are considerably less toxic. Instead, the ready dissociation of  $[\text{Eu.L}^{5b}]^{3+}$  may contribute to increased metabolism of the chromophore, releasing the toxic sulfone.

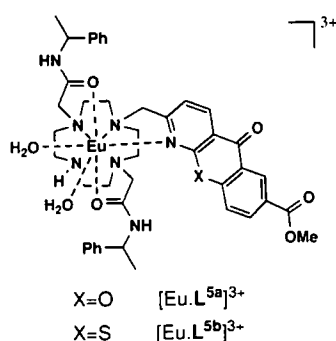
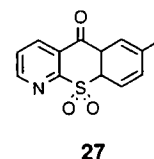
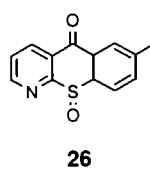
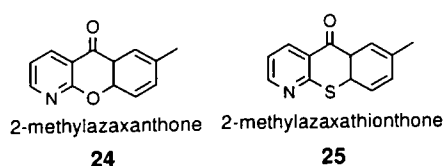


**Table 6.3:** Cytotoxicity data for  $[\text{Eu.L}^{5j}]^{3+}$  and related compounds in NIH 3T3 cells following 24 h incubation, showing standard deviations (SD)

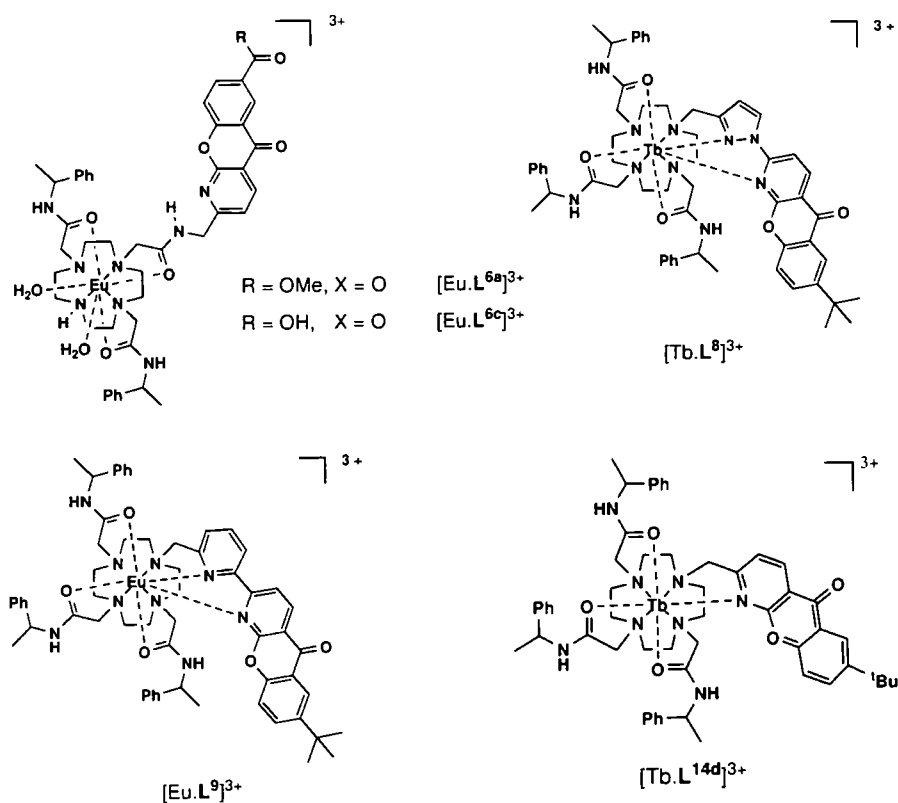
Compound	$IC_{50}$ ( $\mu\text{M}$ )	SD
$[\text{Eu.L}^{5a}]Cl_3$	>200 $\mu\text{M}$	-
<b>L<sup>5a</sup></b>	180 $\mu\text{M}$	15 $\mu\text{M}$
<b>24</b>	>240 $\mu\text{M}$	-
$[\text{Eu.L}^{5b}]Cl_3$	5.6 $\mu\text{M}$	0.3 $\mu\text{M}$
<b>L<sup>5b</sup></b>	4.9 $\mu\text{M}$	1.3 $\mu\text{M}$
<b>25</b>	72.5 $\mu\text{M}$	6.3 $\mu\text{M}$
<b>26</b>	>240 $\mu\text{M}$	-
<b>27</b>	21.2 $\mu\text{M}$	0.2 $\mu\text{M}$



### 6.3 Mitochondrial membrane potential

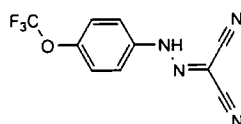
In addition to being non-toxic towards cells, cellular probes must also be designed to have minimal interaction with normal cellular process, and to have as little effect as possible on cellular homeostasis. For mitochondrial probes, this requires a minimal effect on the mitochondrial membrane potential (MMP), which allows for the normal function of the electron transport chain. One means by which the MMP can be monitored is through the use of fluorescent dyes in flow cytometry. One such assay, described by Pendergrass *et al.*,<sup>270</sup> measures the green fluorescence of Mitotracker Green FM (MTG), which stains all mitochondria, independent of their MMP,<sup>271</sup> against the red fluorescence of chloromethyl-X-rosamine (CMXRos), for which mitochondrial uptake increases with MMP.<sup>272</sup>

This method was utilised to study the effects of five complexes which demonstrated some mitochondrial localisation:  $[\text{Eu.L}^{6a}]^{3+}$  and  $[\text{Eu.L}^{6c}]^{2+}$ , which appeared to localise solely in the mitochondria at times up to 12 h, and  $[\text{Tb.L}^{8}]^{3+}$ ,  $[\text{Eu.L}^{9}]^{3+}$  and  $[\text{Tb.L}^{14d}]^{3+}$ , which exhibited a lysosomal / mitochondrial distribution pattern.



CHO cells were treated with 50  $\mu\text{M}$  complex for one or four hours for  $[\text{Eu.L}^6]^{3+}$  and for four or twenty-four hours for the remaining three complexes. 200 nM MTG and CMXRos were added for the final thirty minutes. Cells were then harvested and analysed by flow cytometry, measuring the green (FL1; MTG) fluorescence against the red (FL4; CMXRos).

Carbonyl cyanide *p*-trifluoromethoxyphenyl-hydrazone (FCCP; **28**) was employed to provide a control for cells with disrupted MMP. FCCP is an uncoupling agent which readily crosses the mitochondrial membrane, disrupting the proton gradient and hence destroying the MMP.<sup>273</sup> Cells were treated with either 20  $\mu\text{M}$  or 100  $\mu\text{M}$  FCCP, concentrations which have previously been reported to elicit approximately half-maximal and maximal changes (respectively) in the fluorescence of CMXRos.<sup>270</sup>

**28**

The ratio of red to green fluorescence (FL4/FL1) was calculated for each treatment (Figure 6.3). As previously observed, treatment with increasing concentrations of FCCP led to disruption of the MMP and decreased labelling by CMXRos, and hence a lower FL4/FL1 ratio.<sup>270</sup> This decreased red fluorescence was not observed for  $[\text{Eu.L}^{6a}]^{3+}$  and  $[\text{Eu.L}^{6c}]^{2+}$ ; instead, the red fluorescence appeared to increase with respect to the green. This suggests that these complexes do not disrupt the MMP. Importantly, there is no significant effect of time on the MMP, nor of a change in the complex charge (of 3+ to 2+). This suggests that these complexes localise in the mitochondria without disrupting its membrane potential, confirming the potential for their use as probes of normal mitochondrial conditions.

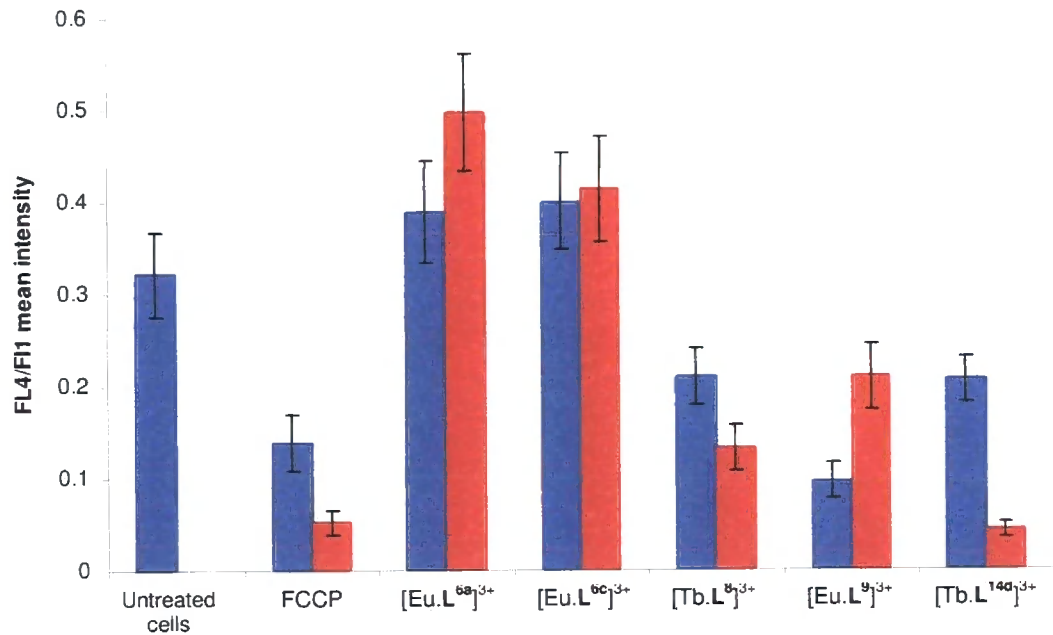


**Figure 6.3:** FL4/FL1 mean intensity from flow cytometric analysis of CHO cells with various treatments. FCCP treatments are 20  $\mu\text{M}$  (blue) and 100  $\mu\text{M}$  (red) for 3 h; [Eu.L<sup>6a</sup>]<sup>3+</sup> and [Eu.L<sup>6c</sup>]<sup>2+</sup> treatments are 50  $\mu\text{M}$  for 1 h (blue) and 4 h (red); [Tb.L<sup>8</sup>]<sup>3+</sup>, [Eu.L<sup>9</sup>]<sup>3+</sup> and [Tb.L<sup>14d</sup>]<sup>3+</sup> treatments are 50  $\mu\text{M}$  for 4 h (blue) and 24 h (red).

The remaining three complexes, on the other hand, demonstrate more noticeable changes in MMP. For all three complexes, the FL4/FL1 intensity is less than for untreated cells at all timepoints. For [Tb.L<sup>8</sup>]<sup>3+</sup> and [Tb.L<sup>14d</sup>]<sup>3+</sup>, this ratio decreases with time, while for [Eu.L<sup>9</sup>]<sup>3+</sup>, the FL4/FL1 ratio indicates a greater uncoupling at 4h, with partial restoration of the MMP after 24 h. In order to better understand this behaviour, an apoptosis-necrosis assay was performed (Figure 6.4). Higher complex concentrations (200  $\mu\text{M}$ ), above the measured IC<sub>50</sub> values (Table 6.1), were employed in order to maximise the number of dead cells that could be observed.

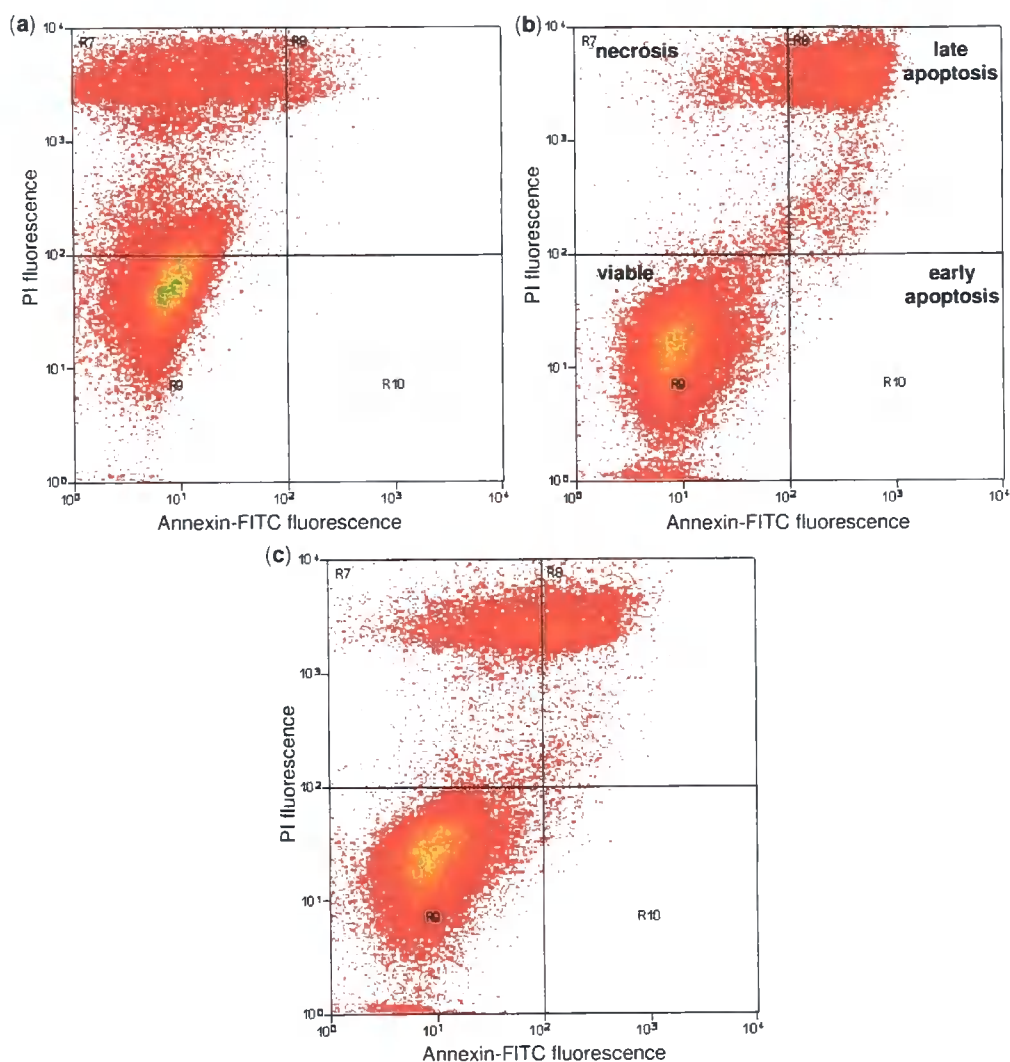


**Figure 6.4:** Flow cytometry plots following staining with propidium iodide and Annexin V-FITC of CHO cells treated for 24 h with (a)  $200 \mu\text{M} [\text{Tb.L}^8]^{3+}$ , (b)  $200 \mu\text{M} [\text{Eu.L}^9]^{3+}$  and (c)  $200 \mu\text{M} [\text{Tb.L}^{14d}]^{3+}$ .

The flow cytometry plots indicate that a population of cells treated with  $[\text{Tb.L}^8]^{3+}$  are stained with PI, and are therefore undergoing necrosis. In contrast, cells treated with  $[\text{Eu.L}^9]^{3+}$  are stained with Annexin-FITC as well as PI, indicative of apoptosis. The flow cytometry plot for  $[\text{Tb.L}^{14d}]^{3+}$  is harder to interpret, with cells lying in both apoptotic and necrotic regions.

These modes of cell death observed for  $[\text{Tb.L}^8]^{3+}$  and  $[\text{Eu.L}^9]^{3+}$  are consistent with the observed mitochondrial membrane potentials. Necrosis is a traumatic event which affects all aspects of cellular function. It is likely that a perturbed MMP is an effect of disrupted mitochondrial membranes rather than a cause of necrosis. Over time, therefore,

the damage to the mitochondria should increase, as is observed with the decreasing MMP of cells treated with  $[\text{Tb.L}^8]^{3+}$ . In contrast, apoptosis occurs *via* a cascade of controlled events which are often mediated by the mitochondria.<sup>269</sup> Cells undergoing apoptosis, such as those treated with  $[\text{Eu.L}^9]^{3+}$ , are therefore expected to exhibit a rapid change in MMP, as evidenced by the low FL4/FL1 ratio after 4 h (Figure 6.3). After 24 h, however, a large proportion of the cells which initially showed a reduced MMP would have completed apoptosis and would be too fragmented to be measured by flow cytometry. The assay will therefore measure a larger proportion of viable cells at this time point, with a higher average MMP.

Each of the three complexes under study contained a <sup>t</sup>Bu group appended to the sensitiser. It was initially thought that this group was responsible for the increased toxicity for complexes such as these. If this were the case, it would be expected that all three complexes should effect cell death by a similar mechanism. This was not found to be the case, so it appears that it is not simply the <sup>t</sup>Bu group itself which is causing the observed cytotoxicity.

## 6.4 Conclusions

In designing probes to report on sub-cellular conditions, it is essential that the probes themselves do not interfere with cellular functions. Principally, it is important to design probes that are non-toxic at the concentrations at which they will be used. Studies of the cytotoxicity of a range of luminescent lanthanide complexes indicate that induction of cell death is the exception, rather than the rule. Studies of these isolated toxic complexes have highlighted some design features which should be avoided. The measurement of cytotoxicity remains of great importance in the assessment of a potential cellular probe.

Another important indicator of cellular homeostasis is the mitochondrial membrane potential, which affects both the energy production of the cell and the induction of apoptosis. The complexes which were noted in Chapter Three (page 76) to localise to the mitochondria alone at early time-points did not appear to perturb the MMP, in agreement with their low toxicity. In contrast, complexes which localised quickly to both the lysosomes and the mitochondria were more toxic, and did result in an altered MMP with concomitant induction of cell death. This provides further confirmation that such a class

of complexes, which does not show one clear localisation pattern, should be avoided in future probe design.

The results reported in this chapter indicate that luminescent lanthanide complexes do not, in general, dramatically perturb cellular homeostasis. They therefore have great promise for application as sub-cellular probes.

# CHAPTER SEVEN

---

## CONCLUSIONS

## 7.1 General conclusions

The design of luminescent lanthanide complexes as luminescent probes has received widespread attention and interest. Reviews of the subject highlight the bias of research towards the design of systems which can respond to their environment, but not to considerations of the cellular behaviour of such systems.<sup>91, 274, 275</sup> Studies of novel complexes generally report only *in vitro* properties and assume that the complex will behave in a similar manner *in cellulo*. The interaction of complexes with cells is, however, an essential design consideration, and warrants greater attention.

This study of luminescent lanthanide complexes has been significantly aided by work in Durham over the past eight years, which has produced a range of complexes which vary in structure and behaviour. The synthesis of one set of complexes, bearing a tetraazatriphenylene chromophore and amino acid-based pendant arms, is described in Chapter Two. Characterisation of these complexes by various spectrometric methods revealed that substitution of alanine- for phenylalanine-based pendant arms results in adoption of a distinctly different geometry, in which the atom occupying the capping apical site of the polyhedron has changed, and a  $\Lambda$ - rather than  $\Delta$ -configuration is observed. Despite these marked structural changes, it appears to be overall complex hydrophobicity rather than geometry that dictates aspects of complex behaviour such as protein association. Each complex within this class exhibits a similar cellular uptake, localisation and toxicity profile. The information derived from these complexes contributed to the study of a broader range of complexes described throughout the rest of this thesis.

The selection of a suitable luminescent lanthanide complex for use as a cellular probe requires the simultaneous fulfilment of a number of properties. A complex which exhibits high luminescence in cellular medium but is cytotoxic, for example, would not be a suitable candidate. Nor would a complex which is sensitive to the concentration of citrate, but which localises in an organelle in which this anion is not of interest. The chapters of this thesis have addressed these issues.

An essential aspect of the design of cellular probes involves directing the complex to an appropriate sub-cellular locality. This work has demonstrated that complexes generally localise in the lysosomes or mitochondria. In addition, nucleolar localisation can be promoted and this tendency has been linked to cases of enhanced membrane

permeability. While these membrane effects perturb the homeostasis of the cell, this technique may prove to be a valuable method by which to probe this protein-rich region of the cell.

In addition to identification of localisation behaviour, structural aspects which promote distribution in each organelle have been defined. While the nature of the pendant arms does not appear to have any effect on the sub-cellular distribution, complexes bearing three identical pendant arms appear to exhibit less well-defined localisation profiles than those possessing a free cyclen NH. A number of modifications to the chromophore structure have been investigated, revealing that it is the nature of the linkage between the chromophore and the cyclen ring which most dramatically influences localisation. In contrast, variation of the substituents on the chromophore does not appear to significantly affect localisation, but can influence other aspects of cellular behaviour, such as sensitivity to quenching, protein affinity and cytotoxicity.

Another essential requirement for a sub-cellular probe is its ability to cross the cell membrane. Some complexes which were poorly visible by microscopy were previously believed to be excluded from the cell. Investigations of uptake and quenching behaviour indicated that these complexes did enter the cell, where their luminescence was strongly quenched. Indeed, all complexes were observed to be transported into the cell at similar rates. Mechanistic studies revealed a common active mode of uptake involving macropinocytosis. This allows for the uptake of structurally diverse complexes, and subsequent release of these complexes into the cytoplasm for trafficking to various organelles.

The sub-cellular speciation of a complex is very important in determining its efficacy. Emission spectroscopy of whole cells which had been treated with complex proved to be an effective method of probing the form adopted by the complex in cells. In this way, it was observed that complexes generally exist in protein-bound form. One interesting case was  $(SSS)-[Ln.L^2]^{3+}$ , which binds enantioselectively to drug site II of serum albumin with a concomitant change in helicity. This change was signalled by inversion of the circularly polarised luminescence.

Finally, it is important that probes cause minimal perturbation to cellular structure and function. Evaluation of cytotoxicity revealed that luminescent lanthanide complexes are generally non-toxic at working concentrations. Isolated complexes which did cause

death did so by readily explained mechanisms, which can be avoided in future probe design. The effect of mitochondrially-localising complexes on mitochondrial membrane potential (MMP) was also investigated. Those complexes which did perturb MMP also exhibited modest cytotoxicity, and should therefore be avoided in future probe design.

While the primary aim of this work was to investigate the cellular behaviour of luminescent lanthanide complexes to aid future probe design, this work has highlighted existing complexes which show particular promise. For example, complexes based on the ligands  $L^6$  exhibit low toxicity and good anion selectivity. In addition, they show clear mitochondrial localisation at time points up to 12 h, without perturbation of the mitochondrial membrane potential.

## 7.2 Implications for probe design

The objective of the work described in this thesis was to gain a greater understanding of the cellular behaviour of luminescent lanthanide complexes to aid in the design of cellular probes. The conclusions which have been reached concerning the interaction of complexes with cells have highlighted a number of important factors for consideration. Each chapter of this thesis has addressed a separate aspect of cellular behaviour. In probe design, however, it is essential to consider all facets together. This section attempts to draw together the various conclusions reached to highlight future directions for the study of luminescent lanthanide complexes.

The design of compounds for use as sub-cellular probes or drugs often employs strategies to induce certain cellular behaviour. For example, compounds might be encapsulated in liposomes to enhance cellular uptake, or conjugated to peptides to improve uptake and localisation. However, these strategies may also alter properties such as selectivity, toxicity or efficacy. It is therefore important to assess whether such modifications are required, or whether cellular behaviour of the native compound is sufficient to achieve its purpose.

For the luminescent lanthanide complexes, it is evident that no such strategy need be employed to induce cellular uptake. All complexes were observed to be transported readily across the cell membrane. The wide range of complexes studied indicates that is likely that any lanthanide complex of a similar structure (bearing a cyclen macrocycle

and heterocyclic sensitiser) will undergo macropinocytosis. Future probe design therefore need not concentrate on inducing cellular uptake.

In a similar manner, if lysosomal or mitochondrial localisation is required, it is not necessary to tag complexes to direct their delivery. Clear structural requirements for mitochondrial localisation have been defined, while a lysosomal localisation appears to be the default distribution. If other localisations are desired, however, it might be necessary to investigate more drastic structural modifications, or to conjugate the complex to a moiety with well-defined cellular behaviour. The studies reported here have indicated that sub-cellular localisation and other aspects of cellular behaviour, such as susceptibility to quenching and protein binding, are regulated by different structural factors. This allows the fine-tuning of probe behaviour by making small structural modifications, without affecting the sub-cellular localisation.

This work has highlighted a number of aspects of cellular behaviour which must be screened at an early stage in the design process to assess for potential use as a cellular probe. This should minimise the time spent in fully optimising and characterising a complex which may exhibit ideal *in vitro* behaviour, but does not function in the cellular environment. Among factors which must be assessed are cytotoxicity and susceptibility to quenching. It is also important to study the effect of protein binding or association on the selectivity and responsiveness of a potential probe.

### 7.3 Future work

This work has elucidated a number of significant biological properties of luminescent lanthanide complexes. However, there remain unanswered questions about the cellular behaviour of these complexes, particularly with respect to their sub-cellular localisation. While the mechanism of cell uptake has been studied and defined, the pathways by which complexes are trafficked between organelles is less clear. The preliminary results from the FRET experiments with RFP-tagged actin and tubulin could be investigated further. For example, it would be valuable to assess *in vitro* association or binding of complexes with either protein. Intracellular trafficking could also be studied by selecting inhibitors of organellar functions, such as polyvinylpyrrolidone, which disrupts lysosomes,<sup>276</sup> or antimycin, which inhibits mitochondrial function.<sup>277</sup>

The sub-cellular distribution of a complex which has been observed here by fluorescence microscopy could be further confirmed by use of a complementary technique, such as electron microscopy or X-ray fluorescence spectroscopy, as discussed in Section 3.6.3 (page 96). It might also be valuable to repeat the preliminary sub-cellular fractionation experiments, and collect a lysosomal fraction in addition to the nuclear and mitochondrial. This could allow for quantification of the relative distribution of complex throughout the cell. By collecting the emission spectra from these separated organelles, a more sophisticated understanding of sub-cellular speciation could be gained. Another aspect of sub-cellular localisation, which has not been explored here, is how localisation behaviour might be controlled by the cell cycle. Future work might involve synchronisation of the cell cycle and subsequent microscopic examination of intracellular localisation during mitosis and interphase.

In addition to these studies, which attempt to better understand cellular behaviour, further work is also required in the assessment of existing complexes for use as cellular probes. Studies thus far have concentrated on only a few indicators of *in cellulo* efficacy, such as susceptibility to quenching and serum albumin binding. Valuable work might involve the identification of other factors which are also important in determining probe efficacy, such as the binding of other common proteins.

The luminescent lanthanide complexes studied in this work have been designed to provide *in cellulo* information by their emission profiles. This is most likely to be manifested in a probe for use in a spectral imaging microscope. Future work in assessing the suitability of complexes for this purpose would require testing in such a set-up, to confirm that the information gained thus far from fluorescence microscopy and emission spectroscopy experiments can be combined to give information with high spatial and temporal resolution.

#### **7.4 Final remarks**

This work has demonstrated that the luminescent lanthanide complexes are very well suited to the purpose of probing cellular conditions. In addition to desirable chemical properties, such as long luminescence lifetimes and information-rich emission spectra, these complexes have been shown to be readily transported across the cell membrane and into cellular compartments, and to minimally perturb normal cellular function.

Luminescent lanthanide complexes therefore fulfil the requirements of an effective cellular probe set out in Section 1.2.3 (page 6), and certainly merit further attention and research in the future.

# CHAPTER EIGHT

---

## **EXPERIMENTAL METHODS**

## 8.1. General experimental

All solvents used were laboratory grade and were dried over an appropriate drying agents when required. All reagents were used as supplied by commercial sources unless otherwise stated. Water and H<sub>2</sub>O refer to high purity water obtained from the “PuriteSTILL Plus” purification system, with conductivity of 0.04  $\mu\text{S cm}^{-1}$ . Reactions requiring anhydrous conditions were carried out using Schlenk-line techniques under an atmosphere of dry argon.

Thin layer chromatography was performed using silica plates (Merck Art 5554) or neutral aluminium oxide plates (Merck Art 5550), both of which are fluorescent under UV irradiation (254 nm). Preparative column chromatography was performed using silica (Merck Silica Gel 60, 230–400 mesh) or neutral aluminium oxide (Merck Aluminium Oxide 90, activity II–III, 70–230 mesh) which had been pre-washed in ethyl acetate.

All pH measurements were performed using a Jenway 3320 pH meter attached to an Aldrich Chemical Company micro-pH combination electrode, calibrated using pH 4, 7 and 10 buffer solutions.

Melting points were recorded using a Reichart-Köfler block and are uncorrected.

### 8.1.1. Spectroscopy

<sup>1</sup>H NMR spectra were recorded at 199.99 MHz on a Varian Mercury-200, 299.91 MHz on a Varian Unity-300, 400.13 MHz on a Bruker Avance spectrometer, 499.78 MHz on a Varian Inova-500 or at 699.73 MHz on a Varian VNMRS-700. <sup>13</sup>C NMR spectra were recorded at 100.57 MHz on a Bruker Avance spectrometer, 125.67 MHz on a Varian Inova-500 or at 175.95 MHz on a Varian VNMRS-700. All spectra were recorded in commercially-available deuterated solvents, and were referenced to solvent residual proton signals.

Electrospray mass spectra were recorded on a Thermo Finnigan LTQ with methanol as the carrier solvent. High resolution mass spectrometry was performed on a Thermo Finnigan LTQ-FT.

Infrared spectra were obtained using a Perkin Elmer Spectrum RX1 with an ATR attachment.

UV/Vis absorbance spectra were recorded on a Perkin Elmer Lambda 900 UV/Vis/NIR spectrometer. Emission spectra and lifetimes were measured on a Fluorolog-3 and a Perkin Elmer LS55 luminescence spectrometer using FL Winlab software. All samples were contained in quartz cuvettes with a path length of 1 cm and measurements obtained relative to a reference of pure solvent contained in a matched cell. Luminescence spectra of the lanthanide(III) complexes were recorded following indirect excitation of the lanthanide(III) ion *via* the chromophore, at the stated maximal excitation wavelength.

Lifetime measurements were obtained by excitation of the sample by a short pulse of light (at  $\lambda_{\max}$ ) followed by monitoring the integrated intensity of light (546 nm for terbium, 612 nm for europium) emitted during a fixed gate time,  $t_g$ , after a delay of  $t_d$  (Figure 8.1). Measurements were made for at least 20 delay times over a period of three or more lifetimes. A gate time of 0.1 ms was used, and the excitation and emission slits were set to 10 and 5 nm respectively. The obtained decay curves were plotted in Microsoft Excel and fitted to equation 8.1:

$$I = A_0 + A_1 e^{-kt} \quad [8.1]$$

where  $I$  is the intensity at time  $t$  after the flash

$A_0$  is the intensity after decay is completed

$A_1$  is the pre-exponential factor

$k$  is the rate constant for decay of the excited state.

The excited state lifetime,  $\tau$ , is the inverse of the rate constant,  $k$ .

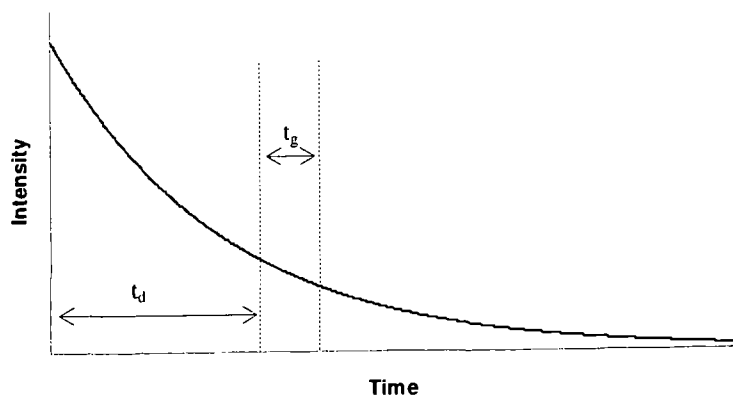


**Figure 8.1:** Measured parameters for lifetime measurements

Absorbance of biological samples in 96-well plates was measured on an Analytik Jena FLASHScan 530 using WinFLASH version 1.5 software.

CPL spectra were measured at the University of Glasgow, with the assistance of Dr R. D. Peacock.

Relaxivity measurements were made at 37 °C and 60 MHz on a Bruker Minispec mq60 instrument. The mean value of three separate measurements was recorded, and values stated were corrected for the diamagnetic contribution ( $R_{1d}=0.27$  at 60 MHz, 310 K).

HPLC analysis was performed using a Perkin Elmer series 200 system. The stationary phase was a Phenomenex Synergy 4  $\mu$  Fusion-RP 80 (150  $\times$  4.6 mm). The solvent system was H<sub>2</sub>O + 0.1% HCOOH / CH<sub>3</sub>CN + 0.1% HCOOH (gradient elution) with a run time of 20 min, according to the gradient outlined in Table 8.1.

**Table 8.1:** HPLC conditions employed for analysis of ligands and complexes. Flow rate: 1 mL/min; solvent A: H<sub>2</sub>O + 0.1% formic acid; solvent B: acetonitrile + 0.1% formic acid

Time / min	Solvent A / %	Solvent B / %	Curvature
0	100	0	0
15	0	100	1
20	0	100	0
25	100	0	-3
27	100	0	0

### 8.1.2. Cellular studies

Three cell lines were selected for cellular studies: CHO (Chinese Hamster Ovary), NIH 3T3 (mouse skin fibroblast) and HeLa (human endothelial carcinoma cells). Cells were maintained in exponential growth as monolayers in F-12 (Ham) medium, DMEM (Dulbecco's Modified Eagle Medium) and RPMI 1640 medium respectively. For each cell line, the medium was supplemented with 10% foetal bovine serum (FBS) and 1% (v/v) penicillin and streptomycin. Cells were grown in plastic culture flasks, with no prior surface treatment. Cultures were incubated at 37 °C, 20% average humidity and 5% (v/v) CO<sub>2</sub>. Cells were harvested by treatment with 0.25% (v/v) trypsin solution for

5 min at 37 °C. Cell suspensions were pelleted by centrifugation at 1000 rpm for 3 min, and were resuspended by repeated aspiration with a glass pipette.

In order to determine cell number, cells were detached from the flask by trypsinisation. Cells were then pelleted and resuspended in 4 mL medium, and an aliquot of the cell suspension injected into a haemocytometer (Fisher). The number of cells in a grid of volume 100 nL was counted using a light microscope, and the values for four separate grids measured to give an average cell count.

#### **8.1.2.1. Microscopy**

Cells were seeded in 12-well plates on glass coverslips and allowed to grow to 40% – 60% confluence, at 37 °C in 5% CO<sub>2</sub>. At this stage, the medium was replaced and cells were treated with drugs and complexes as appropriate. For NIH 3T3 and HeLa cells, DMEM lacking phenol red was used from this point onwards. Following incubation, the coverslips were washed with phosphate-buffered saline (PBS; pH 7.5), mounted on slides and the edges sealed with colourless, quick-dry nail varnish to prevent drying out of the sample.

Epifluorescence images were taken on a Zeiss Axiovert 200M epifluorescence microscope with a digital camera. G365 filters (Zeiss) were employed for excitation of the complexes, 546±12 and 575-625 filters (Comar) used for emission of Tb and Eu respectively and the FITC emission and excitation filter sets were selected for visualisation of LysoTracker and MitoTracker Green. Images were processed, given false colour and overlaid using Zeiss Axiovision and ImageJ software.

#### **8.1.2.2. Uptake studies**

Cells were seeded in 6-well plates and allowed to grow to 80% – 100% confluence, at 37 °C in 5% CO<sub>2</sub>. At this stage, the medium was replaced and cells treated with drugs at concentrations shown in Table 8.1. Complexes (50 µM) were added 30 min later and the cells incubated for a further 4 h. Following incubation, the medium was removed and the cells washed three times with PBS. 500 µL of lysis buffer (10 mM Tris, pH 7.5, 100 mM NaCl, 1 mM EDTA, 1% Triton X-100, 0.1% protease inhibitor cocktail) was then added

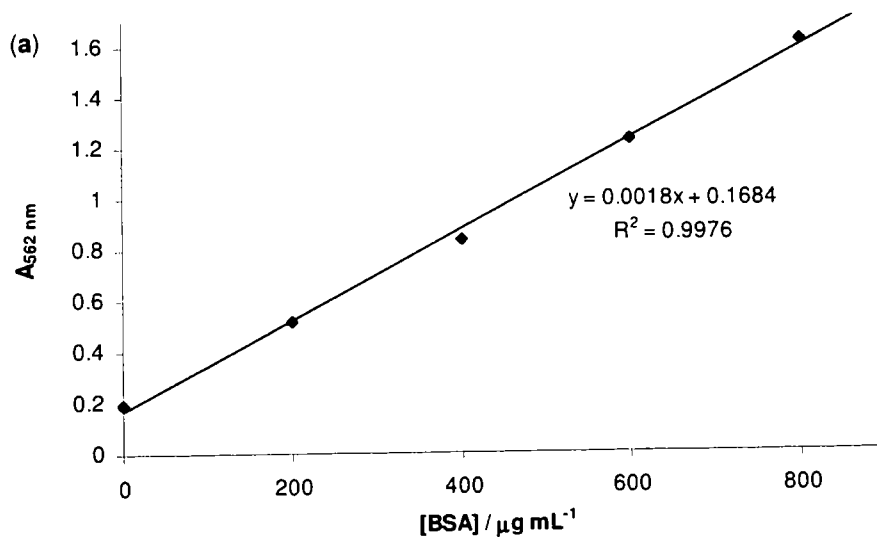
to each well, and the cells incubated at 5 °C for fifteen minutes. 3 × 25 µL aliquots of the supernatant were taken from each well for the BCA assay, as described below, and 400 µL was submitted for ICP-MS analysis.

**Table 8.1:** Inhibitors / activators of uptake pathways and the dosage concentrations utilised

Treatment	Dosage
Sucrose	50 mM
Chlorpromazine	50 µM
Filipin	1 mg/mL
Wortmannin	300 nM
Amiloride	3 mM
Phorbol 12-myristate-13-acetate	50 ng/mL
1,2-Dipalmitoyl- <i>rac</i> -diacylglycerol	500 ng/mL
Monensin	2 µM
Chloroquine	10 µM
Poly-L-lysine <sup>a</sup>	0.01%

<sup>a</sup> Prepared from a 10% solution as commercially available

Total protein content was determined in lysed cells using the bicinchoninic acid protein assay (BCA™ Protein Assay Kit).<sup>278</sup> A BSA standard curve was constructed in the range 0.2 to 1 mg/mL. 25 µL of standards and samples were aliquoted into triplicate wells of a 96-well plate and 200 µL of BCA reagent mix was added to each well. Absorbance at 540 nm was measured after 10 h incubation at room temperature using a microplate reader. Protein concentration for each sample was determined against the standard curve. Example results for a set of cells treated with [Eu.L<sup>9</sup>]Cl<sub>3</sub> are shown in Figure 8.2.



(b)

sample	replicate			average	[protein] μg/mL
	1	2	3		
1	0.291	0.307	0.418	0.339	96.0
2	0.351	0.373	0.320	0.348	101.2
3	0.869	0.984	1.042	0.965	449.5
4	0.714	0.784	0.667	0.722	312.3
5	0.459	0.442	0.402	0.434	150.0
6	0.576	0.643	0.622	0.614	251.3
7	0.533	0.549	0.495	0.526	201.5
8	0.636	0.629	0.618	0.628	259.2
9	0.513	0.567	0.592	0.557	219.4
10	0.316	0.278	0.317	0.304	76.4
11	0.464	0.502	0.491	0.486	179.0

**Figure 8.2:** Example data set for the determination of protein concentration using the BCA assay for cells treated with  $[\text{Eu.L}^9]^{3+}$  showing (a) BSA standard curve and (b) protein concentrations calculated from triplicate readings of each sample from calibration curve

Inductively coupled plasma mass spectrometry determinations of europium, terbium or gadolinium concentrations were made by Dr. C. Ottley in the Department of Earth Sciences at Durham University. Experimental data for the uptake of  $[\text{Eu.L}^2]\text{Cl}_3$  in the presence of various drugs are shown in Table 8.2.

**Table 8.2:** Example data for uptake studies of  $[\text{Eu.L}^2]\text{Cl}_3$  showing (a) calculation of intracellular lanthanide concentration from [protein] (from BCA assay) and  $[\text{}^{151}\text{Eu}]$  (from ICP-MS), and (b) the average and relative uptake calculated from triplicate measurements

(a)	Treatment	[protein] $\mu\text{g} / \text{mL}$	$[\text{}^{151}\text{Eu}]$ $\text{ng} / \text{mL}$	[Eu] $\text{nmol} / \text{mL}$	[Eu] / protein $\mu\text{mol} / \text{g}$
	Blank	249.7	0.087	0.0006	0.0022
	Control	292.1	101.9	0.670	2.30
	Chloroquine	255.6	84.41	0.554	2.17
	Chlorpromazine	197.6	76.8	0.504	2.55
	Filipin	274.0	115.8	0.762	2.78
	Monensin	256.6	74.5	0.489	1.91
	Poly-L-lysine	264.6	108.3	0.715	2.70
	Sucrose	207.3	70.2	0.465	2.24
	Wortmannin	241.4	66.7	0.440	1.82
	Amiloride	278.4	72.5	0.478	1.72
	Phorbol acetate	183.4	76.0	0.503	2.74
	Diacylglycerol	155.9	90.6	0.599	3.84
	5 °C	265.8	37.1	0.245	0.92

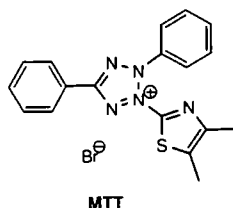
(b)	Uptake				
	$\mu\text{mol Eu} / \text{g protein}$				
	replicate 1	replicate 2	replicate 3	average	% uptake
Control	2.30	3.25	3.59	3.05	100.0
Chloroquine	2.17	3.30	3.4	2.96	97.0
Chlorpromazine	2.55	2.33	4.01	2.96	97.2
Filipin	2.78	2.30	4.35	3.14	103.2
Monensin	1.91	1.92	2.98	2.27	74.5
Poly-L-lysine	2.70	3.53	4.23	3.49	114.4
Sucrose	2.24	2.48	3.51	2.74	90.0
Wortmannin	1.82	1.81	1.85	1.83	60.0
Amiloride	1.72	1.45	1.69	1.62	53.2
Phorbol 12-myristate-13-acetate	2.74	6.15	4.80	4.56	149.8
1,2-dipalmytoylglycerol	3.84	7.84	6.01	5.90	193.5
5 °C	0.92	1.35	0.84	1.04	34.0

### 8.1.2.3. Cytotoxicity

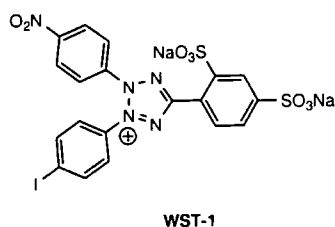
Approximately  $1 \times 10^4$  NIH-3T3 cells in 100  $\mu\text{L}$  DMEM were seeded into each well of flat-bottomed 96-well plates and allowed to attach overnight. Complex solutions were added to triplicate wells to give final concentrations over a 2-log range. After 24 h incubation,  $\text{IC}_{50}$  values were measured by one of two methods: MTT or WST-1. Both

methods utilise the cleavage of the tetrazolium ion by mitochondrial reductase in viable cells.<sup>262, 264</sup>

For the MTT method, 3-(4,5-dimethylthiazol-2-yl)-2,5-diphenyltetrazolium bromide (MTT; 1.0 mM)<sup>262</sup> was added to each well and the plates incubated for a further 4 h. The culture medium was removed, and DMSO (150  $\mu$ L) was added. The plate was shaken for 20 sec and the absorbance measured immediately at 540 nm in a microplate reader against a blank plate containing DMSO.



For the WST-1 assay, 4-[3-(4-iodophenyl)-2-(4-nitrophenyl)-2H-5-tetrazolio]-1,3-benzene disulfonate (WST-1, 10  $\mu$ L)<sup>264</sup> was added to each well and the plates incubated for a further 30 min. The plate was shaken for 20 sec and the absorbance measured immediately at 450 nm in a microplate reader against a blank of DMEM containing 10  $\mu$ L WST-1 per well.



For both methods,  $IC_{50}$  values were determined as the drug concentration required to reduce the absorbance to 50% of that in the untreated, control wells, and represent the mean value for data from at least three independent experiments. Example measurements and calculations for  $[Eu.L^9]Cl_3$  are shown in Figure 8.3.

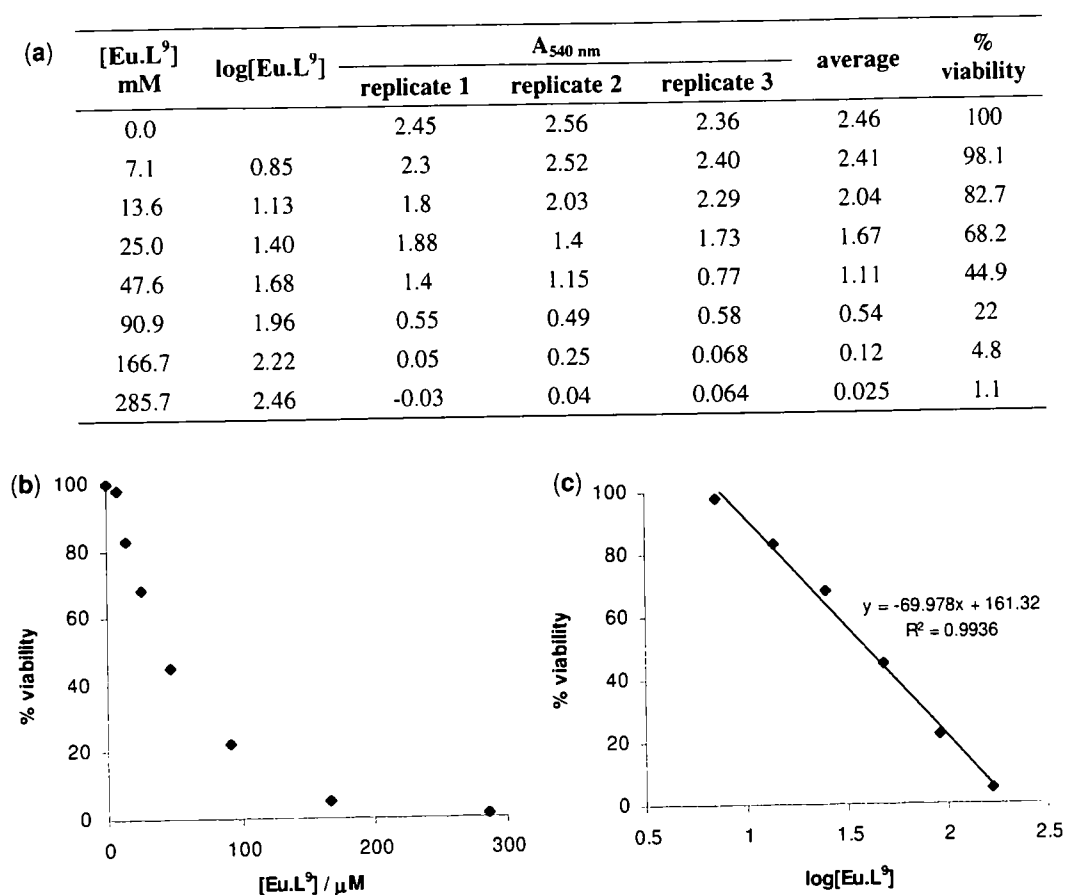


**Figure 8.3:** Example data from IC<sub>50</sub> determination for [Eu.L<sup>9</sup>]Cl<sub>3</sub> by the MTT assay (NIH 3T3 cells, 24 h incubation), showing (a) data from absorbance measurements and calculation of % viability, (b) variation of cell viability with concentration on a linear scale and (c) a logarithmic scale, allowing calculation of an IC<sub>50</sub> value of 41.4 μM.

#### 8.1.2.4. Flow cytometric assays

Flow cytometric analysis and sorting was conducted using a Dakocytomation Inc. MoFlo multi-laser flow cytometer (Fort Collins, CO, USA) operating at 60 psi with a 70 μM nozzle. Samples were interrogated with a 100mW 488 nm solid state laser. Fluorescence signals were detected through interference filters (FL1 530/40, FL2 670/30 nm) and were collected in the logarithmic mode. Data were analysed using Summit v4.3 software (Dakocytomation).

For flow cytometry, cells were grown to confluence in 6-well plates. Medium was replaced and cells were treated with complex. Cells were detached from the plastic surface with 0.25% (v/v) trypsin solution for five minutes at 37 °C. The resulting cell

suspension was pelleted by centrifugation. Immediately prior to flow cytometric analysis, cell suspensions were filtered through a 40  $\mu\text{m}$  filter.

The apoptosis-necrosis assay distinguishes cells which are undergoing different forms of cell death.<sup>265</sup> Propidium iodide (PI) is a marker for necrotic cells as it is excluded from viable cells, but can enter necrotic cells, for which the membrane is compromised. Upon DNA binding, the fluorescence of PI increases 30-fold. The annexin V-FITC conjugate is a marker for apoptotic cells, as it binds to the phosphatidyl serine (PS) which is presented on the membrane of cells in early apoptosis.<sup>266</sup> This binding event is signalled by induced fluorescence of the conjugated fluorescein moiety.<sup>267</sup> In this assay, the cell pellet was resuspended in 500  $\mu\text{L}$  binding buffer (10 mM HEPES at pH 7.5, 0.14 M NaCl and 2.5 mM  $\text{CaCl}_2$ ). This suspension was incubated with 0.5  $\mu\text{g}/\text{mL}$  annexin-FITC and 2  $\mu\text{g}/\text{mL}$  propidium iodide for ten minutes in the dark. Four controls were used, as illustrated in Table 8.3.

**Table 8.3:** Set-up of control wells used for apoptosis-necrosis assay

Control	Stains	Treatment
Blank	-	-
Apoptosis	annexin-FITC	staurosporine (1 $\mu\text{M}$ , 3h)
Necrosis	propidium iodide	ethanol (70%, 5 $^\circ\text{C}$ , 3h)
Untreated cells	annexin-FITC, propidium iodide	[Eu.L <sup>6c</sup> ] <sup>3+</sup> (50 $\mu\text{M}$ , 4h)

The mitochondrial membrane potential assay<sup>270</sup> measures the green fluorescence of Mitotracker Green FM (MTG), which stains all mitochondria, independent of their MMP,<sup>271</sup> against the red fluorescence of chloromethyl-X-rosamine (CMXRos), for which mitochondrial uptake increases with MMP.<sup>272</sup> Cells were incubated with 200 nM MTG and CMXRos for thirty minutes prior to harvesting. Following centrifugation, the cell pellet was resuspended in 500  $\mu\text{L}$  PBS. Relative mitochondrial membrane potential was calculated by measuring the mean intensity of FL1 (green) and FL4 (red) channels. Example data for the measurement of the MMP of [Eu.L<sup>6a</sup>]<sup>3+</sup> and [Eu.L<sup>6c</sup>]<sup>3+</sup> with respect to controls are shown in Table 8.4.

**Table 8.4:** Data from flow cytometric analysis of CHO cells with various treatments. FL4/FL1 gives an indication of relative mitochondrial membrane potential

Sample	Stains	Treatment	FL1 mean	FL4 mean	FL4/FL1
1	-	-	34.0	8.7	0.257
2	MTG	-	480.7	8.5	0.018
3	CMXRos	-	34.8	63.0	1.810
4	MTG, CMXRos	-	518.2	94.4	0.182
5	MTG, CMXRos	FCCP <sup>3</sup> (20 $\mu$ M, 3h)	476.2	52.8	0.111
6	MTG, CMXRos	FCCP (100 $\mu$ M, 3h)	884.7	62.2	0.070
7	MTG, CMXRos	[Eu.L <sup>6a</sup> ] <sup>3+</sup> (50 $\mu$ M, 1h)	719.8	181.5	0.252
8	MTG, CMXRos	[Eu.L <sup>6a</sup> ] <sup>3+</sup> (50 $\mu$ M, 4h)	686.9	228.7	0.333
9	MTG, CMXRos	[Eu.L <sup>6c</sup> ] <sup>3+</sup> (50 $\mu$ M, 1h)	552.7	143.4	0.259
10	MTG, CMXRos	[Eu.L <sup>6c</sup> ] <sup>3+</sup> (50 $\mu$ M, 4h)	560.1	149.8	0.267

<sup>3</sup> FCCP = Carbonyl cyanide *p*-trifluoromethoxyphenyl-hydrazone

### 8.1.2.5 Expression of RFP-tagged proteins

Cells containing RFP-tagged tubulin or actin were cultured using Cellular Lights™ Actin-RFP and Tubulin-RFP kits following the prescribed protocol (Invitrogen).<sup>182</sup> RFP-tagged proteins were expressed in CHO cells which had been grown to confluence on glass coverslips in 6-well plates. Following expression, cells were treated with Tb complex (100  $\mu$ M) for 4 hours. The coverslips were then mounted on microscope slides, as described in Section 8.1.2.1, and visualised using a Zeiss LSM510 Meta confocal microscope using 405 nm and 543 nm lasers, and Zeiss imaging software.

### 8.1.2.6 Sub-cellular fractionation

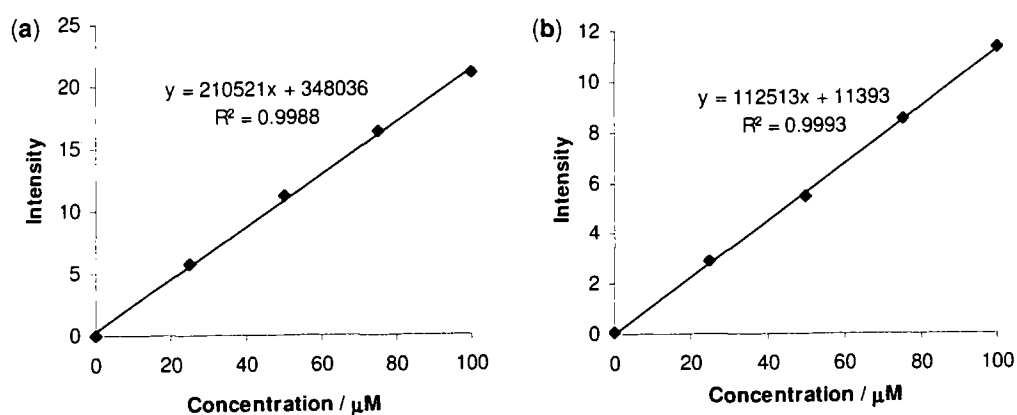
CHO and NIH 3T3 cells were grown in 75 cm<sup>2</sup> culture dishes and harvested by treatment with trypsin (0.1%) followed by centrifugation (1000 rpm, 3 min, 25 °C). Nuclei were extracted from the cell suspension using the Nuclei EZ Prep Kit (Sigma)<sup>279</sup> and Mitochondria were extracted from CHO cell using the Mitochondria Isolation Kit (Pierce Biotechnology)<sup>280</sup> according to the provided instructions.

### 8.1.3. Lipophilicity

Lipophilicity was measured as the relative partitioning of the complex between water and 1-octanol. Water was saturated with 1-octanol, and 1-octanol was saturated with water. Complexes were prepared as 100  $\mu\text{M}$  solutions in water and mixed with 1-octanol in 1:2, 1:1 and 2:1 water:octanol ratios. Mixtures were agitated for twelve hours, after which time emission spectra of the water and 1-octanol layers were collected. The complex concentration was calculated at the emission maximum with reference to calibration curves constructed for at least five concentrations between 0 and 100  $\mu\text{M}$  for water and 0 and 40  $\mu\text{M}$  for 1-octanol. For each mixture, the logP value was calculated according to equation 8.2:

$$\log P = \log_{10} \frac{[X]_{\text{1-octanol}}}{[X]_{\text{water}}} \quad [8.2]$$

Final logP values were calculated as the average of at least two replicates of the three solvent mixtures. Example data for  $[\text{Eu.L}^{4b}]$  are shown in Figure 8.4.



Sample	H <sub>2</sub> O		1-octanol		P	logP
	I <sub>616</sub>	[Eu] <sub>H2O</sub>	I <sub>616</sub>	[Eu] <sub>1-oct</sub>		
A	14.4	67.0	5.0	67.0	0.67	-0.18
B	15.0	69.7	5.0	69.7	0.63	-0.2
C	14.4	66.7	5.4	66.7	0.71	-0.15
D	14.5	67.2	5.6	67.2	0.74	-0.13
E	15.8	73.2	5.6	73.2	0.67	-0.17
F	16.2	75.2	6.3	75.2	0.74	-0.13
					<b>average</b>	-0.16
					<b>S.D.</b>	0.03

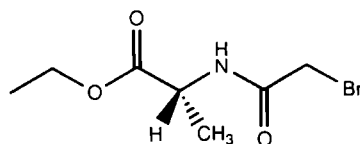
**Figure 8.4:** Calibration curves for  $[\text{Eu.L}^{4b}]$  in (a) H<sub>2</sub>O and (b) 1-octanol, and logP calculations for six replicates

## 8.2. Syntheses

[Eu.L<sup>1</sup>] was synthesised by Robert Poole.<sup>73</sup> [Eu.L<sup>5a</sup>]<sup>3+</sup>, [Eu.L<sup>5b</sup>]<sup>3+</sup>, [Eu.L<sup>6a</sup>]<sup>3+</sup>, [Eu.L<sup>6b</sup>]<sup>3+</sup>, [Eu.L<sup>6c</sup>]<sup>2+</sup> and [Eu.L<sup>7</sup>]<sup>3+</sup> were synthesised by Benjamin Murray,<sup>108, 148</sup> while [Tb.L<sup>8</sup>]<sup>3+</sup>, [Eu.L<sup>9</sup>]<sup>3+</sup> and [Eu.L<sup>10</sup>]<sup>3+</sup> were prepared by Craig Montgomery.<sup>149-151</sup> [Eu.L<sup>11</sup>]<sup>3+</sup> was synthesised by Junhua Yu, and [Eu.L<sup>12</sup>]<sup>3+</sup> and [Eu.L<sup>13</sup>]<sup>2+</sup> by Robert Pal. [Tb.L<sup>14a</sup>]<sup>3+</sup> and [Tb.L<sup>14d</sup>]<sup>3+</sup> were synthesised by Siobhan Richardson and Philip Stenson respectively.<sup>75</sup> [Tb.L<sup>14b</sup>]<sup>3+</sup>, [Tb.L<sup>14c</sup>]<sup>3+</sup>, [Tb.L<sup>15</sup>]<sup>3+</sup> and [Tb.L<sup>16</sup>]<sup>3+</sup> were prepared by Filip Kielar.<sup>155-157</sup>

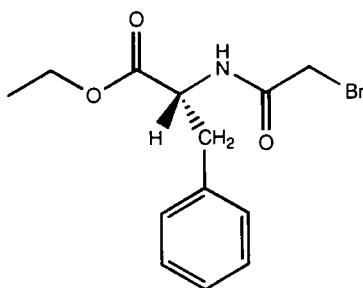
*N*-Bromoacetyl-(*S*)-alanine and *N*-bromoacetyl-(*S*)-phenylalanine ethyl esters were prepared by Junhua Yu. Ethyl esters of (*R*)-alanine and (*R*)-phenylalanine were prepared by esterification in ethanol, catalysed by HCl, using standard procedures.

### *N*-Bromoacetyl-(*R*)-alanine ethyl ester



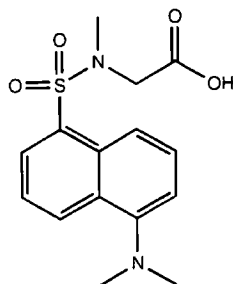
(*R*)-Alanine ethyl ester (5.5 g, 33 mmol) was suspended in dry chloroform (50 mL) and cooled to 0 °C in a salt-ice water bath. Following the addition of triethylamine (7 mL, 5.1 g, 51 mmol), bromoacetyl bromide (4.4 mL, 10.1 g, 50 mmol) was added dropwise to the suspension. The mixture was allowed to warm to room temperature and was stirred under argon overnight. The suspension was washed with an aqueous saturated sodium bicarbonate solution, and the chloroform removed to yield a brown oil. The product was purified by column chromatography (silica, eluted with dichloromethane) to yield *N*-bromoacetyl-(*R*)-alanine ethyl ester as an off-white solid (4.3 g, 18 mmol, 55%).

R<sub>F</sub> (silica; 5% CH<sub>3</sub>OH in CH<sub>2</sub>Cl<sub>2</sub>): 0.46, mp 65 - 66 °C. <sup>1</sup>H NMR (500 MHz, CDCl<sub>3</sub>): δ 1.31 (3H, t, *J* = 7.0, CH<sub>2</sub>CH<sub>3</sub>), 1.46 (3H, d, *J* = 7.0, Ala CH<sub>3</sub>), 3.89 (2H, s, Br-CH<sub>2</sub>), 4.24 (2H, q, *J* = 7.0, CH<sub>2</sub>CH<sub>3</sub>), 4.56 (1H, q, *J* = 7.0, Ala CH), 7.06 (1H, broad, NH). <sup>13</sup>C NMR (500 MHz, CDCl<sub>3</sub>): δ 14.36 (CH<sub>2</sub>CH<sub>3</sub>), 18.50 (Ala CH<sub>3</sub>), 29.01 (CH<sub>2</sub>Br), 49.04 (Ala CH), 62.03 (CH<sub>2</sub>CH<sub>3</sub>), 165.31 (Ala C=O), 172.63 (amide C=O). HRMS (+ *m/z*): [M+H]<sup>+</sup> calculated for C<sub>7</sub>H<sub>13</sub>O<sub>3</sub>N<sup>79</sup>Br, 238.0073; found, 238.0069.

***N*-Bromoacetyl-(*R*)-phenylalanine ethyl ester**<sup>281</sup>

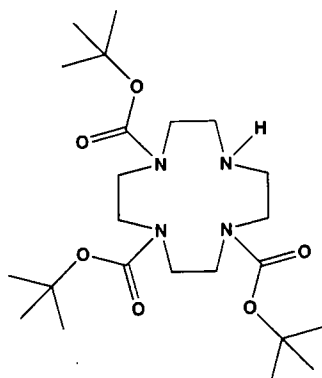
Phenylalanine ethyl ester (1.0 g, 4.1 mmol) was suspended in dry chloroform (30 mL) and cooled to 0 °C in a salt-ice water bath. Following the addition of triethylamine (1.5 mL, 1.1 g, 11 mmol), bromoacetyl bromide (1.0 mL, 2.3 g, 11 mmol) was added dropwise to the suspension. The mixture was allowed to warm to room temperature and was stirred under argon overnight. The suspension was washed with an aqueous saturated sodium bicarbonate solution, and the chloroform removed to yield a brown oil. The product was purified by column chromatography (silica, eluted with 1% MeOH:DCM) to yield *N*-bromoacetyl-(*R*)-phenylalanine ethyl ester as an off-white solid (0.85 g, 2.7 mmol, 66%).

$R_F$  (silica; 5% CH<sub>3</sub>OH in CH<sub>2</sub>Cl<sub>2</sub>): 0.51, mp 71 – 72 °C (lit. value<sup>281</sup> 71 – 72 °C for *S* enantiomer) <sup>1</sup>H NMR (200 MHz, MeOD): δ 1.27 (3H, t,  $J = 7.2$ , CH<sub>2</sub>CH<sub>3</sub>), 3.17 (2H, d,  $J = 6.2$ , Phe CH<sub>2</sub>), 3.86 (2H, s, Br-CH<sub>2</sub>), 4.21 (2H, q,  $J = 7.2$ , CH<sub>2</sub>CH<sub>3</sub>), 4.78 (1H, q,  $J = 6.2$ , Phe CH), 7.15 (2H, d,  $J = 6.5$ , ArH *ortho*), 7.30 (3H, m, ArH *para* and *meta*). <sup>13</sup>C NMR (500 MHz, CDCl<sub>3</sub>): δ 14.36 (CH<sub>2</sub>CH<sub>3</sub>), 28.94 (CH<sub>2</sub>Br), 38.01 (Phe CH<sub>2</sub>), 54.00 (Phe CH), 62.01 (CH<sub>2</sub>CH<sub>3</sub>), 127.55 (ArH *para*), 128.88 (ArH *meta*), 129.61 (ArH *ortho*), 165.36 (Phe C=O), 171.09 (amide C=O). HRMS (+  $m/z$ ): [M+H]<sup>+</sup> calculated for C<sub>13</sub>H<sub>17</sub>O<sub>3</sub>N<sup>79</sup>Br, 314.0386; found, 314.0382

***N*-Dansyl sarcosine**

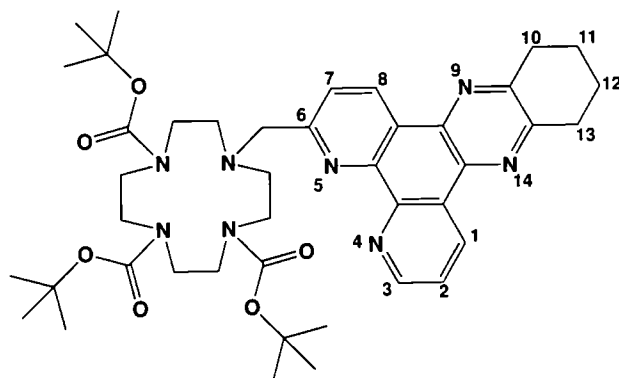
Sarcosine (32 mg, 0.36 mmol) was dissolved in an aqueous saturated  $\text{NaHCO}_3$  solution (10 mL). A solution of dansyl chloride (121 mg, 0.45 mmol) in acetone (2 mL) was added, and the resulting mixture was stirred at room temperature overnight. The mixture was subsequently evaporated to dryness, and the solid residue resuspended in water. The insoluble solids were removed by filtration. The supernatant was acidified to pH 4 by the addition of dilute HCl, at which point a pale green precipitate of dansyl sarcosine was formed. This product was isolated by filtration and was recrystallised from acetone (95 mg, 82%).

mp 198-199 °C.  $^1\text{H}$  NMR (400 MHz,  $\text{CD}_3\text{OD}$ ):  $\delta$  2.19 (3H, s, sarcosine  $\text{CH}_3$ ) 2.85 (6H, s, dansyl  $\text{CH}_3$ ), 4.00 (2H, s, sarcosine  $\text{CH}_2$ ), 7.24 (1H, m, ArH), 7.56 (2H, d,  $J = 8.2$ , ArH), 8.19 (1H, d,  $J = 8.2$ , ArH), 8.31 (1H, d,  $J = 8.7$ , ArH), 8.55 (1H, d,  $J = 8.7$ , ArH).  $^{13}\text{C}$  NMR (400 MHz,  $\text{CD}_3\text{OD}$ ):  $\delta$  34.8 (dansyl  $\text{CH}_3$ ), 47.7 (sarcosine  $\text{CH}_3$ ), 50.9 (sarcosine  $\text{CH}_2$ ), 115.3 (C Ar), 119.7 (C Ar), 123.2 (C Ar), 125.5 (C Ar), 126.4 (C Ar), 127.2 (C Ar), 127.9 (C Ar), 127.9 (C Ar), 129.2 (C Ar), 130.2 (C Ar), 134.9 (C Ar), 151.9 (sarcosine COOH). HRMS (+  $m/z$ ):  $[\text{M}+\text{Na}]^+$  calculated for  $\text{C}_{15}\text{H}_{18}\text{N}_2\text{O}_4\text{SNa}$ , 345.0885; found, 345.0883.

**1,4,7-Tris-*tert*-butoxycarbonyl-1,4,7,10-tetraazacyclododecane**<sup>73</sup>

A solution of di-*tert*-butyl dicarbonate (7.6 g, 35 mmol) in dichloromethane (70 mL) was added dropwise to a stirred solution of 1,4,7,10-tetraazacyclododecane (2.5 g, 15 mmol) in dichloromethane (250 mL). The mixture was stirred at room temperature for 2 h. Evaporation of the solvent afforded a transparent oil, which was purified by column chromatography (silica; gradient elution CH<sub>2</sub>Cl<sub>2</sub> to 5 % CH<sub>3</sub>OH/CH<sub>2</sub>Cl<sub>2</sub>) to give the title compound as a colourless solid (5.0 g, 11 mmol, 73 %).

R<sub>F</sub> (silica; 10% CH<sub>3</sub>OH in CH<sub>2</sub>Cl<sub>2</sub>): 0.29. mp 61-62 °C. <sup>1</sup>H NMR (400 MHz, CDCl<sub>3</sub>): δ 1.28 (27H, br s, CH<sub>3</sub>), 2.67 (4H, br m, CH<sub>2</sub>), 3.0-3.3 (8H, br m, CH<sub>2</sub>), 3.47 (4H, m, CH<sub>2</sub>).

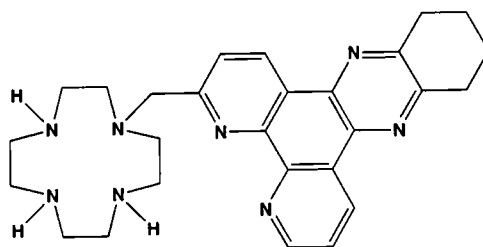
**1-(6-Methyl-10,11,12,13-tetrahydro-4,5,9,14-tetraazabenzotriphenylene)-4,7,10-tris(*tert*-butoxycarbonyl)-1,4,7,10-tetraazacyclododecane**<sup>73</sup>

Potassium carbonate (810 mg, 4.7 mmol) and a catalytic amount of potassium iodide were added to a solution of 1,4,7-tris-*tert*-butoxycarbonyl-1,4,7,10-

tetraazacyclododecane (500 mg, 1.2 mmol) in acetonitrile (20 mL). The mixture was heated to 60°C and a solution of 6-chloromethyl-10,11,12,13-tetrahydro-4,5,9,14-tetraazabenzob[*b*]triphenylene (390 mg, 1.2 mmol) in dichloromethane (3 mL) was added. The reaction mixture was boiled under reflux under argon overnight, after which time the solution was filtered and the salts washed with dichloromethane. Evaporation of the solvent afforded an orange residue, which was purified by column chromatography (silica gel; gradient elution CH<sub>2</sub>Cl<sub>2</sub> to 2.5 % CH<sub>3</sub>OH/ CH<sub>2</sub>Cl<sub>2</sub>) to yield the title compound as a pale yellow solid (424 mg, 0.60 mmol, 52%), identical to an authentic sample.<sup>73</sup>

R<sub>F</sub> (silica; 5% CH<sub>3</sub>OH in CH<sub>2</sub>Cl<sub>2</sub>): 0.29. <sup>1</sup>H NMR (300 MHz, CDCl<sub>3</sub>): δ 0.92-0.71 (27H, br m, CH<sub>3</sub>), 2.04 (4H, m, H10, H13), 2.42-2.99 (4H, m, CH<sub>2</sub> ring), 3.07-3.87 (16H, br m, CH<sub>2</sub> ring, H11, H12), 4.24 (2H, s, CH<sub>2</sub>-dpqC), 7.67 (1H, m, H2), 7.72-7.97 (1H, br s, H7), 9.71 (1H, br s, H3), 9.26-9.44 (2H, br m, H8, H1).

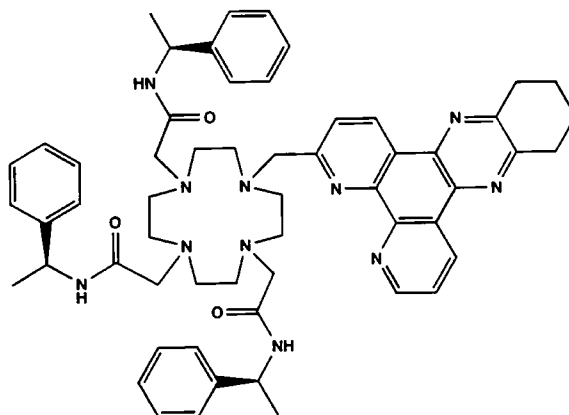
**1-(6-Methyl-10,11,12,13-tetrahydro-4,5,9,14-tetraazabenzob[*b*]triphenylene)-1,4,7,10-tetraazacyclododecane**<sup>73</sup>



Trifluoroacetic acid (9 mL) was added to a solution of 1-(6-methyl-10,11,12,13-tetrahydro-4,5,9,14-tetraazabenzob[*b*]triphenylene)-4,7,10-tris(*tert*-butoxycarbonyl)-1,4,7,10-tetraazacyclododecane (590 mg, 0.77 mmol) in dichloromethane (9 mL). The mixture was stirred at room temperature overnight. The solvent was evaporated and the residue washed with dichloromethane (3 × 10 mL). The residue was resuspended in an aqueous solution of potassium hydroxide (1M; 10 mL) and the product extracted into dichloromethane (3 × 10 mL). The organic layer was dried over K<sub>2</sub>CO<sub>3</sub>, and the solvent removed under reduced pressure to yield the title compound as a pale orange solid (270.3 mg, 0.577 mmol, 75%).

$^1\text{H}$  NMR (400 MHz,  $\text{CDCl}_3$ ):  $\delta$  2.06 (4H, m, H10, H13), 2.60-3.00 (16H, m,  $\text{CH}_2$  ring), 3.21 (4H, m, H11, H12), 4.22 (2H, s,  $\text{CH}_2$ -dpqC), 7.25 (1H, d,  $J = 8.0$ , H7), 7.63 (1H, dd,  $J = 8.2, 4.4$ , H2), 8.03 (1H, dd,  $J = 4.4, 1.4$ , H3), 9.23 (1H, d,  $J = 8.0$ , H8), 9.44 (1H, dd,  $J = 8.2, 1.4$ , H1).

**1-(6-Methyl-10,11,12,13-tetrahydro-4,5,9,14-tetraazabenzob[*b*]triphenylene)-4,7,10-tris[(*S*)-1-(1-phenyl)ethylcarbamoylmethyl]-1,4,7,10-tetraazacyclododecane**<sup>73</sup>



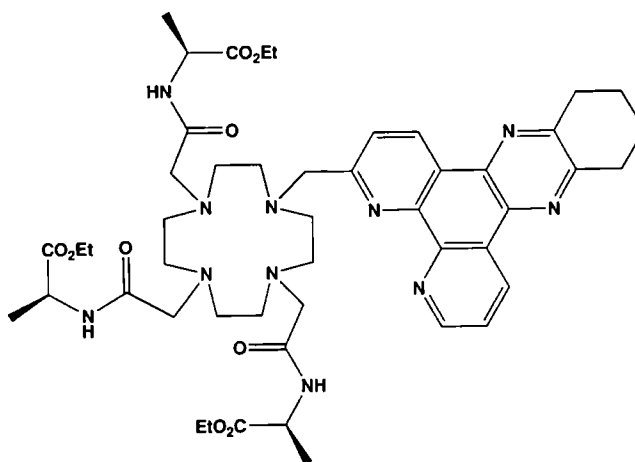
Potassium carbonate (120 mg, 0.85 mmol) and a catalytic amount of potassium iodide were added to a solution of 1-(6-methyl-10,11,12,13-tetrahydro-4,5,9,14-tetraazabenzob[triphénylene])-1,4,7,10-tetraazacyclododecane (80 mg, 0.17 mmol) in acetonitrile (5 mL). The reaction mixture was heated to 60 °C and a solution of (*S*)-*N*-(1-phenyleth-1-yl)chloroacetamide (99 mg, 0.50 mmol) in dichloromethane (5 mL) was added. The reaction mixture was heated to reflux overnight under argon. The solution was filtered and the salts washed with dichloromethane. Evaporation of the solvent resulted in an orange solid which was purified by column chromatography (neutral alumina; gradient elution  $\text{CH}_2\text{Cl}_2$  to 1%  $\text{CH}_3\text{OH}/\text{CH}_2\text{Cl}_2$ ) to give the title compound as a yellow solid (87 mg, 0.091 mmol, 54%).

$R_F$  (neutral alumina; 7.5%  $\text{CH}_3\text{OH}$  in  $\text{CH}_2\text{Cl}_2$ ): 0.55. mp 148-149 °C (lit. value<sup>73</sup> 148 - 150 °C). HRMS (+  $m/z$ ):  $[\text{M}+\text{H}]^+$  calculated for  $\text{C}_{57}\text{H}_{68}\text{N}_{11}\text{O}_3$ , 954.5506; found, 954.5505

**1-(6-Methyl-10,11,12,13-tetrahydro-4,5,9,14-tetraazabenzob[*b*]triphenylene)-4,7,10-tris(*R*)-1-(1-phenyl)ethylcarbamoylmethyl]-1,4,7,10-tetraazacyclododecane**

An analogous procedure to that described for synthesis of the (*SSS*) isomer was followed, using (*R*)-*N*-(1-phenyleth-1-yl)chloroacetamide. All spectroscopic characteristics were identical to those observed for the (*SSS*) isomer.

**1-(6-Methyl-10,11,12,13-tetrahydro-4,5,9,14-tetraazabenzob[*b*]triphenylene)-4,7,10-tris(ethyl-*N*-acetyl-*S*-alanine)-1,4,7,10-tetraazacyclododecane**



Potassium carbonate (80 mg, 0.58 mmol) and a catalytic amount of potassium iodide were added to a solution of 1-(3-methyl-10,11,12,13-tetrahydrodipyrido[3,2-*a*:2',3'-*c*]phenazine)-1,4,7,10-tetraazacyclododecane (55 mg, 0.12 mmol) in acetonitrile (5 mL). The reaction mixture was heated to 60°C and a solution of *N*-bromoacetyl-(*S*)-alanine ethyl ester (77 mg, 0.34 mmol) in dichloromethane (5 mL) was added. The reaction mixture was heated to reflux overnight, under argon. The solution was filtered and the salts washed with dichloromethane. After evaporation of the solvent, the residue was washed with ether to give the title compound as a yellow-brown solid (30 mg, 0.10 mmol, 29 %).

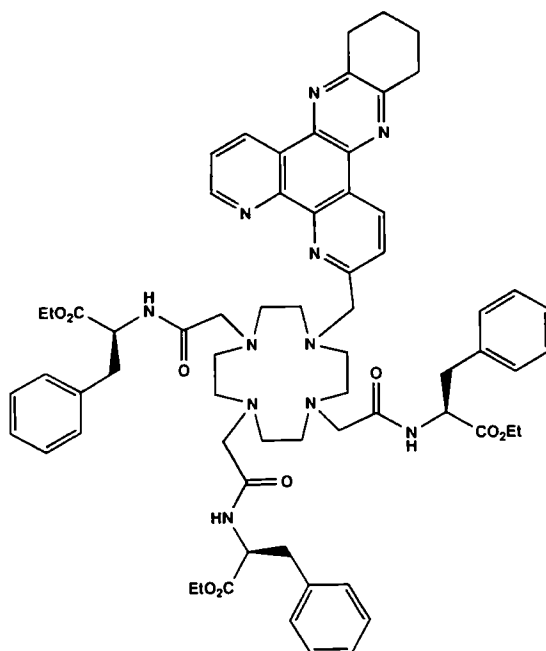
mp 129-130 °C. <sup>1</sup>H NMR (200 MHz, CDCl<sub>3</sub>): δ 1.16 (3H, t, *J* = 6.4, arm CH<sub>2</sub>CH<sub>3</sub>), 1.37 (3H, d, *J* = 7.2, arm Ala CH<sub>3</sub>), 2.09 (4H, m, H10, H13), 2.83 (16H, m, CH<sub>2</sub> ring), 3.24 (4H, m, H11, H12), 4.00-4.15 (4H, m, arm CH<sub>2</sub>CH<sub>3</sub>, CH<sub>2</sub>-dpqC), 4.60 (1H, q, *J* = 7.2, arm Ala CH), 7.27 (1H, d, *J* = 8.0, H7), 7.65 (1H, dd, *J* = 8.2, 4.4, H2), 8.06 (1H, dd, *J* = 4.4, 1.4, H3), 9.20 (1H, d, *J* = 8.0, H8), 9.42 (1H, dd, *J* = 8.2, 1.4, H1).

HRMS (+  $m/z$ ):  $[M+H]^+$  calculated for  $C_{48}H_{68}N_{11}O_9$ , 943.1266; found, 943.1259.  
HPLC:  $t_R = 10.9$  min.

**1-(6-Methyl-10,11,12,13-tetrahydro-4,5,9,14-tetraazabenzotriphenylene)-4,7,10-tris(ethyl-*N*-acetyl-*R*-alanine)-1,4,7,10-tetraazacyclododecane**

An analogous procedure to that described for synthesis of the (*SSS*) isomer was followed, using *N*-bromoacetyl-(*R*)-alanine ethyl ester. All spectroscopic characteristics were identical to those observed for the (*SSS*) isomer.

**1-(6-Methyl-10,11,12,13-tetrahydro-4,5,9,14-tetraazabenzotriphenylene)-4,7,10-tris(ethyl-*N*-acetyl-*S*-phenylalanine)-1,4,7,10-tetraazacyclododecane**



Potassium carbonate (88 mg, 0.63 mmol) and a catalytic amount of potassium iodide were added to a solution of 1-(6-methyl-10,11,12,13-tetrahydro-4,5,9,14-tetraazabenzotriphenylene)-1,4,7,10-tetraazacyclododecane (60 mg, 0.13 mmol) in acetonitrile (5 mL). The reaction mixture was heated to 60 °C and a solution of *N*-bromoacetyl-*S*-phenylalanine ethyl ester (120 mg, 0.38 mmol) in dichloromethane (5 mL) was added. The reaction mixture was heated to reflux overnight, under argon. The solution was filtered and the salts washed with  $CH_2Cl_2$ . Evaporation of the solvent

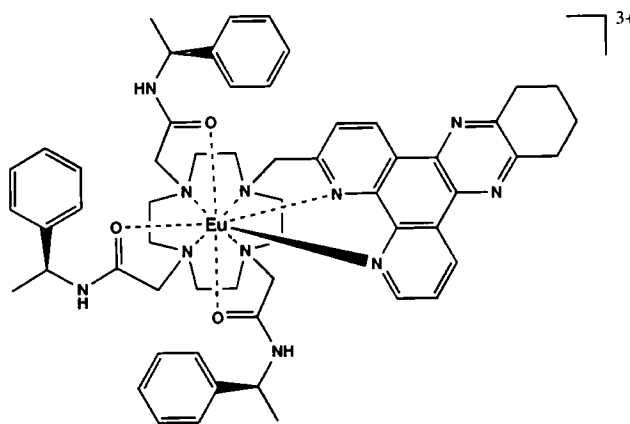
gave rise to an orange residue, which was purified by column chromatography (neutral alumina; gradient elution  $\text{CH}_2\text{Cl}_2$  to 1%  $\text{CH}_3\text{OH}/\text{CH}_2\text{Cl}_2$ ) to give the title compound as a yellow solid (74 mg, 0.079 mmol, 51%).

mp 119-120 °C.  $R_F$  (neutral alumina; 5%  $\text{CH}_3\text{OH}$  in  $\text{CH}_2\text{Cl}_2$ ): 0.33.  $^1\text{H}$  NMR (300 MHz,  $\text{CDCl}_3$ ): 0.95-1.40 (18H, m,  $\text{CH}_2\text{CH}_3$ ,  $\text{CHCH}_3$ ), 2.06 (4H, m, H10, H13), 2.40-3.00 (16H, br m,  $\text{CH}_2$  ring), 3.43 (4H, m, H11, H12), 3.80-4.80 (17H, m,  $\text{CH}_2\text{CO}$ ,  $\text{CH}_2$ -dpqC, CH), 6.95-7.35 (15H, m, phenyl CH), 7.58 (1H, m, H7), 7.70 (1H, br m, H2), 7.98 (1H, br m, H3), 9.38 (1H, m, H8), 9.49 (1H, m, H1). HRMS (+ m/z):  $[\text{M}+\text{H}]^+$  calculated for  $\text{C}_{66}\text{H}_{80}\text{N}_{11}\text{O}_9$ , 1171.4160; found, 1171.4165. HPLC:  $t_R = 14.1$  min

**1-(6-Methyl-10,11,12,13-tetrahydro-4,5,9,14-tetraazabenzotriphenylene)-4,7,10-tris(ethyl-*N*-acetyl-*R*-phenylalanine)-1,4,7,10-tetraazacyclododecane**

An analogous procedure to that described for synthesis of the (*SSS*) isomer was followed, using *N*-bromoacetyl-(*R*)-phenylalanine ethyl ester. All spectroscopic characteristics were identical to those observed for the (*SSS*) isomer.

**(*SSS*)-[Eu.L<sup>2</sup>]Cl<sub>3</sub><sup>73</sup>**

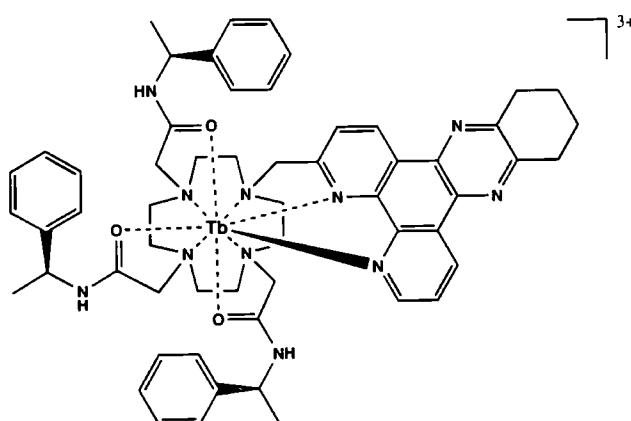


1-(6-Methyl-10,11,12,13-tetrahydro-4,5,9,14-tetraazabenzotriphenylene)-4,7,10-tris[(*S*)-1-(1-phenyl)ethylcarbamoylmethyl]-1,4,7,10-tetraazacyclododecane (16 mg, 0.017 mmol) and europium(III) trifluoromethanesulfonate (10 mg, 0.017 mmol) were dissolved in dry acetonitrile (5 mL) and the resulting solution was heated to reflux under argon overnight. The solution was then added dropwise to ether (20 mL), the precipitate centrifuged and the solvent decanted. The solid was redissolved in acetonitrile and the

process repeated to yield a pale yellow solid. This solid was then converted to the chloride salt by stirring with Dowex 1x8 200-400 mesh Cl which had previously been washed with 1 M hydrochloric acid and neutralised with water. The solid Dowex was removed by filtration and the solvent removed by freeze drying to yield the title compound as an off-white solid (15 mg, 0.013 mmol, 73%).

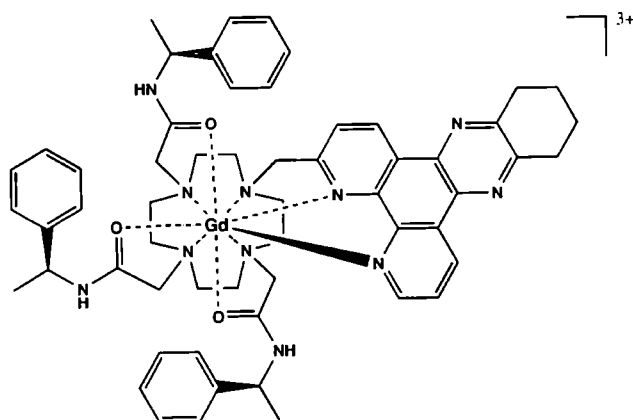
Spectroscopic characteristics were identical to those reported previously.<sup>73</sup> HRMS (+ m/z): [M]<sup>3+</sup> calculated for C<sub>57</sub>H<sub>67</sub>O<sub>3</sub>N<sub>11</sub>Eu, 368.1537; found, 368.1541

(SSS)-[Tb.L<sup>2</sup>]Cl<sub>3</sub><sup>73</sup>



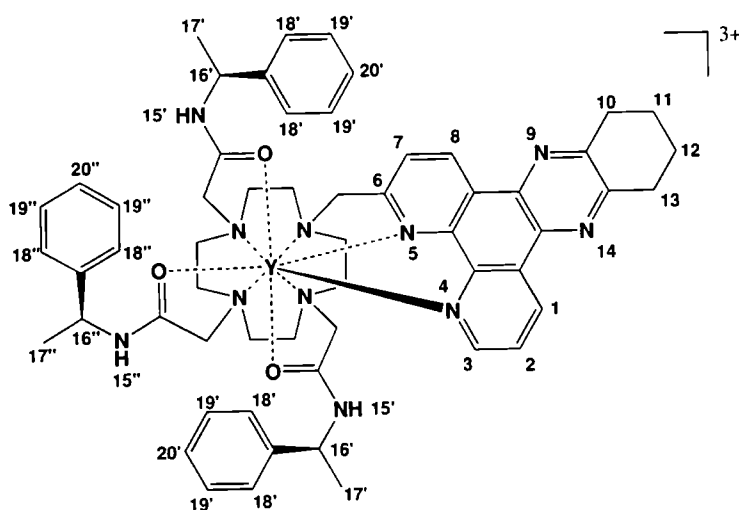
An analogous procedure to that described for synthesis of the Eu complex was followed using 1-(6-methyl-10,11,12,13-tetrahydro-4,5,9,14-tetraazabenzob[*b*]triphenylene)-4,7,10-tris[(*S*)-1-(1-phenyl)ethylcarbamoylmethyl]-1,4,7,10-tetraazacyclododecane (16 mg, 0.017 mmol) and terbium(III) trifluoromethanesulfonate (10 mg, 0.017 mmol) in dry acetonitrile (5 mL), giving the product as a yellow solid (14 mg, 0.012 mmol, 66%).

Spectroscopic characteristics were identical to those reported previously.<sup>73</sup> HRMS (+ m/z): [M]<sup>3+</sup> calculated for C<sub>57</sub>H<sub>67</sub>O<sub>3</sub>N<sub>11</sub>Tb, 370.8222; found, 370.8226

**(SSS)-[GdL<sup>2</sup>]Cl<sub>3</sub>**<sup>73</sup>

An analogous procedure to that described for synthesis of the Eu complex was followed using 1-(6-methyl-10,11,12,13-tetrahydro-4,5,9,14-tetraazabenzob)triphenylene)-4,7,10-tris[(*S*)-1-(1-phenyl)ethylcarbamoylmethyl]-1,4,7,10-tetraazacyclododecane (16 mg, 0.017 mmol) and gadolinium(III) acetate (5.7 mg, 0.017 mmol) in methanol:water (1:1, 5 mL), giving the product as a yellow solid (13.5 mg, 0.011 mmol, 65%).

Spectroscopic characteristics were identical to those reported previously.<sup>73</sup> HRMS (+ *m/z*): [M+2H]<sup>+</sup> calculated for C<sub>57</sub>H<sub>65</sub>N<sub>11</sub>O<sub>3</sub>Gd, 1109.4513; found 1109.4517.

**18. (SSS)-[YL<sup>2</sup>]Cl<sub>3</sub>**

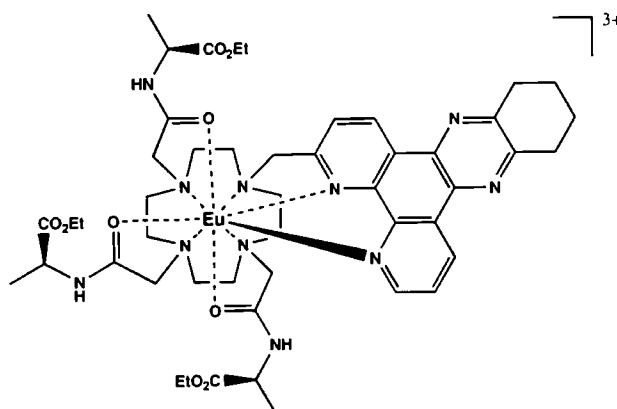
An analogous procedure to that described for synthesis of the Eu complex was followed using 1-(6-methyl-10,11,12,13-tetrahydro-4,5,9,14-tetraazabenzob)triphenylene)-

4,7,10-tris[(*S*)-1-(1-phenyl)ethylcarbamoylmethyl]-1,4,7,10-tetraazacyclododecane (26 mg, 0.027 mmol) and yttrium(III) acetate (6.7 mg, 0.025 mmol) in methanol:water (1:1, 5 mL), giving the product as a yellow solid (23 mg, 0.019 mmol, 75%).

$^1\text{H}$  NMR (700 MHz,  $\text{D}_2\text{O}$ ): 0.79 (3H, m, H16'), 1.11 (3H, m, H17'), 1.25 (1H, m, cyclen  $\text{CH}_2$ ), 1.39 (1H, m, cyclen  $\text{CH}_2$ ), 1.61 (3H, m, H17''), 1.84 (2H, m, amide  $\text{CH}_2$ ), 2.01 (5H, m, H11, H12, cyclen  $\text{CH}_2$ ), 2.17 (3H, m, cyclen  $\text{CH}_2$ ), 2.26 (1H, m, cyclen  $\text{CH}_2$ ), 2.34 (1H, m, amide  $\text{CH}_2$ ), 2.52 (2H, m, amide  $\text{CH}_2$ ), 2.67 (1H, m, H16'), 2.75 (2H, m, cyclen  $\text{CH}_2$ ), 2.97 (1H, m, cyclen  $\text{CH}_2$ ), 3.20 (3H, m, cyclen  $\text{CH}_2$ ), 3.22 (4H, m, H10, H13), 3.33 (1H, m, amide  $\text{CH}_2$ ), 3.68 (1H, m, cyclen  $\text{CH}_2$ ), 4.01 (1H, m, H16'), 5.04 (1H, m, H16''), 6.37 (2H, m, H19''), 6.47 (3H, m, H18'', H20''), 6.76 (1H, m, H15''), 6.87 (2H, m, H15'), 7.33 (4h, m, H17'), 7.38 (4H, m, H19'), 7.40 (2H, m, H20'), 7.75 (1H, m, H7), 8.35 (1H, m, H2), 9.30 (1H, m, H3), 9.53 (1H, m, H8), 9.59 (1H, m, H1). HRMS (+  $m/z$ ):  $[\text{M}]^{3+}$  calculated for  $\text{C}_{57}\text{H}_{65}\text{N}_{11}\text{O}_3\text{Y}$ , 347.4824; found 347.4816.

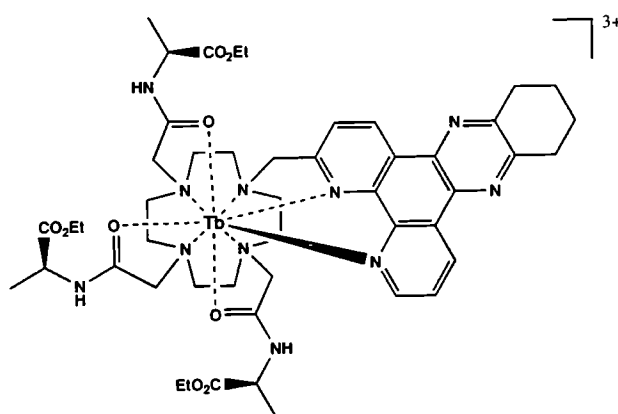
### ***(RRR)*-[Ln.L<sup>2</sup>]Cl<sub>3</sub>**

*(RRR)*-[Eu.L<sup>2</sup>]Cl<sub>3</sub>, *(RRR)*-[Tb.L<sup>2</sup>]Cl<sub>3</sub>, *(RRR)*-[Gd.L<sup>2</sup>]Cl<sub>3</sub> and *(RRR)*-[Y.L<sup>2</sup>]Cl<sub>3</sub> were synthesised by analogous procedures to *(SSS)*-[Eu.L<sup>2</sup>]Cl<sub>3</sub>, *(SSS)*-[Tb.L<sup>2</sup>]Cl<sub>3</sub>, *(SSS)*-[Gd.L<sup>2</sup>]Cl<sub>3</sub> and *(SSS)*-[Y.L<sup>2</sup>]Cl<sub>3</sub> respectively, using *(RRR)*-L<sup>2</sup>. Spectroscopic characterisation was identical to that observed for *(SSS)*-[Ln.L<sup>2</sup>]Cl<sub>3</sub>. Opposite chirality for the Eu and Tb complexes was confirmed by CPL (see main text).

**(SSS)-[Eu.L<sup>3a</sup>]Cl<sub>3</sub>**

An analogous procedure to that described for (SSS)-[Eu.L<sup>2</sup>]Cl<sub>3</sub> was followed, using 1-(6-methyl-10,11,12,13-tetrahydro-4,5,9,14-tetraazabenzob[*b*]triphenylene)-4,7,10-tris(ethyl-N-acetyl-*R*-alanine)-1,4,7,10-tetraazacyclododecane (15 mg, 0.015 mmol) and europium(III) trifluoromethanesulfonate (9 mg, 0.015 mmol) in dry acetonitrile (5 mL). The title compound was obtained as an off-white solid (12 mg, 0.010 mmol, 68%).

<sup>1</sup>H NMR (500 MHz, 283K, D<sub>2</sub>O) Peaks range from 44.0 to -19.5 ppm. Selected peaks at: 44.00, 40.71, 29.93, 25.41, 20.87 ppm; -9.36, -10.37, 13.40, 13.63, 19.54 ppm. HRMS (+ *m/z*): [M]<sup>3+</sup> calculated for C<sub>48</sub>H<sub>67</sub>N<sub>11</sub>O<sub>9</sub>Eu, 359.1435; found, 359.1439. HPLC: *t<sub>R</sub>* = 10.9 min.

**(SSS)-[Tb.L<sup>3a</sup>]Cl<sub>3</sub>**

An analogous procedure to that described for (SSS)-[Eu.L<sup>3a</sup>]Cl<sub>3</sub> was followed, using 1-(6-methyl-10,11,12,13-tetrahydro-4,5,9,14-tetraazabenzob[*b*]triphenylene)-4,7,10-

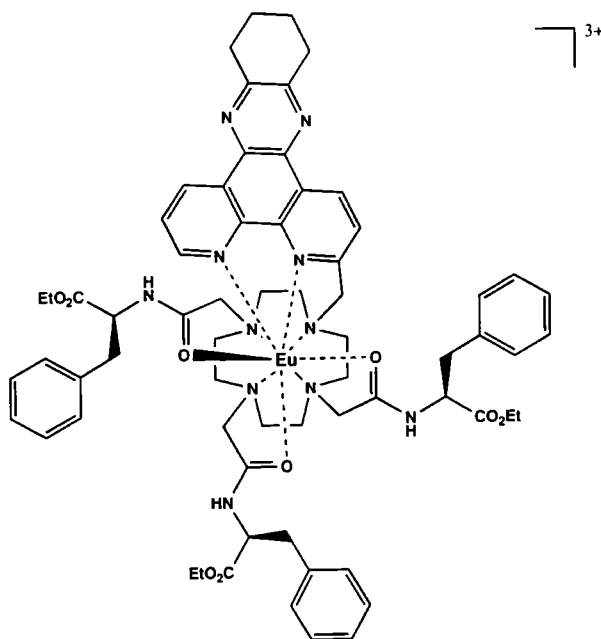
tris(ethyl-N-acetyl-(*S*)-alanine)-1,4,7,10-tetraazacyclododecane (21 mg, 0.022 mmol) and terbium(III) trifluoromethanesulfonate (13mg, 0.022 mmol) in dry CH<sub>3</sub>CN (5 mL), giving the product as an off-white solid (10 mg, 0.0088 mmol, 40%).

HRMS (+ *m/z*):[M]<sup>3+</sup> calculated for C<sub>48</sub>H<sub>67</sub>N<sub>11</sub>O<sub>9</sub>Tb, 366.8120; found, 366.8118. HPLC: *t<sub>R</sub>* = 8.8 min.

### (*RRR*)-[Ln.L<sup>3a</sup>]Cl<sub>3</sub>

(*RRR*)-[Eu.L<sup>3a</sup>]Cl<sub>3</sub> and (*RRR*)-[Tb.L<sup>3a</sup>]Cl<sub>3</sub> were synthesised by analogous procedures to (*SSS*)-[Eu.L<sup>3a</sup>]Cl<sub>3</sub> and (*SSS*)-[Tb.L<sup>3a</sup>]Cl<sub>3</sub> respectively, using (*RRR*)-L<sup>3a</sup>. Spectroscopic characterisation was identical to that observed for (*SSS*)-[Ln.L<sup>3a</sup>]Cl<sub>3</sub>. Opposite chirality was confirmed by CPL (see main text).

### (*SSS*)-[Eu.L<sup>3b</sup>]Cl<sub>3</sub>

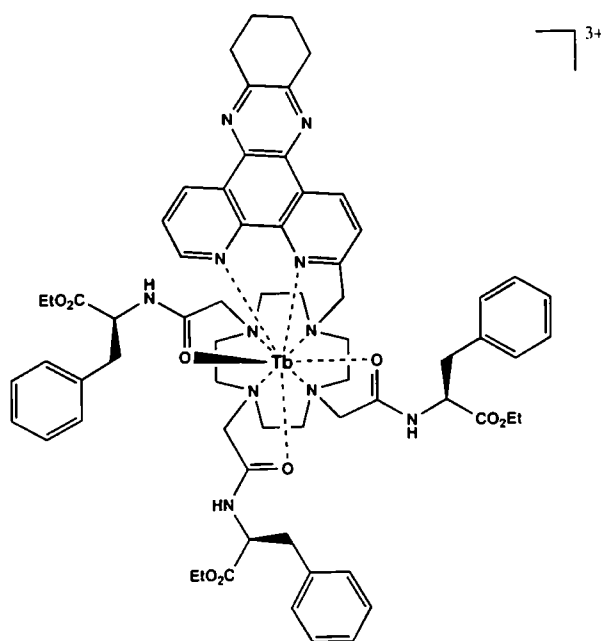


An analogous procedure to that described for (*SSS*)-[Eu.L<sup>2</sup>]Cl<sub>3</sub> was followed, using 1-(6-methyl-10,11,12,13-tetrahydro-4,5,9,14-tetraazabenzob[*b*]triphenylene)-4,7,10-tris(ethyl-N-phenylalanine)-1,4,7,10-tetraazacyclododecane (30 mg, 0.026 mmol) and

europium(III) trifluoromethanesulfonate (15 mg, 0.026 mmol) in dry acetonitrile (6 mL). The title compound was obtained as an off-white solid (20 mg, 0.015 mmol, 58%).

$^1\text{H}$  NMR (500 MHz, 283K,  $\text{D}_2\text{O}$ ) Peaks range from 12.2 to -20.2 ppm. Selected peaks at: 12.21, 12.05, 11.39, 11.04, 10.79 ppm; -8.61, -8.92, -10.64, -12.59, -15.92, -20.24 ppm. HRMS (+  $m/z$ ):  $[\text{M}]^{3+}$  calculated for  $\text{C}_{66}\text{H}_{79}\text{O}_9\text{N}_{11}\text{Eu}$ , 440.1748; found, 440.1752. HPLC:  $t_{\text{R}} = 11.8$  min

**(SSS)-[Tb.L<sup>3b</sup>]Cl<sub>3</sub>**

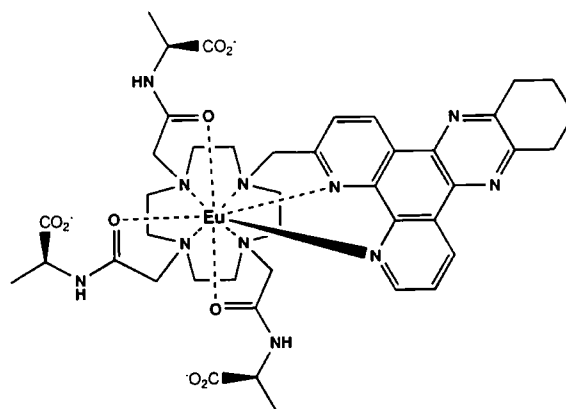


An analogous procedure to that described for (SSS)-[Eu.L<sup>3b</sup>]Cl<sub>3</sub> was followed, using 1-(6-methyl-10,11,12,13-tetrahydro-4,5,9,14-tetraazabenzotriphenylene)-4,7,10-tris(ethyl-N-acetylphenylalanine)-1,4,7,10-tetraazacyclododecane (30 mg, 0.026 mmol) and Tb(III) trifluoromethanesulfonate (15 mg, 0.026 mmol) in dry acetonitrile (6 mL). The product was obtained as an off-white solid (26 mg, 0.020 mmol, 77%).

HRMS (+  $m/z$ ):  $[\text{M}]^{3+}$  calculated for  $\text{C}_{66}\text{H}_{79}\text{N}_{11}\text{O}_9\text{Tb}$ , 422.8433; found, 422.8332. HPLC:  $t_{\text{R}} = 11.0$  min

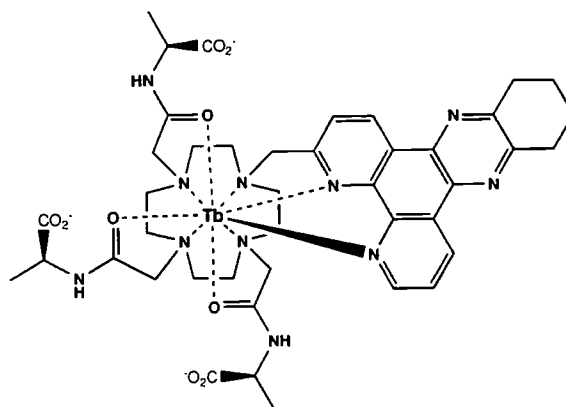
**(*RRR*)-[Ln.L<sup>3b</sup>]Cl<sub>3</sub>**

(*RRR*)-[Eu.L<sup>3b</sup>]Cl<sub>3</sub> and (*RRR*)-[Tb.L<sup>3b</sup>]Cl<sub>3</sub> were synthesised by analogous procedures to (*SSS*)-[Eu.L<sup>3b</sup>]Cl<sub>3</sub> and (*SSS*)-[Tb.L<sup>3b</sup>]Cl<sub>3</sub> respectively, using (*RRR*)-L<sup>3b</sup>. Spectroscopic characterisation was identical to that observed for (*SSS*)-[Ln.L<sup>3b</sup>]Cl<sub>3</sub>. Opposite chirality was confirmed by CPL (see main text).

**(*SSS*)-[Eu.L<sup>4a</sup>]**

To a solution of (*SSS*)-[Eu.L<sup>3a</sup>]Cl<sub>3</sub> (1 mg, 0.0095 mmol) was added an aqueous solution of potassium hydroxide (286  $\mu$ L; 0.02 M) and the mixture stirred at 40 °C for 12 h. The solution was neutralised using dilute HCl, and the product retained in solution for subsequent studies.

<sup>1</sup>H NMR (500 MHz, 283K, D<sub>2</sub>O) Peaks range from 36.8 to -20.9 ppm. Selected peaks at: 36.82, 29.06, 25.66, 24.29, 14.25, 13.53 ppm; -14.42, -15.30, -16.73, -18.64, -20.27, -20.86 ppm. HPLC:  $t_R$  = 9.9 min.

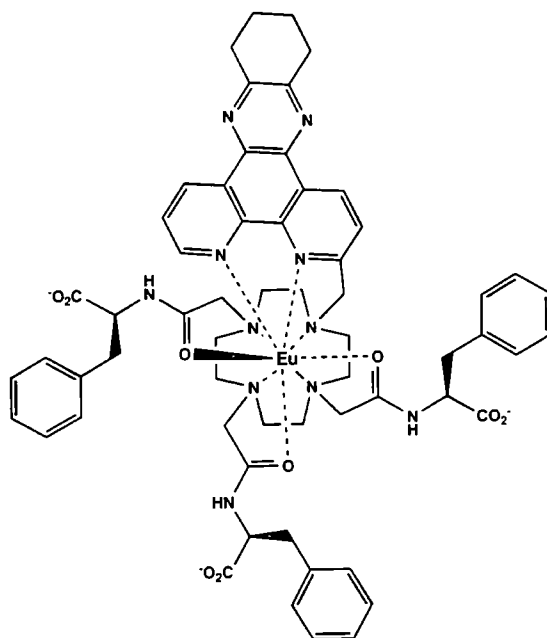
**(SSS)-[Tb.L<sup>4a</sup>]**

An analogous procedure to that described for (SSS)-[Eu.L<sup>4a</sup>] was followed, using (SSS)-[Tb.L<sup>3a</sup>]Cl<sub>3</sub> (1 mg, 0.0095 mmol). The neutral complex was retained in solution for subsequent testing.

HPLC:  $t_R = 8.7$  min

**(RRR)-[Eu.L<sup>4a</sup>]Cl<sub>3</sub>**

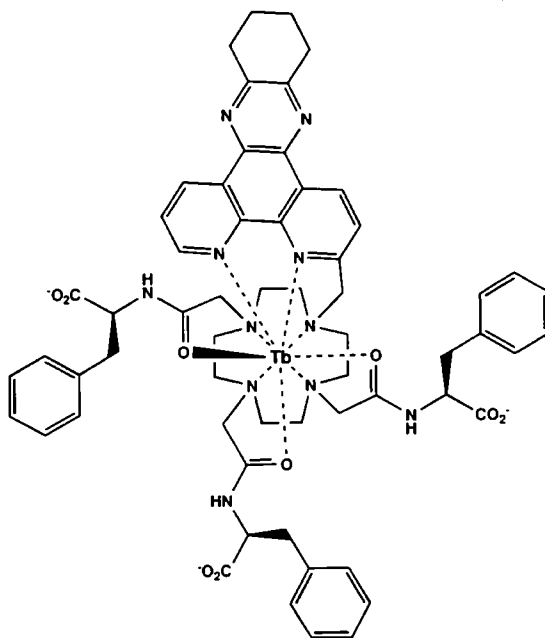
(RRR)-[Eu.L<sup>4a</sup>]Cl<sub>3</sub> was prepared by an analogous procedures to (SSS)-[Eu.L<sup>4a</sup>]Cl<sub>3</sub>, by hydrolysis of (RRR)-[Eu.L<sup>3a</sup>]Cl<sub>3</sub>. Spectroscopic characterisation was identical to that observed for (SSS)-[Eu.L<sup>4a</sup>]Cl<sub>3</sub>. Opposite chirality was confirmed by CPL (see main text).

**(SSS)-[Eu.L<sup>4b</sup>]**

An analogous procedure to that described for (SSS)-[Eu.L<sup>4a</sup>] was followed, using (SSS)-[Eu.L<sup>3b</sup>]Cl<sub>3</sub> (1 mg, 0.0095 mmol). The compound was retained in solution for subsequent testing.

<sup>1</sup>H NMR (500 MHz, 283K, D<sub>2</sub>O) Peaks range from 14.1 to -20.6 ppm. Selected peaks at: 14.12, 13.27, 12.67, 10.63, 10.27 ppm; -14.81, -15.26, -16.97, -17.90, -20.55 ppm.

HPLC: t<sub>R</sub> = 10.88 min.

**(SSS)-[Tb.L<sup>4b</sup>]**

An analogous procedure to that described for (SSS)-[Eu.L<sup>4b</sup>] was followed, using (SSS)-[Tb.L<sup>3b</sup>]Cl<sub>3</sub> (15 mg, 0.0096 mmol). The product was isolated by freeze drying, giving the neutral complex as an off-white solid (6 mg, 0.0055 mmol, 73%).

HPLC:  $t_R = 10.17$  min

**(RRR)-[Eu.L<sup>4b</sup>]Cl<sub>3</sub>**

(RRR)-[Eu.L<sup>4b</sup>]Cl<sub>3</sub> was prepared by an analogous procedure to (SSS)-[Eu.L<sup>4b</sup>]Cl<sub>3</sub>, by hydrolysis of (RRR)-[Eu.L<sup>3b</sup>]Cl<sub>3</sub>. Spectroscopic characterisation was identical to that observed for (SSS)-[Eu.L<sup>4b</sup>]Cl<sub>3</sub>. Opposite chirality was confirmed by CPL (see main text).

---

## **REFERENCES**

---

**REFERENCES**

1. Weissleder, R.; Mahmood, U., *Radiology* 2001, **219**, 316-333.
2. Massoud, T. F.; Gambhir, S. S., *Gene Dev.* 2003, **17**, 545-580.
3. Gadian, D. G., *NMR and its application to living systems*; 10th Ed.; Oxford University Press: Oxford, 1995.
4. Cassidy, P. J.; Radda, G. K., *J. R. Soc. Interface* 2005, **2**, (3), 133-144.
5. Jaffer, F. A.; Weissleder, R., *J. Am. Med. Assoc.* 2005, **293**, (7), 855-862.
6. Willmann, J. K.; van Bruggen, N.; Dinkelborg, L. M.; Gambhir, S. S., *Nat. Rev. Drug Discov.* 2008, **7**, (7), 591-607.
7. Heintzmann, R.; Ficz, G., *Brief. Funct. Genom. Proteom.* 2006, **5**, (4), 289-301.
8. Drezek, R. A.; Richards-Kortum, R.; Brewer, M. A.; Feld, M. S.; Pitris, C.; Ferenczy, A.; Faupel, M. L.; Follen, M., *Cancer* 2003, **98**, (9), 2015-2027.
9. Sutton, E. J.; Henning, T. D.; Pichler, B. J.; Bremer, C.; Daldrup-Link, H. E., *Eur. Radiol.* 2008, **18**, 2021-2032.
10. Jaffer, F. A.; Weissleder, R., *Circ. Res.* 2004, **94**, 433-445.
11. Lakowicz, J. R., *Principles of Fluorescence Spectroscopy*; Kluwer Academic / Plenum Publishers: New York, 1999.
12. Tsien, R. Y., *Meth. Cell Biol.* 1989, **30**, 127-156.
13. Valeur, B., In *Molecular Luminescence Spectroscopy: Methods and Applications Part 3*; Schulman, S. G., Ed.; John Wiley & Sons: New York, 1993.
14. Dibbayawan, T.; Kable, E.; Cox, G., In *Optical Imaging Techniques in Cell Biology*; Cox, G., Ed.; CRC Press: Boca Raton, FL, 2007.
15. Haugland, R. P., *A Guide to Fluorescent Probes and Labelling Technologies*; 10th Ed.; Molecular Probes: Eugene, Oregon, 2005.
16. Lakowicz, J. R., In *Topics in Fluorescence Spectroscopy, Volume 4*; Lakowicz, J. R., Ed.; Plenum Press: New York, 1994.
17. Czarnik, A. W., In *Fluorescent Chemosensors for Ion and Molecule Recognition*; Czarnik, A. W., Ed.; American Chemical Society: Washington, DC, 1993.
18. Tsien, R. Y., In *Fluorescent Chemosensors for Ion and Molecule Recognition*; Czarnik, A. W., Ed.; American Chemical Society: Washington DC, 1993.
19. Bouas-Laurent, H.; Desverge, J.-P.; Fages, F.; Marsau, P., In *Fluorescent Chemosensor for Ion and Molecule Recognition*; Czarnik, A. W., Ed.; American Chemical Society: Washington DC, 1992.
20. Szmanski, H.; Lakowicz, J. R., In *Topics in Fluorescence Sensing, Volume 4*; Lakowicz, J. R., Ed.; Plenum Press: New York, 1994.
21. Hibbs, A. R., *Confocal Microscopy for Biologists*; Plenum Publishers: New York, 2004.
22. Song, L.; Hennink, E. J.; Young, I. T.; Tanke, H. J., *Biophys. J.* 1995, **68**, 2588-2600.
23. Beumer, T. L.; Veenstra, G. J. C.; Hage, W. J.; Destree, O. H. J., *Trends Genet.* 1995, **11**, 9.
24. Bloom, J. A.; Webb, W. W., *J. Histochem. Cytochem.* 1984, **32**, 608-616.
25. Petit, J.-M.; Denis-Gay, M.; Ratinaud, M.-H., *Biol. Cell.* 1993, **78**, 1-13.
26. Lakowicz, J. R.; Maliwal, B. P.; Gryczynski, Z., *Anal. Chem.* 2001, **73**, 4277-4285.
27. Yao, M.; Li, Y., *Chemistrymag.org* 2003, **5**, (58), 65.
28. Johnson, I., *Histochem. J.* 1998, **30**, 123-140.
29. Bright, G. R.; Kuo, N.-T.; Chow, D.; Burden, S.; Dowe, C.; Przybylski, R. J., *Cytometry* 1996, **24**, 226-233.
30. Steinberg, T. H.; Newman, A. S.; Swanson, J. A.; Silverstein, S. C., *J. Biol. Chem.* 1987, **262**, 8884-8888.
31. Tsien, R. Y., *Nature* 1981, **290**, 527-528.

32. Langmuir, M. E.; Yang, J.-R.; LeCompte, K. A.; Durand, R. E., In *Fluorescence Microscopy and Fluorescent Probes*; Slavik, J., Ed.; Springer: New York, 1996.
33. Herschel, J. F. W., *Phil. Trans. Roy. Soc. London* 1845, **135**, 143-145.
34. Udenfriend, S., *Protein Sci.* 1995, **4**, (4), 542-551.
35. Lavis, L. D.; Raines, R. T., *ACS Chem. Biol.* 2008, **3**, (3), 142-155.
36. Ueno, T.; Urano, Y.; Setsukinai, K.; Takakusa, H.; Kojima, H.; Kikuchi, K.; Ohkubo, K.; Fukuzumi, S.; Nagano, T., *J. Am. Chem. Soc.* 2004, **126**, (43), 14079-14085.
37. Urano, Y.; Kamiya, M.; Kanda, K.; Ueno, T.; Hirose, K.; Nagano, T., *J. Am. Chem. Soc.* 2005, **127**, (13), 4888-4894.
38. Yogo, T.; Urano, Y.; Ishitsuka, Y.; Maniwa, F.; Nagano, T., *J. Am. Chem. Soc.* 2005, **127**, (35), 12162-12163.
39. Haugland, R. P., In *Optical Microscopy for Biology*; Herman, B.; Jacobson, K., Eds.; Wiley: New York, 1990.
40. Vo-Dinh, T.; Cullum, B., *Fresenius J. Anal. Chem.* 2000, **366**, 540-551.
41. Glazer, A. N., *J. Biol. Chem.* 1989, **264**, (1), 1-4.
42. Oi, V. T.; Glazer, A. N.; Stryer, L., *J. Cell Biol.* 1982, **93**, (3), 981-986.
43. Shimomura, O.; Johnson, F. H.; Saiga, Y., *J. Cell. Comp. Physiol.* 1962, **59**, 223-239.
44. Prasher, D. C.; Eckenrode, V. K.; Ward, W. W.; Prendergast, F. G.; Cormier, M. J., *Gene* 1992, **111**, 229-233.
45. Tsien, R. Y., *Annu. Rev. Biochem.* 1998, **67**, 509-544.
46. Abbyad, P.; Childs, W.; Shi, X.; Boxer, S. G., *Proc. Natl Acad. Sci. USA* 2007, **104**, (5), 20189-20194.
47. Rossetti, R.; Nakahara, S.; Brus, L. E., *J. Chem. Phys.* 1983, **79**, 1086-1088.
48. Bawendi, M. G.; Steigerwald, M. L.; Brus, L. E., *Annu. Rev. Phys. Chem.* 1990, **41**, 477-496.
49. Chen, W. C. W.; Maxwell, D. J.; Gao, X. H.; Bailey, R. E.; Han, M. Y., *Curr. Opin. Biotech.* 2002, **12**, 40-46.
50. Han, M. Y.; Gao, X. H.; Su, J. Z.; Nie, S. M., *Nat. Biotechnol.* 2001, **19**, 631-635.
51. Gao, X. H.; Nie, S. M., *J. Phys. Chem. B* 2003, **107**, 11575-11578.
52. Wu, X. Y.; Liu, H. J.; Liu, J. Q.; Haley, K. N.; Treadway, J. A.; Larson, J. P.; Ge, N. F.; Peale, F.; Bruchez, M. P., *Nat. Biotechnol.* 2003, **21**, 41-46.
53. Keefe, M. H.; Benkstein, K. D.; Hupp, J. T., *Coord. Chem. Rev.* 2000, **205**, 201-228.
54. Demas, J. N.; DeGraff, B. A., *Coord. Chem. Rev.* 2001, **211**, (1), 317-351.
55. Demas, J. N.; DeGraff, B. A., In *Topics in Fluorescence Spectroscopy, Volume 4*; Lakowicz, J. R., Ed.; Plenum Press: New York, 1994.
56. O'Connor, N. A.; Stevens, N.; Samaroo, D.; Solomon, M. R.; Marti, A. A.; Dyer, J.; Vishwasrao, H.; Atkins, D. L.; Kandel, E. R.; Turro, N. J., *Chem. Commun.* 2009, 2640-2642.
57. Botchway, S. W.; Charnley, M.; Haycock, J. W.; Parker, A. W.; Rochester, D. L.; Weinstein, J. A.; Williams, J. A. G., *Proc. Natl Acad. Sci. USA* 2008, **105**, 16071-16076.
58. Greenwood, N. N.; Earnshaw, A., *Chemistry of the Elements*; Butterworth-Heinemann: Oxford, 1997.
59. Aspinall, H. C., *Chemistry of the f-Block Elements*; CRC Press: Boca Raton, FL, 2001.
60. Atkins, P.; de Paula, J., *Atkins' Physical Chemistry*; Oxford University Press: Oxford, 2002.

61. Parker, D.; Williams, J. A. G., In *Metal Ions in Biological Systems - The Lanthanides and Their Interrelations with Biosystems*; Sigel, A.; Sigel, H., Eds.; Marcel Dekker: New York, 2003.
62. Bünzli, J.-C. G.; Piguet, C., *Chem. Soc. Rev.* 2005, **34**, 1048-1077.
63. Døssing, A., *Eur. J. Inorg. Chem.* 2005, **2005**, 1425-1434.
64. Dexter, D. L., *J. Chem. Phys.* 1953, **21**, (5), 836-850.
65. Förster, T., *Discuss. Faraday Soc.* 1959, **27**, 7-17.
66. Beeby, A.; Faulkner, S.; Parker, D.; Williams, J. A. G., *J. Chem. Soc. Perkin Trans. 2* 2001, **2001**, 1268-1273.
67. Reichert, D. E.; Lewis, J. S.; Anderson, C. J., *Coord. Chem. Rev.* 1999, **184**, 3-66.
68. Lukeš, I.; Kotek, J.; Vojtíšek, P.; Herman, P., *Coord. Chem. Rev.* 2001, **216-217**, 287-312.
69. Sabbatini, N.; Guardigli, M.; Mecati, A.; Balzani, V.; Ungaro, R.; Ghidini, E.; Casnati, A.; Pochini, A., *J. Chem. Soc., Chem. Commun.* 1990, 878-879.
70. Wolbers, M. P. O.; van Veggel, F. C. J. M.; Snellink-Ruël, B. H. M.; Hofstraat, J. W.; Geurts, F. A. J.; Reinhoudt, D. N., *J. Chem. Soc., Perkin Trans. 2* 1998, 2141-2150.
71. Quici, S.; Marzanni, G.; Cavazzini, M.; Anelli, P. L.; Botta, M.; Gianolio, E.; Accorsi, G.; Armaroli, N.; Barigelletti, F., *Inorg. Chem.* 2002, **41**, 2777-2784.
72. Bobba, G.; Frias, J.-C.; Parker, D., *Chem. Commun.* 2002, 890-891.
73. Poole, R. A.; Bobba, G.; Cann, M. J.; Frias, J.-C.; Parker, D.; Peacock, R. D., *Org. Biomol. Chem.* 2005, **3**, 1013-1024.
74. Parker, D.; Yu, J., *Chem. Commun.* 2005, 3141-3143.
75. Atkinson, P.; Findlay, K. S.; Kielar, F.; Pal, R.; Parker, D.; Poole, R. A.; Puschmann, H.; Richardson, S. L.; Stenson, P. A.; Thompson, A. L.; Yu, J., *Org. Biomol. Chem.* 2006, **4**, 1707-1722.
76. Song, Y.; Salinas, D.; Nielsen, D. W.; Verkman, A. S., *Am. J. Physiol. Cell Physiol.* 2006, **290**, (3), C669-671.
77. Gatenby, R. A.; Gawlinski, E. T.; Gmitro, A. F.; Kaylor, B.; Gillies, R. J., *Cancer Res.* 2006, **66**, 5216-5223.
78. Parker, D.; Senanayake, K.; Williams, J. A. G., *Chem. Commun.* 1997, 1777-1778.
79. Parker, D.; Senanayake, K.; Williams, J. A. G., *J. Chem. Soc., Perkin Trans. 2* 1998, 2129-2139.
80. Alberts, B.; Johnson, A.; Lewis, J.; Raff, M.; Roberts, K.; Walter, P., *Molecular Biology of the Cell*; 4th Ed.; Garland Science: New York, 2002.
81. da Silva, A. P.; Gunaratne, H. Q. N.; Rice, T. E., *Angew. Chem. Int. Ed.* 1996, **35**, 2116-2118.
82. Pal, R.; Parker, D., *Chem. Commun.* 2007, 474-476.
83. Bretonniere, Y.; Cann, M. J.; Parker, D.; Slater, R., *Org. Biomol. Chem.* 2004, **2**, 1624-1632.
84. Bretonniere, Y.; Cann, M. J.; Parker, D.; Slater, R., *Chem. Commun.* 2002, 1930-1931.
85. Poole, R. A.; Kielar, F.; Richardson, S. L.; Stenson, P. A.; Parker, D., *Chem. Commun.* 2006, 4084-4086.
86. Kielar, F.; Montgomery, C. P.; New, E. J.; Parker, D.; Poole, R. A.; Richardson, S. L.; Stenson, P. A., *Org. Biomol. Chem.* 2007, **5**, 2055-2062.
87. da Silva, J. J. R. F.; Williams, R. J. P., *The Biological Chemistry of the Elements*; Oxford University Press: Oxford, 2001.
88. Reany, O.; Gunnlaugsson, T.; Parker, D., *J. Chem. Soc. Perkin Trans. 2* 2000, 1819-1831.
89. Reany, O.; Gunnlaugsson, T.; Parker, D., *Chem. Commun.* 2000, 473-474.

90. Viguier, R. F. H.; Hulme, A. N., *J. Am. Chem. Soc.* 2006, **128**, 11370-11371.
91. Thibon, A.; Pierre, V. C., *J. Am. Chem. Soc.* 2009, **131**, 434-435.
92. Schafer, F. Q.; Buetner, G. R., *Free Radic. Biol. Med.* 2001, **30**, (11), 1191-1212.
93. Lee, K.; Dzubeck, V.; Latshaw, L.; Schneider, J. P., *J. Am. Chem. Soc.* 2004, **126**, 13616-13617.
94. Stryer, L., *Biochemistry*; 4th Ed.; W.H.Freeman: New York, 1995.
95. Atkinson, P.; Murray, B. S.; Parker, D., *Org. Biomol. Chem.* 2006, **4**, 3166-3171.
96. Epe, B.; Pfaum, M.; Boiteux, S., *Mutat. Res.* 1993, **299**, (3-4), 135-145.
97. Song, B.; Wang, G.; Tan, M.; Yuan, J., *J. Am. Chem. Soc.* 2006, **128**, (41), 13442-13450.
98. Vandevyver, C. D.; Chauvin, A. S.; Comby, S.; Bünzli, J.-C. G., *Chem. Commun.* 2007, (17), 1716-1718.
99. Kessner, S.; Krause, A.; Rothe, U.; Bendas, G., *Biochim. Biophys. Acta* 2001, **1514**, 177-190.
100. Bünzli, J.-C. G.; Chauvin, A. S.; Vandevyver, C. D.; Song, B.; Comby, S., *Ann. N.Y. Acad. Sci.* 2008, **1130**, 97-105.
101. Deiters, E.; Song, B.; Chauvin, A. S.; Vandevyver, C. D.; Gumy, F.; Bünzli, J.-C. G., *Chemistry* 2009, **15**, (4), 885-900.
102. Yu, J.; Parker, D.; Pal, R.; Poole, R. A.; Cann, M. J., *J. Am. Chem. Soc.* 2006, **128**, 2294-2299.
103. Seveus, L.; Väisälä, M.; Syrjänen, S.; Sandberg, M.; Kuusisto, A.; Harju, R.; Salo, J.; Hemmilä, I.; Kojola, H.; Soini, E., *Cytometry* 1992, **13**, 329-338.
104. Marriott, G.; Heidecker, M.; Diamandis, E. P.; Yan-Marriott, Y., *Biophys. J.* 1994, **67**, 957-965.
105. Manning, H. C.; Goebel, T.; Thompson, R. C.; Price, R. R.; Lee, H.; Bornhop, D. J., *Bioconjugate Chem.* 2004, **15**, (6), 1488-1495.
106. Vieira, O. V.; Botelho, R. J.; Grinstein, S., *Biochem. J.* 2002, **366**, 689-704.
107. Hanaoka, K.; Kikuchi, K.; Kojima, H.; Urano, Y.; Nagano, T., *J. Am. Chem. Soc.* 2004, **126**, (39), 12470-12476.
108. Murray, B. S.; New, E. J.; Pal, R.; Parker, D., *Org. Biomol. Chem.* 2008, **6**, 2085-2094.
109. Parker, D.; Dickins, R. S.; Puschmann, H.; Crossland, C.; Howard, J. A. K., *Chem. Rev.* 2002, **102**, (6), 1977-2010.
110. Aime, S.; Botta, M.; Ermondi, G., *Inorg. Chem.* 1992, **31**, (21), 4291-4299.
111. Aime, S.; Botta, M.; Fasano, M.; Marques, M. P. M.; Geraldes, C. F. G. C.; Pubanz, D.; Merbach, A. E., *Inorg. Chem.* 1997, **36**, (10), 2059-2068.
112. Dickins, R. S.; Howard, J. A. K.; Lehmann, C. W.; Moloney, J. M.; Parker, D.; Peacock, R. D., *Angew. Chem. Int. Ed. Engl.* 1997, **36**, (5), 521-523.
113. Peters, J. A.; Huskens, J.; Raber, D. J., *Prog. Nucl. Magn. Reson. Spectrosc.* 1996, **28**, (3-4), 283-350.
114. Parker, D., *Chem. Soc. Rev.* 2004, **3**, 156-165.
115. Mironov, V. S.; Galyametdinov, Y. G.; Ceulemans, A.; Görlner-Walrand, C.; Binnemans, K., *J. Chem. Phys.* 2002, **116**, (11), 4673-4685.
116. Dickins, R. S.; Parker, D.; Bruce, J. I.; Tozer, D. J., *J. Chem. Soc. Dalton Trans.* 2003, 1264-1271.
117. Beeby, A.; Clarkson, I. M.; Dickins, R. S.; Faulkner, S.; Parker, D.; Royle, L.; de Sousa, A. S.; Williams, J. A. G.; Woods, M., *J. Chem. Soc. Perkin Trans. 2* 1999, **1999**, 493-503.
118. Riehl, J. P.; Richardson, F. S., *Chem. Rev.* 1986, **86**, (1), 1-16.
119. Bruce, J. I.; Parker, D.; Lopinski, S.; Peacock, R. D., *Chirality* 2002, **14**, 562-567.

120. Geraldes, C. F. G. C.; Luchinat, C., In *Metal Ions in Biological Systems*; Sigel, H.; Sigel, A., Eds.; Marcel Dekker, Inc.: New York, 2003; Vol. 40.
121. Aime, S.; Botta, M.; Milone, L.; Terreno, E., *Chem. Commun.* 1996, 1265-1266.
122. Dickins, R. S.; Batsanov, A. S.; Howard, J. A. K.; Parker, D.; Puschmann, H.; Salamano, S., *J. Chem. Soc. Dalton Trans.* 2004, 70-80.
123. Parker, D., *Coord. Chem. Rev.* 2000, **205**, 109-130.
124. Dickins, R. S.; Parker, D.; de Sousa, A. S.; Williams, J. A. G., *Chem. Commun.* 1996, 697-698.
125. Hebbink, G. A.; Reinhoudt, D. N.; van Veggel, F. C. J. M., *Eur. J. Org. Chem.* 2001, 4101-4106.
126. Faulkner, S.; Pope, S. J. A.; Burton-Pye, B. P., *Appl. Spectrosc. Rev.* 2005, **40**, (1), 1-31.
127. Weller, A., *Pure Appl. Chem.* 1968, **16**, 115-123.
128. Poole, R. A. Luminescent lanthanide complexes for cellular applications. PhD, University of Durham, Durham, 2007.
129. Poole, R. A.; Montgomery, C. P.; New, E. J.; Congreve, A.; Parker, D.; Botta, M., *Org. Biomol. Chem.* 2007, **5**, 2055-2062.
130. Law, G.-L.; Parker, D.; Richardson, S. L.; Wong, K.-L., *Dalton Trans.* 2009, accepted.
131. Diwu, Z.; Zhang, Y.-Z.; Haugland, R. P. *Novel site-selective fluorescent probes for lysosome and acidic organelle staining and long-term tracking*, XVII Congress of the International Society for Analytical Cytology, New York, 1994
132. Torchilin, V. P., *Annu. Rev. Biochem.* 2006, **8**, 343-375.
133. Fukuda, T.; Ewan, L.; Bauer, M.; Mattaliano, R. J.; Zaal, K.; Ralson, E.; Plotz, P. H.; Raben, N., *Ann. Neurol.* 2006, **59**, (4), 700-708.
134. Hansford, R. G.; Tsuchiya, N. T.; Pepe, S., *Biochem. Soc. Symp.* 1999, **66**, 141-147.
135. Martoglio, B.; Dobberstein, B., *Trends Cell Biol.* 1998, **8**, 410-415.
136. von Heijne, G., *Curr. Opin. Cell Biol.* 1990, **2**, 604-608.
137. Blobel, G., *Proc. Natl Acad. Sci. USA* 1980, **77**, (3), 1496-1500.
138. Vale, R. D., *Cell* 2003, **112**, 467-480.
139. Sherwood, L., *Human Physiology: From Cells to Systems*; 4th Ed.; Brooks/Cole: Pacific Grove, California, 2001.
140. Hirokawa, N., *Science* 1998, **279**, (5350), 519-526.
141. Huth, U. S.; Schubert, R.; Peschka-Süss, R., *J. Controlled Release* 2006, **110**, 490-504.
142. Weissig, V.; Torchilin, V. P., *Adv. Drug Deliv. Rev.* 2001, **49**, 127-149.
143. Chen, L. B.; Summerhayes, I. C.; Johnson, L. V.; Walsh, M. L.; Bernal, S. D.; Lampidis, T. J., *Cold Spring Harb. Symp. Quant. Biol.* 1982, **46**, 141-155.
144. Barnard, P. J.; Berners-Price, S. J., *Coord. Chem. Rev.* 2007, **251**, 1889-1902.
145. Fernández-Carneado, J.; van Gool, M.; Martos, V.; Castel, S.; Prados, P.; de Mendoza, J.; Giralt, E., *J. Am. Chem. Soc.* 2005, **127**, 869-874.
146. Stewart, K. M.; Horton, K. L.; Kelley, S. O., *Org. Biomol. Chem.* 2008, **13**, 2242-2255.
147. Aronov, O.; Horowitz, A. T.; Gabizon, A.; Fuertes, M. A.; Pérez, J. M.; Gibson, D., *Bioconjugate Chem.* 2004, **15**, 814-823.
148. Murray, B. S. Anion Binding Studies with Responsive Lanthanide Complexes. PhD, Durham University, Durham, 2008.
149. Montgomery, C. P.; Parker, D.; Lamarque, L., *Chem. Commun.* 2007, 3841-3843.
150. Montgomery, C. P. Luminescent lanthanide complexes as cellular imaging agents or HTRF assay components. PhD, Durham University, Durham, 2009.

151. Montgomery, C. P.; New, E. J.; Palsson, L. O.; Parker, D.; Batsanov, A. S.; Lamarque, L., *Helv. Chim. Acta* 2009, in press.
152. Yu, J.; Parker, D., *Eur. J. Org. Chem.* 2005, **2005**, (20), 4249-4252.
153. Pålsson, L.-O.; Pal, R.; Murray, B. S.; Parker, D.; Beeby, A., *Dalton Trans.* 2007, 5726-5734.
154. Pal, R.; Parker, D., *Org. Biomol. Chem.* 2008, **6**, 1020-1033.
155. Kielar, F.; Law, G.-L.; New, E. J.; Parker, D., *Org. Biomol. Chem.* 2008, **6**, 2256-2258.
156. Kielar, F.; Congreve, A.; Law, G.-L.; New, E. J.; Parker, D.; Wong, K.-L.; Castroño, P.; de Mendoza, J., *Chem. Commun.* 2008, 2435-2437.
157. Kielar, F. Development of Lanthanide Probes for Cellular Imaging. PhD, Durham University, Durham, 2008.
158. Mukherjee, S.; Ghosh, R. N.; Maxfield, F. R., *Physiol. Rev.* 1997, **77**, (3), 759-803.
159. Ernster, L.; Schatz, G., *J. Cell Biol.* 1981, **91**, (3), 227s-255s.
160. Hatefi, Y., *Annu. Rev. Biochem.* 1985, **54**, 1015-1069.
161. Olson, M. O. J.; Dundr, M.; Szébeni, A., *Trends Cell Biol.* 2000, **10**, 189-196.
162. Pal, R. Ratiometric Luminescent Probes. PhD, University of Durham, Durham, 2007.
163. Johnson, J. A.; Gray, M. O.; Karliner, J. S.; Chen, C.-H.; Mochly-Rosen, D., *Circ. Res.* 1996, **79**, 1086-1099.
164. Invitrogen *Propidium Iodide Nucleic Acid Stain*; Carlsbad, CA, 1999.
165. Wang, K.; Li, R.; Cheng, Y.; Zhu, B., *Coord. Chem. Rev.* 1999, **190-192**, 297-308.
166. Canada, R. G.; Andrews, P. A.; Mack, K. M.; Haider, A., *Biochim. Biophys. Acta* 1995, **1267**, 25-30.
167. Cheng, Y.; Liu, M.; Li, R.; Wang, C.; Bai, C.; Wang, K., *Biochim. Biophys. Acta* 1999, **1421**, 249-260.
168. Mosely, J. A.; Murray, B. S.; Parker, D., *Eur. J. Mass Spectrom.* 2009, **15**, (2), 145-155.
169. Blazejewski, J.-C.; Anselmi, E.; Wakselman, C., *J. Org. Chem.* 2001, **66**, (3), 1061-1063.
170. Adam, S. A., *Curr. Opin. Cell Biol.* 1999, **11**, 402-406.
171. Graham, J. M.; Rickwood, D., *Subcellular Fractionation - A Practical Approach*; Oxford University Press: Oxford, 1997.
172. Prescott, L., *Microbiology*; Wm C. Brown: Dubuque, Iowa, 1993.
173. Blow, J. J.; Laskey, R. A., *Nature* 1988, **332**, (6164), 546-548.
174. Coverley, D.; Downes, C. S.; Romanowski, P.; Laskey, R. A., *J. Cell Biol.* 1993, **122**, 985-992.
175. Collas, P., *J. Cell Sci.* 1998, **111**, 1293-1303.
176. Bobba, G. Interaction of chiral lanthanide complexes with nucleic acids. PhD, University of Durham, Durham, 2002.
177. Thomas, R., *Practical Guide to ICP-MS*; Marcel Dekker, Inc.: New York, 2004.
178. Fahmi, C. J., *Curr. Opin. Chem. Biol.* 2007, **11**, (2), 121-127.
179. Vázquez, M. D.; Poschenrieder, C.; Corrales, I.; Barceló, J., *Plant Physiol.* 1999, **119**, 435-444.
180. Damjanovich, S.; Edidin, M.; Szöllösi, J.; Trón, L., *Mobility and Proximity in Biological Membranes*; CRC Press: Boca Raton, FL, 1994.
181. Evrogen *Red Fluorescent Protein Tag Description*; Moscow, Russia, 2008.
182. Invitrogen *Cellular Lights™ Intracellular Targeted Fluorescent Proteins*; Carlsbad, CA, 2009.
183. Ishida, S.; Lee, J.; Thiele, D. J.; Herskowitz, I., *Proc. Natl Acad. Sci. USA* 2002, **99**, (22), 14298-14302.

184. Wright, E. M., *Am. J. Physiol. Renal Physiol.* 2001, **280**, F10-F18.
185. Mellman, I.; Warren, G., *Cell* 2000, **100**, 99-112.
186. Mousavi, S. A.; Malerod, L.; Berg, T.; Kjekken, R., *Biochem. J.* 2004, **377**, (1), 1-16.
187. Hummeler, K.; Tomassini, N.; Sokol, F., *J. Virol.* 1970, **6**, 87-93.
188. Anderson, H. A.; Chen, Y.; Norkin, L. C., *Mol. Cell. Biol.* 1996, **7**, 1825-1834.
189. Pelkmans, L.; Helenius, A., *Traffic* 2002, **3**, (5), 311-320.
190. Anderson, R. G., *Annu. Rev. Biochem.* 1998, **67**, 199-225.
191. Mineo, C.; Anderson, R. G. W., *Histochem. Cell Biol.* 2001, **116**, 109-118.
192. Sieczkarski, S. B.; Whittaker, G. R., *J. Gen. Virol.* 2002, **83**, 1535-1545.
193. Hewlett, L. J.; Prescott, A. R.; Watts, C., *J. Cell Biol.* 1994, **124**, 689-703.
194. Torgersen, M. L.; Skretting, G.; van Deurs, B.; Sandvig, K., *J. Cell Sci.* 2001, **114**, (20), 3737-3747.
195. Kay, M. A.; Glorioso, J. C.; Naldini, L., *Nat. Med.* 2001, **7**, (1), 33-40.
196. Dokka, S.; Toledo-Velasquez, D.; Shi, X.; Wang, L.; Rojanasakul, Y., *Pharm. Res.* 1997, **14**, (12), 1759-1764.
197. Pandya, S.; Yu, J.; Parker, D., *Dalton Trans.* 2006, 2757-2766.
198. Frias, J.-C.; Bobba, G.; Cann, M. J.; Hutchinson, C. J.; Parker, D., *Org. Biomol. Chem.* 2003, **1**, 905-907.
199. Shapiro, H. M., *Practical Flow Cytometry*; Wiley Liss: New York, 1994.
200. Lichtenfels, R.; Biddinson, W. E.; Schulz, H.; Vogt, A. B.; Martin, R., *J. Immunol. Meth.* 1994, **172**, 227-239.
201. Kubinyi, H., *Farmaco Sci.* 1979, **34**, (3), 248-276.
202. Leo, A.; Hansch, C.; Elkins, D., *Chem. Rev.* 1971, **71**, (6), 525-616.
203. Lipinski, C. A.; Lombardo, F.; Dominy, B. W.; Feeney, P. J., *Adv. Drug Deliv. Rev.* 1997, **23**, 3-25.
204. Dobson, P. D.; Kell, D. B., *Nat. Rev. Drug Discov.* 2008, **7**, 205-220.
205. Royle, L. In Vivo Stability of Radiolabelled Macrocyclic Complexes. PhD, University of Durham, Durham, 1995.
206. Robillard, M. S.; Galanski, M.; Zimmermann, W.; Keppler, B. K.; Reedijk, J., *J. Inorg. Biochem.* 2002, **88**, 254-259.
207. Dunn, W. A.; Hubbard, A. L.; Aronson, N. N., Jr., *J. Biol. Chem.* 1980, **255**, 5971-5978.
208. Flaten, G. E.; Dhanikula, A. B.; Luthman, K.; Brandl, M., *Eur. J. Pharm. Sci.* 2006, **27**, 80-90.
209. Yslas, E. I.; Durantini, E. N.; Rivarola, V. A., *Bioorg. Med. Chem.* 2007, **15**, 4651-4660.
210. Hall, M. D.; Amjadi, S.; Zhang, M.; Beale, P. J.; Hambley, T. W., *J. Inorg. Biochem.* 2004, **98**, 1614-1624.
211. Barta, C. A.; Sachs-Barrable, K.; Jia, J.; Thompson, K. H.; Wasan, K. M.; Orvig, C., *Dalton Trans.* 2007, (43), 5019-5030.
212. Smith, P. K.; Krohn, R. I.; Hermanson, G. T.; Mallia, A. K.; Gartner, F. H.; Provenzano, M. D.; Fujimoto, E. K.; Goeke, N. M.; Olson, B. J.; Klenk, D. C., *Anal. Biochem.* 1985, **150**, 76-85.
213. Drin, G.; Cottin, S.; Blanc, E.; Rees, A. R., *J. Biol. Chem.* 2003, **278**, (33), 31192-31201.
214. Veldhoen, S.; Laufer, S. D.; Trampe, A.; Restle, T., *Nucleic Acids Res.* 2006, **34**, (22), 6561-6573.
215. Wang, L. H.; Rothberg, K. G.; Anderson, R. G., *J. Cell Biol.* 1993, **123**, (5), 1107-1117.
216. Orlandi, P. A.; Fishman, P. H., *J. Cell Biol.* 1998, **141**, 905-915.
217. Schnitzer, J. E.; Oh, P.; Pinney, E.; Allard, J., *J. Cell Biol.* 1994, **127**, 1217-1232.

218. Arcaro, A.; Wymann, M. P., *Biochem. J.* 1993, **296**, 297-301.
219. Hoffmann, P. R.; deCathelineau, A. M.; Ogden, C. A.; Leverrier, Y.; Bratton, D. L.; Daleke, D. L.; Ridley, A. J.; Fadok, V. A.; Henson, P. M., *J. Cell Biol.* 2001, **124**, 689-703.
220. Keller, H. U., *J. Cell. Physiol.* 2005, **145**, (3), 465-471.
221. Mollenhauer, H. H.; Morr e, D. J.; Rowe, L. D., *Biochim. Biophys. Acta* 1990, **1031**, (2), 225-246.
222. Pless, D. D.; Wellner, R. B., *J. Cell Biochem.* 1996, **62**, (1), 27-39.
223. Plank, C.; Oberhauser, B.; Mechtler, K.; Koch, C.; Wagner, E., *J. Biol. Chem.* 1994, **17**, 12918-12924.
224. Lencer, W. I.; Weyer, P.; Verkman, A. S.; Ausiello, D. A.; Brown, D., *Am. J. Physiol. Cell Physiol.* 1990, **258**, C309-C317.
225. Racoosin, E. L.; Swanson, J. A., *J. Cell Sci.* 1992, **102**, (4), 867-880.
226. Watts, C.; Marsh, M., *J. Cell Sci.* 1992, **103**, 1-8.
227. West, M. A.; Prescott, A. R.; Eskelinen, E.-L.; Ridley, A. J.; Watts, C., *Curr. Biol.* 2000, **10**, 839-848.
228. Araki, N.; Johnson, M. T.; Swanson, J. A., *J. Cell Biol.* 1996, **135**, 1249-1260.
229. Jones, A. T., *J. Cell. Mol. Med.* 2007, **11**, (4), 670-684.
230. Swanson, J. A.; Watts, C., *Trends Cell Biol.* 1995, **5**, 424-428.
231. Gibson, G. G.; Skett, P., *Introduction to Drug Metabolism*; Nelson Thornes: Cheltenham, 2001.
232. Hinson, J. A.; Pumford, N. R.; Nelson, S. D., *Drug Metab. Rev.* 1994, **26**, (1&2), 395-412.
233. Walsh, J. S., In *Optimizing the "Drug-Like" Properties of Leads in Drug Discovery*; Borhardt, R. T.; Kerns, E. H.; Hageman, M.; Thakker, D.; Stevens, J., Eds.; Springer: New York, 2006.
234. Stella, V. J., In *Optimizing the "Drug-Like" Properties of Leads in Drug Discovery*; Borhardt, R. T.; Kerns, E. H.; Hageman, M.; Thakker, D.; Stevens, J., Eds.; Springer: New York, 2006.
235. Kim, Y.; Choi, Y.; Weissleder, R.; Tung, C.-H., *Bioorg. Med. Chem. Lett.* 2007, **17**, (18), 5054-5057.
236. Hama, Y.; Urano, Y.; Koyama, Y.; Kamiya, M.; Bernardo, M. A.; Paik, R. S.; Shin, I. S.; Paik, C. H.; Choyke, P. L.; Kobayashi, H., *Cancer Res.* 2007, **67**, 2791-2799.
237. Garrett, R. H.; Grisham, C. M., *Biochemistry*; Harcourt College Publishers: Fort Worth, 1999.
238. Jones, J. B., *Pure Appl. Chem.* 1990, **62**, (7), 1445-1448.
239. Pal, R.; Parker, D.; Costello, L. C., *Org. Biomol. Chem.* 2009, **7**, 1525-1528.
240. Montgomery, C. P.; New, E. J.; Parker, D.; Peacock, R. D., *Chem. Commun.* 2008, 4261-4263.
241. Peters, T., *Adv. Protein Chem.* 1985, **37**, 161-245.
242. Panjehshahin, M. R.; Yates, M. S.; Bowmer, C. J., *Biochem. Pharmacol.* 1992, **44**, (873-879).
243. Li, Y.-T.; Li, S.-C., *J. Biol. Chem.* 1970, **245**, 825-832.
244. Yoshima, H.; Matsumoto, A.; Mizuochi, T.; Kawasaki, T.; Kobata, A., *J. Biol. Chem.* 1981, **256**, 8476-8490.
245. Sudlow, G.; Birkett, D. J.; Wade, D. N., *Mol. Pharmacol.* 1975, **11**, 824-832.
246. Sudlow, G.; Birkett, D. J.; Wade, D. N., *Mol. Pharmacol.* 1976, **12**, 1052-1061.
247. Caravan, P.; Cloutier, N. J.; Greenfield, M. T.; McDermid, S. A.; Dunham, S. U.; Bulte, J. W. M.; Armedio, J. J. C.; Looby, R. J.; Supkowski, R. M.; Horrocks, J., W.D.; McMurry, T. J.; Lauffer, R. B., *J. Am. Chem. Soc.* 2002, **124**, 3152-3162.

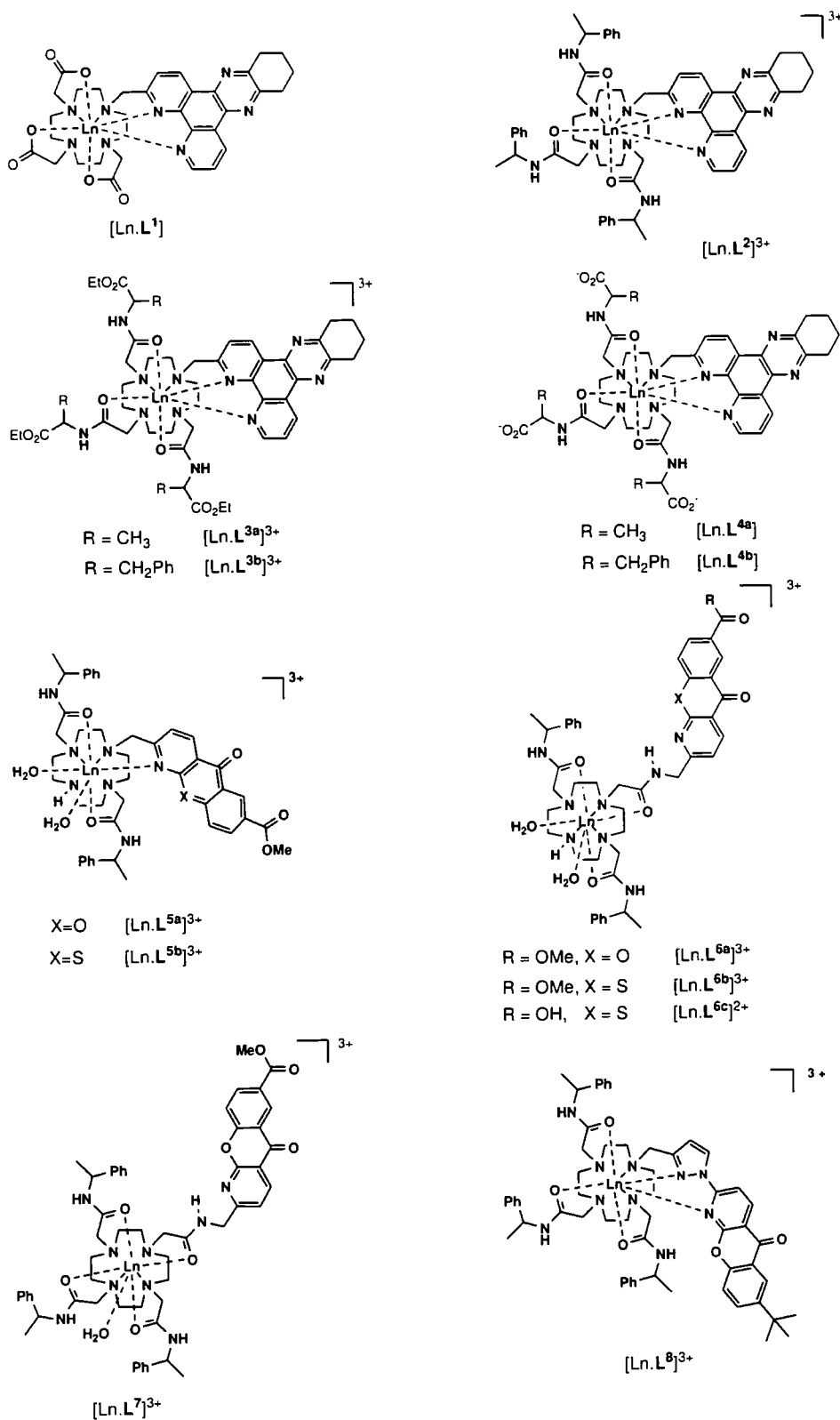
248. Caravan, P.; Parigi, G.; Chasse, J. M.; Cloutier, N. J.; Ellison, J. J.; Lauffer, R. B.; Luchinat, C.; McDermid, S. A.; Spiller, M.; McMurry, T. J., *Inorg. Chem.* 2007, **46**, 6632-6639.
249. Ghuman, J.; Zunszain, P. A.; Petitpas, I.; Bhattacharya, A. A.; Otagiri, M.; Curry, S., *J. Mol. Biol.* 2005, **353**, 38-52.
250. Meyer, B.; Peters, T., *Angew. Chem. Int. Ed.* 2003, **42**, (8), 864-890.
251. Mayer, M.; Meyer, B., *J. Am. Chem. Soc.* 2001, **123**, (5), 6108-6117.
252. Koshland, D. E.; Ray, W. J.; Erwin, M. J., *Fed. Proc.* 1958, **17**, (4), 1145-1150.
253. Pawson, T.; Nash, P., *Science* 2003, **300**, 445-452.
254. Rich, A.; Zhang, S., *Nat. Rev. Genet.* 2003, **4**, 566-572.
255. Rodger, A.; Norden, B., *Circular dichroism and linear dichroism*; Oxford University Press: Oxford, 1997.
256. Mahadevan, S.; Palaniandavar, M., *Inorg. Chem.* 1998, **37**, 3927-3934.
257. Feringa, B. L.; van Delden, R. A.; Koumura, N.; Geertsema, E. M., *Chem. Rev.* 2000, **100**, (5), 1789-1816.
258. Tang, K.; Green, M. M.; Cheon, K. S.; Selinger, K. V.; Garetz, B. A., *J. Am. Chem. Soc.* 2003, **125**, (24), 7313-7323.
259. Zahn, S.; Canary, J. W., *Science* 2000, **288**, (5470), 1404-1407.
260. Miyake, H.; Yoshida, K.; Sugimoto, H.; Tsukube, H., *J. Am. Chem. Soc.* 2004, **126**, (21), 6524-6525.
261. Chen, H.; Parkinson, J. A.; Novakova, O.; Bella, J.; Wang, F.; Dawson, A.; Gould, R.; Parsons, S.; Brabec, V.; Sadler, P. J., *Proc. Natl Acad. Sci. USA* 2003, **100**, (25), 14623-14628.
262. Carmichael, J.; DeGraff, W. G.; Gazdar, A. F.; Minna, J. D.; Mitchell, J. B., *Cancer Res.* 1987, **47**, (4), 936-42.
263. Calabrese, E. J.; Baldwin, L. A., *Toxicol. Pathol.* 1999, **27**, (2), 195-216.
264. Roche Cell Proliferation Reagent WST-1. (18/07/09),
265. Ormerod, M. G., In *Flow Cytometry: A Practical Approach*; Ormerod, M. G., Ed.; Oxford University Press: Oxford, 2000.
266. Kuypers, F. A.; Lewis, R. A.; Hua, M.; Schott, M. A.; Discher, D.; Ernst, J. D.; Lubin, B. H., *Blood* 1996, **87**, (3), 1179-1187.
267. Van Engeland, M.; Nieland, L. J. W.; Ramaekers, F. C. S.; Schutte, B.; Reutelingsperger, C. P. M., *Cytometry* 1998, **31**, 1-9.
268. Martin, S. J.; Reutelingsperger, C. P.; McGahon, A. J.; Rader, J. A.; van Schie, R. C.; LaFace, D. M.; Green, D. R., *J. Exp. Med.* 1995, **182**, (5), 1545-1556.
269. Green, D. R.; Reed, J. C., *Science* 1998, **281**, 1309-1312.
270. Pendergrass, W.; Wolf, N.; Poot, M., *Cytometry* 2004, **61A**, 162-169.
271. Poot, M.; Pierce, R. H., *Cytometry* 1999, **35**, 311-317.
272. Macho, A.; Decaudin, D.; Castedo, M.; Hirsch, T.; Susin, S. A.; Zamzami, N.; Kroemer, G., *Cytometry* 1996, **25**, 333-340.
273. Kessler, R. J.; Tyson, C. A.; Green, D. E., *Proc. Natl. Acad. Sci. USA* 1976, **73**, (9), 3141-3145.
274. Thibon, A.; Pierre, V. C., *Anal. Bioanal. Chem.* 2009, **394**, 107-120.
275. Bünzli, J.-C. G., In *Metal Ions in Biological Systems - The Lanthanides and Their Interrelations with Biosystems*; Sigel, A.; Sigel, H., Eds.; Marcel Dekker: New York, 2003.
276. Gavrilova, N. I.; Putyshev, A. B.; Korolenko, T. A., *Biull. Eksp. Biol. Med.* 1982, **94**, 58-60.
277. Reed, D. J.; Savage, M. K., *Biochim. Biophys. Acta* 1995, **1271**, (1), 43-50.
278. Sigma Aldrich *BCA Assay Kit*; Saint Louis, MO, 2003.
279. Sigma Aldrich *Nuclei EZ Prep Nuclei Isolation Kit*; Saint Louis, MO, 2003.

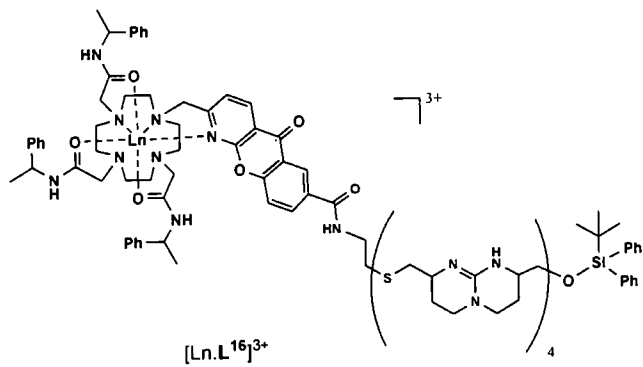
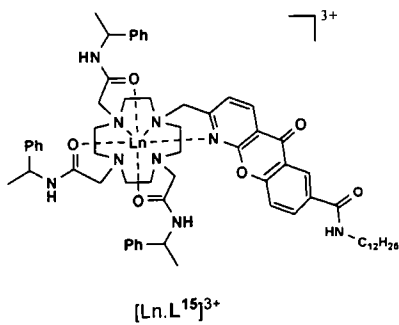
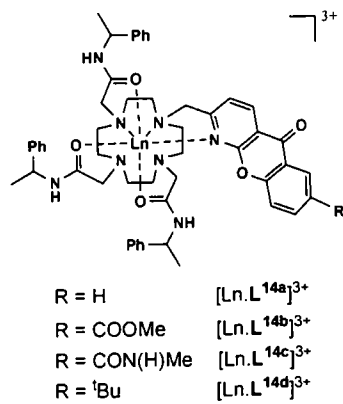
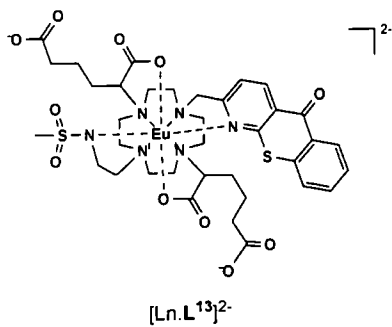
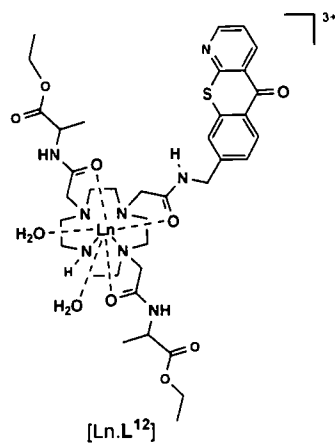
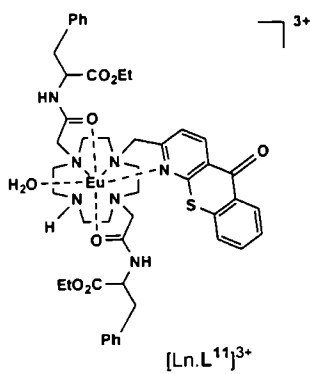
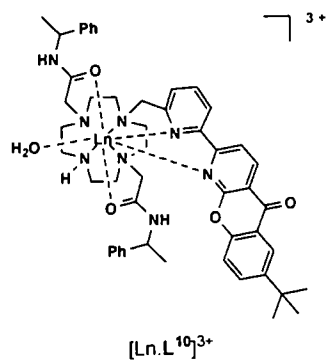
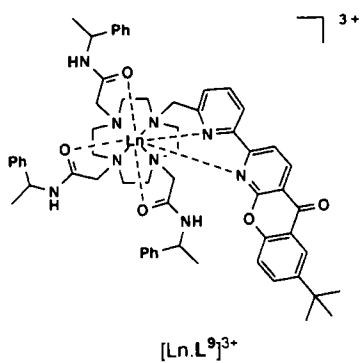
280. Pierce Biotechnology *Mitochondria Isolation Kit for Cultured Cells*; Rockford, IL, 2005.
281. Gibb, B. C.; Mezo, A. R.; Caustan, A. S.; Fraser, J. R.; Tsai, F. C. S.; Sherman, J. C., *Tetrahedron* 1995, **51**, (32), 8719-8732.

---

# APPENDICES

## APPENDIX ONE – SELECTED COMPLEXES





## APPENDIX TWO – RELEVANT PUBLICATIONS

Aspects of the work presented in this thesis have been reported in the following publications:

1. Robert Poole, Craig P. Montgomery, Elizabeth J. New, Aileen Congreve, David Parker and Mauro Botta, 2007, Identification of emissive lanthanide complexes suitable for cellular imaging that resist quenching by endogenous anti-oxidants, *Org. Biomol. Chem.*, **5**, 2055-2062, DOI: 10.1039/b705943d
2. Filip Kielar, Craig P. Montgomery, Elizabeth J. New, David Parker, Robert A. Poole, Siobhan L. Richardson and Philip A. Stenson, 2007, A mechanistic study of the dynamic quenching of the excited state of europium(III) and terbium(III) macrocyclic complexes by charge- or electron transfer, *Org. Biomol. Chem.*, **5**, 2975-2982, DOI: 10.1039/b709062e
3. Benjamin S. Murray, Elizabeth J. New, Robert Pal and David Parker, 2008, Critical evaluation of five emissive europium(III) complexes as optical probes: correlation of cytotoxicity, anion and protein affinity with complex structure, stability and intracellular localisation profile, *Org. Biomol. Chem.*, **6**, 2085-2094, DOI: 10.1039/b803895c
4. Filip Kielar, Aileen Congreve, Ga-Lai Law, Elizabeth J. New, David Parker, Ka-Leung Wong, Pilar Castreño and Javier de Mendoza, 2008, Two-photon microscopy study of the intracellular compartmentalisation of emissive terbium complexes and their oligo-arginine and oligo-guanidinium conjugates, *Chem. Commun.*, 2435-2437, DOI: 10.1039/b803864c
5. Filip Kielar, Ga-Lai Law, Elizabeth J. New and David Parker, 2008, The nature of the sensitiser substituent determines quenching sensitivity and protein affinity and influences the design of emissive lanthanide complexes as optical probes for intracellular use, *Org. Biomol. Chem.*, **6**, 2256-2258, DOI: 10.1039/b804369h
6. Craig P. Montgomery, Elizabeth J. New, David Parker and Robert D. Peacock, 2008, Enantioselective regulation of a metal complex in reversible binding to serum albumin: dynamic helicity inversion signalled by circularly polarised luminescence, *Chem. Commun.*, 4261-4263, DOI: 10.1039/b810978h
7. Elizabeth J. New, David Parker and Robert D. Peacock, 2009, Comparative study of the constitution and chiroptical properties of emissive terbium and europium complexes with a common tetraazatriphenylene sensitiser; the nature of the sensitiser determines quenching sensitivity and cellular uptake, *Dalton Trans.*, 672-679, DOI: 10.1039/b816173a
8. Elizabeth J. New and David Parker, 2009, The mechanism of cell uptake for luminescent lanthanide optical probes: the role of macropinocytosis and the effect of enhanced membrane permeability on compartmentalisation, *Org. Biomol. Chem.*, **7**: 851-855, DOI: 10.1039/b822145f

9. Craig P. Montgomery, Benjamin S. Murray, Elizabeth J. New, Robert Pal and David Parker, 2009, Cell-penetrating metal complex optical probes: Targeted and responsive systems based on lanthanide luminescence, *Acc. Chem. Res.* **42**: 925-937, **DOI**: 10.1021/ar800174z
10. Craig P. Montgomery, Elizabeth J. New, Lars O. Pålsson, David Parker, Andrei S. Batsanov and Laurent Lamarque, 2009, Emissive and cell permeable pyridyl and pyrazoyl-1-azaxanthone lanthanide complexes and their behaviour *in cellulo*, *Helv. Chim. Acta*, in press

